Cell-free regenerative medicine (RM) strategies for cartilage and bone put to the test in the challenging equine in vivo model

Rafael Angel Vindas Bolaños

Cell-free regenerative medicine (RM) strategies for cartilage and bone put to the test in the challenging equine *in vivo* model

Rafael Angel Vindas Bolaños

2019

Cell-free regenerative medicine (RM) strategies for cartilage and bone put to the test in the challenging equine *in vivo* model

(met een samenvatting in het Nederlands)

Proefschrift

Ter verkrijging van de graad van doctor aan de Universiteit Utrecht op gezag van de rector magnificus, prof.dr. H.R.B.M. Kummeling, ingevolge het besluit van het college voor promoties in het openbaar te verdedigen op dinsdag 9 april 2019 des ochtends te 10.30 uur

door

Rafael Angel Vindas Bolaños

geboren op 15 februari 1968 te Zarcero, Costa Rica

Promotoren: Prof. dr. P.R. van Weeren
　　　　　　 Prof. dr. ir. J. Malda

Co-promotor: Dr. J.C. de Grauw

A Dios

A mi familia

Al Profesor Dr. Paul René van Weeren

Content:

Chapter I

General Introduction

"Moveo ergo sum" (I move, so I am). This paraphrase of René Descartes' famous *"Cogito ergo sum"* may, in all its simplicity, well reflect the core of orthopaedics and unveil something of the largely hidden but nevertheless huge clinical need caused by partial or entire failure of the musculoskeletal system. The need to move around is a hallmark of humans and virtually any other mammalian species. Though not immediately life-threatening like cardiovascular disease or cancer, inability to do so means a sharp decline in quality of life with big physical and mental consequences in the long term.

Contemporary challenges to musculoskeletal health

The current epoch sees a combination of increasing lifespan and an almost contemptuous disregard of another Latin saying: "*Natura non facit saltus".* The phrase means: "Nature does not make jumps" and is commonly used to underline the notion that in nature things tend to change gradually rather than abruptly. It is an important principle of natural history and can be found in the works of Linnaeus, Leibniz and Darwin. When looking at the lifestyles of modern human beings, it would seem as though jumping has become the new walking, and fast has replaced gradual in many areas. However, while modern Western life may be fast-paced due to technological (smartphone, internet) advances, our bodies are becoming more sedentary and overweight; our diets and physical activity patterns have changed more rapidly over the past 50 years than ever before in the history of *homo sapiens*. Our musculoskeletal system was not made for this and struggles to cope. For our domesticated animals, many of which go through comparable processes, the same applies.

Against this background, it should not come as a surprise that the crucial tissues supporting our bodies and enabling absorption and transfer of forces during motion, bone and articular cartilage, are under more duress now than ever. The fact that one of the constituting tissues of the osteochondral unit, articular cartilage, is infamous for its limited, if any, self-repair capacity is not very helpful in this context. If articular cartilage structure and integrity deteriorates it can lead to osteoarthritis (OA) (Brittberg et al., 2016; Findlay and Atkins, 2014) and the possibility of pain and loss of function can develop (Lawrence et al., 2008a; Thein, 2014). In an increasingly obese and aging human population, osteoarthritis is one of the leading causes of disability throughout the Western world (CDC., 2018; Ge et al., 2012), affecting more than 90 million people in the United States alone and OA ranks among the most common clinical conditions negatively affecting quality of life (Krishnana and Grodzinsky, 2018).

This is true not only for humans: Osteoarthritic disease affects some species of domestic animals, most notably dogs (Shortkroff et al., 1996) and horses (McIlwraith et al., 2012), as commonly as it does humans. Of these species, the horse is uniquely bred and kept for its athletic potential, and musculoskeletal problems are a major quality of life concern and form a common ground for humane euthanasia of geriatric horses (McGowan and Ireland, 2016). Importantly, equine osteochondral tissue closely

resembles that of humans both morphologically and biochemically (Malda et al., 2012b; Malda et al., 2013). As such, translational research studying novel methods to facilitate osteochondral regeneration in horses will benefit both future human and equine patients (Colbath et al., 2017; Mcllwraith et al., 2011).

The joints are the hinges of the skeleton and are, as any moving part in technical engineering through which forces are transmitted or redirected, most prone to sustaining accidental damage or suffering from wear and tear. In the joint it is the osteochondral unit that mainly deals with the biomechanical challenges and is thus most vulnerable. It is the repair through various regenerative medicine approaches of this unit, consisting of articular cartilage and subchondral bone, which is the main focus of this thesis. Where the osteochondral unit should be seen as a single functional entity, it is made up of two widely different tissues that each poses its own specific requirements and challenges.

Articular cartilage: seemingly simple, but an utterly complex challenge to copy
Articular cartilage is a key element in carrying out the principal function of diarthrodial joints: enabling both the transmission and attenuation of forces generated by locomotion and allowing the almost frictionless articulation of bones. The major components of the extracellular matrix are water (70%), collagen (20%) and proteoglycans (10%)(Fox et al., 2009; Klein et al., 2009; McIlwraith et al., 2016).

At first glance, cartilage may appear to be a relatively simple tissue: It is aneural, avascular and alymphatic in nature, rich in extracellular matrix (ECM) components, with a low density of resident cells (chondrocytes) (Krishnana and Grodzinsky, 2018). When studied in more detail however, cartilage is in fact a complex (Coates and Fisher, 2010; Cole, 2011) and heterogeneous tissue, with an elaborate ECM composed predominantly of collagen type II fibrils and proteoglycans with unique biomechanical characteristics (Coates and Fisher, 2010; Roughley and Lee, 1994), in which a relatively low number of chondrocytes (between approximately 5 and 12% of total volume) are present (Todhunter and C.W., 1996).The proteoglycans are interspersed within the intricate three-dimensional network of collagen fibrils, which conglomerate of fairly inelastic fibrils and strongly hydrophilic proteoglycan aggregates is responsible for the tissue's unique biomechanical characteristics (Coates and Fisher, 2010; Roughley and Lee, 1994). A peculiar and very important feature of the collagen type II network of articular cartilage is the huge turnover rate of collagen type II in mature individuals, reflecting its extremely low metabolic rate. Studies using radio carbon dating techniques to determine the age of components of articular tissue extracellular matrix in humans showed that the collagen that was laid down in early puberty was still there at very advanced ages, implying no turnover (or repair) at all (Heinemeier et al., 2016). This incapacity of collagen II to remodel is seen as one of the most important underlying problems in osteoarthritis and is probably the biggest obstacle for developing real regenerative therapies in joint disease.

The biochemical and biomechanical properties of articular cartilage are not similar in all locations of a joint, but show topographical heterogeneity over the joint surface (Brama et al., 2000; Brommer et al., 2005). A similar heterogeneity exists depth-wise, *i.e.* from the articular surface down to the subchondral bone (Brama et al., 2009). The depth-dependent changes give rise to a typical layered or zonal structure (Klein et al., 2009). Three zones are commonly distinguished in the layer of hyaline cartilage between the articular surface and the layer of calcified cartilage that forms the transition to the subchondral bone (Figure 1). The superficial zone (SZ) accounts for the first 10 to 20% of tissue from the articular surface downwards; the following intermediate or middle zone (MZ) comprises 40-60% of total thickness and the deep zone (DZ) between 30 to 40 % (Buckwalter and Mankin, 1998). This depth-dependent configuration is generally conserved among mammalian species, but there are significant inter-species differences in total articular cartilage thickness, cell distribution, and matrix properties (Frisbie et al., 2006a; Malda et al., 2013; Moran et al., 2016).

The superficial zone has the greatest cell density, but the lowest proteoglycan content and biosynthetic activity (Wong et al., 1996). The chondrocytes have a flattened appearance and are arranged along the collagen fibers, which are arranged parallel to the joint surface, providing the tissue with high tensile strength and therefore great resistance against shear forces (Fox et al., 2009). This is also the layer in which the subpopulation of articular cartilage progenitor cells can be found (Williams et al., 2010).

In the middle zone the chondrocytes are present in low density; they are rounded in shape and have a random distribution. The orientation of the collagen fibrils with respect to the articular surface varies, giving the zone a high degree of anisotropy when studied with polarized light microscopy (Fox et al., 2009; Julkunen et al., 2010). The deep zone is characterized by chondrocytes that are arranged in columns perpendicular to the subchondral bone. The cell population is scarce and chondrocytes are hypertrophic in appearance (Fox et al., 2009; Pool et al., 1984). The DZ has the lowest collagen content and the highest concentration of proteoglycans. The fibrils of the collagen course in vertical direction from their anchoring place within the calcified cartilage layer (CCL) until they will start forming arches in the MZ (Fig.2.). The DZ is separated from the calcified layer by the so-called tidemark (Fig. 1), which is mostly described as a single, hematoxyphil line up to 10 µm in thickness (Gannon and Sokoloff, 1999). In fact, the structure is more complex, as at some places it dips through the entire calcified zone, thus reaching the underlying subchondral bone plate or eventually marrow spaces. This means there is direct contact at given places between hyaline cartilage and the underlying subchondral bone (Lyons et al., 2006).

SUPERFICIAL ZONE

MIDDLE ZONE

DEEP ZONE

Tidemark
CALCIFIED CARTILAGE
Cement line
SUBCHONDRAL BONE PLATE

CANCELLOUS BONE
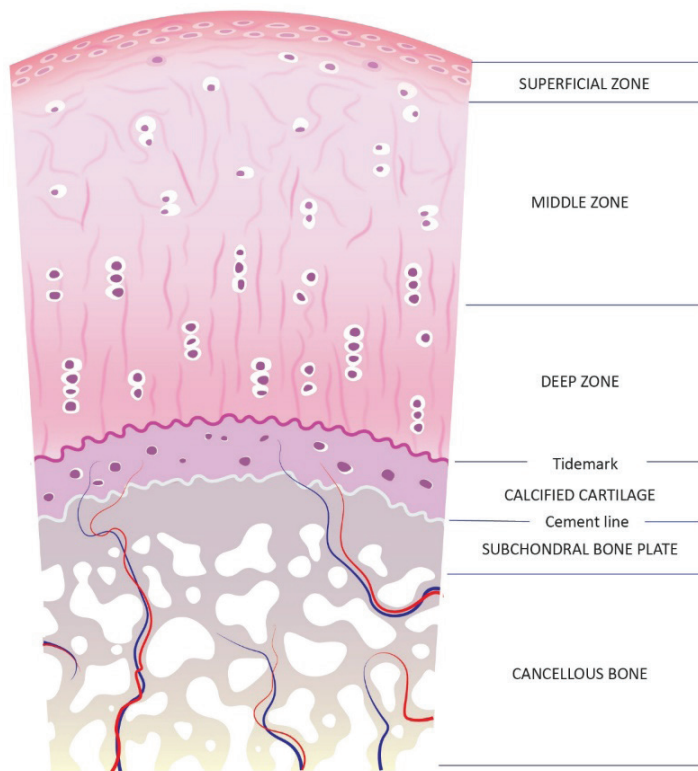
Figure 1. Schematic drawing of the structure of mature articular cartilage and subchondral bone. The tissue consists of a hyaline cartilage layer with three distinct zones: the superficial, middle and deep zone; the calcified cartilage layer and the subchondral bone.

While articular cartilage in fact is a very simple tissue that contains only extracellular matrix and a limited number of cells of the same breed, it is a tissue that is able to withstand enormous, and hugely varying, loads. This simplicity and immutability in mature individuals of the main structural element of the tissue, the collagen skeleton, may well be key elements in the success with which the tissue is able to cope with the demanding biomechanical challenges it is subjected to. Those same elements, however, make it extremely difficult to create a replacement tissue through regenerative medicine approaches that in a functional sense even comes close to what the native tissue is capable of.

ARTICULAR CARTILAGE

CALCIFIED CARTILAGE

SUBCHONDRAL BONE PLATE

CANCELLOUS BONE
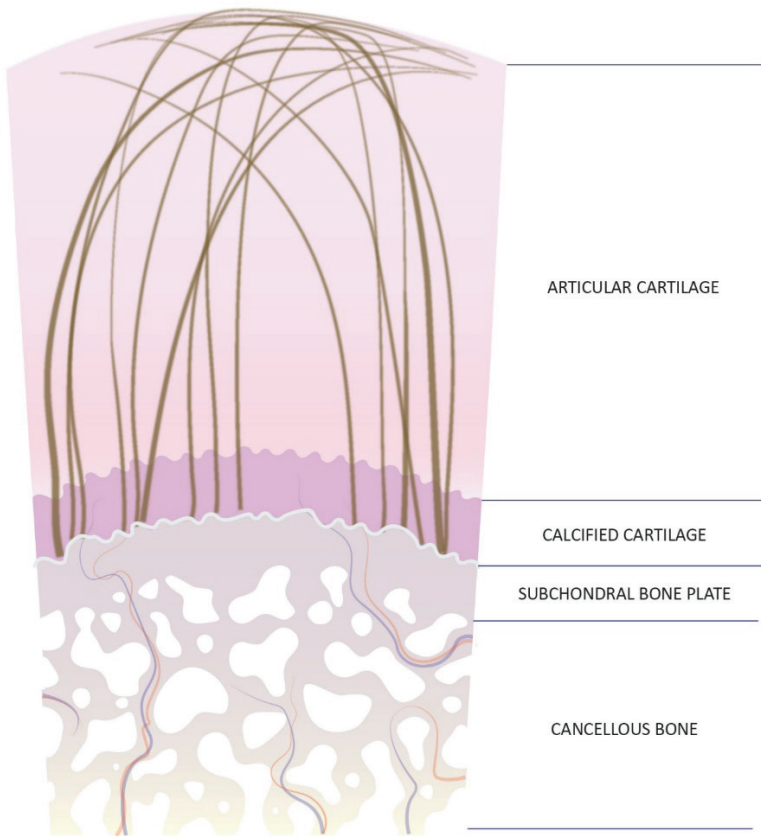
Figure 2. *Schematic drawing of the arch-like configuration of the collagen fibers in articular cartilage. Fiber orientation in the superficial zone is tangential to the cartilage surface, in the deep zone perpendicular to it. In the middle zone the fibers describe an arc, resulting in an anisotropic configuration.*

Subchondral bone: the more versatile but indispensable base

Articular cartilage composition, morphology and function cannot be seen as separate from the underlying subchondral bone. Together, articular cartilage and subchondral bone constitute what is known as the osteochondral unit (Goldring, 2012; Lajeunesse and Reboul, 2003; Stewart and Kawcak, 2018).

Typically, subchondral bone consists of a subchondral plate that is made up of compact bone and located directly adjacent to the layer of calcified cartilage, which plate is supported by trabecular bone at a greater distance from the joint cavity. There is a huge difference between articular cartilage and bone in their responses to biomechanical

loading. Bone has long been known to respond to mechanical loading, a response that, albeit to a lesser extent at advanced age and in conditions such as osteoporosis, will remain functional throughout the entire lifetime of an individual. This mechanism, which was first described by the German physician Julius Wolff in the late 1800s, is commonly known as Wolff's law which states that bone will adapt to the loading to which it is subjected (Frost, 2004; Wolff, 1982). In cartilage, a similar mechanism has been described, but only during the juvenile period in which growth takes place and during which the collagen skeleton network is still able to remodel in what has been termed the "process of functional adaptation" (Brama et al., 2002).

Mechanically, the compact subchondral plate provides firm support, but has some rigidity; the trabecular component provides some elasticity. This dual functionality of bone is made possible by its biochemical composition. The joint effect of the inorganic components of the bone (65%), such as calcium and phosphorus that form the basis of the hydroxyapatite crystals, and the organic components (35%), such as collagen I, proteoglycans, glycosaminoglycans and glycoproteins, permit the combination of strength and stiffness with a certain degree of elasticity (Gartner.L.P, 2017; McIlwraith et al., 2016). This has important physiological and pathological consequences. In a physiological sense, it is above all the trabecular zone that will adapt to magnitude and especially direction of loading. The capacity to modify the subchondral bone shape is approximately 10 times greater compared to that of the cortices of long bones (Mankin and Radin, 1993). This phenomenon can be driven by subtle differences, as has recently been illustrated in studies on the development of the mature structure of the subchondral bone in precocious species like the horse and the cow (Gorissen et al., 2016; Gorissen et al., 2018). It is not only bone structure that responds to loading during development. Like in articular cartilage, the biochemical composition of the bone has also been shown to be influenced by loading conditions in the early juvenile period (Brama et al., 2001; van de Lest et al., 2003). In a pathological sense, it is sclerosis of the subchondral plate that precedes fatigue injury that may result in catastrophic fracture in racehorses (Whitton et al., 2018), which is an issue that gets increasing attention in the ongoing debate about the ethical acceptability of the use of the horse for certain equestrian activities, especially racing.

All in all, the subchondral bone is an integral and extremely important part of the osteochondral unit. Due to its rich vascularization and (most probably related) lifelong capacity of remodeling it is a much more responsive and versatile tissue than articular cartilage and hence more amenable in terms of attempts at regeneration once damage has occurred. It is, however, also the tissue the overlying articular cartilage layer is attached to, Therefore, knowledge of the response of bone to any regenerative medicine approach that envisages restoration, repair or regeneration of the entire osteochondral unit is paramount for such an attempt to have any chance of success.

Regenerative medicine: approaches to (osteo)chondral defect treatment
Natural healing of cartilage lesions comprises the formation of fibrocartilaginous repair tissue, wich is functionally and biomechanically inferior to the original hyaline cartilage (Benders et al., 2013b). While in some cases repair tissue may appear to adequately fill up the defect bed or even to integrate with the adjacent cartilage, due to its inferior biomechanical properties, fibrocartilaginous repair tissue does not provide long-lasting protection from further trauma, and degeneration will ensue. Articular cartilage is above all a tissue that has to resist the biomechanical challenges it is subjected to. We therefore do not need solutions that look like or even anatomically resemble cartilage, they need to emulate its functional properties: *Esse quam videri (To be rather than to seem;* Cicero, 106-43 BC).

The Holy Grail in articular cartilage research has therefore long been to obtain repair tissue that is structurally and biomechanically equivalent to the original cartilage. Much research has been dedicated to attempts at stimulating or improving the body's own repair response to chondral or osteochondral damage. However, none so far have resulted in repair tissue of adequately comparable composition or biomechanical quality (López and Jarazo, 2015; Sridhar et al., 2015). Realizing the very limited potential for functional repair of osteochondral defects, and with the advent of new molecular and biopolymer techniques, research in recent years has shifted focus from methods for improving cartilage repair to those enabling true tissue regeneration – i.e., the aim is not merely to heal a defect through stimulation of natural repair, but by actually restoring the damaged tissue (Filardo et al., 2013; Kon et al., 2010), This so-called regenerative medicine (RM) and tissue engineering, approach represents a whole new paradigm in treatment of chondral or (osteo)chondral defects. While current routine clinical treatments involve debridement and facilitated access to endogenous repair factors in the subchondral bone, regenerative medicine aims at restoring damaged tissue using a combination of scaffolding materials or hydrogels and added biological components like growth factors, peptides, or mix of matrix (Moreira et al., 2012; Pot et al., 2016; Ruvinov et al., 2018). The thus far poor clinical results in repair or regeneration of chondral and osteochondral lesions prompt the development of new approaches that make use of new technologies in regenerative medicine, such as three-dimensional (3D) bioprinting (Mouser et al., 2017) and nano-technology (Abou Neel et al., 2013). However, whilst these and other avenues are generally seen as very promising, it should be understood that they also pose a multitude of inherent challenges (Mouser et al., 2017).

The lesions that are clinically encountered in diarthrodial joints can be grossly divided in three categories (Figure 3): partial thickness defects include lesions that extend to a certain extent, but not to full depth, into the layer of hyaline cartilage; the full thickness defect goes deeper, but does not extend to the subchondral bone, and the osteochondral defect penetrates into the subchondral bone (Frisbie et al., 2006a; Madry et al., 2010).

Unlike osteochondral defects, purely chondral defects represent damage limited to the articular cartilage alone. These are perhaps even more challenging to treat than the osteochondral ones, as such defects forego inputs from the vascular bone marrow, and any biomaterial approach aiming to treat these will need a method of fixation to prevent loss of the implant from the defect bed into the synovial cavity (Mancini et al., 2017; Moreira et al., 2012; van der Goes, 2010). Several strategies could be used to address this: one would be to anchor the scaffold, construct or implant to the subchondral bone. Prerequisites for such a strategy are the proper integration (*i.e.*, without significant pathological bone reaction) of the bone anchor into the surrounding bone. An alternative strategy would be to retain the implant in the defect bed through use of a self-sealing material, which could attach to adjacent cartilage and thus maintain the implant in the correct position until further tissue integration has occurred (Mancini et al., 2017; Moreira et al., 2012).
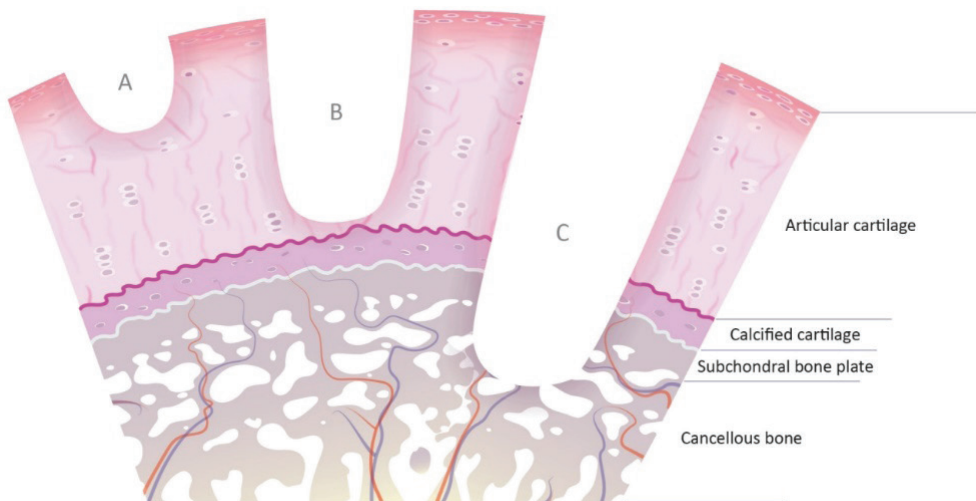
Figure 3. *A. Partial thickness defect; B. Full thickness defect excluding the calcified cartilage layer; C. Osteochondral defect.*

On the other hand, in osteochondral defects the entire osteochondral unit is injured and both tissue types should be taken into account in a more comprehensive approach when attempting the repair or regeneration of this type of lesions. Osteochondral defects have more clinical impact than chondral defects, as they will progress much quicker than defects that are limited to the chondral part alone and hence develop earlier into OA, which is a highly relevant disorder in both humans and horses (Anderson et al., 2011; Benders et al., 2013b; Kawcak et al., 2001; Lawrence et al., 2008a; Nukavarapu and Dorcemus, 2013).

To seed or not to seed; that's the question

The many approaches that have been tried and tested can broadly be classified into those employing either cell-seeded or unseeded (*i.e.*, cell-free) scaffolds of different origins. Biomaterials used as scaffolds for this purpose may in turn be divided into two groups: natural (biological) or synthetic (artificial) (Abou Neel et al., 2013; Benders et al., 2013b; Koch et al., 2009). While cellular components could have great potential in long-lasting regeneration, there are many drawbacks to their incorporation in scaffold material for osteochondral lesion repair: they cannot be incorporated in matrices subjected to higher temperatures (as may occur in some bioprinters, depending on the material involved and the printing technique used, or during sterilization), promoting and maintaining appropriate (stem) cell differentiation is difficult, and there are various other obstacles including autologous vs. xenograft issues and associated regulatory (legal) barriers that limit potential preclinical or clinical application at this time (Ahern et al., 2008; Benders et al., 2013b; Mouser et al., 2017; Pot et al., 2016). For these reasons there is an ongoing quest for optimized cell-free approaches, which are the focus of the work reflected in this thesis and to which this review is limited.

Material choices for cell-free cartilage repair

The field of tissue engineering has expanded exponentially in recent years, as has the range of potential biomaterials for regenerative strategies (Abou Neel et al., 2013). The choice of biomaterial for cell-free approaches depends on the intended application, but most are designed to aid the function of the extracellular matrix in supporting endogenous cellular attachment, proliferation and differentiation. Components of the extracellular matrix, including structural proteins, glycosaminoglycans, glycoproteins or even pieces of intact matrix have been used as scaffold materials (Abou Neel et al., 2013). Decellularized natural scaffolds have been used successfully in various areas of regenerative medicine, including approaches to intestine, bladder and skin defect healing (Badylak et al., 2008). While hardly used for orthopaedic purposes, this approach was marked as potentially useful for osteochondral defects, and an eight-week pilot in a horse seemed very promising (Benders et al., 2013b).

Regenerative scaffold-based interventions are gaining increasing interest as a potential treatment for chondral and osteochondral lesions, which is reflected in the high number of publications every year on *in vitro* research as well as pre-clinical experimental animal studies (Filardo et al., 2013). As mentioned previously, engineered implants, constructs or scaffolds will need to be retained at the site of the defect; they may either be fixed in the defect bed by anchoring the implant to the subchondral bone, by using some kind of glue, or they may be retained in the defect by using sealing gels.

Whenever anchoring to subchondral bone is to be carried out, integration and interaction of the proposed 'anchoring' biomaterial with surrounding bone must be critically evaluated prior to actual clinical application in the *in vivo* joint situation.

Materials such as tricalcium phosphate (TCP) and biphasic calcium phosphate (BCP) are osteo-inductive, readily available and have shown success in the regeneration of critical-size bone defects (Yuan et al., 2010). These materials are therefore excellent candidates as bone anchors for constructs treating osteochondral defects. The next logical step would be to create a biphasic construct of such a successful ceramic, combining it with for instance bioactive decellularized cartilage, which on its own seems to drive tissue regeneration *in vivo* (Benders et al., 2013b; Pot et al., 2016). The use of such ECM-based scaffolds would perfectly suit an unseeded (i.e., non-cell-laden) approach to osteochondral repair, as these scaffolds would attract cells from the implant site, which then could differentiate into the appropriate cell type and elicit endogenous repair. Ideally, such an approach could lead to natural off-the-shelf products that might be applied for a wide range of osteochondral defects (Benders et al., 2013b; Pot et al., 2016).

As an alternative to subchondral bone anchoring, the latest technology in hydrogels promotes interaction with the surrounding tissue to allow attachment to the (osteo) chondral lesion, the gel itself thus becoming a medium to facilitate cellular ingrowth (Moreira et al., 2012). This was exemplified in a recent study where cartilage defects were filled with natural polymers (hydrogel Dextran-Tiramine), showing the gel to become firmly attached to the cartilage ECM by covalent bonding to tyrosine residues in collagen fibrils. In addition the gel showed the capacity to attract and facilitate cellular ingrowth of chondrocytes or chondrocyte progenitor cells by combination of natural polymers like dextran-tiramine with Heparine-tiramine (Moreira et al., 2012; Moreira et al., 2011).

Though the rationale behind these regenerative strategies is elegantly simple and the underlying science seems sound, this rapidly developing field still faces many challenges. As for the materials themselves, scaffolds should have excellent biocompatibility and maintain a suitable microenvironment for cell proliferation and differentiation (Nino-Fong et al., 2013); they need to have optimal pore structure to allow ingrowth and exchange of cells and biological cues between the construct and the surrounding tissue (Seo et al., 2014); they should show adequate and predictable biodegradability where appropriate (Seo et al., 2014); and they need to display mechanical stability in order to promote lasting tissue regeneration (Seo et al., 2014). Having depicted this ideal and comfortably reassuring desired course of events, this may, however, be the moment to launch an utterly disturbing *caveat.* This *caveat* is that the described scenario stems from the reigning paradigm in regenerative medicine that temporary tissues and scaffolds will at some stage be replaced by functional native tissues. This paradigm may have proven true in certain applications for soft tissue repair, for instance in regenerative medicine of bladder or intestinal tissue (Badylak et al., 2008), but there are strong biological reasons to believe that the applicability of the paradigm might be less universal than originally thought and some musculoskeletal tissues, especially

articular cartilage, might well be the proverbial exception (Heinemeier et al., 2016). That being said, it should be recognized that scientifically speaking both paradigms and *caveats* need to be proven or disproven and consequently no choice can be made between the somewhat rosy or bleak views on the potential of articular regenerative medicine as pointed out above. The jury is still out and the jury is Nature itself.

Animal models for cartilage repair – Natura, artis magistra

While many different approaches to osteochondral defect treatment have been used and investigated in recent years, the overall aim remains the same: To obtain as optimal a restoration as possible of tissue composition and structure, but above all of functionality, with long-term (preferably life-long) effect. The benchmark for any novel approach aimed at improving cartilage repair is a comparison to an untreated ('control') defect of similar size, depth and location. Although traditional *in vitro* tests have been and still are of great importance in the initial developmental stages (e.g. biocompatibility and toxicity screening) of novel regenerative approaches, they are not sufficient for evaluation of cartilage repair or regeneration, let alone of clinical outcomes (Hurtig et al., 2011).

The evaluation of long-term outcome of potential novel regenerative strategies would ideally be performed *in vivo* over the natural course of a human life. It cannot be performed or even mimicked under laboratory conditions, and as demand for improved clinical solutions is high, results need to become available within months to years, not a lifetime – Therefore, predictive animal models of the human *in vivo* situation are much needed and sought after. The key issue for selection of an appropriate animal model is to best match the model to the clinical question being investigated and the hypothesis to be tested (Reinholz et al., 2004).

The American Food and Drug Administration (FDA) has provided guidance on the use of animal models for products intended to repair or replace knee cartilage (F.D.A., 2011). The FDA's guidance documents do not establish legally enforceable responsibilities, but these recommendations can be considered as the best guideline for obtaining approval for clinical use. For the given purpose, large animal models, of which the equine model has the biomechanics most resembling the human situation, are seen as necessary for truly translational research (Cook et al., 2014). This is not only due to closer similarity in outcome parameters that can be investigated, but also to fundamental differences in biomechanical and cellular responses in large animals and humans vs. small laboratory animal species. While laboratory animal studies using small mammals like rabbits and rodents will likely remain important for toxicology and biocompatibility screening at the earlier developmental stage, serious limitations preclude the use of such models for end-stage pre-clinical testing (Cook et al., 2014; Moran et al., 2016). These include the vast difference in body weights, limb angulations and therefore biomechanical environment in rabbit and rodent joints, as well as the much higher cellularity found in

rodent cartilage compared to that in humans (Malda et al., 2013).

Laboratory animal species like mice, rats, and rabbits make for low cost models due to easy animal husbandry and management, but their joints are inevitably small, precluding some surgical and/or monitoring options like repeated arthrocentesis and arthroscopy. Alternatively, the dog is used a lot as a human pre-clinical model in drug testing, naturally occurring OA is common in many canine breeds, and dogs are generally cooperative during recovery and rehabilitation from surgery (Moran et al., 2016). However, the limited body weight of most breeds and relatively thin articular cartilage are drawbacks to their use when trying to mimic the human situation (Cook et al., 2014; Moran et al., 2016). Pigs show comparable bone biochemistry, bone apposition rate and trabecular thickness to humans, and present the possibility of creating partial thickness cartilage defects, but they are relatively expensive to keep and require specialized management given their temperament, resistance to restrain and difficult vascular access (Ahern et al., 2008; Moran et al., 2016). Mini pigs have a thickness of articular cartilage of 1-2 mm in the femoral trochlear groove and can be a good option for short-term studies (Fisher et al., 2015). Goats and sheep have stifle joint anatomy similar to humans, are easily maintained and handled and partial thickness defects can be surgically created, but in both species subchondral cyst formation is a problem (Moran et al., 2016).

The horse is an increasingly popular species for the *in vivo* evaluation of regenerative medicine approaches, as it constitutes one of the closest approximations of the human situation and one of the most biomechanically challenging models for various orthopaedic ailments (Chu et al., 2009; McIlwraith et al., 2011; Moran et al., 2016). Because of the high prevalence and large economic and welfare impact of OA in horses, substantial research effort has historically been dedicated to its treatment, providing a unique base of knowledge on equine articular tissue composition and joint responses (McIlwraith et al., 2012). Conveniently, the anatomical size of most equine joints allows close monitoring of the healing process by sequential sampling of synovial fluid and imaging facilities like ultrasound, MRI, CT, and arthroscopy. Additionally, the animal is easy to handle and training a horse provides the opportunity to perform extensive quantitative functional assessments such as kinematic and kinetic analyses, and permits the use of treadmills for a well-defined rehabilitation program (Colbath et al., 2017; de Grauw, 2010; McIlwraith et al., 2012; McIlwraith et al., 2011).

Over the last decade, the horse has increasingly been used to study regenerative approaches aimed at cartilage (Colbath et al., 2017; López and Jarazo, 2015; Malda et al., 2012b; Mancini et al., 2017; McIlwraith et al., 2011; Nixon et al., 2015; Schnabel et al., 2013; Vindas Bolaños et al., 2017), bone (López and Jarazo, 2015; Vindas Bolaños et al., 2017) and tendon (Colbath et al., 2017; Estrada et al., 2014; Guercio et al., 2015; López and Jarazo, 2015; Renzi et al., 2013; Romero et al., 2017; Schnabel et al., 2013).

An important asset of the equine joint model is that the characteristics of equine cartilage are virtually identical to those of human cartilage (Malda et al., 2012b) (Figure 4). Similarities in bone mineralization density of the medial femoral condyle in horses and the lateral bone plate in humans have also been found, and in the lateral trochlea of both species, the bone mineral density is similar at a depth of 3 mm (Chevrier et al., 2014). The equine stifle joint has in fact been proposed as the best matching animal model to date for human knee OA, with a defect on the equine medial femoral condyle emulating medial femoral condylar injuries in humans (McIlwraith et al., 2011).
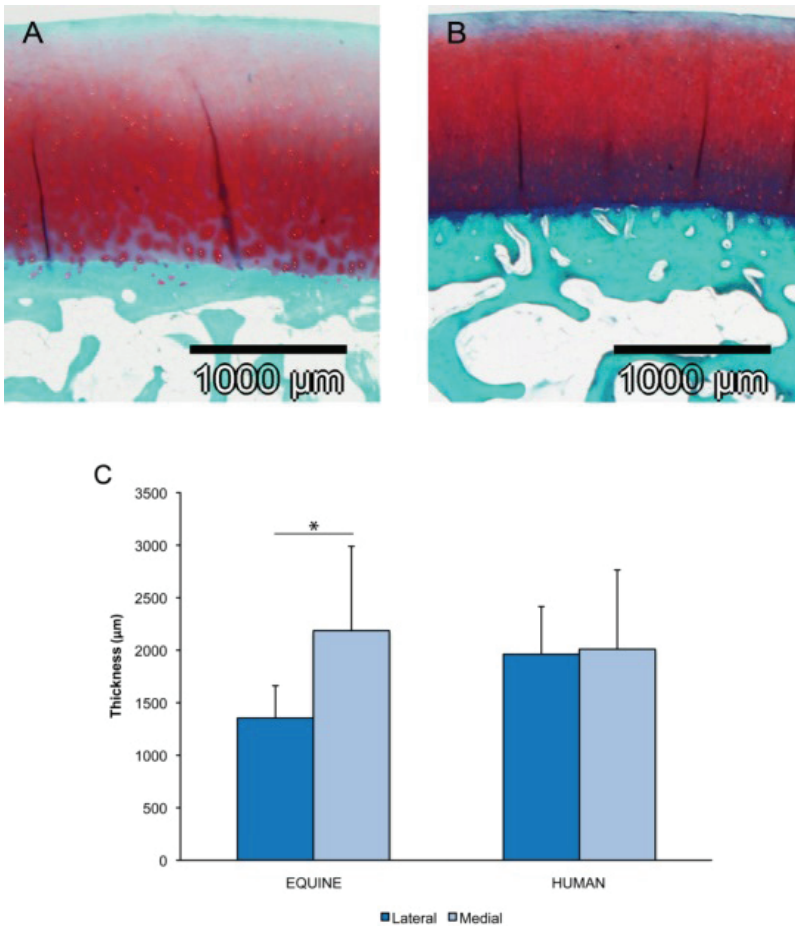
Figure 4. *Safranin-O staining of equine (A) and human (B) articular cartilage from the central sites of the femoral condyles, showing the strong optical resemblance. Average thickness of equine (n = 15) and human (n = 23) cartilage from the central sites of the femoral condyles (C). Whereas a significant difference was observed between the lateral and medial condyle of equine samples (P = 0.003) in contrast to human samples, overall thickness is comparable. Error bars indicate 95% confidence intervals. (Malda et al., 2012b), reprinted with permission).*

Other strengths of the equine model include the fact that in horses, most cartilage injuries occur during sporting activities and like in humans they frequently lead to clinical osteoarthritis (Nixon et al., 2015); also similar to the human situation, developmental joint diseases like osteochondrosis can predispose to OA. Societal resistance to experimentation with horses may be sizeable and ethical approval for equine studies could be more difficult to obtain. However, in terms of animal ethics, an important point to be made is that horses are themselves bred and kept primarily for their athletic potential. This means that they frequently suffer from orthopaedic injuries and hence represent an important target species for (osteo)chondral repair studies, unlike any other species with the possible exception of the dog (Williams et al., 2001; Wright, 2017). In this way, human preclinical studies on equine joints do not merely constitute animal experimentation for the benefit of humans, but may benefit the horse itself (Malda et al., 2012b).

Disadvantages of the horse are the substantial cost and specialized housing, husbandry and management facilities needed for *in vivo* trials, the horse's inability to reduce weight bearing on the joint in the recovery phase, and the dense subchondral bone placing demands on drills and other instruments (Moran et al., 2016).

Aim and outline of this thesis
Considering that osteochondral injuries predispose to osteoarthritis, which is a human and equine health problem that diminishes the quality of life of both species and causes great economic losses around the world, the overall aim of this thesis was to evaluate the long-term outcome of promising cell-free biomaterial approaches (*i.e.*, strategies that have shown promise in *in vitro* and small laboratory animal studies) to (osteo)chondral defect treatment in the equine *in vivo* setting.

The benefit of evaluation in such equine *in vivo* studies is two-fold: the performance of novel biomaterial-based approaches in this challenging environment represents formal clinical evaluation for its potential routine application in the horse, and it is considered the ultimate preclinical test for possible future use in humans.

Chapter II sets off with an investigation of a putative method to enhance intrinsic cartilage defect repair, avoiding the use of exogenous biomaterials altogether. It describes the technical details and feasibility of the *in vivo* application of nano-fracturing, a potential advancement to micro-fracturing which is the current clinical standard in humans, to enhance endogenous cartilage repair in the equine stifle joint partial thickness cartilage defect model.

Chapters III and IV address the suitability of novel biomaterials as potential subchondral bone anchors for constructs or scaffolds to be used in osteochondral defect treatment. As integration to surrounding bone with minimal pathology at the implant site is a

prerequisite for their eventual successful intra-articular application, these materials were in the horse first studied *in vivo* in an ectopic implant site: the tuber coxae.

Chapter III details the *in vivo* performance of low temperature direct 3D-printed bioceramics scaffold, aimed at improving the bone anchor for RM approaches to cartilage defect treatment, in the equine tuber coxae bone model.

Chapter IV builds on the findings of chapter III by evaluating the *in vivo* performance of new printed bone scaffolds, based on the CaP scaffolds implanted in the study reported in chapter III.

Chapter V is the first of the chapters addressing the performance and outcome of biomaterial-based approaches in the equine *in vivo* intra-articular situation. It describes the technical challenges associated with the *in vivo* application, fixation and long term evaluation of hydrogel constructs for cartilage repair in the equine stifle joint full-thickness cartilage defect model.

Chapter VI describes the long-term *in vivo* evaluation of a cartilage decellularized matrix scaffold for the repair of osteochondral defects in the equine *in vivo* stifle joint model using a composite osteochondral plug.

Chapter VII uses another approach to articular cartilage defect repair. The chapter describes, as chapter VI, the results of a long-term *in vivo* study using the same equine stifle joint model, but this time using a self-sealing hydrogel that covalently links to exposed cartilage collagen fibrils in the defect to treat chondral (not osteochondral) lesions.

The general discussion (chapter VIII) summarizes key findings from each study, highlighting strengths as well as limitations and identifying areas and directions for future research. This is in the humble recognition that finding the truth in science is following a long, winding and possibly never ending road, which is true for any scientific product, including this thesis. This recognition, however, does not alter in any form the drive of scientific researchers, as so eloquently expressed by Cicero (103-43BC): *Imprimis hominis est propria veri inquisitio atque investigatio* (It is humanity's dear plight to research and investigate the truth).

References

Abou Neel, E.A., Bozec, L., Knowles, J.C., Syed, O., Mudera, V., Day, R., Hyun, J.K., 2013. Collagen — Emerging collagen based therapies hit the patient. Advanced Drug Delivery Reviews 65, 429-456.

Anderson, D.D., Chubinskaya, S., Guilak, F., Martin, J.A., Oegema, T.R., Olson, S.A., Buckwalter, J.A., 2011. Post-Traumatic Osteoarthritis: Improved Understanding and Opportunities for Early Intervention. J Orthop Res 29, 802–809.

Badylak, S.F., Freytes, D.O., Gilbert, T.W., 2008. Reprint of: Extracellular matrix as a biological scaffold material: Structure and function. Acta Biomaterialia 23, S17-S26.

Benders, K.E.M., van Weeren, P.R., Badylak, S.F., Saris, D.B.F., Dhert, W.J.A., Malda, J., 2013. Extracellular matrix scaffolds for cartilage and bone regeneration. Trends in Biotechnology 31, 169-175.

Brama, P.A., Tekoppele, J.M., Bank, R.A., Karssenberg, D., Barneveld, A., van Weeren, P.R., 2000. Topographical mapping of biochemical properties of articular cartilage in the equine fetlock joint. Equine Vet J. 32, 19-26.

Brama, P.A.J., TeKoppele, J.M., Bank, R.A., 2001. Training affects the collagen framework of subchondral bone in foals. Vet J. 162, 24-32.

Brama, P.A.J., TeKoppele, J.M., Bank, R.A., Barneveld, A., van Weeren, P.R., 2002. Development of biochemical heterogeneity of articular cartilage: influences of age and exercise. Equine vet. J. 34, 265-269.

Brama, P.A., Holopainen, J., van Weeren, P., R., Firth, E., C., Heiminen, H.J., Huttinen, M.M., 2009. Influence of exercise and joint topography on depth-related spatial distribution of proteoglycan and collagen content in immature equine cartilage. Equine vet. J. 41, 557-563.

Brittberg, M., Gomoll, A.H., Canseco, J.A., Far, J., Lind, M., Hui, J., 2016. Cartilage repair in degenerative ageing knee. Acta Orthopaedica 87, 26-38.

Brommer, H., Brama, P.A., Laasanen, M.S., Helminen, H.J., van Weeren, P.R., Jurvelin, J.S., 2005. Functional adaptation of articular cartilage from birth to maturity under the influence of loading: a biomechanical analysis. Equine Vet J. 37, 148-154.

Buckwalter, J.A., Mankin, H.J., 1998. Articular Cartilage: Tissue design and chondrocyte-matrix interactions: Instruction Course Lecture. 47, 477-486.

CDC, 2018. Osteoarthritis. (accessed August, 25th 2018).

Coates, E.E., Fisher, J.P., 2010. Phenotypic Variations in Chondrocyte Subpopulations and Their Response to In Vitro Culture and External Stimuli. Ann Biomed Eng. 38(11), 3371-3388.

Colbath, A.C., Frisbie, D.D., Dow, S.W., Kisiday, J.D., McIlwraith, C.W., Goodrich, L.R., 2017. Equine Models for the Investigation of Mesenchymal Stem Cell Therapies in Orthopaedic Disease. Sports Medicine 25, 41-49.

Cole, A., G., 2011. A review of diversity in the evolution and development of cartilage: the search for the origin of the chondrocyte. European Cells and Materials 21, 122-129.

Cook, J.L., Hung, C.T., Kuroki, K., Stoker, A.M., Cook, C.R., Pfeiffer, F.M., Sherman, S.L., Stannard, J.P., 2014. Animal models of cartilage repair. Bone Joint Res 3, 89-94.

Chevrier, A., Kouao, A.S.M., Picard, G., Hurtig, M.B., Buschmann, M.D., 2014. Interspecies comparison of subchondral bone properties important for cartilage repair. J Orthop Res. 33, 63-70.

Chu, C.R., Szczodry, M., Bruno, S., 2010. Animal Models for Cartilage Regeneration and Repair. Tissue Engineering 16. Part B, 105-115.

Estrada, R.J., van Weeren, P.R., van de Lest, C.H.A., Boere, J., Reyes, M., Lonita, J.C., Estrada, M., Lischer, C.J., 2014. Comparison of healing in forelimb and hindlimb surgically induced core lesions of the equine superficial digital flexor tendon. Veterinary and Comparative Orthopaedics and Traumatology 27, 358-365.

F.D.A., 2011. Preparation of IDEs and INDs for Products Intended to Repair or Replace Knee Cartilage. Office of Communication, Outreach and Development (OCDO), Rockville, MD, USA., pp. 1-18.

Filardo, G.M.D., Kon, E.M.D., Roffi, A.B.S.D., Di Martino, A.M.D., Marcacci, M.M.D., 2013. Scaffold-Based Repair for Cartilage Healing: A Systematic Review and Technical Note. Arthroscopy: The Journal of Arthroscopic and Related Surgery. 29, 174-186.

Findlay, D.M., Atkins, G.J., 2014. Osteoblast-Chondrocyte Interactions in Ostearthritis. Curr Osteoporosis Resp 12, 127-134.

Fisher, M.B., Belkin, N.S., Milby, A.H., Henning, E.A., Bostrom, M., Kim, M., Pfeifer, C., Meloni, G., Dodge, G.R., Burdick, J.A., Schaer, T.P., Steinberg, D.S., Mauck, R.L., 2015. Cartilage Repair and Subchondral Bone Remodeling in Response to Focal Lesions in a Mini-Pig Model: Implications for Tissue Engineering. Tissue Engineering Part A 21, 850-859.

Fox, A.J.S., Bedi, A., Rodeo, S.A., 2009. The Basic Science of Articular Cartilage: Structure, Composition, and Function. Sports Health 1, 461-468.

Frisbie D.D. (2012). Synovial joint biology and pathobiology. In: Auer J.A., Stick J.A. (eds). Equine Surgery (4th ed) (pp. 1096-1114). St. Louis, MO: Elsevier-Saunders.

Frisbie, D.D., Cross, M.W., McIlwraith, C.W., 2006. A comparative study of articular cartilage thickness in the stifle of animal species used in human pre-clinical studies compared to articular cartilage thickness in the human knee. Veterinary and Comparative Orthopaedics and Traumatology 19, 142-146.

Frost, H.M., 2004. A 2003 Update of Bone Physiology and Wolff's Law for Clinicians. Angle Orthodontist 74, 3-15.

Gannon, F.H., Sokoloff, L., 1999. Histomorphometry of the aging human patella: histologic criteria and controls. . Osteoarthritis and Cartilage 7, 173-181.

Gartner.L.P, 2017. Textbook of Histology, 4th ed. Elsevier, Philadelphia,USA.

Ge, Z., Li, C., Heng, B., C., Cao, G., Yang, Z., 2012. Functional biomaterials for cartilage regeneration. J Biomed Mater Part A, 2526–2536.

Goldring, S.R., 2012. Alterations in periarticular bone and cross talk between subchondral bone and articular cartilage in osteoarthritis. Ther Adv Musculoskelet Dis 4, 249–258.

Gorissen, B.M., Wolschrijn, C.F., van Vilsteren, A.A., van Rietbergen, B., van Weeren, P.R., 2016. Trabecular bone of precocials at birth; Are they prepared to run for the wolf(f)? J Morphol. 277, 948-956.

Gorissen, B.M.C., Wolschrijn, C.F., van Rietbergen, B., Rieppo, L., Saarakkala, S., van Weeren, P.R., 2018. Trabecular and subchondral bone development of the talus and distal tibia from foal to adult in the warmblood horse. Anat Histol Embryol. Jun;47, 206-215.

Heinemeier, K.M., Schjerling, P., Heinemeijer, J., M.B., M., Krogsgaard, M.R., Grum-Schwensen, T., Petersen, M.M., Kjaer, M., 2016. Radiocarbon dating reveals minimal collagen turnover in both healthy and osteoarthitic human cartilage. Sci Transl Med 8, 346-390.

Hurtig, M.B., Buschmann, M.D., Fortier, L.A., Hoemann, C.D., Hunziker, E.B., Jurvelin, J.S., Mainil-Varlet, P., McIlwraith, C.W., Sah, R.L., Whiteside, R.A., 2011. Preclinical Studies for Cartilage Repair: Recommendations from the International Cartilage Repair Society. Cartilage2(2), 137-52.

Julkunen, P., Livarinen, J., Brama, P.A., Arokoski, J., Jurvelin, J.S., Helminen, H.J., 2010. Maturation of collagen fibril network structure in tibial and femoral cartilage of rabbits. Osteoarthritis and Cartilage 18, 406-415.

Kawcak, C.E., McIlwraith, W.C., Norrdin, R.W., Park, R.D., James, S.P., 2001. The rol of subchondral bone in joint disease: a review. Equine Vet J. 33, 120-126.

Klein, J.T., Malda, J., Sah, R.L., Dietmar W. Hutmacher, D.W., 2009. Tissue Engineering of Articular Cartilage with Biomimetic Zones. Tissue Engineering 15, 143-157.

Koch, T.G., Berg, L.C., Betts, D.H., 2009. Current and future regenerative medicine - Principles, concepts, and therapeutic use of stem cell therapy and tissue engineering in equine medicine. Can Vet Journal. 50, 155-165.

Kon, E., Mutini, A., Arcangeli, E., Delcogliano, M., Filardo, G., Aldini, N.N., 2010. Novel nanostructured scaffold for osteochondral regeneration: pilot study in horses. Tissue Eng Reg Med 4, 300-318.

Krishnana, Y., Grodzinsky, A.J., 2018. Cartilage diseases. Matrix Biology. Oct;71-72:51-69.

Lajeunesse, D., Reboul, P., 2003. Subchondral bone in osteoarthritis: a biologic link with articular cartilage leading to abnormal remodeling. Current opinion in rheumatology 15, 628-633.

Lawrence, R.C., Felson, D.T., Helmick, C.G., Lesley, M., Arnold, M.D., Hyon Choi, H., Deyo, R.A., Gabriel, S., Hirsch, R., Hochberg, M.C., G. Hunder, G.G., Jordan, J.M., Katz, J.N., Kremers, H.M., Wolfe, F., 2008. Estimates of the Prevalence of Arthritis and Other Rheumatic Conditions in the United States, Part II. Arthritis Rheum 58, 26-35.

López, M.J., Jarazo, J., 2015. State of the art: Stem cells in equine regenerative medicine. Equine Veterinary Journal 47, 145-154.

Lyons, T.J., McClure, S.F., Stoddart, R.W., McClure, J., 2006. The normal human chondro-osseous junctional region: evidence for contact of uncalcified cartilage with subchondral bone and marrow. BMC Musculoskeletal Disorders 7, 1-8.

Madry, H., van Dijk, N., Mueller-Gerbl, M., 2010. The basic science of the subchondral bone. Knee Surg Sports Traumatol Arthrosc, 18(4), 419-433.

Malda, J., Benders, K.E.M., Klein, T.J., Grauw, J.C., Kik, M.J.L., Hutmacher, D.W.S., D.B.F., van Weeren, P., R., Dhert, W.J.A., 2012. Comparative study of depth-development characteristics of equine and human osteochondral tissue from medial and lateral femoral condyles. Osteoarthritis and Cartilage. 20, 1147-1151.

Malda, J., de Grauw, J.C., Benders, K.E.M., Kik, M.J.L., van de Lest, C.H.A., Creemers, L.B., Dhert, W.J.A., van Weeren, P.R., 2013. Of Mice, Men and Elephants: The Relation between Articular Cartilage Thickness and Body Mass. PLOS ONE 8, 1-8.

Mankin H.J., Radin E.L. (1993). Structure and function of joints. In: McCarthy D.J. (ed.). Arthritis and allied conditions: a textbook of rheumatology (12th ed) (p. 189). Philadelphia, PA: Lea & Febiger [cited by Frisbie, 2012].

McGowan, C., Ireland, J.L., 2016. Welfare, Quality of Life, and Euthanasia of Aged Horses. Veterinary Clinics of North America: Equine Practice 32, 355-367.

McIlwraith, C.W., Frisbie, D.D., Kawcak, C.E., 2012. The horse as a model of naturally occurring osteoarthritis. Bone Joint Res 1, 297-309.

McIlwraith, W.C., Fortier, L.A., Frisbie, D.D., Nixon, A.J., 2011. Equine Models of Articular Cartilage Repair. Cartilage 2, 317-326.

Moran, C.J., Ramesh, A., Brama, P.A., O'Byrne, J.M., O'Brien, F.J., Levingstone, T.J., 2016. The benefits and limitations of animal models for translational research in cartilage repair. J Exp Orthop. 3(1), 1.

Moreira Teixeira, L.S., Bijl, S., Pully, V.V., Otto, C., Jin, R., Feijen, J., van Blitterswijk, C.A., Dijkstra, P.J., Karperien, M., 2012. Self-attaching and cell-attracting in-situ forming dextran-tyramine conjugates hydrogels for arthroscopic cartilage repair. Biomaterials 33, 3164-3174.

Moreira Teixeira, L.S., Feijen, J., van Blitterswijk, C.A., Dijkstra, P.J., Karperien, M., 2011. Enzyme-catalyzed crosslinkable hydrogels: Emerging strategies for tissue engineering. Biomaterials 33, 1281-1290.

Mouser, V.H.M., Levato, R., Bonassar, L.J., Lima, D.D.D., Grande, D.A., Travis J. Klein, T.J., Saris, D.B.F., Zenobi-Wong, M., Gawlitta, D., Malda, J., 2017. Three-Dimensional Bioprinting and Its Potential in the Field of Articular Cartilage Regeneration. Cartikage 8, 327-340.

Nino-Fong, R., McDuffee, L., Esparza, B.P., Kumar, M.R., Merschod, E.F., Podusca, K.M., 2013. Scaffold Effects on Osteogenic Differentiation of Equine Mesenchymal Stem Cells: An In Vivo Comparative Study. Macromolecular Bioscience. 13, 348-355.

Nixon, A.J., Rickey, E., Butler, T.J., Scimeca, M.S., Moran, N., Matthews, G.L., 2015. A chondrocyte infiltrated collagen type I/III membrane (MACI® implant) improves cartilage healing in the equine patellofemoral joint model. Osteoarthritis and Cartilage 23, 1-13.

Nukavarapu, S.P., Dorcemus, D.L., 2013. Osteochondral tissue engineering: Current strategies and challenges. Biotechnology Advances 31, 706-721.

Pot, M., W., Gonzales, V., K., Buma, P., IntHou, J., van Kuppevelt, T., H., de Vries, R., B.M., Daamen, W.F., 2016. Improved cartilage regeneration by implantation of acellular biomaterials after bone marrow stimulation: a systematic review and meta-analysis of animal studies. PeerJ Sep 8;4:e2243

Reinholz, G.G., Lu, L., Saris, D.B., Yaszemski, M.J., O'Driscoll, S.W., 2004. Animal models for cartilage reconstruction. Biomaterials 25, 1511-1521.

Renzi, S., Riccò, S., Dotti, S., Sesso, L., Grolli, S., Cornali, M., Carlin, S., Patruno, M., Cinotti, S., Ferrari, M., 2013. Autologous bone marrow mesenchymal stromal cells for regeneration of injured equine ligaments and tendons: A clinical report. Research in Veterinary Science 95, 272-277.

Romero, A., Barrachina, L., Ranera, B., Remacha, A.R., Moreno, B., de Blas, I., Sanz, A., Vázquez, F.J., Vitoria, A., Junquera, C., Zaragoza, P., Rodellar, C., 2017. Comparison of autologous bone marrow and adipose tissue derived mesenchymal stem cells, and platelet rich plasma, for treating surgically induced lesions of the equine superficial digital flexor tendon. The Veterinary Journal 224, 76-84.

Roughley, P.J., Lee, E.R., 1994. Cartilage proteoglycans: structure and potencial functions. Microsc Res Tech 28, 385-397.

Schnabel, L.V., Fortier, L.A., McIlwraith, C.W., Nobert, K.M., 2013. Therapeutic use of stem cells in horses: Which type, how, and when? The Veterinary Journal . 197(3), 570-577.

Seo, S.J., Mahapatra, C., Singh, R.K., Knowles, J.C., Kim, H., 2014. Strategies for osteochondral repair:Focus on scaffolds. Journal of Tissue Engineering 5, 2041731414541850.

Shortkroff, S., Barone, L., Hsu, H.P., Wrenn, C., Gagne, T., Chi, T., Breinan, H., Minas, T., Sledge, C.B., Tubo, R., Spector, M., 1996. Healing of chondral and osteochondral defects in a canine model: the role of cultured chondrocytes in regeneration of articular cartilage. Biomaterials 17(2), 147-154.

Sridhar , V.B., Dailing , E.A., Brock, L.J., Stansbury, J.W., Randolph, M., Anseth, K.S., 2015. A Biosynthetic Scaffold that Facilitates Chondrocyte-Mediated Degradation and Promotes Articular Cartilage Extracellular Matrix Deposition. Regen Eng Transl Med. 1(1-4), 11-21.

Stewart, H.L., Kawcak, C.E., 2018. The importance of Subchondral Bone in the Pathophysiology of Osteoarthritis. Frontiers in Veterinary Science 5, 1-9.

Thein, L., B, 2014. Knee osteoarthritis: Clinical connections to articular cartilage structure and function. Physical Therapy in Sport 16, 301-3016.

Todhunter, 1996. Anatomy and physiology of synovial joints. In: *Joint disease in the horse*, 1st ed. Eds: McIlwraith, C.W. and Trrotter, G.W. Saunders, Philadelphia.

Van de Lest, C.H.A., Brama, P.A.J. and van Weeren, P.R. (2003) The influence of exercise on bone morphogenic enzyme activity of immature equine subchondral bone. Biorheol., 40, 377-382.

van der Goes, T.I.F., 2010. Histología y biología celular Segunda ed, México.

Whitton, R.C., Ayodele, B.A., Hitchens, P.L., Mackie, E.J., 2018. Subchondral bone microdamage accumulation in distal metacarpus of Thoroughbred racehorses. Equine Vet J. Nov; 50, 766-773.

Williams, R., Khan, I., M, Richardson, K., Nelson, L., McCarthy, H.E., Analbelsi, T., Singhrao, S.K., Dowthwaite, G.P.-., Jones, R., E. , Baird, D.M., Lewis, H., Roberts, S., Shaw, H.M., Dudhia, J., Fairclough, J., Briggs, T., Archer, C.W., 2010. Identification and Clonal Characterisation of a Progenitor Cell Sub-Population in Normal Human Articular Cartilage. PLOS ONE 5 e13246.

Williams, R.B., Harkins, L.S., Hammond, C.J., Wood, J.L., 2001. Racehorse injuries, clinical problems and fatalities recorded on British racecourses from flat racing and National Hunt racing during 1996, 1997 and 1998. Equine Vet J. 33, 478-486.

Wolff, J., 1892. Das Gesetz der Transformation der Knochen. Berlin: Hirschwald.

Wong, M., Wuethrich, P., Eggli, P., Hunziker, E., 1996. Zone-specific cell biosynthetic activity in mature bovine articular cartilage: a new method using confocal microscopic stereology and quantitative autoradiography. J Orthop Res. 14, 424-432.

Yuan, H., Fernandes, H., Habibovic, P., de Boer, J., Barradas, A.M., de Ruiter, A., Walsh, W.R., van Blitterswijk, C.A., de Bruijn, J.D., 2010. Osteoinductive ceramics as a synthetic alternative to autologous bone grafting. PNAS 107, 13614-13139.

Chapter II

Technical note - Nanofracturing as a new needling technique for bone marrow stimulation in equine cartilage repair

(Submitted)

Technical note - Nanofracturing as a new needling technique for bone marrow stimulation in equine cartilage repair.

Stefan M. Cokelaere[a], Rafael A. Vindas Bolaños[b], Sanne K. Both[d], Mariëlle Vullers[a], Nicoline M. Korthagen[a,c], Janny C. de Grauw[a], P. René van Weeren[a]

[a] Department of Equine Sciences, Faculty of Veterinary Medicine, Utrecht University, Yalelaan 112, 3584 CM, Utrecht, The Netherlands.

[b] Catedra de Cirugía de Especies Mayores, Escuela de Medicina Veterinaria, Universidad Nacional, Costa Rica

[c] Department of Orthopaedics, University Medical Center Utrecht, Heidelberglaan 100, 3584 CX, Utrecht, The Netherlands

[d] Developmental BioEngineering, Faculty Technical Nature Science, University of Twente, Drienerlolaan 5, 7522 NB, Enschede, The Netherlands

Corresponding author
Stefan M. Cokelaere, Sporthorse Medical Diagnostic Centre, Hooge Wijststraat 7, 5384 RC, Heesch, The Netherlands. T + 31 412 745500 E: cokelaere@sporthorsemdc.com

Keywords
Horse, bone marrow stimulation, nanofracture, cartilage repair

Abstract

Background: Although microfracture is the current standard for treatment of cartilage defects in horses, it has been associated with variable outcome. Nanofracturing is a novel technique that uses a commercially developed device to yield smaller perforations with deeper penetration into the subchondral space. It is applied via a standardized simple procedure, which can be performed arthroscopically alone or via mini-arthrotomy in combination with other procedures. Experimentally, in rabbits and sheep, nanofracturing has been shown to result in superior repair in comparison with microfracture.

Objectives: To study the feasibility of nanofracturing using a commercial device for treatment of cartilage defects in horses.

Methods: Nanofracturing was tested in two studies: 1) a cadaveric study in n = 2 equine stifle joints and 2) an *in vivo* study in n = 8 horses with experimental partial thickness cartilage defects in the stifle joint. These were treated with nanofracturing or a novel biomaterial and repair tissue was studied macroscopically (ICRS-I score) and microscopically (histology and microCT) after 7 months.

Results: The nanofracturing device allowed easy penetration of the subchondral bone in horses and could readily be applied both arthroscopically and via mini-arthrotomy. Compared to clinical experience with conventional microfracturing, smaller and deeper holes could be created without visible compaction of adjacent tissue. Repair tissue after 7 months was graded near-normal on the ICRS-I score, while histologically, the abundant repair tissue proved mainly fibrocartilaginous in nature. MicroCT revealed near-full restoration of cartilage thickness and acceptable subchondral bone microarchitecture.

Main limitations: The *in vivo* study did not include a control group treated with conventional microfracture.

Conclusions: This is the first report on the feasibility of bone marrow stimulation through nanofracturing as a method to enhance chondral defect repair in horses. In the *in vivo* study, no clinical adverse effects were observed and promising defect filling was seen 7 months after treatment.

Introduction

Articular cartilage has limited capacity for repair of lesions that do not extend into the underlying bone (Gomoll and Minas, 2014; Mankin, 1982; Martin et al., 2004) As such, chondral injuries contribute to progressive articular cartilage loss and the eventual development of osteoarthritis (Akatsu et al., 2018; Guermazi et al., 2017; Martin et al., 2004; Squires et al., 2003; Widuchowski et al., 2007), a major issue in human healthcare and equine practice (Cokelaere et al., 2016; Dillon et al., 2006; Guermazi et al., 2017; Lawrence et al., 2008b). Strategies to improve repair of chondral defects are therefore imperative in the effort to reduce the disease burden of osteoarthritis (Cokelaere et al., 2016). Over the years, it has become increasingly apparent that the osteochondral unit rather than cartilage alone needs to be the focus of cartilage surgery, as the articular cartilage and subchondral bone form a complex system featuring many (mechanical, paracrine) interactions between the two tissues (Gomoll et al., 2010).

Microfracture is the most frequently used technique to access bone marrow cells and growth factors for enhancement of endogenous articular cartilage repair (Frisbie et al., 2006b; Frisbie et al., 1999; Steadman et al., 2001). While considered a current clinical standard of treatment in horses and humans (Cokelaere et al., 2016; Frisbie et al., 2006b; Steadman et al., 2001), long-term clinical outcomes have varied (Bae et al., 2006; Goyal et al., 2013; Kreuz et al., 2006a; Kreuz et al., 2006b; Mithoefer et al., 2005). Variability in the amount and quality of repair tissue, along with the observation of significant subchondral bone changes after microfracture, has also been reported (Bae et al., 2006; Frisbie et al., 2006b; Goyal et al., 2013; Kreuz et al., 2006a; Kreuz et al., 2006b; Minas et al., 2009; Mithoefer et al., 2016; Mithoefer et al., 2005). The amount and quality of repair cells available to the cartilage defect are likely key variables in the success or failure of bone marrow stimulated cartilage repair (Madry et al., 2016; Shapiro et al., 1993). Recently however, surgical compromise of the subchondral bone during microfracture has been postulated to negatively affect success rates of other subsequently applied cartilage repair techniques (Cokelaere et al., 2016; Minas et al., 2009). The variable and limited penetration of the subchondral bone and the relatively large diameter of the awl are thought to play key roles in formation of suboptimal repair tissue, as well as in subchondral bone compaction around the perforations and in intralesional osteophyte formation (Cokelaere et al., 2016). To overcome the mechanical limitations and associated variable outcomes of microfracture, the nanofracturing technique using a specially developed device was recently introduced. It provides for smaller diameter and deeper subchondral bone needle perforations with improved access to the bone marrow (Behrens and Benthien, 2011). Both techniques are compared in the figure 1.

Nanofracturing of osteochondral lesions in adult sheep has been shown to provide

better repair tissue than microfracturing, with a more satisfactory restoration of articular cartilage architecture and greater type II collagen content (Zedde et al., 2017). This technical note reports on the use and feasibility of this second generation needling technique for the treatment of partial thickness cartilage defects in horses.

Materials & Technique

The nanofracture device (NanoFx®)[a] consists of a reusable hand instrument and a single-use disposable 1 mm diameter nitinol needle (PleuriStik™)[a] that is advanced through the cannulated pick to perform the subchondral needling. The handle[a] of the device comes either with a 15° angled tip or with an A-Curve tip, which is specifically designed for hard-to-access lesions.

The nanofracturing technique itself has been previously described by Behrens & Benthien (2011) and is performed in a systematic, spiral fashion starting from the periphery of the lesion, upon completion of cartilage defect preparation (superficial debridement). The 1 mm diameter needle is inserted into the cannula of the pick. The tip of the pick is placed onto the prepared defect bed and slight hammer strikes on the proximal end of the needle advance the tip into the subchondral bone to a consistent, stop-controlled depth of 9 mm with minimal thermal damage to the tissue. The needle is removed and consecutive subchondral bone channels are placed throughout the defect bed approximately 3 mm apart, to give an even distribution and to maintain adequate bone bridges between channels.

Methods

1) *Cadaver study*

Two fresh cadaver stifle joints obtained from n = 2 adult horses euthanized for reasons other than stifle joint pathology were used to test the feasibility of nanofracture. All cartilage defects were created and treated by the same board-certified equine surgeon (SC), who did not have previous clinical experience with the device. After creation of multiple partial- and full-thickness cartilage defects in the femoral trochlear ridges and condyles via arthrotomy, nanofracturing of the defect beds was undertaken. Numbers of perforations, success or failure to penetrate the subchondral bone, as well as any special observations or remarks were recorded.

2) *In vivo equine chondral defect model*

The study protocol was approved by the institutional ethical and animal welfare

committee from the Veterinary School at the National University of Costa Rica. Eight healthy Criollo breed horses (mean age 7.1 years; range 5 - 9; mean weight 319 kg; range 275-375) were used. All horses were sound on clinical lameness examination and did not show clinical or radiographic evidence of stifle joint pathology. They were housed in individual box stalls and fed a standard daily maintenance ration of 0.5 kg concentrate with hay ad libitum and free access to water.

Prior to surgery, one limb of each animal was randomly assigned to receive nanofracture treatment, while the other was assigned to be treated with an experimental biomaterial (Both et al, manuscript in preparation). Surgery was performed under general anaesthesia, with peri- and post-operative analgesia provided by phenylbutazone. One partial-thickness chondral defect (1 mm depth) was created via mini-arthrotomy in the mid-medial trochlear ridge of each stifle joint by the same surgeon (SC) using a 7-mm diameter biopsy punch. For nanofracture, each cartilage lesion was treated with three perforations distributed across the 7-mm defect (Figure 1a and b). Defects were flushed with saline to remove any debris left-over from defect creation or nanofracturing. Incisions were routinely closed and horses returned to their stalls immediately after surgery.

Post-operative care and monitoring
Post-operatively, horses received antibiotics for 5 days (procaine penicillin (Phenix, Belgium; 15000 IU/kg IM SID) and gentamicin (Kepro BV, the Netherlands; 6.6 mg/kg IV SID)) and non-steroidal anti-inflammatory drugs (phenylbutazone (Lisan, Costa Rica; 2.2 mg/kg PO BID) for 10 days. The animals were clinically monitored on a daily basis for rectal temperature, heart rate and respiratory rate, as well as stance, demeanor and general appearance; hematology and serum biochemistry were checked one, three and six months post-operatively. From three months post-operatively, horses were turned out at free pasture allowing natural exercise until the end of the experiment at 7 months, when horses were humanely euthanized.

Repair tissue assessment: Macroscopic and microscopic scoring
Osteochondral plugs were obtained and fixed in formalin for histopathologic and micro-CT analysis. The ICRS-I Visual Assessment Scale (Table 1) was used for macroscopic scoring of cartilage repair. Three images of each cartilage defect were selected. These images were randomly labelled and scored by three blinded observers. Microscopic assessment was performed on images of Hematoxylin-Eosin (HE), Safranin-O and Alcian Blue (AB) stained histological slides obtained from each of the borders of the defect as well as mid-defect. Scores were assigned using the ICRS-II scoring system (Table 2) by three blinded observers, with the exception that no polarized light microscopy was performed.
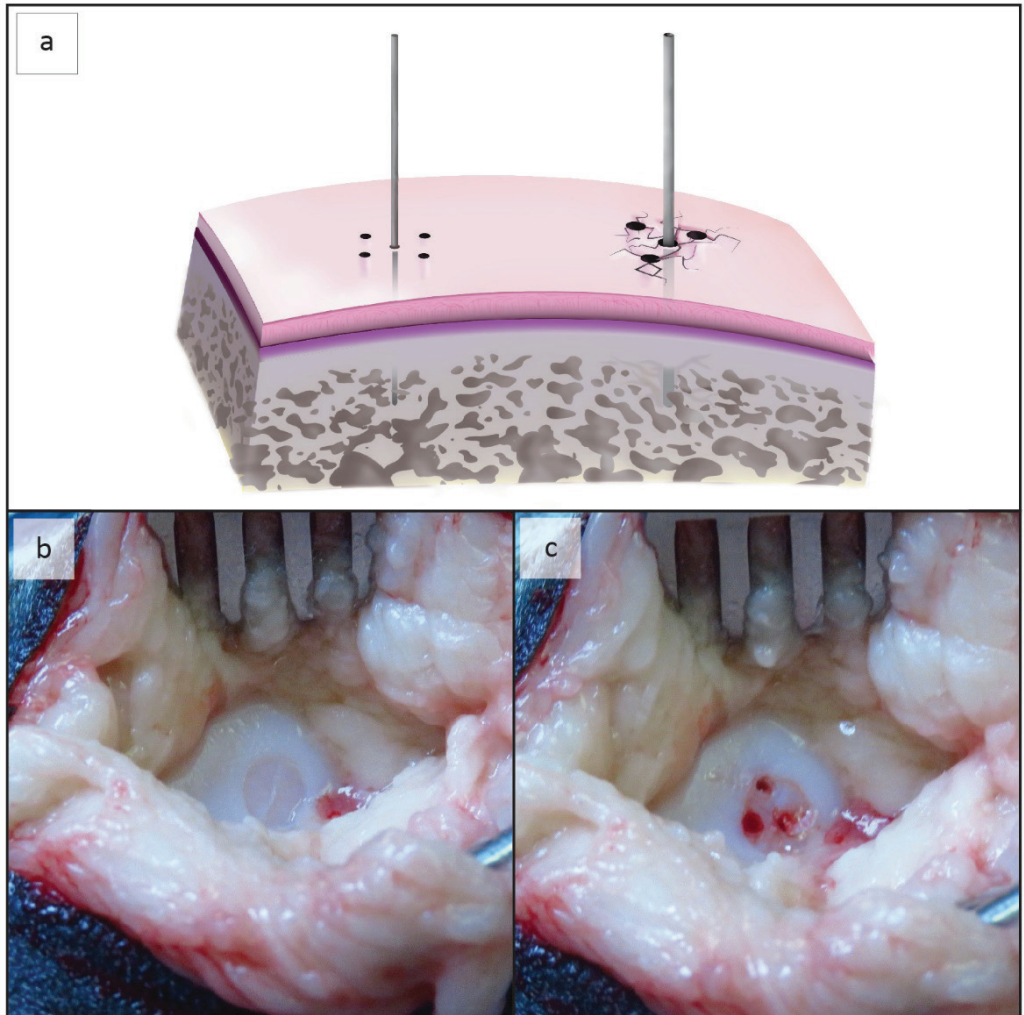
Figure 1 (a) Schematic diagram of nanofracture (left) compared to microfracture (right), showing more adjacent tissue compaction and the wider awl causing more subchondral bone damage with the latter technique (b) photograph of a freshly created partial thickness cartilage defect (c) the same defect after nanofracture was applied.

Table 1 – International Cartilage Repair Society Visual Assessment Score (ICRS-I; Van den Borne et al., 2007)

Cartilage repair assessment ICRS	Points
Degree of defect repair	
In level with surrounding cartilage	4
75% repair of defect depth	3
50% repair of defect depth	2
25% repair of defect depth	1
0% repair of defect depth	0
Integration to border zone	
Complete integration with surrounding cartilage	4
Demarcating border < 1mm	3
¾ of graft integrated, ¼ with notable border > 1mm width	2
½ of graft integrated with surrounding cartilage, ½ with a notable border	1
>1mm	0
From no contact to ¼ of graft integrated with surrounding cartilage	
Macroscopic appearance	
Intact smooth surface	4
Fibrillated surface	3
Small, scattered fissures of cracks	2
Several, small or few but large fissures	1
Total degeneration of grafted area	0
Overall repair assessment	
Grade I: normal	12
Grade II: nearly normal	8-11
Grade III: abnormal	4-7
Grade IV: severely abnormal	1-3

Table 2 – ICRS-II scoring system for histological assessment of cartilage repair tissue (Mainil-Varlet et al., 2010)

Histological Parameter	Score
1.Tissue morphology (viewed under polarized light)	0%: Full-thickness collagen fibers 100%: Normal cartilage birefringence
2.Matrix staining (metachromasia)	0%: No standing 100%: Full metachromasia
3.Cell morphology	0%: No round/oval cells 100%: Mostly round/oval cells
4.Chondrocyte clustering (4 or more grouped cells)	0%: Present 100%: Absent
5.Surface architecture	0%: Delamination, or mayor irregularity 100%: Smooth surface
6.Basal integration	0%: No integration 100%: Complete integration
7.Formation of tidemark	0%: No calcification front 100%: Tidemark
8.Subchondral bone abnormalities	0%: Abnormal 100%: Normal marrow
9.Inflammation	0%: Present 100%: Absent
10.Abnormal calcification/ossification	0%: Present 100%: Absent
11.Vascularization (within the repaired tissue)	0%: Present 100%: Absent
12.Surface/Superficial assessment	0%: Total loss or complete disruption 100%: Resembles intact articular cartilage
13.Mid/deep zone assessment	0%: Fibrous tissue 100%: Normal hyaline cartilage
14.Overall assessment	0%: Bad (fibrous tissue) 100%: Good (hyaline cartilage)

Micro-CT

The samples were dried and manually positioned in the µCT system[b]. Specific settings included voltage of 90 kV, current of 200 µA, field of view (FOV) of 20 mm and scan time of 4.5 minutes. These settings were equal for all samples and created 512 µCT images per sample. Fiji software (version Image J 1.52g) was used to edit µCT images for further analyses, with manual selection of regions of interest (ROI) at the level of the defect.

Results

1) Cadaver study

Perforations could successfully be made, with the needle penetrating the subchondral bone with relative ease in diverse joint locations; of 20 perforations attempted, 19 were immediately successful, with only the first attempt giving slight slippage of the device during hammer strikes. Blood could be observed to appear from each of the channels upon removal of the device. The needle could be re-used up to 10 times without breakage.

2) In vivo study

Technical nanofracturing performance
The subchondral bone needling was easy to perform in a clinical setting and was consistently associated with visible bleeding out of the holes (100% of perforations). A small depression left by the device in the adjacent cartilage or very minor cartilage debris surrounding the perforations could be observed in 2 out of 7 defects.

Post-operative monitoring
One of the horses showed dehiscence of the skin wound, which was immediately treated by re-suturing which resulted in further uneventful healing of the wound. Over the 7 months follow-up, 7 out of 8 horses recovered uneventfully and coped well during the post-surgical rehabilitation period. Two months postoperatively, one horse unfortunately died due to an unrelated traumatic head injury; osteochondral tissue blocks were harvested but no photographs were obtained from this horse. In the remaining horses, no significant (≥ 1/5 on AAEP scale) lameness was observed at any time, and clinical parameters as well as routine hematology and serum biochemistry parameters remained within normal physiologic limits throughout the experiment. Radiographs were taken at baseline but not subsequently, as the clinical course was deemed very satisfactory.

Macroscopic assessment
Scoring showed good inter-observer reliability (Cronbach's alpha 0.86; $p < 0.001$). Median overall repair assessment score for nanofracture treated defects was 9 (interquartile range, IQR 7 – 10), denoting near normal cartilage (where normal cartilage receives a score of 12; Table 1). Defects were still readily recognizable (Figure 2a) but showed promising degrees of filling and integration with adjacent tissue; degree of defect repair received the highest sub scores (median 3, IQR 2.25 – 4), followed by integration to border zone (median 3, IQR 2 – 3).
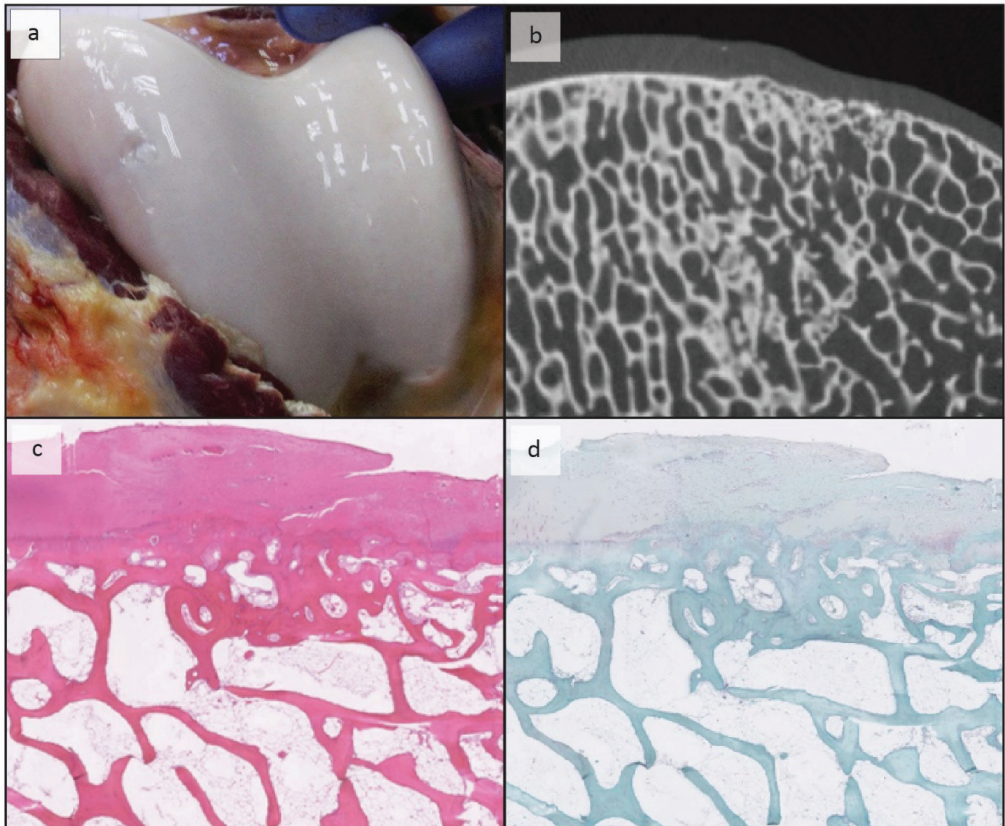
Figure 2 (a) Typical macroscopic outcome 7 months after nanofracture treatment of a surgically created partial thickness cartilage defect on the medial femoral trochlea of a horse (b) MicroCT image of the same nanofracture treated defect 7 months after surgery, revealing mild distiurbance of subchondral bone microarchitecture where surgical perforations were made (c) Image of Hematoxyllin-Eosin (HE) stained section of the same nanofracture treated defect 7 months postoperatively, showing abundant repair tissue with good basal integration but relatively poor cell morphology, tidemark disturbance and mild subchondral bone changes underlying the defect (d) Image of Safranin-O stained section of the same nanofracture treated defect 7 months postoperatively, showing poor cartilage matrix staining.

Histopathologic analysis
Histopathologic assessment using the ICRS-II scoring system (Mainil-Varlet et al., 2010; Table 2) by three blinded observers yielded a Cronbach's alpha of 0.78, which is considered acceptable (where > 0.8 is rated as good). After 7 months, defects demonstrated ample but mainly fibrocartilaginous repair tissue, with acceptable integration to the underlying calcified cartilage and adjacent cartilage, but limited matrix staining (Figure 2c and d). Total ICRS-II score was 48% ± 10% (mean ± SD), where 100% denotes normal cartilage; highest scores were assigned for the criterion 'basal integration' (67% ± 9%), while 'superficial assessment' received the lowest scores of all ICRS-II criteria (32% ± 12%).

MicroCT analysis
Mean cartilage thickness mid-defect was 97.6 ± 7.7% (mean ± SD) of adjacent cartilage thickness. MicroCT showed moderate subchondral bone disruption surrounding nanofracture channels in all treated defects 7 months post-operatively (Figure 2b).

Discussion

In the work reported here, we found that nanofracturing using a commercially available device for small-diameter needle perforation into cartilage defect beds is a feasible and ready-to-use technique in horses for bone marrow stimulated cartilage repair. Some mechanical limitations of microfracture are overcome using this nanofracturing technique, which makes it possible to have standardized smaller and deeper holes into the subchondral bone.

The use of clinical standard microfracture awls is being debated, based on recent scientific evidence, that suggests that every effort should be made to minimize bone injury from marrow-stimulation procedures through use of narrower awls, small-diameter drills (Cokelaere et al., 2016; Eldracher et al., 2014), subchondral bone needles, or by the development of alternative treatment strategies. Indeed, in a mature rabbit model, cartilage repair was impaired due to compaction and fracturing of bone around microfracture holes. In that study, shearing and crushing of adjacent bone during microfracture caused more osteocyte death than heat by drilling (Chen et al., 2009), while deeper penetration resulted in enhanced repair (Chen et al., 2011). A study in sheep showed that the use of small-diameter awls of 1 mm instead of larger awls decreased the extent of subchondral bone damage and improved articular cartilage repair (Orth et al., 2016). Indeed, *"deeper, smaller, better"* may be the new paradigm when it comes to bone marrow stimulation procedures (Chen et al., 2009; Zedde et al., 2016).

Microfracture has shown variable long-term clinical outcome in humans and horses.

Studies in humans have shown that the repair tissue is a form of fibrocartilage at best and that the clinical outcome deteriorates after 2 years of follow-up, with inconclusive durability and possible treatment failure beyond 5 years (Goyal et al., 2013; Kreuz et al., 2006a; Mithoefer et al., 2005). Subchondral bone alterations such as subchondral cystic lesions or intralesional osteophytes were also seen in up to one-third of patients treated with microfracture (Kreuz et al., 2006b; Mithoefer et al., 2005). Horses, (Frisbie et al., 1999) showed improvement in the quantity of repair tissue and type II collagen content and earlier bone remodelling at 4 and 12 months after microfracture of full-thickness defects compared to control defects. At 12 months however, degeneration of repair tissue was noted in the femoral condyles, probably due to biomechanical instability caused by enzymatic tissue degradation.

Nanofracture of full-thickness chondral lesions in adult sheep resulted in better repair tissue than microfracture at 6 months, with a more satisfactory cartilage architecture restoration and tissue having greater type II collagen content (Zedde et al., 2017). Our study represents the first application of nanofracture for cartilage defect treatment in horses. We found ample defect filling for all nanofracture treated chondral defects; at 7 months, defects were well filled-in with repair tissue that appeared grossly hyaline-like and appeared to have good integration with surrounding tissue. Objective macroscopic scoring yielded ICRS-I scores between 7 and 10 with a median of 9, which is considered 'near normal cartilage'. However, more detailed histopathological assessment revealed no more than intermediate quality of repair, with repair tissue scoring on average only 48% of normal cartilage tissue. Subjectively, histopathological analysis showed better basal integration after nanofracture of chondral defects in the current study, compared to that historically reported for microfracture when the calcified cartilage layer was retained (Frisbie et al., 1999). Microscopic assessment scores were indeed highest for the criterion 'basal integration', but poor for surface architecture and overall matrix staining. While microCT analysis confirmed the observed excellent filling of defects with repair tissue in terms of relative tissue thickness, histologically, tissue appeared to be fibrous or fibrocartilaginous in nature rather than hyaline.

Interestingly, qualitative microCT image analysis also showed altered subchondral bone microarchitecture underlying the defects (compared to remote subchondral bone) at 7 months post-nanofracturing. It is difficult to compare the extent of disturbance of the subchondral and cancellous bone with the nanofracture technique applied in this study to what has been previously reported for microfracture in equine stifle joints (Frisbie et al., 1999). In the current study, outcome was assessed at 7 months instead of 4 or 12 months post-operatively, and in the previous work by Frisbie et al. (1999), microCT was not performed. Importantly, we did not perform a head-to-head comparison of nanofracture vs. microfracture in the current study, nor should any such inferences be made from our data. The microCT images do highlight that even with the small-

diameter needle used for nanofracturing, subchondral bone changes are inevitable, and more importantly that such changes are either underestimated or simply not appreciated at all, respectively, when repair tissue is only evaluated histologically or macroscopically. The fact that these subchondral changes were not associated with clinical signs does not rule out their possible clinical relevance if follow-up had been prolonged to 1-2 years or even longer (Bae et al., 2006; Goyal et al., 2013; Kreuz et al., 2006a; Kreuz et al., 2006b; Mithoefer et al., 2005)

Our results can be summarized as macroscopically adequate looking filling of defects with acceptable basal integration and mild disturbance of subchondral bone architecture, but with poor restoration of the articular cartilage surface. This is largely similar to what has previously been found for microfracture, and does not (yet) convey a distinct benefit of nanofracture over microfracture at this stage.

Several limitations to the work reported here must be noted: First and foremost, this work represents a preliminary investigation of the feasibility of nanofracturing as a clinical procedure for bone marrow stimulated cartilage repair in horses. As the contralateral stifle joints were treated with an experimental biomaterial (the subject of a human pre-clinical investigation), we were unfortunately unable to compare nanofracture to conventional microfracture in this study. The defects in the current study were created in a non-weightbearing region of the joint, meaning that no conclusion can be drawn regarding the extent of repair and/or likely occurrence of subchondral cystic lesions in condylar defects treated with nanofracture (Changoor et al. 2006, Chen et al., 2013). Previous reports showed benefit of removal of the calcified cartilage layer in horses to enhance basal integration of repair tissue after microfracture (McIlwraith and Frisbie, 2010); as the current study was designed to specifically address chondral, not osteochondral, defect repair, defect depth was limited to 1 mm and thus deeper cartilage layers were retained, complicating comparison to previous work on full thickness stifle joint defects (McIlwraith and Frisbie, 2010). As a further limitation, detailed longitudinal monitoring (e.g., motion analysis or radiographic imaging) was not available and neither was outcome assessed at intermediate time points. Subjectively, the one horse that died prematurely due to an unrelated accident, showed more marked subchondral changes than those at 7 months, suggesting that nanofractured defects at 7 months were past the peak for subchondral bone remodeling.

In conclusion, this is the first report on the feasibility and outcome of nanofracturing in the equine stifle joint. Treated lesions were experimentally created chondral defects on the medial trochlea of the femur. Given what is known about topographic variation in osteochondral tissue properties (Changoor et al. 2006, McIlwraith and Frisbie 2010), no extrapolation of results to other joints (Frisbie et al., 1999), other regions within the stifle joint (Changoor et al. 2006, Chen et al., 2013) or to other defect depths

are warranted. Whether nanofracturing results in superior cartilage repair with less subchondral bone disturbance compared to conventional microfracture techniques needs to be addressed in a randomized experimental trial prior to its clinical application in horses.

Manufacturers' addresses
[a] NanoFx®, Nanofracture, Arthrosurface, MA, USA
[b] μ-CT 80, ScancoMedicalAG, Switzerland

References

Bae, D. K., Yoon, K. H., & Song, S. J. (2006). Cartilage healing after microfracture in osteoarthritic knees. *Arthroscopy, Apr;22*(4), 367-374.

Behrens, J. P., & Benthien, P. (2011). The treatment of chondral and osteochondral defects of the knee with autologous matrix-induced chondrogenesis (AMIC): method description and recent developments. *Knee Surg Sports Traumatol Arthrosc, 19*(8), 1316 – 1319. doi: 10.1007/s00167-010-1356-1

Cokelaere, S. M., Malda, J., & van Weeren, P. R. (2016). Cartilage defect repair in horses: current strategies and recent developments in regenerative medicine of the equine joint with emphasis on the surgical approach. *The Veterinary Journal, 2014*(2016), 61-71.

Chen, H., Sun, J., Hoemann, D. D., Lascau-Coman, V., Ouyang, W., McKee, M. D., Shrive, M.S., Buschmann, M. D. (2009). Drilling and microfracture lead to different bone structure and necrosis during bone-marrow stimulation for cartilage repair. *J. Orthop. Res.,* 27, 1432-1438. doi: 10.1002/jor.20905

Chen, H., Chevrier, A., Hoemann, C. D., Sun, J., Ouyang, W., & Buschmann, M. D. (2011). Characterization of subchondral bone repair for marrow-stimulated chondral defects and its relationship to articular cartilage resurfacing. *The American Journal of Sports Medicine, 39*(8), 1731 – 1740. doi: 10.1177/0363546511403282

Chen, H., Chevrier, A., Hoemann, C.D., Sun, J., Lascau-Coman, V., Buschmann, M.D. Bone marrow stimulation induces greater chondrogenesis in trochlear vs condylar cartilage defects in skeletally mature rabbits. Osteoarthritis Cartilage. 2013 Jul;21(7):999-1007. doi: 10.1016/j.joca.2013.04.010.

Eldracher, M., Orth, P., Cucchiarini, M., Pape, D., & Madry, H. (2014). Small subchondral drill holes improve marrow stimulation of articular cartilage defects. *The American Journal of Sports Medicine, 42*(11), 2741–2750. doi: 10.1177/0363546514547029

Frisbie, D. D., Morisset, S., Ho, C. P., Rodkey, M.-G., Steadman, R., & McIlwraith, C. W. (2006). Effects of calcified cartilage on healing of chondral defects treated with microfracture in horses. *The American Journal of Sports Medicine, 34*(11), 1824-1831.

Frisbie, D. D., Trotter, G. W., Powers, B. E., Rodkey, W. G., Steadman, J. R., Howard, R. D., Park, R.D., McIlwraith, C. W. (1999). Arthroscopic subchondral bone plate microfracture technique augments healing of large chondral defects in the radial carpal bone and medial femoral condyle of horses. *Vet Surg., Jul-Aug;28*(4), 242-255.

Gomoll, A. H., Madry, H., Knutsen, G., van Dijk, N., Seil, R., Brittberg, M., & Kon, E. (2010). The subchondral bone in articular cartilage repair: current problems in the surgical management. . *Knee Surg Sports Traumatol Arthrosc, 2010*(18), 434-447.

Gomoll, A. H., & Minas, T. (2014). The quality of healing: Articular cartilage. *Wound Repair and Regeneration, 22*(2014), 2230-2238.

Goyal, D., Keyhani, S., Lee, E. H., & Hui, J. H. (2013). Evidence-based status of microfracture technique: A systematic review of level I and II studies. *Arthroscopy: The Journal of Arthroscopic and Related Surgery, 29*(2013), 1579-1588

Kreuz, P. C., Erggelet, C., Steinwachs, M. R., Krause, S. J., Lahm, A., Niemeyer, P., Ghanem, M., Uhl, M., Südkamp, N. (2006a). Is microfracture of chondral defects in the knee associated with different results in patients aged 40 years or younger? *Arthroscopy, November,22*(11), 1180-1186.

Kreuz, P. C., Steinwachs, M. R., Erggelet, C., Krause, S. J., Konrad, G., Uhl, M., & Südkamp, N. (2006b). Results after microfracture of full-thickness chondral defects in different compartments in the knee. *Ostearthritis and Cartilage, Nov;14*(11), 1119-1125. doi: 10.1016/j.joca.2006.05.003

Lawrence, R. C., Felson, D. T., Helmick, C. G., Lesley, M., Arnold, M. D., Hyon Choi, H., Deyo, R.A., Gabriel, S., Hochberg, M.C., Hunder G.G., Jordan, J.M., Katz, J.N., Kremers, H.M., Wolfe, F. (2008). National Arthritis Data Workgroup. Estimates of the prevalence of arthritis and other rheumatic conditions in the United States. Part II. *Arthritis Rheum, Jan;58*(1), 26-35. doi: 10.1002/art.23176

Madry, H., Orth, P., & Cucchiarini, M. (2016). Role of the subchondral bone in articular cartilage degeneration and repair. *J Am Acad Orthop Surg., Apr;24*(4), e45-46. doi: 10.5435/JAAOS-D-16-00096

Mainil-Varlet, P., Van Damme, B., Nesic, D., Knutsen, G., Kandel, R., Roberts, S. A new histology scoring system for the assessment of the quality of human cartilage repair: ICRS II. Am J Sports Med. 2010 May;38(5):880-90.

Mankin, H. J. (1982). The response of articular cartilage to mechanical injury. *J Bone Joint Surg Am., Marz; 64*(3), 460-466.

Martin, J. A., Brown, T., Heiner, A., & Buckwalter, J. A. (2004). Post-traumatic osteoarthritis: the role of accelerated chondrocyte senescence. *Biorheology, 41*(3-4), 479-491.

McIlwraith, W. C., & Frisbie, D. D. (2010). Microfracture: Basic Science Studies in the Horse. *Cartilage, 1*(2), 87-95. doi: 10.1177/1947603510367427

Minas, T., Gomoll, A. H., Rosenberger, R., Royce, R. O., & Bryant, T. (2009). Increased failure rate of autologous chondrocyte implantation after previous treatment with marrow stimulation techniques. . *Am J Sports Med., May;37*(5), 902-908. doi: 10.1177/0363546508330137

Mithoefer, K., Venugopal, V., & Manaqibwala, M. (2016). Incidence, degree, and clinical effect of subchondral bone overgrowth after microfracture in the knee. *Am J Sports Med., 44*(8), 2057-2063. doi: 10.1177/0363546516645514

Orth, P., J. Duffner, J., D. Zurakowski, D., M. Cucchiarini, M., & H. Madry, H. (2016). Small-diameter awls improve articular cartilage repair after microfracture treatment in a translational animal model. *The American Journal of Sports Medicine, 2016 Jan;44*(1), 209-219. doi: 10.1177/0363546515610507

Squires, G. R., Okouneff, S., Ionescu, M., & Poole, A. R. (2003). The pathobiology of focal lesion development in aging human articular cartilage and molecular matrix changes characteristic of osteoarthritis. *Arthritis Rheum., May;48*(5), 1261-1270.

Steadman, J. R., Rodkey, W. G., & Rodrigo, J. J. (2001). Microfracture: surgical technique and rehabilitation to treat chondral defects. 2001. *Clin Orthop Relat Res., Oct*((391 Suppl)), S362-369.

Zedde, P., Cudoni, S., Giachetti, G., Manunta, M. L., Masala, G., Brunetti, A., & Manunta, A. F. (2016). Subchondral bone remodeling: comparing nanofracture with microfracture. An ovine study. . *Joints, 4*(2), 87 – 93. doi: 10.11138/jts/2016.4.2.087

Zedde, P., Cudoni, S., Manunta, L., Passino, E. S., Masala, G., Brunetti, A., Uboldi, F.M., Manunta, A. F. (2017). Second generation needling techniques for the treatment of chondral defects in animal model. Joints *Joints, 5*(1), 27-33. doi: 10.1055/s-0037-1601412

Chapter III

Long term *in vivo* performance of low temperature 3D printed bioceramics in an equine model

(Submitted)

Long term *in vivo* performance of low temperature 3D printed bioceramics in an equine model

Rafael Vindas Bolaños[1,2,3]*, Miguel Castilho[3,4]*, Janny de Grauw[2], Stefan Cokelaere[2], Saskia Plomp[2,3], Jürgen Groll[5], P. René van Weeren[2,3], Uwe Gbureck[5], Jos Malda[2,3,4]

[1] Cátedra de Cirugía de Especies Mayores, Escuela de Medicina Veterinaria, Universidad Nacional, Costa Rica

[2] Department of Equine Sciences, Faculty of Veterinary Medicine, Utrecht University, the Netherlands

[3] Regenerative Medicine Utrecht, Utrecht, The Netherlands

[4] Department of Orthopaedics, Division of Surgical Specialties, University Medical Center Utrecht, Utrecht University, Utrecht, the Netherlands

[5] Department of Functional Materials in Medicine and Dentistry, University of Würzburg, Würzburg, Germany

*Shared first authorship

Corresponding author: M.DiasCastilho@umcutrecht.nl

Abstract

Bone has great self-healing capacity, but above a certain critical size bone defects will not heal spontaneously, requiring intervention to achieve full healing. Autografts or allografts are the standard of care, but these techniques are associated with strong disadvantages, such as limited availability, donor site morbidity or adverse immunological responses. Synthetic ceramics, usually based on calcium phosphate (CaP) chemistry have been developed as implants and form an alternative. Of these, brushite-base materials are of particular interest, because of their degree of solubility and the related high potential to promote bone regeneration after dissolution. They can be produced tailor-made using modern 3D printing technology. While this type of implant has been widely tested *in vitro*, there is only limited *in vivo* data and less so in a relevant large animal model. In this study, the material properties of a 3D-printed brushite-based scaffold are characterized, after which the material is tested by *in vivo* orthotopic implantation in the equine tuber coxae for 6 months.

The implantation procedure was easy to perform and was well tolerated by the animals who showed no detectable signs of discomfort. *In vitro* tests showed that compressive strength along the vertical axis of densely printed material was around 13 Mpa, which was reduced to approximately 8 MPa in the cylindrical porous implant. *In vivo,* approximately 40% of the visible volume of the implants was degraded after 6 months and replaced by bone, showing the capacity to stimulate new bone formation. Histologically, ample bone ingrowth was observed. In contrast, empty defects were filled with fibrous tissue only, confirming the material's osteoconductive capacity.

It is concluded that this study provides proof that the 3D-printed brushite implants were able to promote new bone growth after 6 months implantation in a large animal model and that the new equine tuber coxae bone model that was used is a promising tool for bone regeneration studies.

Introduction

Bone is a complex dynamic tissue that provides biomechanical stability to the body and plays an important role in hematopoietic cell production and calcium homeostasis (Reichert et al., 2012). Despite its self-healing capabilities, bone defects with geometries larger than their critical healing size (≈10 mm), do not stand a chance to heal at all. In such situations, there is a need for external intervention to support bone repair, *e.g.*, by grafting with biomaterials or harvested bone (Olszta et al., 2007). After decades of intensive bone research, autografting procedures remain the gold standard in orthopaedic surgery. Bone autografts can guide the in-growth of osteoblasts and induce the differentiation of undifferentiated bone cells into the osteogenic lineage (Urist, 1965). Unfortunately, autografting is associated with donor-site morbidity and limited availability. As an alternative, a broad spectrum of bone graft biomaterials has been investigated (LeGeros, 2002; Szpalski and Gunzburg, 2002).

Amongst different types of candidate biomaterials, synthetic ceramics, usually based on calcium phosphate (CaP) chemistry, are of particular interest due to their similar composition to bone mineral and resorption potential. There are several known CaPs, with CaPs phases depending on their calcium-to-phosphate (Ca/P) molar ratio (Rey, 1998). The most common are hydroxyapatite (HA), tricalcium phosphate (TCP) in two crystalline forms, β-tricalcium phosphate (β-TCP) and α-tricalcium phosphate (α-TCP), and dicalcium phosphate dihydrate (or brushite). The performance of these CaPs is greatly dependent on specific material properties. It is known that phase composition, crystal size and porosity, are key factors that determine the speed of resorption and mechanical stability of these materials, and their subsequent success or failure in promoting bone regeneration *in vivo* (Yuan et al., 2010). While sintered hydroxyapatite is practically non-degradable *in vivo*, TCP or brushite are more soluble phases with higher potential to promote bone regeneration after dissolution (Cameron et al., 1977; Ferraro, 1979). These unique characteristics have drawn increasing attention to brushite-based materials (Castilho et al., 2014a; Habibovic et al., 2008).

In case of large and complex bone defects, the capacity to mould the biomaterial according to the shape needed, together with the desired rate of biodegradation, is a determining factor. Such bone defects can hardly be treated with pasty bone materials, but require the implantation of preformed bone scaffolds, often with complex geometry (Klammert et al., 2010; Probst et al., 2010). Current CaP bone substitutes are mostly available in injectable pastes or standard shapes that do not fit patient-specific defect requirements. Recently, we have shown that three-dimensional (3D) powder printing (3DPP) is a promising manufacturing technique for the fabrication of individual ceramic-based bone grafts (Castilho et al., 2014b; Gbureck et al., 2007; Vorndran et al., 2008). In previous works, we have used a low temperature processing regime to produce

personalised ceramic matrices composed of TCP and/or brushite ceramic phases. (Castilho et al., 2014b; Gbureck et al., 2007). The suitability of these materials for bone replacement has been confirmed by few *in vivo* implantation experiments. Habibovic *et al.* have tested 3D printed brushite-based scaffolds on the decorticated lumbar transverse processes of goats for 3 months (Habibovic et al., 2008), while Tamini *et al.* have tested implants with a similar composition in a calvarial bone surface of rabbits (Tamini et al., 2013). Although promising, translational animal studies of biomaterial performance for intended human application should ideally be performed in large animal species, as small laboratory animals like rabbits possess superior regenerative ability compared to humans and larger animals (Muschler et al., 2010). Also, *in vivo* studies should be of sufficient duration to allow assessment of long-term effects and durability (Frisbie et al., 2010).

In fact, there is still no consensus on the ideal *in vivo* model to study the osteopromotive potential of biomaterials. In orthopaedic regenerative medicine however, evaluation of novel interventions in large animal models is a pre-requisite to human clinical application, while such studies constitute end-stage testing for veterinary application in the animal species involved (Carlton Gyles, 2016). Like humans and unlike other perhaps more common animal model species like goats or sheep, horses participate in athletic competitions, where osteochondral injuries cause great economic losses as well as animal welfare concerns (Bigham-Sadegh and Oryan, 2015; Williams et al., 2001; Wright, 2017). Studies addressing bone regenerative capacity are, therefore, also of potential interest for equine healthcare and welfare.

The aim of this study was to characterize the material properties of 3D printed brushite-based scaffolds, as well as to evaluate their *in vivo* orthotopic bone regenerative potential in a long-term large animal study. The structural and mechanical properties of the printed materials was carefully investigated prior to implantation. For the *in vivo* evaluation, experimentally created defects in the equine tuber coxae bone were used as a new model for large animal pre-clinical bone regeneration studies. Implants were inserted into experimentally created defects in both tuber coxae of n = 8 horses and were retrieved 6 months after implantation; implant degradation and bone regeneration was evaluated by micro-computed tomography (uCT) and histological analysis.

Materials and Methods

Implant preparation and material characterization

Ceramic implants (cylindrical diameter = 11 mm, depth = 10 mm with open channel

diameter 3 mm, Fig. 1) and dense samples for structural and mechanical testing were printed from α/ß-tricalcium phosphate (α/ß-Ca$_3$PO$_4$) powder and 20v/v% phosphoric acid binder (Merck, Darmstadt, Germany) on a Z-Corp 310 (Z-Corporation, Burlington, USA) powder printer. Detailed description of powder synthesis and printing process parameters is provided elsewhere (Gbureck et al., 2007). After removal from the powder bed, the printed constructs were cleaned with compressed air and post-hardened by immersion in the binding liquid for 2 x 30 s to increase the degree of cement setting. Micro-porosity and pore-size distribution characteristics of the 3D printed constructs were measured with Hg porosimetry (PASCAL 140/440, Porotec GmbH, Hofheim, Germany). The micro-structure was visualized using scanning electron microscopy (SEM) Phenom Pro (Phenom-World, the Netherlands), at an acceleration voltage of 5-10kV. Prior to scanning, specimens were sputter-coated with a 5nm layer of gold.
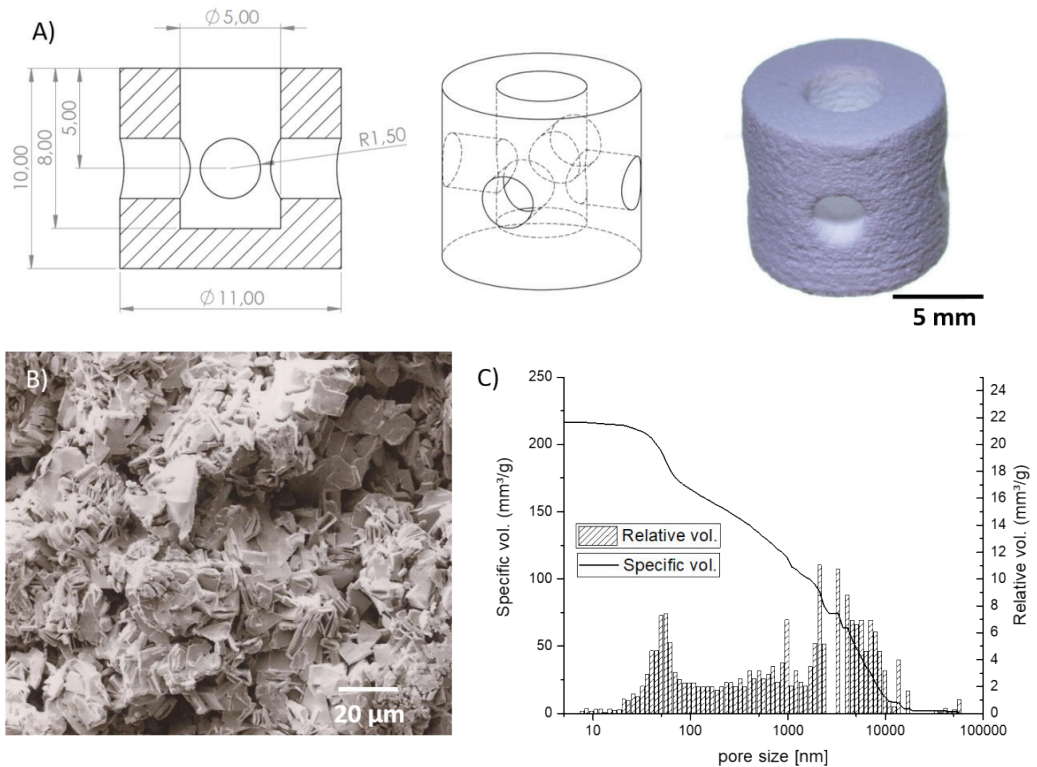

Fig. 1 Implant design and structural characterization. A) CAD design and photograph of the printed implant. B) Implant micro-structure and C) pore size distribution prior to implantation.

Mechanical characterization

Mechanical properties were evaluated under two stress-loading conditions by performing uniaxial compression and diametral compression tests. Dense specimens of appropriate geometry and printed according to the three directions of the printing process, x, y, and z, were used. All tests were performed with a universal testing machine Zwick/Roell Z010 (Zwick GmbH & Co. KG, Ulm, Germany) equipped with a 5kN load cell, according to a protocol described elsewhere (Castilho et al., 2015). Briefly, for uniaxial compression, dense cylindrical samples with height = 12 mm and diameter = 6 mm were tested at a rate of 1 mm/min. Compressive strength (CS) was defined as the ratio between the force at failure and the specimen's unloaded cross-sectional area. For diametral compression, disc-shaped specimens with a thickness = 4 mm and diameter = 8 mm were tested at 0.5 mm/min. The diametral tensile strength (DTS) was calculated by,

$$DTS\ (MPa) = 2F_{max}/(\pi dt) \qquad\qquad (1)$$

where F_{max} is the failure load, d and t are the sample diameter and thickness, respectively. Implant compressive strength was only determined under axial compression and calculated on the basis of cross-sectional area of the bottom of the implant without taking care of the central or horizontal pores.

Experimental design

The protocols and study described were approved by the ethical and animal welfare committee of the National University of Costa Rica. Eight healthy Criollo breed horses (5 mares, 3 geldings; mean age 6 years, range 4 – 9 years; mean body weight 288 kg, range 275 – 350 kg) were used. All horses were free of lameness and did not have clinical or radiographic evidence of acute or chronic injuries. They were housed in individual box stalls and were fed a standard maintenance ration of 0.5 kg concentrate daily, with hay ad libitum and free access to water.

Surgical procedure

After IV premedication with xylazine (1.1 mg/kg; Pisa, Mexico), a 12G jugular venous catheter was placed and phenylbutazone (2.2 mg/kg; Holliday, Argentina) administered IV for peri-operative analgesia. Anaesthesia was induced with midazolam (0.05 mg/kg; Holliday, Argentina) IV and ketamine (2.2 mg/kg; Holliday, Argentina) IV and the horse was positioned in dorsal recumbence. General anesthesia was maintained with isoflurane in oxygen.

For the tuber coxae model, a vertical incision through the skin and subcutaneous tissue of approximately 10 cm length was made by a board-certified equine surgeon (SC) over the tuber coxae to expose the underlying bone (Fig. 2). Once the bony surface of the tuber coxae was exposed, one cylindrical defect (11 mm diameter, 10 mm depth) was created perpendicular to the bony surface using a stop-controlled power-driven drill. Defects were flushed with saline (Baxter,USA) before press-fit implantation of the scaffolds (n = 8). Control defects (n = 8) of the same size and depth were created in a similar fashion in the contralateral tuber coxae and were left empty. Finally, the skin was closed using nylon sutures (Ethilon 0). These surgeries were performed during the same anesthetic episode as was used for surgical creation of defects in both stifle joints for an unrelated cartilage repair study that has been reported elsewhere (Vindas Bolaños et al., 2017).
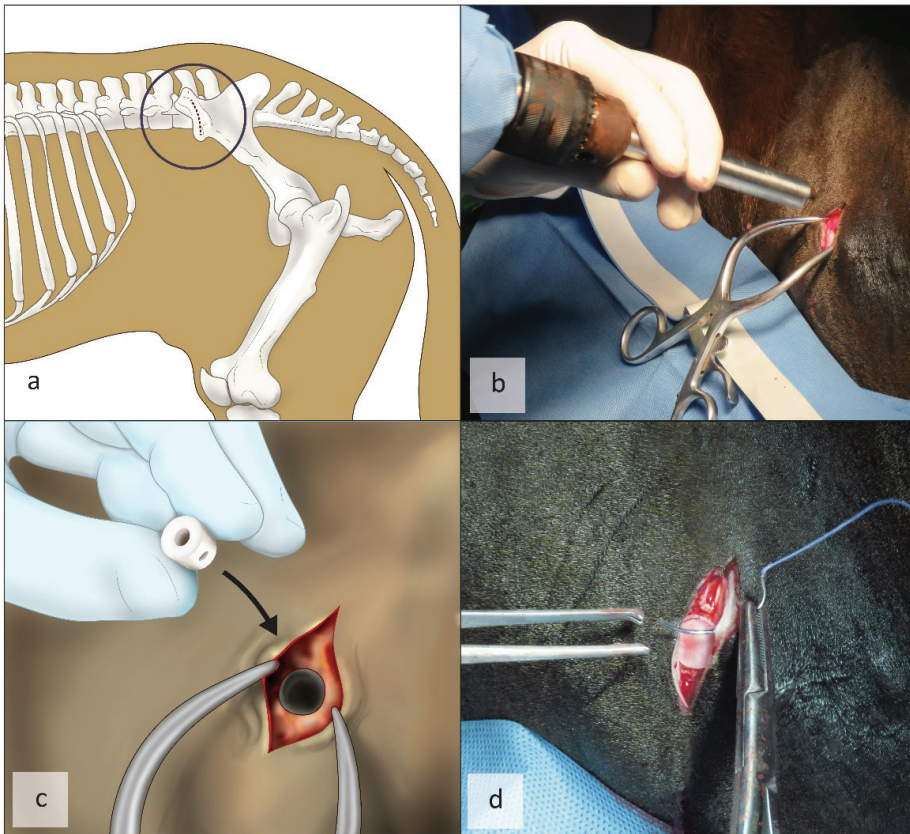

Fig. 2. Surgical implantation of 3D printed ceramic implants in the tuber coxae model. A) Position of the tuber coxae of the ileum wing in the horse, B) The defect was made using a power drill, C), Schematic drawing of placement of the scaffold into the defect D) Wound closure.

Post-operative care and rehabilitation

Post-operatively, horses received antibiotics for 8 days (procaine penicillin 15,000 IU/kg intramuscularly SID, Alfasan, the Netherlands, and IV gentamicin 6.6 mg/kg BID, Alfasan, the Netherlands), and non-steroidal anti-inflammatory drugs (phenylbutazone (2.2 mg/kg, Lisan, Costa Rica, orally BID)) during the first 14 days. As the horses were enrolled in a parallel cartilage repair study, from week 3, horses were subjected to an incremental exercise program as detailed elsewhere (Vindas Bolaños et al., 2017).

Monitoring during experimental period

The animals were clinically monitored on a daily basis for rectal temperature, heart rate and respiratory rate, as well as stance, demeanor and general appearance; hematology and serum biochemistry were checked 1, 2, 4 and 6 months post-operatively.

Euthanasia and sample harvesting

All horses were euthanized at 6 months post-operatively using a combination of xylazine (1 mg/kg IV, Pisa) and ketamine-midazolam (3 mg/kg and 0.05 mg/kg IV, Holliday, Argentina) to induce profound anesthesia. After this, a bolus of oversaturated magnesium sulphate (200 g/L) and chloral hydrate (200 g/L) solution was administered to effect and death confirmed by cessation of breathing, ictus and corneal reflex.

After opening the skin and subcutaneous tissue over the tuber coxae, macroscopic pictures were taken and blocks of tissue containing the defects were excised. A piece containing the treated defect was fixed in 10% formalin for micro-CT analysis, X-ray diffraction analysis and histological evaluation after embedding in polymethylmethacrylate (MMA).

Micro-computed tomography and X-ray diffraction

To visualize the calcified tissue at the defect site, the formalin-fixed tissue underwent micro-CT analysis (Quantum FX-Perkin Elmer). The newly fabricated implants were also analysed with micro-CT. The scan parameters were 90 kV tube voltage, 180 mA tube current, 60 µm resolution and 3 min scan time. Reconstruction of 2D projections was automatically performed using the inbuilt software of the micro-CT while pre-processing (image calibration and noise reduction) of the images was undertaken with Analyze-11.0 software. Implant degradation was quantified by comparing the reconstructed volumes of the implants before and after 6 months of implantation.

Before and 6 months after the implantation, the diffraction patterns of the ceramic implants were analysed using a powder diffractometer (D5005, Siemens, Karlsruhe, Germany) with monochromatic Cu K_1 radiation at an acceleration voltage of 40kV. Data were collected in a 2Theta range of 20-40° with a step size of 0.02°. Diffraction patterns were qualitatively analysed using the following reference patterns from the powder diffraction database: brushite (PDF-ref. 09-0077), monetite (PDF-No. 09-0080), α-TCP (PDF-ref 09-0348), ß-tricalcium phosphate (PDF-ref. 09-0169) and hydroxyapatite (HA) (PDF-ref. 09-0432).

Histological processing

The tuber coxae bone samples were fixed in Neutral Buffered Formalin at 10% and dehydrated through an ethanol series, cleared in xylene and embedded in polymethylmethacrylate (MMA). Embedded samples were cut with a Leica 4 SP1600 Saw Microtome system (Leica, Germany) to yield 20-30μm sections. The sections were stained with methylene blue and basic fuchsin for analysis of tissue-scaffold integration and bone growth. Samples were also stained with picrosirius red and analyzed with polarized light for collagen analysis. Stained sections were imaged using an Olympus BX51 light microscope.

Statistical analysis

A one-way ANOVA post hoc test (Tukey's test) was used to compare the means of the different groups. Differences were considered significant at a probability error (p) of $p < 0.05$.

Results

3D-printed material characterization

Implants were successfully 3D-printed based on the hydraulic setting reaction of a reactive α/ß-TCP powder with a phosphoric acid binder. This reaction led to the precipitation of brushite and, thus, to the formation of a stable 3D structure (Fig. 1A). No significant dimensional changes were observed between the as-printed constructs and the computer designed geometry. Evaluation of the implants' dimensions revealed a deviation of less than ±0.1 mm.

While analyzing the printed constructs' microstructure, we observed that all specimens had a porous microstructure composed of random oriented brushite crystals (Fig. 1B). The total micro-porosity of all specimens was in the range of 28-30 vol%, with a

bimodal pore size distribution and with the main pore size fraction in the range of 90 nm – 10 µm (Fig. 1C).

The results from compression strength testing revealed no significant differences between the three different directions, with final strengths of approximately 13 MPa (Fig. 3). In contrast, tensile strength was significantly higher for the samples printed along the z-direction, while compared to x- and y-direction, with strengths reaching approximately 2.2 MPa (Fig 3). As expected, printed constructs were stronger under compression and weaker under tension, as in any ceramic material. Based on both compression and tensile strength, macro-porous implants for subsequent *in vivo* tests were printed along the z-direction and tested under compressive loading. Stress-strain behavior of macro-porous implants was similar to the dense specimens. However, a significant decrease in compression strength, from approximately 13 MPa to 8.2±2.1 MPa, was observed.
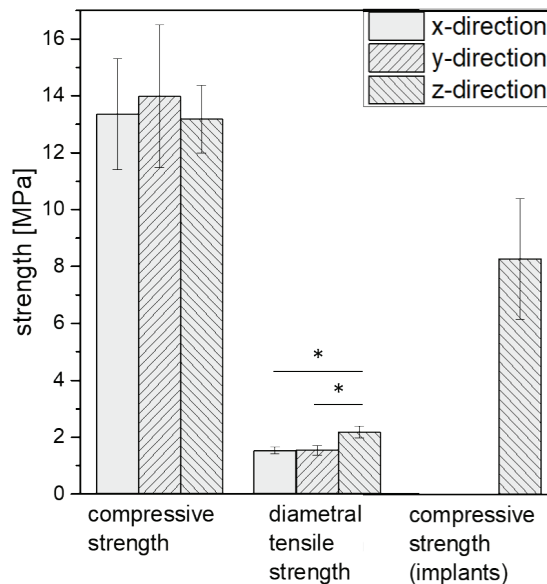

Fig. 3 Mechanical properties of densely printed brushite material (tri-axial compressive strength and diametral tensile strength) and porous implants (uniaxial compressive strength only) prior to implantation. Compressive strength (CS) and diametral tensile strength (DTS) were evaluated in three different directions of the printing process.

Surgery, post-operative care and monitoring

The surgical procedure proved straightforward, with the approach providing ample access to the proposed surgical site (Fig. 2). Defect creation was likewise easily performed, as was press-fit implantation of scaffolds. Post-operatively, 7 out of 8 horses recovered uneventfully and had uncomplicated healing of the surgical incisions. One horse showed signs of a local surgical site infection (tenderness, swelling, drainage) three days after surgery, which was treated with antibiotics and cleaning; signs resolved within the first week post-operatively. In all other horses, no local tissue reaction or signs of infection (heat, pain, swelling) were seen. In all horses, routine blood parameters remained within normal physiologic limits throughout the experiment.

MicroCT and phase composition analysis

MicroCT analysis was performed on the tuber coxae specimens with and without implants (Fig. 4). Six months after implantation, we observed significantly higher new bone deposition in all the defects containing the 3D-printed implants, compared to the empty defects (Fig. 4A, 4B). Bone ingrowth was found throughout the defect, predominantly inside the implant macro-pores and in contact with the printed material (indicated by the white arrows in Fig. 4B). In contrast, and as expected, the empty defects were not filled with new bone after 6 months. As it was possible to distinguish between the implant geometry and newly formed bone, the implant resorption was quantified by comparing the implants' volume before and after the *in vivo* period. Approximately 40% of the visible volume of the implants was degraded at 6 months, suggesting that the brushite implants were able to stimulate new bone formation.

Moreover, XRD patterns of implants before and after implantation displayed different CaP phases (Fig. 5). Before implantation, the printed implants were predominantly composed of brushite and unreacted TCP phases. After implantation, they were composed of predominantly hydroxyapatite and TCP, suggesting a re-precipitation of brushite into less soluble CaP phases.

A) Empty defect
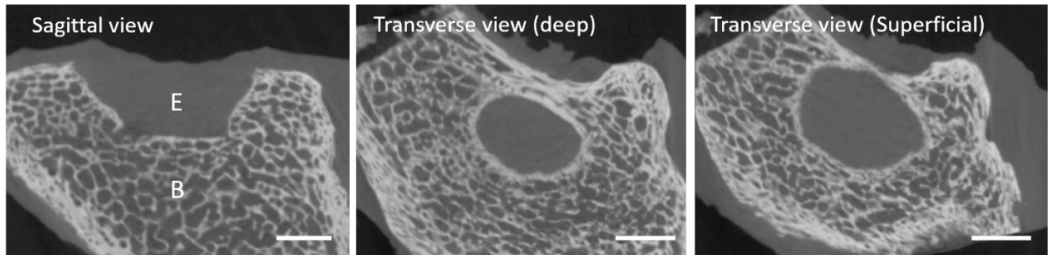
B) Implant after 6months
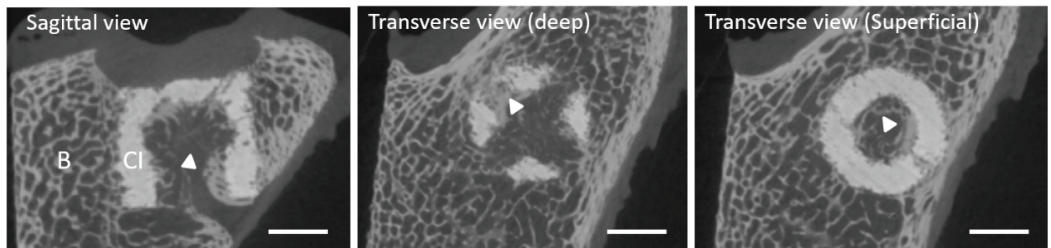
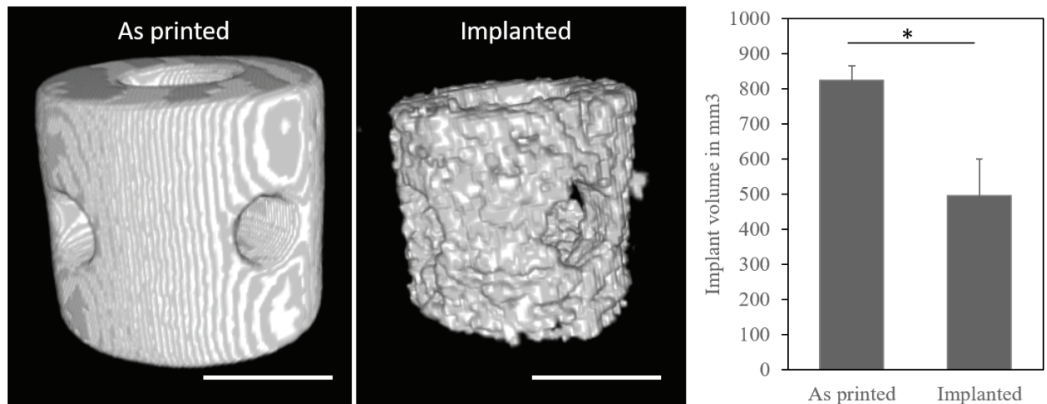## C) Quantification of implant volume after 6months

Fig. 4 μCT analysis of 3D printed implants after 6 months of implantation. Representative μCT images of A) Untreated defect showing empty space (E) and native bone at base of defect (B). B) Treated defect after 6 months with native surrounding bone (B) and remains of ceramic implant (CI). C) Quantification of implant volume after printing and after implantation using 3D reconstructed volumes from μ-CT images. Arrow indicates region where new bone was formed. Scale bars are 5 mm. * indicates a significant difference, p = 0.05
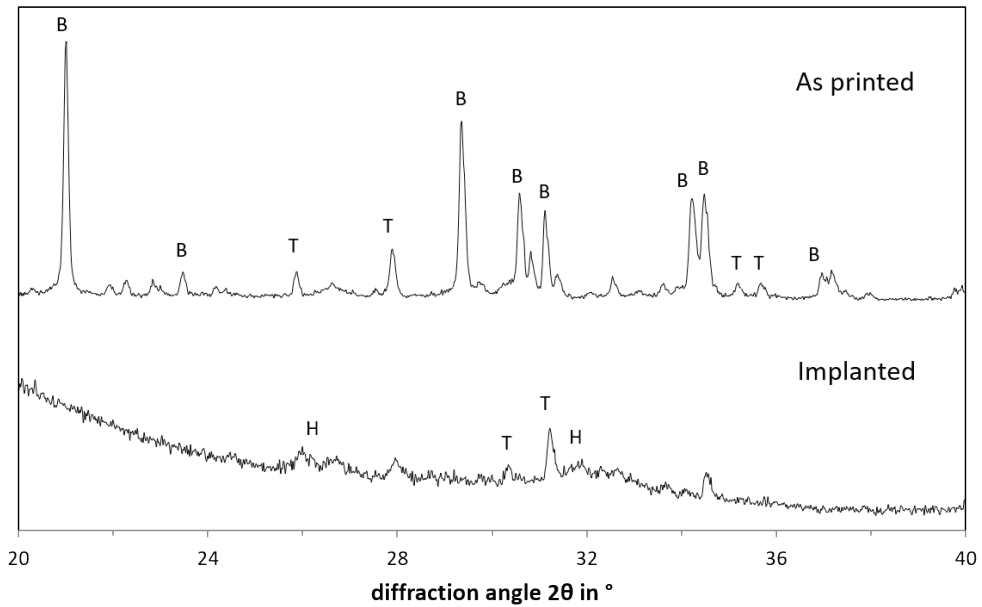
Fig. 5 X-ray diffraction analysis of 3D printed ceramic implants before (as printed) and after explantation after a 6-month *in vivo* period. Most prominent peaks of Brushite (B), b-Tricalcium phosphate (T) and hydroxyapatite (H) are labelled.
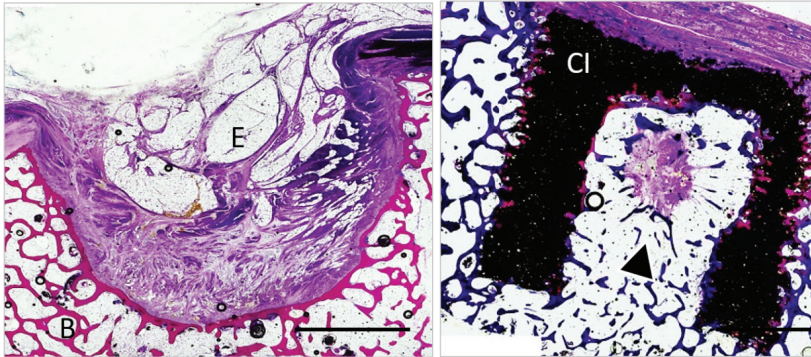
Histological analysis

Histological analysis on the MMA-embedded sections confirmed the micro-CT findings (Fig. 6). Methylene blue and basic fuchsin staining showed new bone in-growth inside the implants macro-pores, together with a tight bond between the newly formed bone and the host bone. In contrast, little new bone formation was detected in the empty defects, which were filled with fibrotic scar tissue. Picrosirius red staining confirmed the presence of collagen inside the macro-pores of the implants and at the implant surface cavities. Only minor traces of mineralized tissue were observed in the empty defects.

A) Macroscopic images
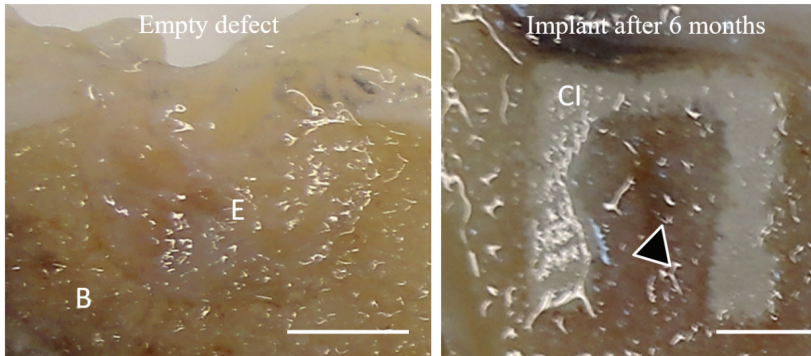
B) MF staining

C) Picrosirius red staining
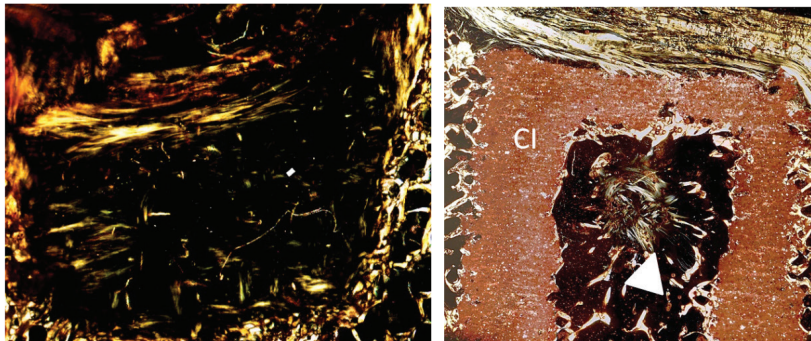
Fig. 6 Histologic analysis of 3D printed implants after 6 months of implantation. Representative images of A) post-mortem processed samples; B) Methylene blue and basic fuchsin (MF) stained samples; and C) picrosirius red stained samples under polarized light. CI – Ceramic implant, B- Bone, E- Empty defect. Arrows indicate some of the regions where new bone was formed. Scale bars are 5mm.

Discussion

As physical properties and 3D structure of biomaterial constructs are known to be critical to their osteopromoting regenerative performance (Bose et al., 2012; Yuan et al., 2010), implant architecture and material characteristics were studied in detail in vitro prior to their in vivo application. The cement system used was formed mostly by a brushite phase obtained by the reaction of α/ß- $Ca_3(PO_4)_2$ (tricalcium phosphate) with a phosphoric acid solution according to:

α/ß-$Ca_3(PO_4)_2$ + H_3PO_4 + $6H_2O$ → $3CaHPO_4 \cdot 2H_2O$
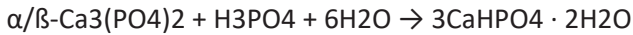
The high reactivity of the powder-binder system allowed the production of implants with a high accuracy and minimal dimensional variations from the computer designed geometry. This findings confirm the potential of this 3D printing methodology for individual implant fabrication, and is in line with our previous results (Castilho et al., 2014a; Habibovic et al., 2008; Klammert et al., 2010). Moreover, by using this printing method, we were able to combine a highly soluble ceramic phase with a porous microstructure of around 30%. These two material properties could explain the observed in vivo performance and, in part, explain its osteoconductive and, eventual, osteoinductive properties. These findings also align well with the previous literature, although some open questions remain to be answered: e.g. which is the exact material property that influences the osteogenic process? And which cell signaling pathways are activated by the brushite resorption and consequent release of Ca ions?

Also, it is important to mention that after 6 months of implantation both hydroxyapatite and TCP phases were detected. Such CaP phases are less soluble under physiological conditions, and tend to occur due to re-precipitation of brushite. This may slow down the overall implant resorption speed and thus raise some concerns regarding an eventual complete resorption of the brushite implants. As an alternative to the CaP based materials, magnesium phosphates have captured increasing attention, since Mg^{2+} ions can suppress the formation of an insoluble hydroxyapatite phase (Kanter et al., 2018).

The influence of the printing direction on the printed constructs' mechanical properties was carefully characterized. Interestingly, significant improvements were only evidenced under diametral tensile strength for the specimens printed along the z-direction. This might be explained by small micro-porosity differences between the different axes, as we have previously demonstrated (Castilho et al., 2015; Christ et al., 2015). Importantly, the final mechanical properties of the implants were in accordance with the strength of the native cancellous bone, 4- 12 MPa (Karageorgiou and Kaplan, 2005).

It is known that any biomaterial approach aimed at human application needs to not only undergo thorough biocompatibility and toxicity screening, as well as material

characterization in vitro, but ultimately will also need to show proof of in vivo bone regenerative capacity in animal model studies. To the best of our knowledge, no formal consensus has been reached on the ideal animal model to be used for translational studies of biomaterial osteopromotive performance. It has, however, become clear that large animal models are preferable to small laboratory species, as the former models are more comparable to humans in terms of intrinsic regenerative capacity (Muschler et al., 2010). While goats and sheep are commonly used animal model species for human orthopaedic interventions, partly owing to their ease of handling and economic husbandry, bone xenograft compatibility in humans has been shown to be superior for equine bone compared to porcine or ovine bone (Tetè et al., 2014) and equine bone performed better than human, bovine or even ovine bone in a sheep subchondral bone model (Waselau et al., 2005). Importantly, from an animal ethics perspective, sheep nor goats themselves constitute veterinary target species for bone regeneration studies, while horses perform athletic activities and represent substantial economic and/or emotional value; restoration of osteochondral injury and large bone defects is therefore of great relevance to equine veterinary practice and to equine welfare.

In horses, a bone regeneration and osteoinductivity study has previously been performed in equine third metacarpal bone defects, showing favorable results (Tsuzuki et al., 2012). However, this defect location is challenging both in terms of surgical approach and in terms of potential for significant discomfort to the horse. There is a long history of osteochondral defect studies for cartilage repair in horses (McIlwraith and Frisbie, 2010). Prior to any application of a biomaterial as a bone anchor in the biomechanically challenging environment of the equine joint, the proposed biomaterial should show promising bone regenerative potential in an orthotopic location; if it proves unsuccessful here, it should not be tried in a load-bearing situation, while if promising, further testing in such an application could be warranted. As a further advantage of testing of bone regeneration is studied in an orthotopic site such as the tuber coxae, is the possibility of concurrent investigation of novel therapies at different sites. This was done in the present study with a concurrent study into the effect of osteochondral implants in the stifle joint (Vindas Bolaños et al., 2017). This simultaneous study was possible thanks to the very limited (if any) impact of the orthotopic bone implant on the animal. In this way better use is made of the animals involved in the study, contributing to the refinement and reduction of animal experimentation (Guhad, 2005).

The equine tuber coxae to date has not formally been used as a site for bone regeneration studies, but it has several distinct advantages: It is easily accessible, is representative of long compact bones, and does not affect locomotion of the animals during recovery from anesthesia. In fact, we have refined the technique in ponies and have found that bone defects at this site can be created in the standing sedated animal, using systemic opioids and local anesthetic injections, with the animals showing both great tolerance of the procedure during surgery and an uncomplicated recovery

thereafter. The equine tuber coxae bone was also recently used as a donor site for an equine bone autograft study for mandibular symphysis repair in a horse (Ogden et al., 2018) without significant donor site morbidity or problems with incisional healing. As an anatomical site, the tuber coxae bone is easily accessible, shows little overlying tissue movement during ambulation, and it is remote from the ground, all of which might favor uncomplicated wound healing.

Conclusion

In conclusion, our results provided clinical proof that the 3D-printed brushite implants were able to promote new bone growth after 6 months implantation in a large animal model. Also, we demonstrated that the new equine tuber coxae bone model is a promising tool for bone regeneration studies.

Acknowledgements

References

Bigham-Sadegh, A., Oryan, A., 2015. Selection of animal models for pre-clinical strategies in evaluating the fracture healing, bone graft substitutes and bone tissue regeneration and engineering. Connect Tissue Res 56, 175-194.

Bose, S., Roy, M., Bandyopadhyay, A., 2012. Recent advances in bone tissue engineering scaffolds Trends Biotechnol 30, 546-554.

Cameron, H.U., MacNeb, I., Pilliar, R.M., 1977. Evaluation of a bidegradable ceramic. J Biomed Mater Res 11, 179-186.

Castilho, M., Moseke, C., Ewald, A., Gbureck, U., Groll, J., Pires, I., Teßmar, J., Vorndran, E., 2014b. Direct 3D powder printing of biphasic calcium phosphate scaffolds for substitution of complex bone defects. Biofabrication 6, 1-12.

Castilho, M., Rodrigues, J., Pires, I., Gouveia, B., Pereira, M., Moseke, C., Groll, J., Ewald, A., Vorndran, E., 2015. Fabrication of individual alginate-TCP scaffolds for bone tissue engineering by means of powder printing Biofabrication 7, 1-19.

Castilho, M., Vorndran, E., Gbureck, U., Fernandes, P., Pires, I., Gouveia, B., ArmésH., Pires, E., Rodrigues, J., 2014a. Application of a 3D printed customized implant for canine cruciate ligament treatment by tibial tuberosity advancement. Biofabrication 6.

Christ, S., Schnabel, M., Vorndran, E., Groll, J., Gbureck, U., 2015. Fiber reinforcement during 3D printing. Materials Letters 139, 165-168.

Ferraro, J.W., 1979. Experimental evaluation of ceramic calcium-phosphate as a substitute for bone grafts. Plast Reconstruct Surg 63, 634-640.

Frisbie, D.D., Mc Ilwraith, C.W., Arthur, R.M., Blea, J., Baker, V.A., Billinghurst, R.C., 2010. Serum biomarker levels for musculoskeletal disease in two- and three-year-old racing Thoroughbred horses: A prospective study of 130 horses. Equine vet. J. 42, 643-651.

Gbureck, U., Hozel, T., Klammert, U., Wurzler, K., Muller, F.A., Barralet, J.E., 2007. Resorbable dicalcium phosphate bone substitutes prepared by 3D powder printing. Advanced Functional Materials 17, 3940-3945.

Guhad, F., 2005. Introduction to the 3Rs (Refinement, Reduction and Replacement). Journal of the American Association for Laboratory Animal Science 44, 58-59.

Gyles, C., 2016. One Medicine, One Health, One World. Can Vet J. 57, 345–346.

Habibovic, P., Gbureck, U., Doillon, C.J., Bassett, D.C., van Blitterswijk, C.A., Barralet, J.E., 2008. Osteoconduction and osteoinduction of low-temperature 3D printed bioceramic implants. Biomaterials 29, 944-953.

Kanter, B., Vikman, A., Brückner, T., Schamel, M., Gbureck, U., Ignatius, A., 2018. Bone regeneration capacity of magnesium phosphate cements in a large animal model. Acta Biomater 69, 352-361.

Karageorgiou, V., Kaplan, D., 2005. Porosity of 3D biomaterial scaffolds and osteogenesis. Biomaterials 26, 5474 – 5491.

Klammert, U., Gbureck, U., Vorndran, E., Rödiger, J., Meyer-Marcotty, P., Kübler, A.C., 2010. 3D powder printed calcium phosphate implants for reconstruction of cranial and maxillofacial defects. J Craniomaxillofac Surg 38, 565-570.

LeGeros, R.Z., 2002. Properties of Osteoconductive Biomaterials: Calcium Phosphates. Clinical Orthopaedics and Related Research, 81-98.

Mcllwraith, W.C., Frisbie, D.D., 2010. Microfracture: Basic Science Studies in the Horse. Cartilage 1, 87-95.

Muschler, G.F., Raut, V.P., Patterson, T.E., Wenke, J.C., Hollinger, J.O., 2010. The Design and Use of Animal Models for Translational Research in Bone Tissue Engineering and Regenerative Medicine. Tissue Engineering: Part B. 16, 123-145.

Ogden, N.K.E., Jukic, C.C., Zedler, S.T., 2018. Management of an extensive equine juvenile ossifying fibroma by rostral mandibulectomy and reconstruction of the mandibular symphysis using String of Pearls plates with cortical and cancellous bone autografts. Vet Surg 28, 1-7.

Olszta, M.J., Cheng, X., Jee, S.S., Kumar, R., Kim, Y., Kaufman, M., Douglas, E., Gower, L., 2007. Bone structure and formation: a new perspective. Materials Science and Engineering R58, 77-116.

Probst, F.A., Hutmacher, D.W., Müller, D.F., Machens, H.G., Schantz, J.T., 2010. Calvarial reconstruction by customized bioactive implant Handchir Mikrochir. Plast Chir 42, 369-373.

Reichert, J.C., Cipitria, A., Epari, D.R., Saifzadeh, S., Krishnakanth, P., Berner, A., Woodruff, M.A., Schell, H., Mehta, M., Schuetz, M.A., Duda, G.N., Hutmacher, D.W., 2012. A Tissue Engineering Solution for Segmental Defect Regeneration in Load-Bearing Long Bones. Sci Transl Med 4, 141-193.

Rey, C., 1998. Calcium Phosphates for Medical Applications. In: Zahid Amjad, editor. Calcium Phosphates in Biological and Industrial Systems. Boston, USA: Kluwer Academic Publishers, 217-251.

Szpalski, M., Gunzburg, R., 2002. Applications of calcium phosphate-based cancellous bone void fillers in trauma surgery. Orthopedics. 25, 601-609.

Tamini, F., Corneau, P., Nihouannen, D., Zhang, Y., Bassett, D., Khalili, S., Gbureck, U., Tran, S., Komarova, S., Barralet, J., 2013. Perfluorodecalin and bone regeneration. Eur. Cells Mater 25, 22–36.

Tetè, S., Zizzari, V.L., Vinci, R., Zara, S., Di Tore, U., Manica, M., Cataldi, A., Mortellaro, C., Piattelli, A., Gherlone, E., 2014. Equine and porcine bone substitutes in maxillary sinus augmentation: a histological and immunohistochemical analysis of VEGF expression. J Craniofac Surg 25, 835-839.

Tsuzuki, N., Otsuka, K., Seo, J., Yamada, K., Haneda, S., Furuoka, H., Tabata, Y., Sasaki, N., 2012. In vivo osteoinductivity of gelatin β-tri-calcium phosphate sponge and bone morphogenetic protein-2 on an equine third metacarpal bone defect. Research in Veterinary Science 93, 1021-1025.

Urist, M.R., 1965. Bone: Formation by autoinduction. Science 150, 893–899.

Vindas Bolaños, R.A., Cokelaere, S.M., Estrada McDermott, J.M., Benders, K., E.M., Gbureck, U., Plomp, S.G.M., Weinans, H., Groll, J., van Weeren, P.R., Malda, J., 2017. The use of cartilage decellularized matrix scaffold for the repair of osteochondral defects: the importance of long-term studies in large animal model. Ostearthritis and Cartilage 25, 413-420.

Vorndran, E., Klarner, M., Klammert, U., Grover, L.M., Patel, S., Barralet, J.E., 2008. 3D Powder Printing of beta-Tricalcium Phosphate Ceramics Using Different Strategies. Advanced Engineering Materials. 10, B67-B71.

Waselau, A.C., Nadler, D., Müller, J.M., Zlinszky, K., Hilbe, M., Auer, J.A., von Rechenberg, B., 2005. The effect of cartilage and bone density of mushroom-shaped, photooxidized, osteochondral transplants: an experimental study on graft performance in sheep using transplants originating from different species. BMC Musculoskelet Disord 6, 1-12.

Williams, R.B., Harkins, L.S., Hammond, C.J., Wood, J.L., 2001. Racehorse injuries, clinical problems and fatalities recorded on British racecourses from flat racing and National Hunt racing during 1996, 1997 and 1998. Equine Vet J. 33, 478-486.

Wright, I., M., 2017. Racecourse fracture management. Part 1: Incidence and principles. Equine Veterinary Education 29, 391-400.

Yuan, H., Fernandes, H., Habibovic, P., de Boer, J., Barradas, A.M., de Ruiter, A., Walsh, W.R., van Blitterswijk, C.A., de Bruijn, J.D., 2010. Osteoinductive ceramics as a synthetic alternative to autologous bone grafting. PNAS 107, 13614-13139.

Chapter IV

Orthotopic bone regeneration within 3D printed bioceramic scaffolds with region-dependent porosity gradients in an equine model

(Submitted)

Orthotopic bone regeneration within 3D printed bioceramic scaffolds with region-dependent porosity gradients in an equine model

Rafael Vindas Bolaños[2],* Paweena Diloksumpan[1,*], Stefan Cokelaere[1], Behdad Pouran[3] Janny de Grauw[1], Mattie van Rijen[3], Saskia Plomp[1], P. René van Weeren[1], Riccardo Levato[3,4], Jos Malda[1,3,4,#]

[1]Department of Equine Sciences, Faculty of Veterinary Medicine, Utrecht University, the Netherlands
[2]Cátedra de Cirugía de Especies Mayores, Escuela de Medicina Veterinaria, Universidad Nacional, Costa Rica
[3]Department of Orthopaedics, University Medical Center Utrecht, Utrecht University, Utrecht, the Netherlands
[4]Regenerative Medicine Center, Utrecht, Utrecht University.
*equal contribution

[#]correspondence to j.malda@umcutrecht.nl

Abstract

Methods for bone regeneration in large defects require tissue transplant or biomaterials to promote and facilitate the healing process. To improve this capacity when using scaffolds, multiple factors, including internal pore architecture as well as biomaterial composition and incorporation of exogenous cues have been extensively investigated. Previously, we developed a printable calcium phosphate (PCaP) based biomaterial that showed potential for driving osteogenic differentiation of progenitor cells, and tested this in potential *in vitro* for bone tissue engineering in osteochondral constructs. To further investigate long term *in vivo* performance of this bone substitute, PCaP scaffolds were printed with different internal architecture, displaying either a biomimetic designed porosity gradient or a constant pore distribution, and implanted in experimentally created equine tuber coxae bone defects. Bone ingrowth was allowed only from one direction of the scaffold by encasing the ceramic in a polycaprolactone shell. No adverse effects of surgery or scaffold implantation were seen. After 7 months, total volume of new bone ingrowth and material degradation in scaffolds with constant porous structure was significantly greater than when implants with a gradient porous structure were used. Interestingly, in gradient scaffolds, the local extent of the remodeling and regenerative processes in areas having the same porosity as the constant scaffolds was lower, and depended on the degree of material degradation and tissue repair within adjacent regions displaying less porosity. These results underline the influence of implant macro-pore pattern on the extent of bone healing and material degradation *in vivo*.

Introduction

In the quest for methods to heal large bone defects, bioceramic-based bone scaffolds can overcome the drawbacks of both harvesting and implantation of either autografts or allografts, including limited donor material availability and donor site morbidity. Bioceramics based on calcium phosphates (CaP) have been extensively researched as substitute biomaterials to guide bone regeneration, due to their composition mimicking that of the inorganic phase of native bone, and their proven osteoconductivity (Legeros, 2002). CaP based implants have been processed and investigated for several decades to establish how properties like solubility, particle size, crystallinity, surface roughness and surface charge affect their bioactivity and interaction with host tissue. Both chemical and physical properties of such implants may, alone or in interaction, affect the rate and quality of new tissue formation (Samavedi et al., 2013).

The role of biomaterial porosity and its influence on regenerative processes has been a major topic of investigation since the early stages of tissue engineering (Karageorgiou et al., 2005; Li Loh et al., 2013). Recent studies have highlighted how the pore size, shape and interconnection are essential in driving the exchange of nutrients and bone remodeling factors, cellular and vascular infiltration, progenitor cell differentiation, material degradation, and immune reaction (Ratner et al., 2016; Serra et al., 2015). Pore features including size, geometry and directionality can to a certain extent be controlled with conventional scaffold fabrication techniques, but the recent developments in three-dimensional (3D) printing technologies have greatly enhanced the capacity of designing and fine-tuning the specific architecture of implantable scaffolds.

Anisotropic pore distributions can be introduced in printed materials to mimic the native gradient from highly porous cancellous bone to less porous cortical bone or in the subchondral bone layer in the osteochondral unit of articulating joints (Luca et al., 2016; Cai et al., 2012). However, even though a pore size of over 300 µm has often been recommended as facilitating bone and vascular ingrowth within porous scaffolds (Karageorgiou et al., 2005), the *in vivo* performance of biomimetic anisotropic yet geometrically defined porous printed ceramic implants has not been fully elucidated.

Recently, low-temperature self-setting CaP cements based on α-tricalcium phosphate (α-TCP) microparticles, which are also used as injectable bone cements (Pérez et al., 2012), have emerged as promising materials for printable ceramic formulations. In fact, by accurately controlling the rheology of the cement precursor paste, this can be utilized as an ink for extrusion-based printing. After printing, the printed structure is exposed to a humidified environment at physiological pH to initiate the setting reaction by converting the α-TCP paste into calcium deficient hydroxyapatite cement (CDHA). This is a mild reaction that permits co-printing of CaP cements and cell-laden hydrogels

within the same constructs (Ahlfeld et al., 2018). This mechanism has already been successfully exploited to obtain printed CaP cements with osteoinductive properties, either by encapsulation of growth factors in the paste precursor (Akkineni et al., 2015) or by tuning PCaP nanotopography (Barba et al., 2018). As new 3D printed CDHA-based scaffolds with controllable macro- and microscale architectures are created, it becomes more and more important to investigate their relative regenerative potential not only *in vitro*, but also in reliable animal models (Moran et al., 2016; Pearce et al., 2007].

In orthopaedic regenerative medicine, the evaluation of novel interventions in large animal models is a pre-requisite for their eventual human clinical application; at the same time, such human pre-clinical studies constitute end-stage testing for veterinary application in the animal species involved (Gyles, 2016). Much like humans and unlike other more common large animal models like goats or sheep, horses participate as athletes in competitions, in which bone and osteochondral injuries regularly lead to both great economic losses and serious animal welfare concerns (Bigham-Sadegh et al., 2015; Williams et al., 2001; Wright, 2017). This makes studies addressing bone regenerative capacity in the horse not only of great interest for human medicine, but also for the equestrian industry and equine health care.

A previous study on osteoinductive gelatin/β-TCP sponges demonstrated favorable bone regeneration in third metacarpal bone defects in horses (Tsuzuki et al., 2012). This location of defect is, however, challenging in terms of surgical approach and interventions at this site easily lead to severe discomfort in the animals, which will manifest as lameness. The equine tuber coxae has not formally been used as a site for bone regeneration studies thus far, but presents several advantages: it is easily accessible, contains compact and trabecular bone, is hardly affected by skin displacement, and surgery can even be performed in the standing horse. The limited impact of surgical interventions at this site also allows the simultaneous investigation of novel regenerative approaches at different sites (e.g., stifle joints for cartilage repair), thus contributing to the refinement and reduction of experimental animal use, in compliance with the 3R principle (Guhad, 2005).

This study aimed at studying the *in vivo* bone regenerative potential of a novel CaP-based bioceramic scaffold with variation in pore architecture of the material as a variable. Low temperature setting CaP-based bioceramic-hydrogel composite scaffolds, consisting of alpha-tricalciumphosphate (α-TCP), hydroxyapatite nanoparticles (nanoHA) and a biodegradable, crosslinkable poloxamer derivative were fabricated via 3D printing, to create scaffolds with either an isotropic, homogenous pore distribution or a biomimetic, anisotropic gradient of porosity. Finally, to better assess the ability of bone to grow within large constructs with anisotropic porosity, the regenerative process was challenged by encasing the CaP scaffold within a polycaprolactone cage, which

prevented infiltration of progenitor cells from the periosteum and allowed preferentially unidirectional tissue ingrowth. The scaffolds were implanted orthotopically in the tube coxae bone of horses, and bone regeneration was evaluated after a 7-month period.

Materials and Methods

Printable calcium phosphate (PCaP) Paste preparation

As ceramic precursor, PCaP paste was prepared by mixing a powder particle phase and a liquid phase. The optimal distribution of the particles and liquid phases that allowed the paste to be printable was 70% and 30% w/w respectively. The powder consisted of microparticles of milled α-tricalciumphosphate (α-TCP, average size 3.37 µm, Cambioceramics, The Netherlands) with a 4% w/w substitute by hydroxyapatite nanoparticles (nano-HA, average size 200 nm, Sigma-Aldrich). The liquid phase consisted of a shear-thinning, hydrogel dissolved in PBS, supplemented with 25 mM ammonium persulphate (APS, Sigma Aldrich), to form a 40% (w/v) solution. This hydrogel carrier is constituted by a biodegradable and crosslinkable poloxamer derivative (P-CL-MA), synthesized by grafting onto both terminal hydroxyl groups of poloxamer 407 (Sigma-Aldrich) one biodegradable ε-caprolactone ester block and a methacrylate group, as previously reported [Melchels et al., 2016]. Before mixing, the powder and liquid phases were stored separately at 4 °C for 30 minutes and finally the P-CL-MA solution was added to a composite solid particle at 4 °C and manually mixed with a spatula. To ensure homogeneous distribution of solid particles, the mixing process was performed for 3 minutes at 4 °C. Finally, the PCaP paste was loaded into a 5 ml dispensing cartridge, closed with retainer caps and stored at 4°C until used.

Scaffold preparation

Porous PCaP scaffold
Porous cylindrical PCaP scaffolds (diameter: 9.8 mm. height: 9.5 mm) were designed and produced using a pneumatic extrusion printer (RegenHU, Villaz-St-Pierre, Switzerland). Scaffold architecture was designed and converted to printing path and eventually g-code with the BioCAD software (RegenHU, Villaz-St-Pierre, Switzerland). The PCaP paste was extruded through a conical nozzle (inner diameter = 250 µm, pressure = 0.21 MPa, translation speed 2 mm/s and layer height of 250 µm.) at ambient temperature (20 - 25 °C). All scaffolds were printed with a 0-0-90-90° laydown pattern, stacking two contiguous layers in the same direction in order to ensure a constant lateral porosity of 500 µm. Two types of axial pore structures were formed: i) a gradient of porosity with a discrete 4-steps reduction of the strand-to-strand distance (750 µm, 650 µm, 550 µm and 450 µm), and ii) a constant pore pattern, created by printing within each layer PCaP filaments with a strand-to-strand distance of 750 µm. For both types of scaffolds,

a non-porous last layer was printed (**Fig. 1**). These procedures resulted in scaffolds with porosities of 40.03 $\pm$ 1.78 % and 51.14 $\pm$ 0.78 % for the gradient and constant architectures, respectively. Consequently, the tangent modulus and ultimate strength of the scaffolds within a range of porosity between 40 – 50% under compression were 208.73 $\pm$ 84.90 MPa and 3.09 $\pm$ 1.17 MPa, respectively. After finishing the printing process, PCaP scaffolds were set by leaving them in a humidified environment, saturated with water vapor at 37°C for three days. Subsequently, the scaffolds were immersed in 25 mM tetramethylethylenediamine (TEMED, Life Technologies) solution in PBS at 37°C for one hour, to allow the polymerization of the P-MA component of the PCaP cement, initiated by TEMED diffusing into the APS-enriched cement formulation. Finally, crosslinked scaffolds were rinsed and washed with PBS twice, dried in air at ambient temperature, and stored until further use.

PCL cylindrical shell, implant assembly and sterilization
To allow tissue growth into the construct from only one direction, the entire scaffold, except for the side that was positioned on the bottom of the osteal defect, was insulated with a bucket-shaped polycaprolactone (PCL) shell (height: 10 mm., inner diameter: 10 mm., outer diameter: 10.47 mm.). This shell was 3D printed in medical-grade PCL (Purasorb® PC 12 Corbion PURAC, The Netherlands with printing temperature of 80°C, translation speed 1 mm/sec, and layer thickness of 200 µm) by using the same pneumatic-driven printer as described for the PCaP paste. Hardened and crosslinked PCaP scaffolds were press-fitted inside the PCL shell, with the non-porous PCaP layer at the closed side of the shell (**Fig. 1**). All assembled scaffolds were sterilized by gamma irradiation (8kGy) and kept separately in sterile falcon tubes until implantation.
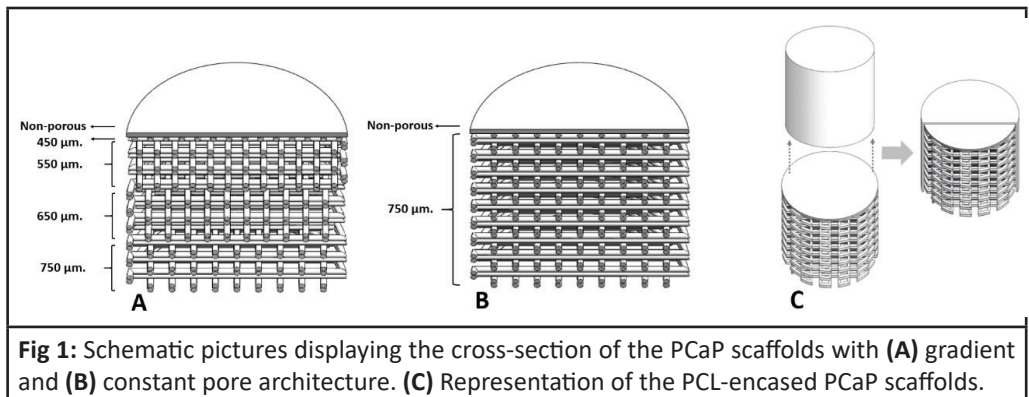

Fig 1: Schematic pictures displaying the cross-section of the PCaP scaffolds with **(A)** gradient and **(B)** constant pore architecture. **(C)** Representation of the PCL-encased PCaP scaffolds.

Implantation

Study design
Cylindrical defects were drilled into the tuber coxae of the ilium in each horse (n = 8) (one defect per side) (**Fig. 2**). Each horse received both one gradient and one constant porous scaffold (with random left/tight distribution). Scaffolds were placed by letting the open circular side of the PCL cylindrical shell in contact with native bone at the bottom of the defect while the closed circular side was covered with periosteum.

Animals
The protocols and studies described were approved by the ethical and animal welfare committee from the Veterinary School at the National University of Costa Rica. Eight healthy adult Criollo breed horses (mean age 7.1 years, range 5-9 years; mean weight 319 kg, range 275-375 kg) were used. Horses were clinically sound on lameness examination and did not have clinical or radiographic evidence of joint pathology. They were housed in individual box stalls and fed a standard maintenance ration of concentrate with hay ad libitum and had free access to water during the first three months of the study. After this period, they had free exercise at pasture at the University farm, with unlimited access to hay and water.

Surgical procedure
After premedication with xylazine (1.1 mg/kg IV; Pisa, Mexico) and the placement of a 12G catheter in one jugular vein, anaesthesia was induced with midazolam (0.05 mg/kg IV; Holliday, Argentina) and ketamine (2.2 mg/kg IV; Holliday, Argentina). General anesthesia was maintained with isoflurane in oxygen. The horse was positioned in dorsal recumbence, with the hindquarters slightly turned to the side of surgery for improved surgical access. An incision was made in the skin and subcutaneous tissue 10 cm above the tuber coxae to expose the underlying bone of the ileal tuberosity. Once the tuberosity was exposed, a cylindrical microdefect of 11 mm wide x 10 mm deep was created using a power-driven drill. Defect sites were flushed with saline (Baxter, USA) and the experimental scaffolds were implanted using a press-fit approach. Subcutaneous tissue and skin were sutured in routine fashion, and the horses were allowed to recover without wound dressings.

Post-operative care and monitoring
Post-operatively, horses received antibiotics for 5 days (procaine penicillin (Phenix, Belgium) 15000 IU/kg IM SID and gentamicin (Kepro BV, the Netherlands) 6.6 mg/kg IV SID), and non-steroidal anti-inflammatory drugs (phenylbutazone, Holliday, Argentina; 2.2 mg/kg PO BID) during the first 10 days. Horses were clinically monitored on a daily basis for rectal temperature, heart rate and respiratory rate, as well as stance, demeanor and general appearance. The surgical wounds were inspected and the area

gently palpated for local heat, swelling and tenderness. Locomotion was evaluated at walk on a daily basis and horses were occasionally trotted up to check for eventual subtle lameness. Routine blood analysis (CBC, chemistry panel) was performed at month 1, 3 and 6 post-operatively. From three months post-operatively, horses were turned out at pasture allowing free exercise until the end of the experiment.

Euthanasia and sample harvesting

Seven horses were euthanized 7 months post-operatively. One horse died because of an accident unrelated to the study at 2 months post-operatively and was excluded from the study. Deep anesthesia was induced with a combination of xylazine (1 mg/kg IV, Pisa, Mexico) followed by ketamine and midazolam (3 mg/kg IV and 0.05 mg/kg IV respectively; Holliday, Argentina), after which a bolus of oversaturated magnesium sulphate (200 g/L; Agreagro S.A., Costa Rica) and chloral hydrate (200 g/L) solution was administered IV to effect and death confirmed by absence of breathing, ictus and corneal reflex.

After dissection of the skin and subcutaneous tissues, the tuber coxae bone was exposed and the surgical sites were readily recognizable. Macroscopic pictures were taken and blocks of tissue containing the defects were excised. A piece containing the defect was fixed and stored in formalin in individual plastic containers.

Micro-computed tomography (μ-CT) evaluation

Three assembled implants of either constant or gradient porous PCaP scaffolds were randomly selected for scanning before an implantation in a μ-CT scanner (Quantum FX-Perkin Elmer). All formalin-fixed tissue explants, containing the implant and the surrounding native tissue that were harvested postmortem at the endpoint of an experiment were also scanned (voltage = 90 kV, current = 200 μA, voxel size = 20 μm^3 and total scanning time = 3 minutes). Subsequently, the acquired images were processed and analyzed using image J (Schindelin et al., 2012) and Bone J (Doube et al., 2010) software, respectively. As 2D-region of interest (ROI) or 3D-volume of interest (VOI), the volume of the defect filled with the ceramic scaffold was selected. Seven main parameters were quantified including total volume of newly-formed bone in overall VOI, volume of newly-formed bone in each zonal VOI, percentage of new bone ingrowth ((new bone volume/VOI) * 100), percentage of remaining PCaP ((volume of ceramic/ VOI) * 100), estimated percentage of other, non-mineralized tissue infiltration (100 – (percentage of new bone ingrowth + percentage of remaining ceramic)), total volume ceramic material of scaffolds before and after implantation, and percentage of PCaP volume loss. μ-CT 3D reconstructions of new bone formation and remaining ceramic were generated using the 3D Slicer software (4.10.0, BWH and 3D Slicer contributors).

Histological assessment

After retrieval, all formalin-fixed samples were kept in 4% formalin and cut through the defect area and therefore through the scaffold longitudinally to obtain two rectangular cross sections for embedding in either paraffin or methyl methacrylate (MMA) resin. For paraffin embedding, tissue explants were decalcified with 0.5 M EDTA disodium salt for 6 weeks. Dehydration was performed through a graded ethanol series, followed by clearing in xylene and embedding in paraffin. Embedded samples were sectioned into 5μm thin slices. Thereafter, all sections were stained separately with hematoxylin and eosin (H&E), Goldner's trichrome, picosirius red, tartrate-resistant acid phosphatase (TRAP) to reveal tissue structure and cell infiltration, osteoid formation and neo-bone maturation, alignment of collagen fibers, and TRAP-positive osteoclasts, respectively. Immunohistochemistry was performed to detect osteonectin (Osteonectin AB SPARC AON-1, DSHB) and collagen type I (Anti-Collagen I antibody (EPR7785), Abcam).

For MMA embedding, formalin-fixed tissue sections were dehydrated through a graded ethanol series, embedded in MMA resin and allowed to harden at 37°C in water bath overnight. Embedded samples were sectioned into 330 μm-thick slices. Thereafter, all sections were stained with basic fuchsin and methylene blue to visualize new bone ingrowth and soft tissue infiltration. Stained histological slides were imaged using a light microscope (Olympus BX51, Olympus Nederland B.V.) equipped with a digital camera (Olympus DP73, Olympus Nederland B.V.).

For analysis of both μ-CT derived bone distribution and histological data, the implant region was divided into three equally thick zones across the depth of the scaffold, starting from the native bone-scaffold interface. Relative amounts of TRAP-positive stain, osteonectin-positive stain and collagen type I-positive stain were semi-quantified. Dimensions and number of blood vessels that penetrated into scaffolds were also quantified. Dimensions were measured manually by using the image J software.

Statistical analysis

Measurements at the endpoint of the *in vivo* experiment were performed on seven horses (n=7). Calculated values for the constant and gradient porosity scaffolds were reported as mean ± standard deviation. Statistical analysis was performed using Matlab (R2018a, The MathWorks, Inc.). A Mann-Whitney U-test was performed to investigate the differences between the groups in terms of total bone volume, zonal bone volume, percentage of PCaP volume loss, including size and number of blood vessels. The same test was used for evaluating the bone volume fraction, remaining material volume fraction and non-mineralized tissue volume fraction in the VOI. Two-way ANOVA was performed for analyzing the total PCaP volume before and after implantation. Statistical significance was considered for $p < 0.05$.

Results

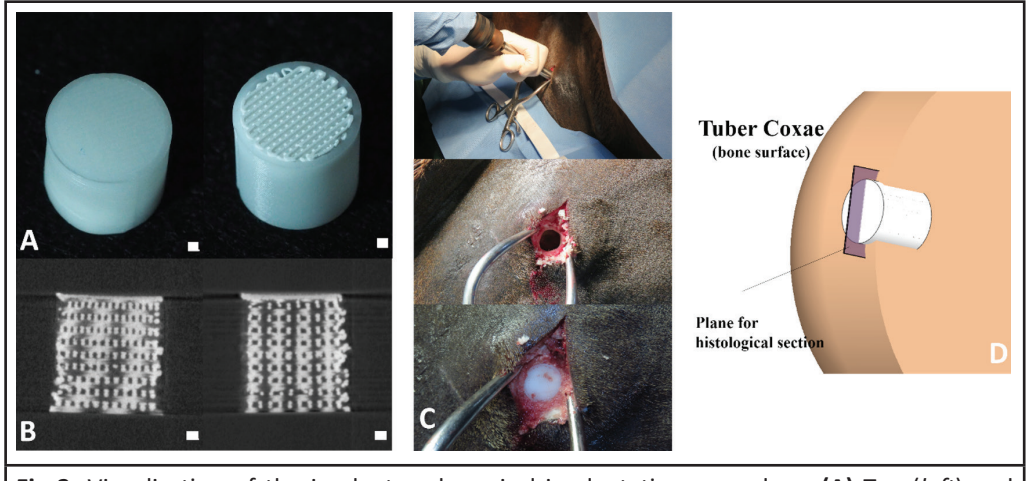### *Architecture of the implant and implantation procedure*

Fig 2: Visualization of the implant and surgical implantation procedure. **(A)** Top (*left*) and bottom (*right*) view of the PCaP implants embedded into the PCL shell. **(B)** Representative µ-CT images of an implant with gradient pore size (*left*) and constant pore size (*right*) before implantation. **(C)** Sequence of implantation of the scaffolds in the tuber coxae, including drilling and exposure of the defect, followed by scaffold implantation. **(D)** Schematic representation of the implant location in the coxal tuberosity. Scale bar = 1mm.

Implantation

Clinical monitoring

Over the 7 months follow-up, 7 out of 8 horses recovered uneventfully and coped well during the post-surgical rehabilitation period. The surgical incisions healed without complications, and no local inflammatory reactions (heat, swelling, tenderness) or gross signs of pain or discomfort were observed at any time. Likewise, the animals did not experience any detectable pain or lameness relating to the tuber coxae implantations during the post-operative period, and clinical and routine blood parameters remained within normal physiological limits. Two months postoperatively, one horse unfortunately died due to an unrelated traumatic head injury; this horse was lost to follow-up for this study.

Macroscopic appearance at necropsy

At the time of euthanasia, surgical sites were easily identified both visually and by palpation. In general, in some cases a slight depression was observed at the site of the

defects; in others there was some thickening because of scar tissue formation. After removal of the overlying soft tissues, the implants all appeared to be well attached to the surrounding osseous tissue. There was no sign of local inflammation or other adverse tissue response.

Quantitative analysis

At 7 months after implantation neo-bone formation was studied throughout the scaffolds that were divided into three zones **(Fig 3A)**. The amount of new bone ingrowth in the constant porosity scaffold group (109.80 ± 54.50 mm^3) was significantly more than in the gradient scaffold group (31.49 ± 11.02 mm^3) **(Fig 3B)** This difference was particularly evident in zones 1 (constant: 42.82 ± 20.94 mm^3; gradient: 11.49 ± 3.00 mm^3) and 2 (constant: 30.86 ± 12.74 mm^3; gradient: 10.53 ± 3.24 mm^3) **(Fig 3C)**. Likewise, the amount of bone appeared higher in zone 3 as well for constant (26.07 ± 16.77 mm^3) against gradient (8.85 ± 4.99 mm^3) porosity scaffolds, but this difference was not significant. Additionally, the bone distribution in each printed layer varied, as a function of the distance to the scaffold-native bone interface (basal side of the scaffold). In terms of ratio over the VOI, constant porosity scaffolds showed more bone volume (constant: $25.06 \pm 8.60\%$; gradient: $10.73 \pm 4.62\%$), as well as non-mineralized repair tissue (constant: $48.24 \pm 7.25\%$; gradient: $42.7 \pm 10.48\%$) **(Fig 3D)**. The percentage of remaining ceramic material was significantly lower in the constant porosity group ($26.7 \pm 6.28\%$) than in the gradient group ($46.58 \pm 6.31\%$) **(Fig 3D-E)**, suggesting a faster resorption of the material. Quantitative analysis of the total volume of ceramic before and after implantation **(Fig 3E-F)** from μ-CT data reveal an estimated percentage of scaffold degradation of $59.26 \pm 13.52\%$ for the constant scaffold group and of $38.38 \pm 11.07\%$ for the gradient scaffold.

Three-dimensional (3D) reconstruction images from μCT data **(Fig 4)** showed the distribution of new bone formation in all scaffolds. The spatial distribution of the neo-tissue in the planes perpendicular to the longitudinal axis of the scaffold was analyzed in correspondence with the 3 main zones. Notably, new bone formation between the basal periphery and the transitional zone between zone 2 and zone 3 of the scaffold was more homogeneous in the constant scaffold than in the gradient scaffold. Bone formation appeared less uniform in zone 3 for both scaffold types, with the constant pore group having a considerably higher amount of neo-bone tissue overall.
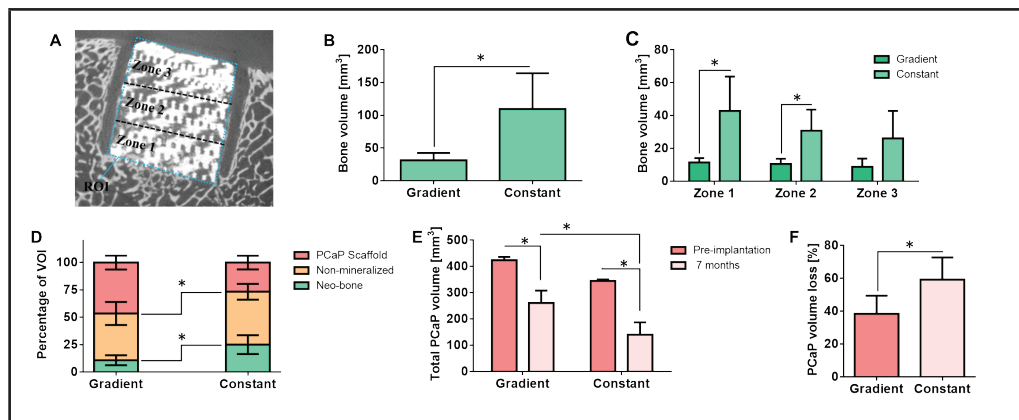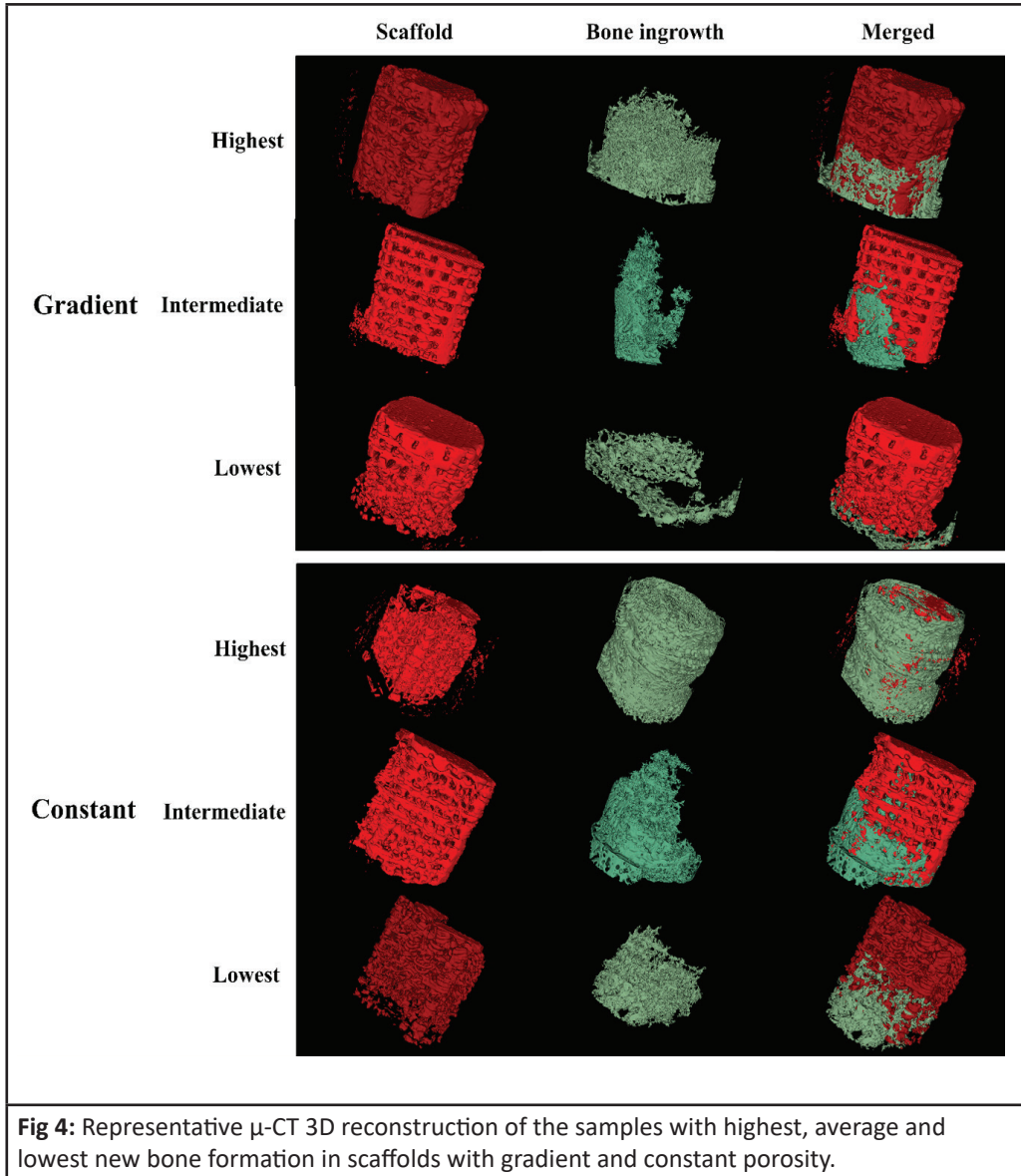
Fig 3: Quantification of bone regeneration. **(A)** The three zones that were analyzed inside the scaffold. Quantification of new bone volume **(B)** within the defect and **(C)** within each zone, and **(D)** ratio of the VOI occupied by new bone, non-mineralized tissue and remnants of PCaP scaffold after 7 months *in vivo*. **(E, F)** Degradation of both types of scaffolds was highlighted by the quantification of the PCaP volume prior to implantation and at the end of the experiment. Asterisks indicate p < 0.05.

Fig 4: Representative µ-CT 3D reconstruction of the samples with highest, average and lowest new bone formation in scaffolds with gradient and constant porosity.

Qualitative analysis

Macroscopic assessment
In formalin-fixed samples that were cut transversely through both circular surfaces of the cylindrical scaffolds, the positions of the implant were easily visible. PCL shells were visible in all samples as opaque white colored struts surrounding the area of the

ceramic scaffold. From the cross-sectional surface, a few samples (both gradient and constant porosity scaffolds) showed a subtle brownish discoloration surrounding the implant. **(Fig 5)**.
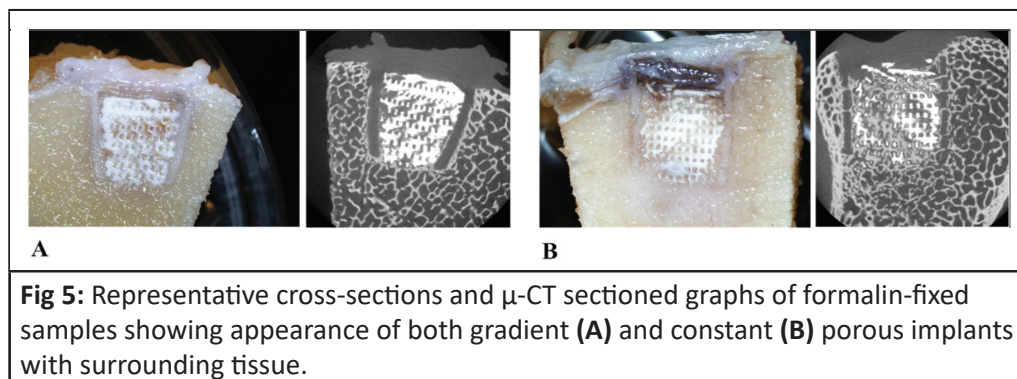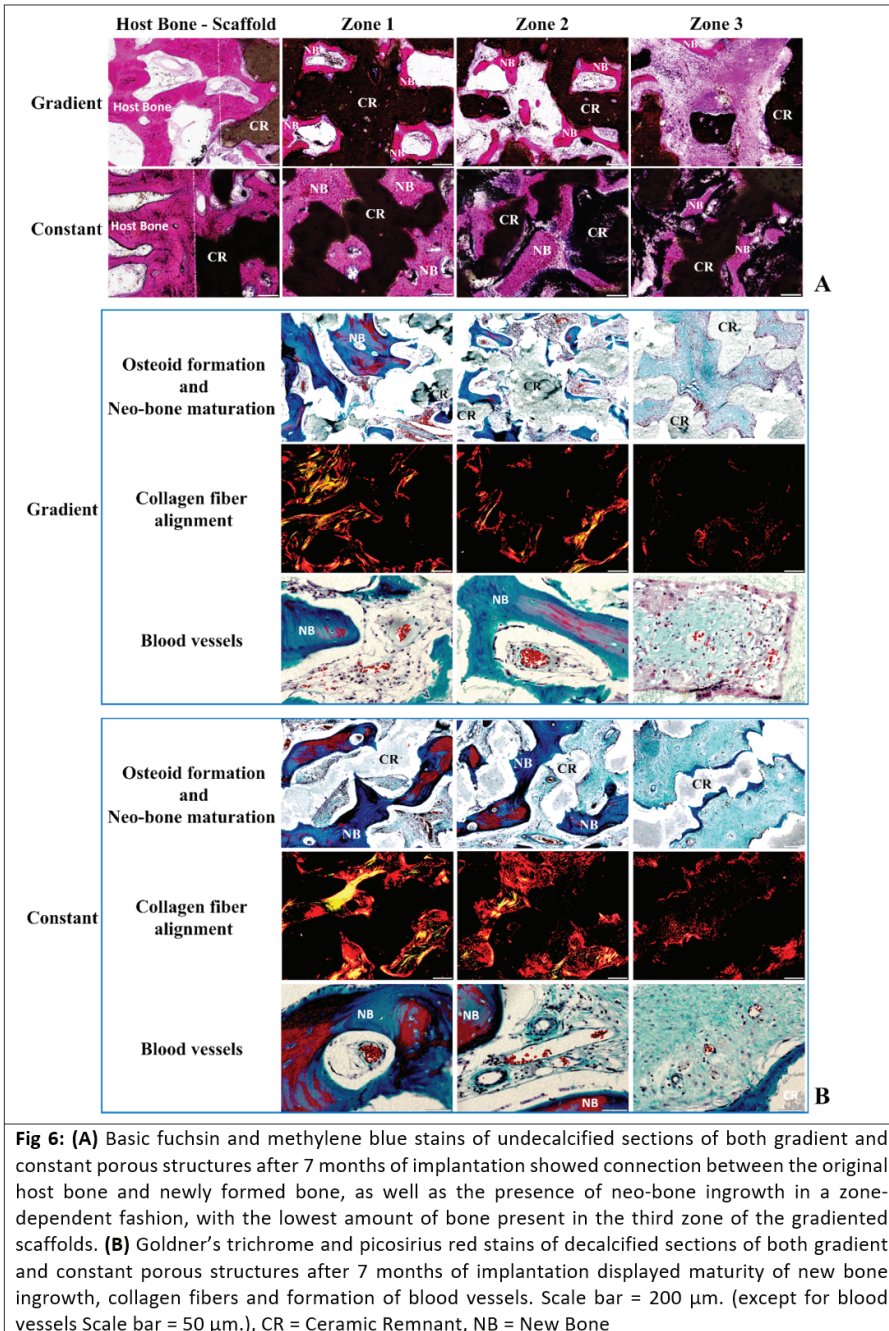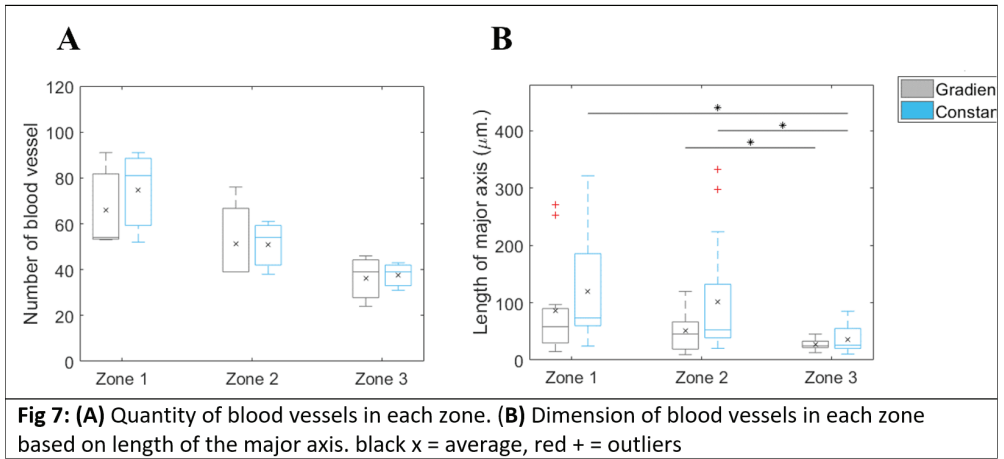

Fig 5: Representative cross-sections and μ-CT sectioned graphs of formalin-fixed samples showing appearance of both gradient **(A)** and constant **(B)** porous implants with surrounding tissue.

Microscopic assessment of the extent of bone healing

Microscopic analysis of the basic fuchsin and methylene blue stains of MMA embedded sections showed areas of new bone ingrowth between the macro-pores of the ceramic scaffolds in both gradient and constant scaffolds, displaying good attachment and integration between the neo-bone and the ceramic material (**Fig 6A**, **Supplementary Figure S1**). Histological analysis together with μ-CT images revealed the continuous connection between the host bone and the new bone ingrowth that penetrated into the scaffold from the host bone at the basal periphery of all scaffolds, regardless of the type of porosity, as well as the presence of non-calcified tissue, which was predominantly located in the regions of the scaffold further away from the interface with the native bone. The extent of new bone ingrowth varied per scaffold type. On the constant porosity scaffolds, new bone extended from the basal periphery of the scaffold, throughout the entirety of zone 2 to zone 3 (close to one side of the cylindrical wall) and towards the non-porous layer. In the gradient scaffolds, new bone extended to the middle region of zone 2 but not or hardly to zone 3. The newly-formed bone inside the gradient porous scaffold was predominantly woven (immature) bone with some lamellar (mature) bone in zone 1. In the constant pore scaffolds both woven bone and lamellar bone were found, with a preponderance of lamellar bone, and found in higher amounts in all zones. Lamellar bone structures were found organized concentrically in a Haversian pattern around blood vessels, typical of native osteons **(Fig 6B)**. New blood vessels from zone 1 to zone 3 in both constant and gradient scaffolds were most prevalent in newly formed lamellar bone and between the macro-pores of the ceramic printed structures. The number of blood vessels decreased slightly from zone 1 to zone 3 in both architectures **(Fig 7 A)**. The dimension of the lumen, estimated by the length of the major axis **(Fig 7 B)**, diminished from zone 1 to zone 3, and larger vessels were detected in the scaffolds with constant porosity (Fig. 7). For gradient porous scaffolds, the sizes of blood vessels (mean±SD) were: 86.44 ± 85.33 μm (zone 1), 51.01 ± 36.74

µm (zone 2) and 27.30 ± 9.50 µm (zone 3). For the constant porosity scaffolds these figures were: 120.22 ± 90.60 µm (zone 1), 101.11 ± 99.16 µm (zone 2) and 35.41 ± 22.79 µm (zone 3).

Fig 6: (A) Basic fuchsin and methylene blue stains of undecalcified sections of both gradient and constant porous structures after 7 months of implantation showed connection between the original host bone and newly formed bone, as well as the presence of neo-bone ingrowth in a zone-dependent fashion, with the lowest amount of bone present in the third zone of the gradiented scaffolds. **(B)** Goldner's trichrome and picosirius red stains of decalcified sections of both gradient and constant porous structures after 7 months of implantation displayed maturity of new bone ingrowth, collagen fibers and formation of blood vessels. Scale bar = 200 µm. (except for blood vessels Scale bar = 50 µm.), CR = Ceramic Remnant, NB = New Bone

Fig 7: (A) Quantity of blood vessels in each zone. (**B**) Dimension of blood vessels in each zone based on length of the major axis. black x = average, red + = outliers
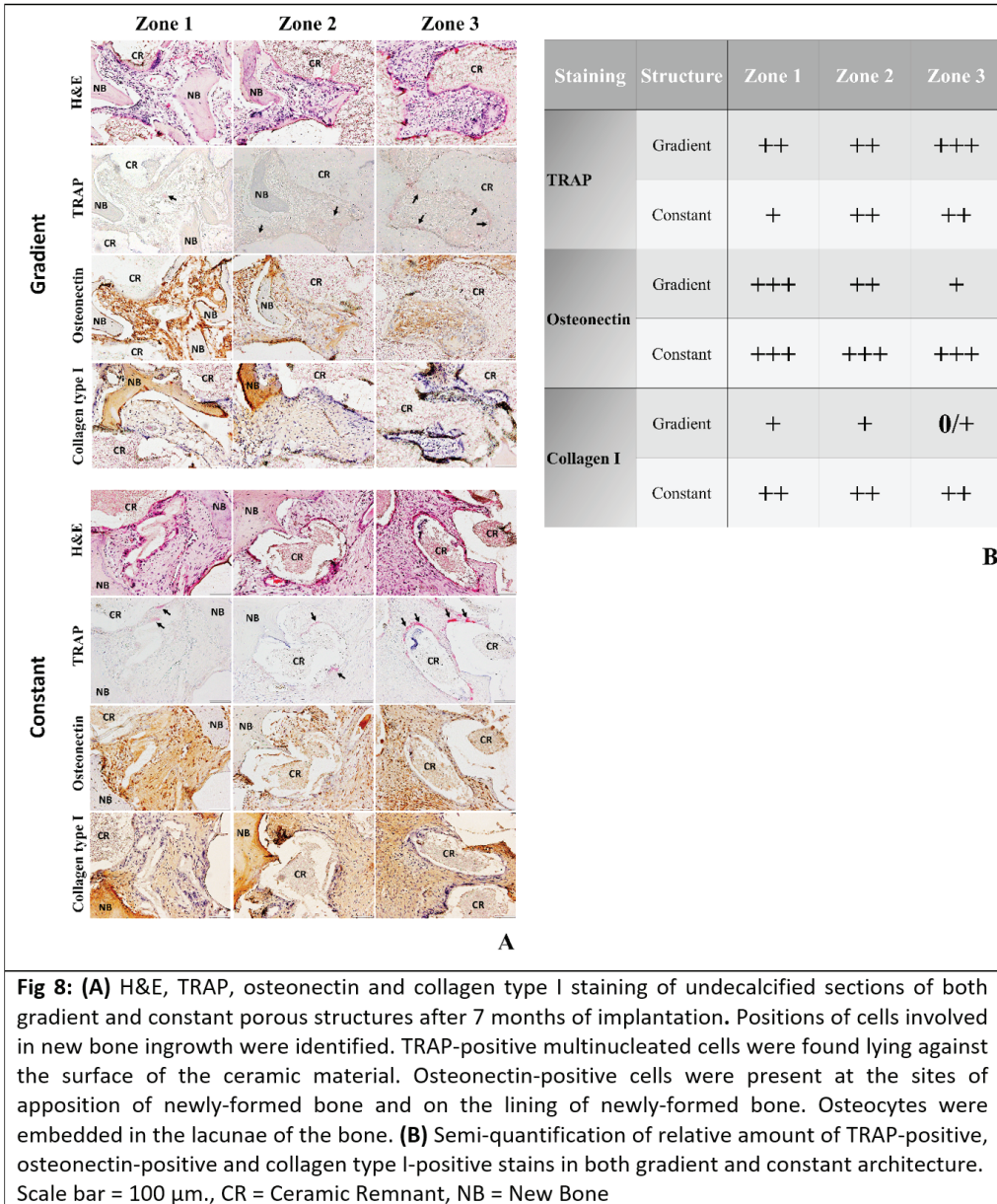
Microscopic assessment: cellular and molecular indicators of bone healing and remodeling

All types of scaffold showed areas of non-calcified tissue infiltration with different volumes in each zone. At the site of new bone formation, there were areas with positive staining for osteonectin, a marker of osteocytes, and a fundamental component of the extracellular matrix, which is able to bind collagen and known to facilitate bone mineralization (John D.Termine *et al*., 1981), in indicating osteoblastic activity. Osteonectin-positive osteocytes were found embedded in lacunae inside newly-formed mineralized bone osteons, and TRAP-positive multinucleated cells were found in contact and in the proximity of the ceramic remnants, indicating osteoclastic activity that can mediate PCaP resorption **(Fig 8)**.

In gradient structures, TRAP-positive multinucleated cells could be found throughout the scaffold from the basal periphery until zone 3 and were relatively higher in number than in the constant pore structure. In the gradient pore structures there were less osteonectin-positive cells from zone 1 towards zone 3. For collagen type I, areas with positive staining could be found mostly on the newly-formed bone, which in the gradient structure was situated mostly in zone 1 and declined from there to zones 2 and 3. In the constant pore structure these areas were found throughout the structure from zone 1 to zone 3.

Staining	Structure	Zone 1	Zone 2	Zone 3
TRAP	Gradient	++	++	+++
	Constant	+	++	++
Osteonectin	Gradient	+++	++	+
	Constant	+++	+++	+++
Collagen I	Gradient	+	+	0/+
	Constant	++	++	++

Fig 8: (A) H&E, TRAP, osteonectin and collagen type I staining of undecalcified sections of both gradient and constant porous structures after 7 months of implantation**.** Positions of cells involved in new bone ingrowth were identified. TRAP-positive multinucleated cells were found lying against the surface of the ceramic material. Osteonectin-positive cells were present at the sites of apposition of newly-formed bone and on the lining of newly-formed bone. Osteocytes were embedded in the lacunae of the bone. **(B)** Semi-quantification of relative amount of TRAP-positive, osteonectin-positive and collagen type I-positive stains in both gradient and constant architecture. Scale bar = 100 µm., CR = Ceramic Remnant, NB = New Bone

Discussion

Native bone possesses a remarkable spontaneous regenerative ability, which is, however, not unlimited. Large bone defects caused by trauma, degenerative diseases or tumor resection, as well as non-healing fractures, are common problems in musculoskeletal

medicine and require new strategies and biomaterials to help unlock, restore and guide bone repair. In this study, we investigated the long-term pro-regenerative performance of a new formulation of 3D printed CaP-based bioceramic scaffolds in vivo in an equine model, as a function of the printed pore architecture.

All scaffolds showed the ability to promote neo-bone formation. Importantly, the incorporation and covalent crosslinking of the biodegradable poloxamer hydrogel, of which biocompatibility had been previously demonstrated in vitro (Melchels et al., 2016) and that ensured the printability and shape fidelity of the cement paste precursors, did not impede the healing process in vivo, and did not appear to provoke any detrimental inflammatory response. In both types of architecture, common features of the regenerative process can be identified. The volume within the pores of the scaffolds is filled with new bone and collagenous, non-calcified tissue. The latter is rich in osteonectin-positive cells, a marker of osteoblasts and a key matrix molecule for the initiation of the mineralization process (Florencio-Silva et al., 2015). This osteocalcin abundance suggests the formation of an osteoid-like tissue, which is a preliminary step for the maturation towards neo-bone (Robey, 2008). The amount of neo-bone and non-mineralized tissue differed between the gradient and the constant porosity scaffolds, with the latter displaying a significantly higher amount of both tissue types. This consistent difference in the degradation rate of the two architectures, albeit produced with the same materials, as well as its association with a difference in neo-bone deposition, suggests an active, cell-driven resorption. Indeed, there was ample osteoclast activity, as evidenced by the histological data (Supplementary Figure S2). Osteoclast activity was higher in the more remote zones of both scaffold types (zones 2 and 3), possibly indicating an ongoing more intense remodeling activity in those areas that are still in an early stage of neo-bone development.

Previous studies on CDHA and nanoHA, the main components of the PCaP scaffolds tested in this study have convincingly shown their osteoconductive capacity (A. Barba et al., 2018). Also, our work shows an osteoconductive component of the regenerative process, as neo-bone is progressing through the scaffold from the host tissue, and integrates tightly with the ceramic remnants, but our analysis at a single time point provides no clear evidence for intrinsic osteoinduction. In other studies, osteoinductive properties in the absence of exogenously added growth factors have already been demonstrated, first for nanoHA (Hu et al., 2014), but also for CDHA, depending on the nanostructure of the biomimetic apatite particles resulting from the hardening process of the cement (Barba et al., 2017). The superior performance of the constant porosity scaffolds as compared to the biomimetic gradient group may not be intuitive. The gradient scaffolds do indeed present a lower degree of porosity, but all pores are well interconnected, with minimum size and geometry compatible with what is reported in the literature as necessary to permit bone ingrowth (Karageorgiou et al., 2005; Li Loh

et al., 2013; Marrella et al., 2018). Perhaps in part, the answer lies in the challenging environment created by the unilateral PCL cap.

In this study, the bone restorative process promoted by the 3D printed scaffolds was challenged by encasing the PCaP scaffolds in a PCL shell, to prevent infiltration of progenitor cells from the periosteum, and to facilitate only unidirectional bone ingrowth. Interestingly, this approach could possibly simulate features of large bone defects, in which areas towards the center of the scaffold have more difficulties in interacting with the host bone, and thus in receiving all cells and signals necessary to trigger the regenerative process. In a previous study on the degradation and osteoconductive properties of α- and β-Tricalcium phosphate, an 8mm-diameter titanium chamber was used to ensure equal space and prevent soft tissue interference (Yamada et al., 2006).

In the specific environment of this study, the overall design and architecture of the macro-pores greatly influenced the extent, quality, homogeneity and spatial distribution of the new bone and of the repair tissue, in an anisotropic, region-dependent fashion. While for both the gradient and the constant architecture neo-bone was consistently well integrated with the native bone at the interface at the open side of the PCL cage, the constant pore diameter scaffolds exhibited significantly higher bone formation, as well as the presence of more mature lamellar bone over woven bone. This was seen already from zone 1, even though the macro-pore architecture in this region was the same for both gradient and constant constructs. Furthermore, in the constant group, the neo-bone was more homogenously distributed throughout the section of the scaffold in the plane parallel to the open face of the PCL shell, and these differences were also evident further away inside the scaffold, in zone 2. A similar trend could be appreciated in zone 3, although differences were not statistically significant in this area. All horses showing the best healing capacity, i.e. full bridging of the defect with bone present throughout the whole scaffold, belonged to the constant porosity group.

Vascularization is a critical step for bone regeneration (García and García, 2016). Blood vessels, associated with bone (either lamellar, as Haversian canals, or woven) and non-mineralized tissue were present throughout all zones, regardless of the architecture. The size of these vessels, which is an indicator of vessel stability and vascularization potential of the scaffolds (Scaglione et al., 2009), decreased significantly from zone 1 to zones 2 and 3, for both architectures. There was a trend towards a larger average lumen size for the vessels in the constant porosity group. Vascular infiltration is a necessary element for bone tissue remodeling, and the degree of maturation and amount of blood vessels (Fig 7) can affect the influx of nutrients, biochemical cues and cells (i.e. osteoclasts, progenitor cells and osteoblasts) that accelerate neo-bone deposition and development (Filipowska et al., 2017; Malhotra et al., 2016). The decrease in the abundance and maturity of blood vessels from zone 1 to zone 3 in both architectures

did not completely mirror our findings for neo-bone formation, which was consistently better for the constant group regardless of zone. The trend for a larger average lumen size in the constant porosity scaffolds however is in line with better neo-bone formation seen in this group.

Importantly, our results suggest that areas further away from the front of mineralization influence other regions that are located elsewhere. This is particularly relevant, as areas with poor regeneration may limit osteoconductive repair also in regions close to the native bone. In the constant group, vascularization and repair tissue can progress with relatively more ease from zone 1 to 2 (and finally to 3), compared to the gradient group, leading to faster degradation and remodeling of the scaffold, accompanied by a satisfactory regeneration of bone in zones 1 and 2. Conversely, in gradient scaffolds, the hindrance of neo-bone progression in the deeper zones also negatively affects the quality and kinetics of the remodeling of the repair tissue in the first zone. Although such phenomena might not be experienced in a relatively small scaffold in which the porous architecture is accessible from all sides, this would be relevant for large scaffolds and the observation may hence be important for bone scaffold design and especially scaling-up of these scaffolds.

Finally, in the perspective of scaling up bone regenerative scaffolds, the selection of appropriate animal models is fundamental. Most biomaterials for bone regeneration are tested in small animals, which possess superior regenerative ability compared to humans and larger animals (Muschler et al., 2010). While these models provide important information on the osteoconductive and osteoinductive properties of a material, they poorly represent human musculoskeletal biology and the associated mechanical loads. Therefore, they are insufficient to translate new biomaterials to human and veterinary clinical practice. The equine model used in this study may aid significantly towards this objective.

Conclusion

In this work, the long-term in vivo performance of 3D-printed porous PCaP based scaffolds with different pore architecture (vertical gradient and constant porosity) was tested in an equine orthotopic bone defect model. The challenging environment created by PCL capping gave valuable insights on the influence of scaffold pore architecture. In this setting, the macro-pore pattern of the scaffolds, which were produced from compositionally equivalent material, was shown to influence new bone ingrowth and material degradation. This is important information for scaffold manufacturing, especially with regard to the possible upscaling of scaffolds for healing of large bone defects, as this study has shown that the –porosity-influenced- bone ingrowth and vascularity characteristics in turn have an effect on what happens further away from

the interfaces of the scaffold with the native bone. This study also highlights the value of the equine tuber coxae model for orthotopic testing of bone scaffolds. Apart from many advantages including ease of surgery, maximum size of implants, and limited experimental animal welfare impact, there is the important ethical consideration that for orthopaedic regenerative medicine studies, the horse is not merely an experimental animal, but a target species in its own right, and thus may benefit from possible positive outcomes of experimental studies.

References

Ahlfeld, T., Doberenz, F., Kilian, D., Vater, C., Korn, P., Lauer, G., Lode, A., Gelinsky, M., 2018. Bioprinting of mineralized constructs utilizing multichannel plotting of a self-setting calcium phosphate cement and a cell-laden bioink. Biofabrication 10, 1-14.

Akkineni, A., Rahul, A.A., Luo, Y., Schumacher, M., Nies, B., Lode, A., Gelinsky, M., 2015. 3D plotting of growth factor loaded calcium phosphate cement scaffolds. Acta Biomaterialia 27, 264-274.

Barba, A., Diez-Escudero, A., Maazouz, Y., Rappe, K., Espanol, M., Montufar, E.B., Bonany, M., Sadowska, J.M., Guillem-Marti, J., Öhman-Mägi, C., Persson, C., Manzanares, M.C., Franch, J., Ginebra, M.P., 2017. Osteoinduction by Foamed and 3D-Printed Calcium Phosphate Scaffolds: Effect of Nanostructure and Pore Architecture. ACS Appl Mater Interfaces 9, 41722-41736.

Barba, A., Maazouz, Y., Diez-Escudero, A., Rappe, K., Espanol, M., Montufar, E.B., Öhman-Mägi, C., Persson, C., Zontecha, P., Manzanares, M.C., Franchc, J., Ginebra, M., 2018b. Osteogenesis by foamed and 3D-printed nanostructured calcium phosphate scaffolds: Effect of pore architecture. Acta Biomaterialia 79, 135-147.

Benders, K.E.M., van Weeren, P.R., Badylak, F., 2013. Extracellular matrix scaffold for cartilage and bone regeneration. Trends in Biotechnology 31, 169-176.

Biggemann, J., Pezoldt, M., Stumpf, M., Greil, P., Fey, T., 2018. Modular ceramic scaffolds for individual implants. Acta Biomaterialia 80, 390 – 400.

Brown, A., Zaky, S., Ray, H.J., Sfeir, C., 2015. Porous magnesium/PLGA composite scaffolds for enhanced bone regeneration following tooth extraction. Acta Biomaterialia 11, 543–553.

Burr, D.D., Akkus, O., 2014. Bone Morphology and Organization. Basic and Applied Bone Biology

Butscher, A., M.Bohner, M., S.Hofmann, S., L.Gauckler, L., and R.Müller, R., 2011. Structural and material approaches to bone tissue engineering in powder-based three-dimensional printing. Acta Biomaterialia 7, 907-920.

Cai, S., Juntong, Xi., and Chee, K. Ch., 2012. A Novel Bone Scaffold Design Approach Based on Shape Function and All-Hexahedral Mesh Refinement, Computer-Aided Tissue Engineering, Methods in Molecular Biology 868, 45 – 56.

Di Luca, A., Longoni, A., Criscenti, G., Mota, C., van Blitterswijk, C., Moroni, L., 2016a. Toward mimicking the bone structure: design of novel hierarchical scaffolds with a tailored radial porosity gradient. Biofabrication 8, 6-7.

Di Luca, A., Lorenzo-Moldero, I., Mota, C., Lepedda, A., Auhl, D., van Blitterswijk, C., Moroni, L., 2016b. Tuning Cell Differentiation into a 3D Scaffold Presenting a Pore Shape Gradient for Osteochondral Regeneration. Advanced Healthcare Materials 5, 1753-1763.

Doube, M., Kłosowski, M.M., Arganda-Carreras, I., Cordelières, F.P., Dougherty, R.P., Jackson, J.S., Schmid, B., Hutchinson, J.R., Shefelbine, S.J., 2010. "BoneJ: Free and extensible bone image analysis in ImageJ",. Bone 47, 1076-1079.

Ferry, P., Melchels, W., Blokzijl, M.M., Levato, R., Peiffer, Q.C., de Ruijter, M., Hennink, W.E., Vermonden, T., Malda, J., 2016. Hydrogel-based reinforcement of 3D bioprinted constructs. Biofabrication 8 8, 1-9.

Filipowska, J., Tomaszewski, K.A., wiedzki2, Ł.N., Walocha, J.A., Niedz´wiedzki2, T., 2017. The role of vasculature in bone development, regeneration and proper systemic functioning. Angiogenesis 20, 291-302.

Florencio-Silva, R., Rodrigues da Silva Sasso, G., Sasso-Cerri, E., Simões, M.J., Paulo Sérgio Cerri, P.S., 2015. Biology of Bone Tissue: Structure, Function, and Factors That Influence Bone Cells. BioMed Research International 2015, 1-17.

Forero, J.C., Roa, E., Reyes, J.G., Acevedo, C., Osses, N., 2017. Development of Useful Biomaterial for Bone Tissue Engineering by Incorporating Nano-Copper-Zinc Alloy (nCuZn) in Chitosan/Gelatin/NanoHydroxyapatite (Ch/G/nHAp) Scaffold. Materials 10, 1-15.

García, J.R., García, A.J., 2016. Biomaterial-mediated strategies targeting vascularization for bone repair. Drug Deliv Transl Res 6, 77-95.

Gehron, P.R., 2008. Noncollagenous Bone Matrix Proteins Principles of Bone Biology, 3rd Edition ed.

Gruber, R., Weich, H.A., Dullin, C., Schliephake, H., 2009. Ectopic bone formation after implantation of a slow release system of polylactic acid and rhBMP-2. Clin. Oral Impl. Res 20, 24–30.

Guhad, F., 2005. Introduction to the 3Rs (Refinement, Reduction and Replacement). Journal of the American Association for Laboratory Animal Science 44, 58-59.

Gyles, C., 2016. One Medicine, One Health, One World. Can Vet J 57, 345–346.

Houmard, M., Fu, Q., Saiz, E., Tomsia, A.P., 2012. Sol–gel method to fabricate CaP scaffolds by robocasting for tissue engineering. Mater Sci: Mater Med J 23, 921–930.

Hu, J., Zhou, Y., Jun Liu, L.H., Lu, H., 2014. Effect of nano-hydroxyapatite coating on the osteoinductivity of porous biphasic calcium phosphate ceramics. BMC Musculoskeletal Disorders 15, 1-11.

Jain, R.K., 2003. Molecular regulation of vessel maturation. Nat Med Jun; 9, 685-693. Karageorgiou, V., Kaplan, D., 2005. Porosity of 3D biomaterial scaffolds and osteogenesis. Biomaterials 26, 5474 – 5491.

Karageorgiou, V., Kaplan, D., 2005. Porosity of 3D biomaterial scaffolds and osteogenesis. Biomaterials 26, 5474 – 5491.

LeGeros, R.Z., 2002. Properties of Osteoconductive Biomaterials: Calcium Phosphates. Clinical Orthopaedics and Related Research 2002 Feb;(395), 81-98.

Li, G., Yin, J., Gao, J., Cheng, T.S., Pavlos, N.J., Zhang, C., Zheng, M.H., 2013. Subchondral bone in osteoarthritis: insight into risk factors and microstructural changes. Arthritis Research & Therapy 15, 1-12.

Li Loh, Q., Choong, C., 2013. Three-Dimensional Scaffolds for Tissue Engineering Applications: Role of Porosity and Pore Size. Tissue Engineering: Part B 19, 485 – 502.

Lieberman, J., Daluiski, A., Einhorn, T.A., 2002. The rol of growth factors in the repair of bone Journal of Bone and Joint Surgery-American 84, 1032-1044.

Lode, A., Meissner, K., Luo, Y., Sonntag, F., Glorius, S., Nies.B., Vater, C., Despang, F., Hanke, T., Gelinsky, M., 2014. Fabrication of porous scaffolds by three-dimensional plotting of a pasty calcium phosphate bone cement under mild conditions. J Tissue Eng Regen Med 8, 682-693.

Loozen, L.D., van der Helm, Y.J.M.v.d.H., Oner, F.C., Wouter, J.A.D., Kruyt, M.C., Alblas, J., 2015. Bone Morphogenetic Protein-2 Nonviral Gene Therapy in a Goat Iliac Crest Model for Bone Formation. Tissue Engieneering 21, 1672-1679.

Malhotra, A., Habibovic, P., 2016. Calcium Phosphates and Angiogenesis: Implications and Advances for Bone Regeneration. Trends in Biotechnology 34, 983 – 992.

Marrella, A., Lee, T.Y., Lee, D.H., Karuthedom, S., Syla, D., Chawla, A., Khademhosseini, A., Lin Jang, H., 2018. Engineering vascularized and innervated bone biomaterials for improved skeletal tissue regeneration. Mater Today (Kidlington) 4, 362-376.

Moran, C.J., Ramesh, A., Brama, P.A., O'Byrne, J.M., O'Brien, F.J., Levingstone, T.J., 2016. The benefits and limitations of animal models for translational research in cartilage repair. J Exp Orthop. 3(1):1.

Muschler, G.F., Raut, V.P., Patterson, T.E., Wenke, J.C., Hollinger, J.O., 2010. The Design and Use of Animal Models for Translational Research in Bone Tissue Engineering and Regenerative Medicine. Tissue Engineering: Part B. 16, 123-145.

Pearce, A.I., Richards, R.G., Milz, S., Schneider, E., Pearce, S.G., 2007. Animal models for implant biomaterial research in bone: a review. Eur Cell Mater 13, 1-10.

Pérez, R.A., Ginebra, M.P., 2013. Injectable collagen/α-tricalcium phosphate cement: collagen-mineral phase interactions and cell response. J Mater Sci Mater Med 24, 381-393.

Perrier, M., Lu, Y., Nemke, B, K., H, P., A, M.M., 2008. Acceleration of Second and Fourth Metatarsal Fracture Healing with Recombinant Human Bone Morphogenetic Protein-2/ Calcium Phosphate Cement in Horses. Veterinary Surgery 37, 648-655.

Ratner, B.D., 2016. A pore way to heal and regenerate: 21st century thinking on biocompatibility. Regenerative Biomaterials 3, 107–110.

Satyavrata,S., Whittington A.R., Goldstein A.S., 2013 Calcium phosphate ceramics in bone tissue engineering: a review of properties and their influence on cell behavior. Acta Biomater. 2013 Sep;9(9):8037-45.

Scaglione, S., Ilengo, C., Fato, M., Quarto, R. Hydroxyapatite-coated polycaprolacton wide mesh as a model of open structure for bone regeneration. Tissue Eng Part A. 2009 15, 155-63. doi: 10.1089/ten.tea.2007.0410.

Schindelin, J., Arganda-Carreras, I., Frise, E., Kaynig, V., Longair, M., Pietzsch, T., Preibisch, S., Rueden, C., Saalfeld, S., Schmid, B., Tinevez, J.Y., White., D.J., Hartenstein, V., Eliceiri,

K., Tomancak, P., Cardona, A., 2012. "Fiji: an open-source platform for biological-image analysis". Nature methods 9, 676-682

Serra, I.R., Fradique, R., Vallejo, M.C., Correia, T.R., Miguel, S.P., Correia, I.J., 2015. Production and characterization of chitosan/gelatin/b-TCP scaffolds for improved bone tissue regeneration. Materials Science and Engineering C 55, 592-604.

Shengyong, C., Juntong, X., Chee Kai, C., 2012. A Novel Bone Scaffold Design Approach Based on Shape Function and All-Hexahedral Mesh Refinement, Computer-Aided Tissue Engineering. Methods in Molecular Biology 868, 45-56.

Takahashi, Y., Yamamoto, M., Tabata, Y., 2005. Enhanced osteoinduction by controlled release of bone morphogenetic protein-2 from biodegradable sponge composed of gelatin and β-tricalcium phosphate. 26.

Takahashi, Y., Yamamoto, M., Yamada, K., Kawakami, O., Tabata, Y., 2007. Skull Bone Regeneration in Nonhuman Primates by Controlled Release of Bone Morphogenetic Protein-2 from a Biodegradable Hydrogel. Tissue Engineering 13.

Termine, J.D., Kleinman, H.K., Whitson, S.W., Conn, K.M., McGarvey, M.L., Martin, G.R., 1981. Osteonectin, a bone-specific protein linking mineral to collagen. Cell press 26, 99-105.

Tsuzuki, N., Otsuka, K., Seo, J., Yamada, K., Haneda, S., Furuoka, H., Tabata, Y., Sasaki, N., 2012. In vivo osteoinductivity of gelatin β-tri-calcium phosphate sponge and bone morphogenetic protein-2 on an equine third metacarpal bone defect. Research in Veterinary Science 93, 1021-1025.

Williams, R.B., Harkins, L.S., Hammond, C.J., Wood, J.L., 2001. Racehorse injuries, clinical problems and fatalities recorded on British racecourses from flat racing and National Hunt racing during 1996, 1997 and 1998. Equine Vet J. 33, 478-486.

Wright, I., M., 2017. Racecourse fracture management. Part 1: Incidence and principles. Equine Veterinary Education 29, 391-400.

Yamada M., Shiota M., Yamashita Y. and Kasugai S., 2006. Histological and Histomorphometrical Comparative Study of the Degradation and Osteoconductive Characteristics of α- and β-Tricalcium Phosphate in Block Grafts,Journal of Biomedical Materials Research Part B: Applied Biomaterials, 139-148

Yuan, H., Fernandes, H., Habibovic, P., de Boer, J., Barradas, A.M., de Ruiter, A., Walsh, W.R., van Blitterswijk, C.A., de Bruijn, J.D., 2010. Osteoinductive ceramics as a synthetic alternative to autologous bone grafting. PNAS 107, 13614-13139.
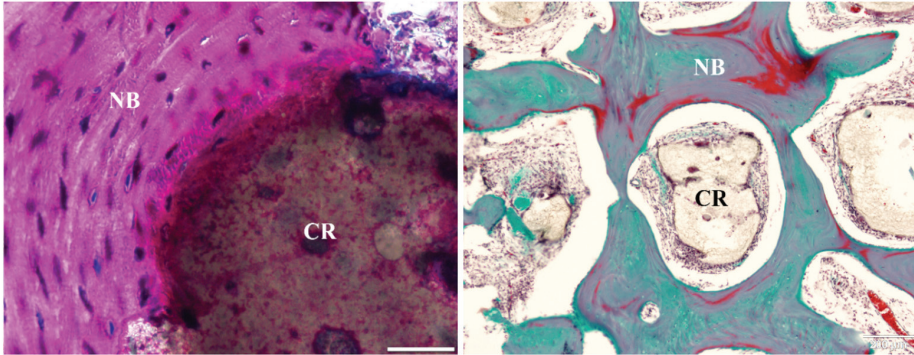
Supplementary data

Fig S1: (Left) Basic fuchsin & Methylene blue staining section displaying area of integration between ceramic remnant and new bone formation. **(Right)** Goldner's trichrome stained section displaying new bone formation on the surface of ceramic and following macro-spacing between the ceramic strands (Left: Scale bar = 50 μm., Right: Scale bar = 200 μm.). CR = Ceramic Remnant, NB = New Bone Ingrowth

In all scaffolds and experimental groups, new bone was found tightly connected to the surface of the PCaP material, suggesting good integration of the scaffold with the host tissue. Such tight interconnection cannot be appreciated in the samples treated for paraffin embedding, possibly because of tissue shrinking due to the processing.
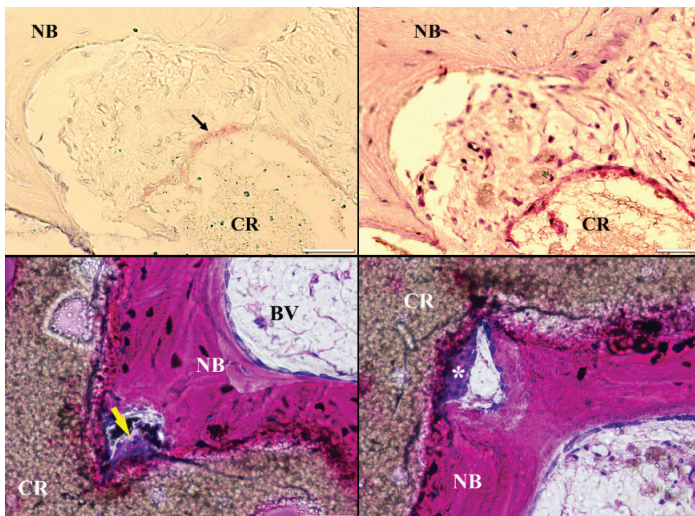
Fig S2: Osteoclastic resorption paired with bone apposition: (Top left) TRAP staining section displaying positive area (black arrow), (Top right) Comparative H&E staining at the same position, (Bottom left and right) Basic fushsin & Methylene blue staining section displaying multinucleated osteoclast aligned against the ceramic (yellow arrow (left), and white asterisk (right)). Scale bar = 50 μm, CR = Ceramic Remnant, NB = New Bone Ingrowth, BV = Blood Vessel

Chapter V

Fixation of hydrogel constructs for cartilage repair in the equine model: a challenging issue

Summary

Objective: To report on the experiences with the use of commercial and autologous fibrin glue (AFG) and of an alternative method based on a 3D-printed polycaprolactone (PCL) anchor for the fixation of hydrogel-based scaffolds in an equine model for cartilage repair.

Methods: In the first study, three different hydrogel-based materials were orthotopically implanted in nine horses for 1–4 weeks in 6mm diameter full-thickness cartilage defects in the medial femoral trochlear ridge and fixated with commercially available fibrin glue (CFG). One defect was filled with CFG only as a control. In a second study, CFG and AFG were compared in an ectopic equine model. The third study compared the efficacy of AFG and a 3D-printed PCL-based osteal anchor for fixation of PCL-reinforced hydrogels in three horses for 2 weeks, with a 4-week follow up to evaluate integration of bone with the PCL anchor. Short-term scaffold integration and cell infiltration were evaluated by microcomputed tomography and histology as outcome parameters.

Results: The first study showed signs of subchondral bone resorption in all defects, including the controls filled with CFG only, with significant infiltration of neutrophils. Ectopically, CFG induced clear inflammation with strong neutrophil accumulation; AFG was less reactive, showing fibroblast infiltration only. In the third study the fixation potential for PCL-reinforced hydrogels of AFG was inferior to the PCL anchor. PCL reinforcement had disappeared from two defects and showed signs of dislodging in the remaining four. All six constructs fixated with the PCL anchor were still in place after 2 weeks. At 4weeks, the PCLanchor showed good integration and signs of new bone formation.

Conclusions: The use ofAFGshould be preferred to xenogeneic products in the horse, butAFGis subject to individual variations and laborious to make. The PCL anchor provides the best fixation; however, this technique involves the whole osteochondral unit, which entails a different conceptual approach to cartilage repair.

Introduction

Articular cartilage is a highly specialized tissue in diarthrodial joints. Its roles are to provide smooth motion between joint surfaces, to transmit the forces generated by locomotion, and to attenuate these by redistributing mechanical stress to the underlying bone. However, because of its avascular nature, cartilage has poor intrinsic capacities for self-repair (Fox et al., 2009). Cartilage injuries in young adults due to sports injuries may, therefore, lead in the long term to degeneration of the tissue; this is one of the causes of osteoarthritis, which is a major cause of disability among the elderly (Steinert et al., 2007; Yang et al., 2009).

Many potential solutions for the treatment of cartilage defects have been investigated, leading to a wide variety of repair techniques being proposed over the years (Makris et al., 2015; Smith et al., 2005; Temenoff and Mikos, 2000). However, despite the researchers' efforts, no method for true regeneration of tissue has been found yet, and the quest for the successful induction of native-like hyaline cartilage is still ongoing(Hunziker et al., 2015). In this quest, tissue engineering is a promising and appealing approach.

Tissue engineering combines cells, scaffolds, and bioactive molecules to support, guide, and maintain the restoration of native tissue through controlled degradation rates that should balance with the process of tissue regeneration (Kuo et al., 2006). In particular, researchers have focused on providing an appropriate degradablematrix for cells to survive and differentiate.Hydrogels have shown to be suitable biomaterials for this purpose because of their intrinsic hydrated nature, their capacity to incorporate chemical cues, and their potential biocompatibility (Kuo et al., 2006; Slaughter et al., 2009). Before possible clinical application, *in vitro* tissue-engineered constructs need to be tested and, despite growing availability of *in silico* (Kock et al., 2012) and *ex vivo* (LeBaron and Athanasiou, 2000; Schwab et al., 2016) models, large animal models are still deemed essential as final proof of concept. In the case of orthopaedic disorders in general and cartilage repair in particular, the equine model has been often described as a very suitable model, as the articular cartilage in the equine stifle joint closely resembles that in the human knee with respect to thickness and biochemical composition, and both species present a very challenging mechanical environment (Malda et al., 2012; Mcllwraith et al., 2011)

A crucial issue in cartilage repair is the fixation of implants. A range of approaches has been reported in literature, but all have significant drawbacks. For example, fascial/periosteal flaps sutured over the defect cause osteoarthritis-like changes in adjacent cartilage (Hunziker and Stähli, 2008), and the use of transosseous sutures or biodegradable pins alters the architecture of 3Dscaffolds (Bekkers et al., 2010). While

it is possible to directly cast materials into defects, or to use hydrogels as a glue (Kerker et al., 2008), these techniques are laborious, difficult for translation to human clinics, and greatly limit the possibility to control the design of the implants.

Fibrin glue has been extensively described in literature as a fixation tool for various type of scaffolds for cartilage repair in animal models (Lind et al., 2008; Nixon et al., 2015) and is currently used in human clinics (Bekkers et al., 2013). It has the advantage of not physically altering either the scaffold or the tissues adjacent to the defect; however, its use is not uncontested. First, there may be a species issue. Brehm et al. described how the use of fibrin glue of human origin caused a massive cell infiltration in the subchondral bone of goats (Brehm et al., 2006). Although thus far not reported in literature, a similar situation may exist in the horse. Problems have been reported in studies where equine fibrin is used as a vehicle for cellular therapies in the horse (McIlwraith, pers. comm. 2016), including demonstration of the lack of ability for mesenchymal stem cells (MSCs) to migrate and proliferate in full strength fibrin and the requirement of dilution of the fibrin to allow these processes (Hale et al., 2012), and that the addition of MSCs to autologous platelet-enhanced fibrin scaffolds in chondral defects had inferior results to the platelet-enhanced fibrin scaffolds alone, including ossification of repair tissue (Goodrich et al., 2016). Second, there is increasing evidence that the use of (fiber) reinforcements in the hydrogels meant for cartilage repair may greatly enhance their efficacy and may even be indispensable (Visser et al., 2015). This poses an additional challenge to the fixation efficacy of sealants such as fibrin glue (Frenkel and Di Cesare, 2004; Knecht et al., 2007).

Given the importance of the equine model for joint-related disorders and the ethical pressure of reducing the number of animal experiments to the minimum, there is, therefore, a need for the critical assessment and, where possible, optimization of fixation methods for hydrogel-based scaffolds, with and without reinforcement, in an equine cartilage defect model.

The data presented in this article emanate from a series of pilot studies focusing on the optimization of the fixation of hydrogel-based scaffolds in (osteo) chondral defects. Starting with a widely described and seemingly harmless commercial fibrin glue (CFG) that is considered the standard for fixation, we discovered that use of the material in the specific equine large animal model is fraught with difficulties (study 1). Based on this observation, we proceeded to compare commercial and autologous fibrin glue (AFG) from an immunogenic point of view in an equine ectopic model (study 2). Finally, we compared the efficacy of the AFG with a custom-made alternative fixation method for specific fiber-reinforced hydrogel constructs based on a 3D-printed polycaprolactone (PCL)-based anchor for the fixation of PCL-reinforced hydrogels (study 3).

Materials and Methods

Animal experiments

1. Use of CFG for the fixation of hydrogel-based constructs in an orthotopic equine model

The study had been approved by the ethical and animal welfare from the Veterinary School at the National University of Costa Rica. Nine criollo horses (age 4–10 years, weight 275–375 kg) were used for surgery. The horses were free of lameness and without any clinical or radiographic evidence of acute or chronic injuries. They were housed in individual boxes and fed a standard maintenance ration of concentrate with hay *ad libitum* and free access to water.

General anesthesia was induced with diazepam (0.05 mg/kg), ketamine (2.2 mg/kg), and lidocaine (2 mg/kg), after premedication with acepromazine (0.025 mg/kg) and xylazin (1.1 mg/kg); anesthesia was maintained with isoflurane in oxygen with an end tidal concentration of 1.0–1.5%. The medial trochlear ridge of the stifle joint was exposed by arthrotomy through a subpatellar approach; two fullthickness cylindrical cartilage defects with a diameter of 6mm were created using a manual drill guided by a drill sleeve. Remnants of cartilage in the defect were removed using a sharp surgical spoon. In each horse one of the defects was filled with 3D-printed porous constructs made of one of three different hydrogels (M10P10-HAMA,25 star- PEG/heparin (Knecht et al., 2007), and P(AGE/G)-HA-SH (Thorn et al., 2004), which had been previously tested both *in vitro* and *in vivo* for safety and biocompatibility and were deemed safe), so N= 3 per gel, and fixated with CFG (Tissucol_, Baxter), the other (control) defect was filled with fibrin glue (*0.3 mL) only (N= 9). The glue was allowed 10 min for cross-linking; the wound was then closed in four layers, and full weight bearing was allowed after recovery from anesthesia.

Postoperatively, horses received antibiotics for 3 days (procaine penicillin 15,000 IU/kg IM, SID, and gentamicin 6.6 mg/kg IV, BID) and nonsteroidal anti-inflammatory drugs (phenylbutazone 2.2 mg/kg, PO BID) during the first 5 days. The animals were subjected to daily monitoring of clinical parameters (temperature, heart rate, and respiratory rate). After 7, 14, and 28 days (n = 3 with one animal/gel per time point), the horses were euthanized, and the stifle joints were harvested, fixated in formalin 4%, and processed for histology.

2. Comparison of commercial and AFG in an equine ectopic model

This study aimed at comparing the *in vivo* tissue reaction, safety, and degradation of commercial and AFG in an ectopic equine model. This study had been approved

by the Ethics Committee for Animal Experimentation of Utrecht University and was performed in accordance with the Institutional Guidelines on the Use of Laboratory Animals in compliance with the Dutch Act on Animal Experimentation.

AFG production. The protocol for production of the fibrin component of the fibrin glue was obtained by adapting the method described by Thorn et al., 2004. with the addition of a cryoprecipitation step to enhance fibrin precipitation (Cavichiolo et al., 2013).

A blood sample (40mL) was collected from each animal in a tube previously filled with heparin (20 IU/mL of blood) and medical grade citrate to obtain a citrate concentration of 3.2%. The plasma was separated by centrifugation for 18min at 400 g at room temperature. The top half of the plasma layer was then transferred by pipetting into a new tube, carefully avoiding the surface containing platelets. Cryoprecipitation was performed by storing overnight the sample at -20˚C.28 The sample was then allowed to thaw at room temperature; next, we initiated precipitation by adding 176 µL of 100% ethanol and, subsequently, mixing by inversion and placing the plasma on ice for 20min. Centrifugation for 10 min at 1000 g followed to allow formation of a fibrin pellet on the bottom of the tube.27 The pellet was isolated, warmed at 37˚C to allow solubilization, and loaded in a two-syringe system together with a commercially available thrombin solution (TISSEEL™; Baxter). The system was kept at 37˚C with warm water and transferred to the surgical theater.

Surgical procedure. Two adult equines were sedated with detomidine (10 mg/kg). Under local anesthesia achieved by subcutaneous injection of 1mL of mepivacaine solution (20mg/ mL) in the dorsal region of the neck, a series of subcutaneous pockets were created through small incisions on the skin (6 x, ~ 10mm in length). A small quantity of 0.3mL of fibrin glue (commercial or autologous, randomized, n = 3) was deposited in each pocket and allowed to cross-link for 5 min, after which the wounds were sutured.

Animals were monitored daily for signs of reaction (temperature, swelling, and general aspect of incision area). After 14 days, the two animals were euthanized by administration of pentobarbital (50 mg/kg of body weight), and the entire soft tissue area containing the constructs was harvested for analysis.

3. Comparative fixation study with AFG and 3D-printed osteal PCL anchor in an equine orthotopic model.

This study aimed at comparing the fixation potential of two techniques (osteal anchor and AFG) for the fixation of reinforced hydrogel-based scaffolds intended to be used

for articular cartilage repair. These studies had been approved by the Local Ethics Committee for Animal Experimentation of Utrecht University and were performed in accordance with the Institutional Guidelines on the Use of Laboratory Animals in compliance with the Dutch Act on Animal Experimentation.

Preparation of osteal anchor. Osteochondral plugs were fabricated by extrusion-based 3D printing of GMP-grade PCL (Purasorb ® PC 12, Corbion, The Netherlands) using a screw-based extruder on a 3D Discovery printer (regenHU, Switzerland). The osteochondral plug was designed on BioCAD software (regenHU) as a cylinder with 6mm diameter, featuring a square-grid scaffold structure with six zones with different porosities. The lower zones were designed for bone osteoconduction and formed a gradient of decreasing porosity from the bottom to the top, mimicking the transition from trabecular to cortical bone. The top zone of the scaffold represented the endochondral interface and was designed as completely closed to separate the hydrogel materials for cartilage repair from the osteal anchor (Fig. 1A). The uppermost zone in the osteochondral plug was designed for fiber reinforcement of the chondral portion (Fig. 1B), to enhance fixation of the hydrogels and to increase biomechanical resistance of the chondral layer (Schuurman et al., 2011).

Before printing, the PCL was first molten in the extruder heating tank at 90°C for at least 30 min to ensure consistent material viscosity. The osteochondral plugs were then fabricated using the following printing parameters: feeding pressure of 0.5 bar, 32G extrusion nozzle, temperature of 80°C, spindle speed of 4 rpm, and printing speed of 4 mm/s.

Preparation of chondral and osteochondral hydrogel reinforced constructs for implantation. To compare fixation potential of AFG and PCL osteal anchor, reinforced hydrogel constructs were prepared. The hydrogels selected for this purpose were M10P10-HAMA (Mouser et al., 2017), starPEG/heparin (Hesse et al., 2017), and P(AGE/G)-HA-SH (Stichler et al., 2016).
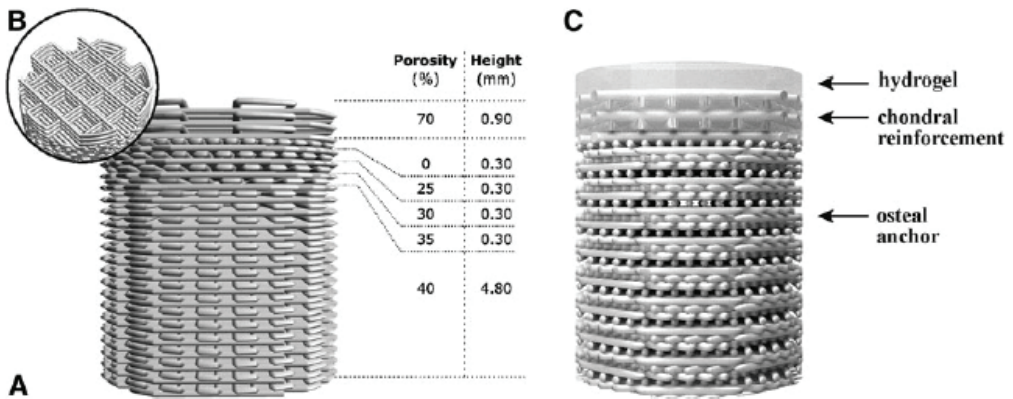
FIG. 1. The osteal anchor was designed to have a decreasing porosity leading to a closed interface between the osteal and chondral parts of the construct, to mimic the natural architecture of the subchondral bone (A), as showed in the 3D-model of the PCL-based anchor design (A). A fiber reinforcement was added in the chondral layer to enhance fixation of hydrogel materials and biomechanical resistance of the chondral layer (B). The hydrogel materials can be cast on top (C). AFG, autologous fibrin glue; PCL, polycaprolactone.

Preparation of chondral and osteochondral hydrogel reinforced constructs for implantation. To compare fixation potential of AFG and PCL osteal anchor, reinforced hydrogel constructs were prepared. The hydrogels selected for this purpose were M10P10-HAMA (Mouser et al., 2017), starPEG/heparin (Hesse et al., 2017), and P(AGE/G)-HA-SH (Stichler et al., 2016).

The osteochondral plugs were inserted into a polytetrafluoroethylene (teflon) custom-made mould of 7.5mm height. This system allowed to cast hydrogel materials in a confined area, thus obtaining a uniform layer integrated with the osteal anchor (Fig. 1C). Casting of M10P10-HAMA and P(AGE/G)-HA-SH was performed infusing 0.42 µL of polymer solution mixed with a photoinitiator (0.05% w/w, Irgacure ®2959; BASF, Ludwigshafen, Germany). Subsequently, chemical cross-linking was induced with a UV lamp at 3 cm distance (UV-Handleuchte Lamp, A. Hartenstein, Germany; wavelength: 365 nm, intensity at 3 cm: 1.2 mW/cm^2). Casting of starPEG/heparin was achieved by mixing equal quantities of the two polymer solutions, which then cross-linked by click reaction.

To allow direct comparison of the two fixation methods, including AFG, the hydrogels were cast in a mould of 1.5mm height together with the PCL reinforcement following the methodology previously described. The constructs were then transported to the surgical theater for implantation.

Surgical procedure. Three Shetland ponies (age 3–10 years, weight 170–240 kg) were used. The horses were free of lameness and without any clinical evidence of acute or chronic injuries. They were housed in individual boxes and fed a standard maintenance ration of concentrate with hay ad libitum and free access to water.

Two defects were made in the medial trochlear ridge of the femur of each stifle joint. On one side, hydrogel based reinforced constructs were implanted and fixated with AFG (N = 2 per joint, distally and proximally, one material for each animal); on the contralateral side, the same constructs were implanted and fixated with the osteal anchor.

General anesthesia was induced with midazolam and ketamine intravenously (0.06 + 2.2 mg/kg), after premedication with detomidine and morphine (10 mcg/kg +0.1 mg/kg); anesthesia was maintained with isoflurane in oxygen with an end tidal concentration of 1.0–1.5%. The medial trochlear ridge of the stifle joint was exposed by arthrotomy through a subpatellar approach; on one side two full-thickness cylindrical cartilage defects with a diameter of 6mm were created using a drill guided in a drill sleeve. On the contralateral side two osteochondral defects with a diameter of 6mm and a depth of 7.5mm were created using a surgical drill guided with a 7.5mm custom-made drill. Defects fixated with fibrin glue were filled with 0.2mL of AFG, prepared as described previously, after which the hydrogel construct was immersed in the defect and left to sit for 10 min to allow cross-linking and fixation. On the contralateral side, the osteal anchor with the hydrogel constructs was inserted press fit into the defects.

The wounds were then closed in 4 layers, and full weight bearing was allowed after recovery from anesthesia. Postoperatively, the ponies received NSAIDS (meloxicam, 0.6 mg/kg, PO, BID-SID) up to 7 days and opiates (tramadol, 5 mg/kg, PO, BID-SID) up to 3 days postoperatively. For antibiotic prophylaxis, ampicillin (10–15 mg/kg) was administered intravenously once before and procaine penicillin (20 mg/kg, IM) once after surgery.

Clinical parameters of the animals were monitored daily for signs of inflammation and lameness. After 14 days, the animals were euthanized by administration of pentobarbital (50 mg/kg of body weight), and the entire osteochondral area containing the constructs was harvested for analysis with the aid of a surgical bone saw.

With the aim of evaluating the bone integration for a longer period, a follow-up study of 4 weeks was performed on three other ponies (age 4–10 years, weight 190–240 kg), where only the PCL osteal anchor implantation was performed bilaterally, following the methodology described above.

Postmortem processing

Microcomputed tomography. Each construct with osteal anchor was scanned before and after implantation in a micro- CT scanner (m-CT 80, Scanco Medical AG, Switzerland) at a resolution of 20 µm. All defects were scanned postmortem. The acquisition parameters were set to a voltage of 70 kVp, an intensity of 114 mA, and an integration time of 300ms. Subsequently, the acquired images were processed by first applying a Gauss filter (sigma = 2, support = 0.8 voxel) and then segmentation. A global threshold of 55 and 120/mile was used for the constructs before and after implantation, respectively. The segmented images of the constructs before implantation were also used to determine the porosity of the printed chondral reinforcement and osteal region. The adjacent healthy bone tissue was also scanned. The images obtained were processed with ImageJ to obtain the bone volume data before and after implantation.

Histological processing and stainings. Soft tissue samples were fixated in 4% formalin, dehydrated through a graded ethanol series, cleared in xylene, and embedded in paraffin. Osteochondral samples for histology were fixated in 4% formalin, decalcified with Formical-2000 (EDTA/ formic acid; Decal Chemical Corporation, Tallman, NY) for 14 days, dehydrated through a graded ethanol series, cleared in xylene, and embedded in paraffin. Samples were sectioned into 5 mm slices and stained with hematoxylin and eosin (HE) to allow for morphological analysis and the evaluation of tissue-scaffold integration according to a modified Drobnic's scoring (Bekkers et al., 2010; Drobnicˇ et al., 2006) and cell infiltration using an Olympus BX51 light microscope. Samples were also stained with picrosirius red and analyzed with polarized light microscopy for visualization of collagen fibril orientation.

Results

1. The use of CFG for the fixation of hydrogel-based constructs in an orthotopic equine model

Clinical parameters of the animals were normal for the duration of the experiment, with no evidence of lameness or inflammation.

Macroscopically, all defects were filled with tissue. Microcomputed tomography (micro-CT) showed signs of bone loss in the subchondral area directly beneath the defect, irrespective of the hydrogel used (Fig. 2). There was some individual variability, but the phenomenon was seen in all
horses. In addition, no correlation with specific implanted materials was found. This bone loss (Fig. 3A–D; Supplementary Table S1 and S2; Supplementary materials available at http://www.liebertpub.com/tec) was also consistently visible in all control defects only filled with the fibrin glue (Fig. 3E–H). At histology, the middle of the defect

displayed an area of bone reaction surrounding the site of bone loss (Fig. 3C, G). As shown by the HE staining, this reaction was characterized by infiltration of fibroblasts and predominantly neutrophil granulocytes (Fig. 3D, H).
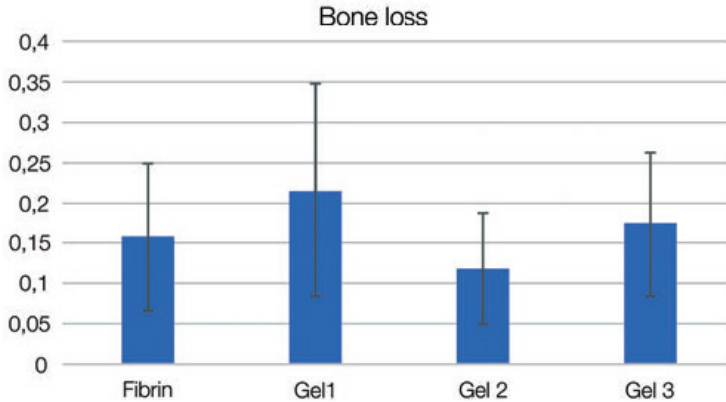

FIG. 2. Bone volume loss from study 1. The area beneath the defects and healthy adjacent tissue was scanned postmortem with micro-CT imaging. Images obtained were processed with ImageJ to obtain bone volume values before and after implantation. Statistical analysis showed no correlation of bone loss with any of the materials. micro-CT, microcomputed tomography. Color images available online at www.liebertpub.com/tec
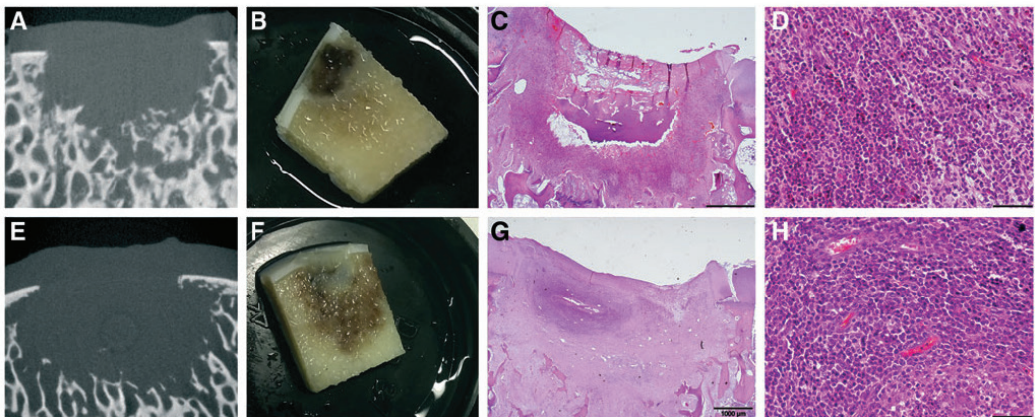
FIG. 3. Inflammatory reaction in control defects filled with CFG (14 days postoperatively). First and second rows show representative examples from two different animals. micro-CT imaging showed loss of the trabecular structure and bone resorption (A, E). Upon sectioning the bone loss was confirmed, and a reaction of the surrounding area with inflammation was visible to the naked eye (B, F). HE staining showed a focal reaction (C, G) with recruitment of neutrophil granulocytes with loss of architecture and bone structure (D, H). CFG, commercial fibrin glue; HE, hematoxylin and eosin. Color images available online at www.liebertpub.com/tec

2. Comparison of commercial (CFG) and AFG in an equine ectopic model

No local or systemic adverse reactions were observed in the horses during the experiment. Upon harvest, the excised tissue appeared macroscopically normal. Histological evaluation with HE staining of the CFG showed that the glue was clearly identifiable within the tissue (Fig. 4; Supplementary Fig. S2). It appeared contracted and was surrounded by a front of neutrophil granulocytes (Fig. 4A, arrow). The AFG was not clearly identifiable through different sections of the implantation area, although a structure compatible with its expected appearance was detected in the soft tissue (Fig. 4B, C). The neighboring tissue did not display any abnormal cell infiltration.
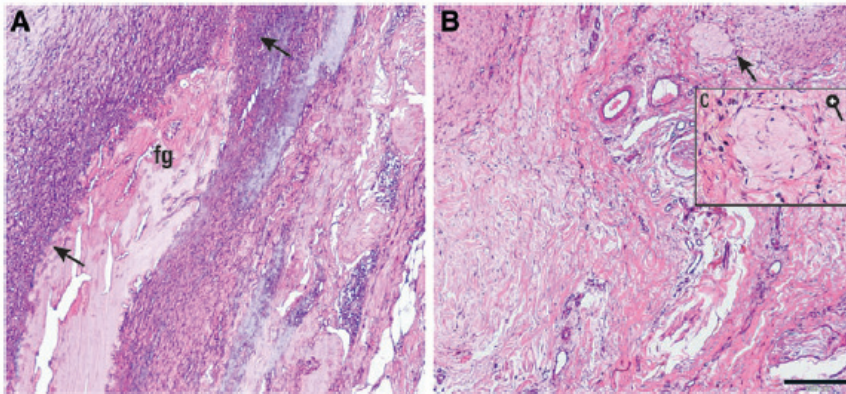
FIG. 4. Histological sections of commercial (A, left) and autologous (B, right) fibrin glue, implanted in an equine ectopic model for 14 days. CFG appears contracted and is easily recognizable (A, fg); the glue is surrounded by a front of neutrophil granulocytes (A, black arrows); this is not present in the area where the autologous fibrin was implanted (B), where some macrophages and fibroblasts are present (C) (black bar = 200 m). Color images available online at www.liebertpub.com/tec

3. Comparative fixation study with AFG and 3D-printed osteal PCL anchor in an equine orthotopic model

PCL osteal anchor and constructs for implantation. 3D osteochondral constructs with a hierarchical porous architecture were successfully fabricated by means of an extrusion-based 3D printing technique (Fig 5).
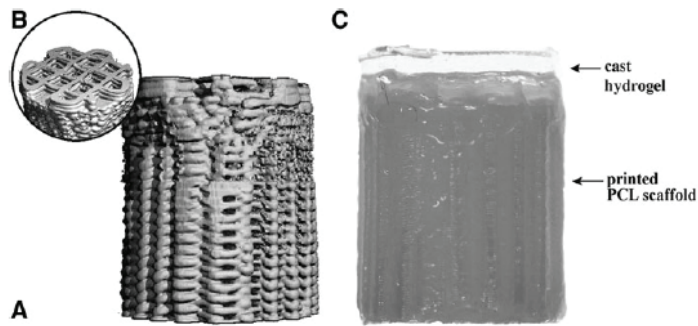
FIG. 5. micro-CT 3D render of the osteochondral anchor before implantation (lateral view, A and top view, B) showing the closure of the layers to allow casting of hydrogels. Aspect of the PCL-based osteal anchor with cast hydrogel on top before implantation (C).

Design (Fig. 1) and built architecture (Fig. 5A) revealed the high accuracy of the printing technique. From the micro-CT data of the printed constructs porosity was also assessed and compared to the design values. Chondral and osteal regions showed porosities of 32%±3% (designed 40%) and 66%±2% (designed 70%), respectively. Furthermore, the 3D reconstructions showed that interconnected pores are presented on the lateral surface of the constructs (Fig. 5A). This is an important factor for the successful mechanical interlocking between the osteal anchor and surrounding natural bone tissue at construct/bone interface.

Animal study
Surgical implantation of the constructs was successful. AFG was kept at 37˚C before implantation, and mixed with the thrombin solution in the defect, to allow immersion of the hydrogel reinforced constructs (Fig. 6A, B). Osteochondral constructs were fixated by press fit, exerting pressure with a forceps on the PCL osteal anchor to avoid damage to the hydrogel portions (Fig. 6C, D).

In the 2-week study all animals had an uneventful course of the experiment, temperature and other clinical parameters were well within normal range. However, when challenged by a flexion test, one animal showed some signs of discomfort on the limb in which the scaffolds had been fixated with the osteal anchor.
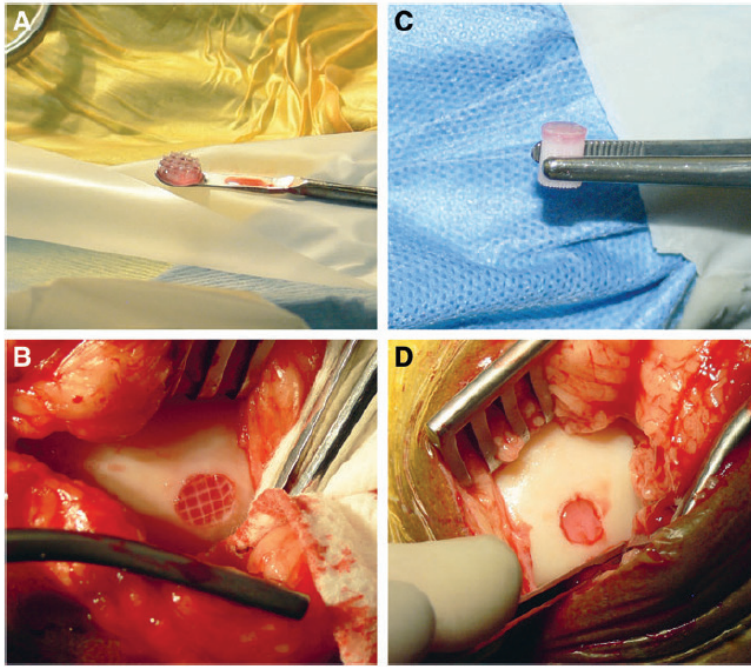
FIG. 6. Surgical implantation of materials for comparison of fixation with fibrin glue (left) versus osteal anchor (right). The reinforced hydrogel (A) was implanted in a full-thickness chondral defect and fixated with autologous fibrin glue (B). The hydrogel with PCL osteal anchor (C) was inserted in the osteochondral defect and secured by press fit (D). Color images available online at www.liebertpub.com/tec

At postmortem, the 2-week study comparing the two fixation techniques showed that the fixation potential of AFG was inferior compared to the PCL osteal anchor. Although in two out of three animals AFG could keep the reinforced constructs in place, in one animal both defects were empty. Moreover, in the remaining four defects, the constructs displayed evidence of slipping out of the defects (Fig. 7A). All six hydrogels with PCL reinforcement fixated by means of the PCL anchor were still in place after 2 weeks (Fig. 7D). In the single animal that showed discomfort at the flexion test, the soft tissue opposing the defect showed signs of inflammation.
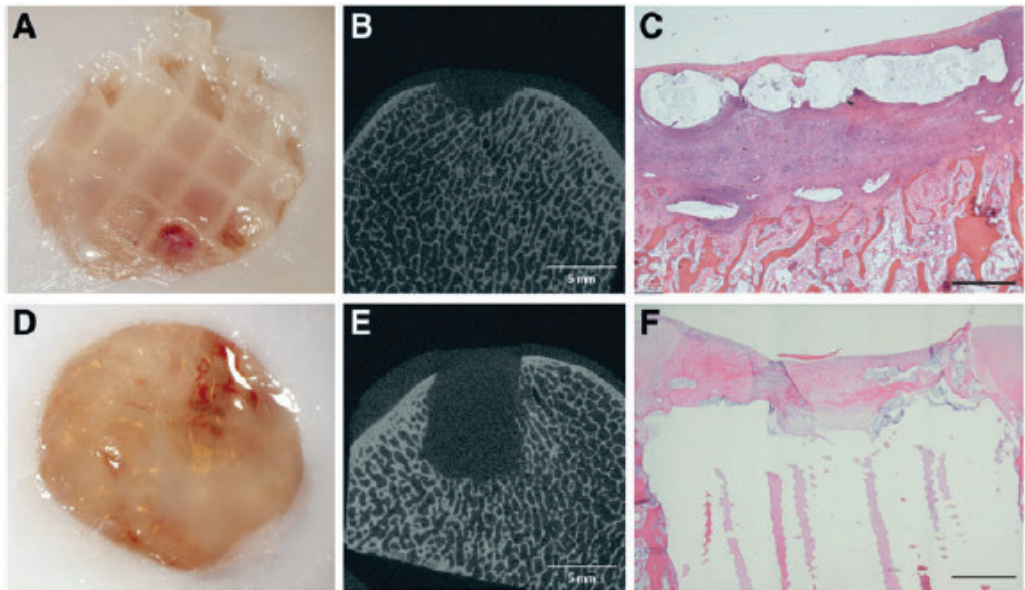
FIG. 7. Fixation potential of two techniques, autologous fibrin glue (top) and PCL osteal anchor (bottom), 14 days after implantation. Reinforced chondral constructs appeared still in place in two of three cases; however, the scaffolds looked as if they were starting to slip out proximally (A). micro-CT of AFG fixation showed some bone resorption (B), confirmed by the HE staining (C), which showed loss of architecture directly underneath the defect with significant infiltration of neutrophil granulocytes and fibroblasts. Constructs fixated with the PCL anchor were all still in place (D), and micro-CT imaging showed a conserved trabecular architecture surrounding the construct (E). The chondral portion of the defect appears filled with repair tissue with a predominance of fibroblasts (F) (Black bar = 1mm). Color images available online at www.liebertpub.com/tec

Micro-CT of the defects and surrounding area in the AFG group (Fig. 7B) showed again the subchondral inflammatory reaction that had been observed in the first study in which CFG had been used, although to a lesser extent. The defects in the PCL group showed no signs of bone reaction (Fig. 7E). Semiquantitative fixation scores showed that PCL gave better results both from an attachment point of view and from a scaffold integrity aspect (Table 1). One-way ANOVA confirmed a significant difference between the two groups ($p < 0.05$).

Table 1. Criteria for Fixation Scoring According to a Modified Drobnic Scoring

Outline attachment	Area coverage	Scaffold integrity
Unchanged (5)	Unchanged (5)	Unchanged (5)
<25% (4)	<75-100% (4)	Minor deformities unrelated to fixation (4)
25-50% (3)	50-75% (3)	Minor cracks close to fixation site (3)
50-75% (2)	25-50% (2)	Fissures that jeopardize the fixation (2)
75-100% (1)	<25% (1)	Fissures and scaffold disorganization in outer area (1)
100% (0)	0% (0)	Fissures and scaffold disorganization in general (0)
	AFG	PCL
Outline attachment	1.7 ± 1.50	4.8 ± 0.41
Area coverage	2.7 ± 2.06	4.8 ± 0.41
Scaffold integrity	2 ± 1.79	4 ± 0
Total score	6.3 ± 5.12	13.7 ± 0.82*

Scores show the difference between AFG and PCL efficacy in fixation. AFG shows high variability in results; overall efficacy for fixation with PCL was significantly higher than with AFG (*$p < 0.05$). AFG, autologous fibrin glue; PCL, polycaprolactone.

Histological analysis confirmed the findings from the micro- CT. In the AFG group, an inflammatory response was observed in the bone underlying the defect, characterized by the presence of fibroblastic cells, neutrophils, and multinucleated cells (Fig. 7C). Bone resorption was consistently present in all defects. In the PCL group, a fibroblast-based infiltration from the bone surrounding the osteal part of the plug was observed, to a degree that can be expected after implanting an osteal scaffold (Fig. 7F; Supplementary Fig. S1).

In the follow-up 4-week study none of the animals showed any clinical sign. micro-CT imaging showed signs of mineralization within the PCL osteal anchor (Fig. 8A), which was confirmed upon histology (Fig. 8B, C).
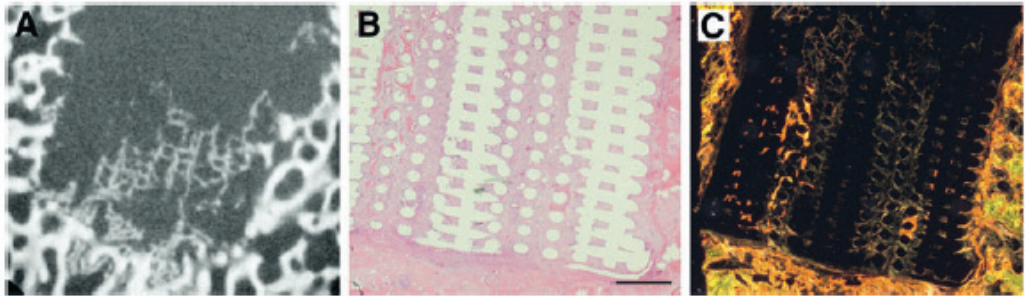
FIG. 8. Bone regeneration after 28 days. micro-CT imaging showed signs of mineralization and new bone formation within the PCL osteal anchor (A). HE staining showed good integration of the anchor with the surrounding tissue (B) and picrosirius red staining under polarized light confirmed presence of new bone (C) (Black bar = 1 mm). Color images available online at www.liebertpub.com/tec

Discussion

In the quest for the optimal tissue-engineered construct that can be implanted in an articular cartilage defect to incite regeneration of the tissue, the fixation of such constructs within the surrounding non-degraded native tissue is a pivotal issue. Improper fixation will inevitably lead to implant failure, irrespective of the qualities of the materials and/or cells that are to be tested (Hutmacher, 2000). In large animal models, fixation is especially important as loading is almost immediate after surgery and as constructs are exposed to substantial biomechanical compressive and shear forces.

Thus far, the focus in the field has predominantly been directed at material development, production methods (e.g., 3D bio-printing), structural aspects of the construct (e.g., zonal composition), and cellular aspects (e.g., use of differentiated versus undifferentiated cells) (Groen et al., 2017; Huey et al., 2012), but surprisingly little attention has been given to the fixation of the implants.

In the advanced techniques used for cartilage defect repair in human healthcare, such as autologous chondrocyte implantation (ACI) and matrix-assisted ACI, the use of fibrin glue is regarded as the gold standard for fixation of implanted cells and/or materials (Bekkers et al., 2013; Cucchiarini et al., 2014; Kon et al., 2012). For this purpose, commercially available fibrin glue obtained from human blood components is used. In many animal studies in which various types of implants for cartilage repair were assessed, this practice has been copied without further investigation, notwithstanding the fact that by doing so the use of fibrin glue changed from allogeneic in humans to xenogeneic in any other animal (Lind et al., 2008; Marmotti et al., 2013; Nixon et al., 1999). Long-term results in some studies did not give rise to suspicions that the

use of CFG might have negative side effects (Nixon et all., 2015), but no short-term assessments of a possible acute reaction to the product have been performed and there were some indications that the use of the product might be less innocuous than assumed in both goats and horses (McIlwraith, pers. comm. 2016).

In this article we present data from a series of short-term studies that were originally executed as preliminary work for long-term experiments focusing on the assessment of hydrogels for cartilage repair. (Supplementary Table S3) Well aware of the limitations of these studies that were originally never meant to be stand-alone studies, we nevertheless felt it useful to report the outcome to the scientific community, given the unexpected events at short term after implantation that came to light, the importance of construct fixation in cartilage repair, and the need to avoid as much unnecessary wastage of experimental animals as possible.

In the first orthotopic study the panel of cells that had infiltrated the defects in which CFG had been used for fixation showed a large predominance of neutrophils that suggest a recruitment of inflammatory cells far beyond expectations 1–4 weeks post-implantation. The most striking point was that this inflammatory reaction, which was accompanied by severe bone loss, was similar in all defects, irrespective of the hydrogel used. Two possible explanations for this phenomenon were formulated based on the observations and literature. The first potential explanation was that the use of xenogeneic material (human origin glue in an equine model) might have led to an inflammatory reaction based on an immune response, as had been supposed by Brehm (Brehm et al., 2006) in their goat model. Alternatively, the subchondral bone reaction might have been caused by the mechanical stress exerted by weight bearing on the exposed bone triggering a biological response (Fisher et al., 2014). Vasara (Vasara et al., 2004) described how a subchondral reaction with bone resorption was detected in goats, 3 months after implantation. Moreover, Kold (Kold et al., 1986) reported the formation of cystic lesions in the femoral condyle of horses after creating a slit-like lesion in the articular cartilage. Timewise, it might have been the case that in our study the bone did not have sufficient time to complete remodeling, and hence, the bone resorption was more evident than in other reported studies. Since bone remodeling occurs starting from the third or fourth week (White et al., 1977), it may even be possible that this phenomenon is more common than suspected, but may go undetected, as most large animal studies are longer than 4 weeks (Ahern et al., 2009). However, in our pilot study lesions were created on the medial trochlear ridge of the femur, which is an area that is not or hardly loaded during rest and only affected by principally shear forces during locomotion. For this reason, we focused first on the CFG as potential cause of the heavy reaction.

In order to carry out a study on the potential inflammatory effect of CFG, a procedure

for the production of AFG had to be developed. The use of partially AFG was deemed acceptable, as the most immunogenic component was suspected to be the one containing fibrinogen (Seegers, 2013). We, therefore, elected to still use the commercial thrombin component. While being successful, the efforts to develop a reproducible protocol yielding a usable product confirmed that the synthesis of AFG is laborious and subject to individual variation in concentration and characteristics, based on the animal's health, nutrition, and immune condition at the moment of blood collection (Meade et al., 1979). This results in a final product that is not standardized and that may introduce additional variation to the experiments. This is a disadvantage compared to the use of a commercially available fibrin glue that offers a ready-to-use consistent product.

The difference in cell recruitment observed in the ectopic model between the CFG and AFG strongly suggested that indeed the xenogeneic nature of the CFG resulted in an undesired inflammatory response. This response was clearly less prominent when using AFG, although not entirely nonexistent. This outcome suggests that the fibrin component may indeed have had a predominant role in the provocation of this response; however, it also hinted at the presence of some residual immunogenic effect, possibly caused by the still xenogeneic thrombin.

Given the fact that the use of this form of AFG was not also entirely reaction free and the inherent difficulty of the use of any type of fibrin glue for the fixation of fiber-reinforced scaffolds, a different approach was considered. The first part of the third study compared the efficacy of AFG versus an entirely different osteochondral concept for the fixation of fiber reinforced hydrogels for cartilage repair. Multicomposite scaffolds for cartilage regeneration envisage solving the problem of the relatively low stiffness that is inherent to hydrogels by altering the architecture of the scaffolds.

One of the approaches to overcome this is the use of fiber reinforcement (Schuurman et al., 2011). While this technology allows for the creation of scaffolds of which the stiffness approaches that of native cartilage (Visser et al., 2015), it poses an ulterior problem for the fixation of the scaffold. This is particularly important when treating chondral defects that are usually not more than 1–2mm deep and in which the risk of the reinforcing mesh being swept out by shear forces is real. For this reason, in this study the AFG-based fixation was compared to fixation of the mesh and hydrogel to an osteal anchor that itself was placed press fit in an osteochondral defect. The PCL osteal anchor was designed to mimic the natural architecture and transition of subchondral bone to cartilage. The reinforcement in the chondral portion was added to enhance integration and mechanical properties of the hydrogel cast on top. In this case, casting was used, but the design can easily be adapted to allow 3D co-printing of the hydrogel and reinforcement fibers (Schuurman et al., 2011).

The hydrogels used were the same as in the first study and all of them had been previously tested for safety and biocompatibility in the horse (data not shown), suggesting that the materials were not likely to cause reaction. The last fixation study showed that bone resorption was still an issue in the AFG, although the bone destruction seemed considerably less than in the case of CFG. It was concluded that apparently only replacing the fibrin component of the glue by an autologous product was not enough to avoid this unwanted side effect and/or that the influence of the mechanical component was larger than anticipated.

Another important finding was that the fixation potential of the AFG was apparently not enough to keep the fiber reinforcement in place in all cases. After 14 days 33% of the defects were empty, and the remaining constructs were in place but showed early signs of the mesh slipping out. In that aspect, the PCL fixation group showed more promising results, with a good integration of the anchor with the surrounding tissue at early stages, which were confirmed by the second, 4-week follow-up, study. The infiltration of the PCL osteal anchor by tissue and the formation of new bone suggest a good integration and adequate response of the native tissue to the construct. However, a long-term evaluation is necessary to confirm these preliminary findings and draw more definitive conclusions (Vindas Bolaños et al., 2017).

The PCL anchor technique solves the fixation issue, as the construct is kept in place by the press fit fixation of the anchor in the osteochondral defect, but it should be realized that this is a conceptually different approach that is valid only for osteochondral defects and not for chondral ones. There has been debate in literature whether chondral or osteochondral defects lead to better results in cartilage repair (Frisbie et al., 2003; Kold et al., 1986), but there is no consensus. An equine study in which the spontaneous repair after 1 year of standardized chondral and osteochondral lesions in the same animal was compared showed better cartilage healing in the osteochondral defects, but these also featured almost invariably subchondral bone changes, which were seen to a much lesser extent in the chondral lesions (Salonius, et al., 2018).

Taken together, it can be concluded from the pilot investigations reported in this study that the use of xenogeneic fibrin glue for the fixation of scaffolds intended for regeneration of articular cartilage can be advised against. The use of AFG reduces the unwanted side effects seen with the xenogeneic glue, but its fabrication process is tedious, susceptible to variability, and should probably focus on the manufacturing of an entirely autologous product, as use of a partly autologous product did not result in the complete avoidance of the inflammatory response. Even if this would be solved, the limited capacity of any type of fibrin glue to fixate composite scaffolds featuring fiber reinforcement remains an issue. The use of osteochondral plugs that are implanted press fit solves the fixation issue, but this versatile and relatively easy surgical approach implies the application of an entirely different concept of cartilage healing that includes the total osteochondral unit and not only the chondral part of the joint surface.

It is very well possible that in the near future, with the advent of sophisticated bioreactor systems that will be able to mimic physiological loading of joint tissues for prolonged periods, the need for large animal *in vivo* studies for the assessment of potential regenerative therapies for articular cartilage defects will decline. However, at this stage of orthopaedic research, no valid alternatives that can fully replace large animal models have been described yet (Cook et al., 2014; Chu et al., 2010) and the equine model is still considered as one of the most representative models available (Malda et al., 2012; McCoy, 2015). In these large animal models, fixation represents a fundamental issue and will continue to do so particularly in the perspective of future translation of composite scaffolds to clinical use, where obviously humans will be in first place, followed however by companion animals such as horses and dogs, which are in this respect not only experimental animals but also patients in their own right.

Disclosure Statement
No competing financial interests exist.

References

Ahern, B.J., Parvizi, J., Boston, R., Schaer, T.P., 2009. Preclinical animal models in single site cartilage defect testing: a sistematic review. Ostearthritis and Cartilage 17, 705-713.

Bekkers, J., Tsuchida, A., Malda, J., Creemers, L., Castelein, R., Saris, D., Dhert, W., 2010. Quality of scaffold fixation in a human cadaver knee model. Osteoarthritis Cartilage 18, 266-272.

Bekkers, J.E., Tsuchida, A.I., van Rijen, M.H., Vonk, L.A., Dhert, W.J., Creemers, L.B., Saris, D.B., 2013. Single-stage cell-based cartilage regeneration using a combination of chondrons and mesenchymal stromal cells comparison with microfracture. . Am J Sports Med 41, 2158-2166.

Brehm, W., Aklin, B., Yamashita, T., Rieser, F., Tru̇b, T., Jakob, R., Mainil-Varlet, P., 2006. Repair of superficial osteochondral defects with an autologous scaffold-free cartilage construct in a caprine model: implantation method and short-term results. Osteoarthritis Cartilage 14, 1214-1226.

Cavichiolo, J.B., Buschle, M., Carvalho, B., 2013. Comparison of fibrin adhesives prepared by 3 different methods. Arch Otorhinolaryngol 17, 62-65.

Cook, J.L., Hung, C.T., Kuroki, K., Stoker, A.M., Cook, C.R., Pfeiffer, F.M., Sherman, S.L., Stannard, J.P., 2014. Animal models of cartilage repair. Bone Joint Res 3, 89-94.

Cucchiarini, M., Madry, H., Guilak, F., Saris, D., Stoddart, M., KoonWong, M., Roughley, P.A., 2014. Vision on the future of articular cartilage repair. Eur Cell Mater 27, 12-16.

Chu, C.R., Szczodry, M., Bruno, S., 2010. Animal models for cartilage regeneration and repair. Tissue Eng Part B Rev 16, 105-115.

Drobnič, M., Radosavljevič, D., Ravnik, D., Pavlovčič, V., Hribernik, M., 2006. Comparison of four techniques for the fixation of a collagen scaffold in the human cadaveric knee. Osteoarthritis Cartilage 14, 337-344.

Fisher, M.B., Belkin, N.S., Milby, A.H., Henning, E.A., Bostrom, M., Kim, M., Pfeifer, C., Meloni, G., Dodge, G.R., Burdick, J.A., Schaer, T.P., Steinberg, D.S., Mauck, R.L., 2014. Cartilage Repair and Subchondral Bone Remodeling in Response to Focal Lesions in a Mini-Pig Model: Implications for Tissue Engineering. Tissue Engineering: Part A 21, 850-860.

Fox, A.J.S., Bedi, A., Rodeo, S.A., 2009. The Basic Science of Articular Cartilage: Structure, Composition, and Function. Sports Health 1, 461-468.

Frenkel, S.R., Di Cesare, P.E., 2004. Scaffolds for articular cartilage repair. Ann Biomed Eng 32, 26-34.

Frisbie, D.D., Oxford, J.T., Southwood, L., Trotter, G.W., Rodkey, W.G., Steadman, J.R., Goodnight, J.L., McIlwraith, C.W., 2003. Early events in cartilage repair after subchondral bone microfracture. Clin Orthop Relat Res 407, 215-227.

Goodrich, L.R., Chen, A.C., Werpy, N.M., Williams, A.A., Kisiday, J.D., Su, A.W., Cory, E., Morley, P.S., McIlwraith, C.W., Sah, R.L., 2016. Addition of Mesenchymal stem cells to autologous platelet-enhanced fibrin scaffolds in chondral defects. J Bone Joint Surg Am 98, 23.

Groen, W.M., Diloksumpan, P., van Weeren, P.R., Levato, R., Malda, J., 2017. From intricate to integrated: biofabrication of articulating joints. J Orthop Res 35, 2089-2097.

Hale, B.W., Goodrich, L.R., Frisbie, D.D., McIlwraith, C.W., Kisiday, J.D., 2012. Effect of scaffold dilution on migration of mesenchymal stem cells from fibrin hydrogels. Am J Vet Res 73, 313-318.

Hesse, E., Freudenberg, U., NiemietzT., Greth, C., Weisser, M., Hagmann, S., Binner, M., Werner, C., Richter, W., 2017. Peptide-functionalized starPEG/heparin hydrogels direct mitogenicity, cell morphology and cartilage matrix distribution in vitro and in vivo. J Tissue Eng Regen Med 12, 229-239.

Huey, D.J., Hu, J.C., Athanasiou, K.A., 2012. Unlike bone,cartilage regeneration remains elusive. Science 338, 917-921.

Hunziker, E.B., Lippuner, K., Keel, M., Shintani, N., 2015. An educational review of cartilage repair: precepts & practice–myths & misconceptions–progress & prospects. Osteoarthritis Cartilage 23, 334-350.

Hunziker, E.B., Stähli, A., 2008. Surgical suturing of articular cartilage induces osteoarthritis-like changes. Osteoarthritis Cartilage 16, 1067-1073.

Hutmacher, D.W., 2000. Scaffolds in tissue engineering bone and cartilage. Biomaterials 21, 2529-2543.

Kerker, J.T., Leo, A.J., Sgaglione, N.A., 2008. Cartilage repair: synthetics and scaffolds: basic science, surgical techniques, and clinical outcomes. Sports Med Arthrosc Rev 16, 208-216.

Knecht, S., Erggelet, C., Endres, M., Sittinger, M., Kaps, C., Stüssi, E., 2007. Mechanical testing of fixation techniques for scaffold-based tissue-engineered grafts. J Biomed Mater 83, 50.

Kock, L., van Donkelaar, C.C., Ito, k., 2012. Tissue engineering of functional articular cartilage: the current status. Cell Tissue Res 2012, 613-627.

Kold, S., Hickman, J., Melsen, F., 1986. An experimental study of the healing process of equine chondral and osteochondral defects. Equine Vet J 18, 18-24.

Kon, E., Filardo, G., Di Martino, A., Marcacci, M., 2012. ACI and MACI. Knee Surg 25, 17-22.

Kuo, C.K., Li, W.-J., Mauck, R.L., Tuan, R.S., 2006. Cartilage tissue engineering: its potential and uses. Current opinion in rheumatology 18, 64-73.

LeBaron, R., Athanasiou, K.A., 2000. Ex vivo synthesis of articular cartilage. Biomaterials 21, 2575-2587.

Lind, M., Larsen, A., Clausen, C., Osther, K., Everland, H., 2008. Cartilage repair with chondrocytes in fibrin hydrogel and MPEG polylactide scaffold: an in vivo study in goats. Knee Surg Sports Traumatol Arthrosc 16, 690-698.

Makris, E.A., Gomoll, A.H., Malizos, K.N., Hu, J.C., Athanasiou, K.A., 2015. Repair and tissue engineering techniques for articular cartilage. Nat Rev Rheumatol 11, 21-34.

Malda, J., Benders, K.E.M., Klein, T.J., de Grauw, J.C., Kik, M.J.L., Hutmacher, D.W., Saris, D.B.F., van Weeren, P.R., Dhert, W.J.A., 2012. Comparative study of depth-dependent characteristics of equine and human osteochondral tissue from the medial and lateral femoral condyles. Ostearthritis and Cartilage 20, 1147-1151.

Marmotti, A., Bruzzone, M., Bonasia, D.E., Castoldi, F., Von Degerfeld, M.M., Bignardi, C., Mattia, S., Maiello, A., Rossi, R., Peretti, G.M., 2013. Autologous cartilage fragments in a composite scaffold for one stage osteochondral repair in a goat model. Eur Cell Mater 26, 15-31.

McCoy, A., 2015. Animal models of osteoarthritis comparisons and key considerations. Vet Pathol 52, 803-818.

McIlwraith, W.C., Fortier, L.A., Frisbie, D.D., Nixon, A.J., 2011. Equine Models of Articular Cartilage Repair. Cartilage 2, 317-326.

Meade, T., Chakrabarti, R., Haines, A., North, W., Stirling, Y., 1979. Characteristics affecting fibrinolytic activity and plasma fibrinogen concentrations. Br Med J 1, 153-156.

Mouser, V.H., Abbadessa, A., Levato, R., Hennink, W.E., Vermonden, T., Gawlitta, D., Malda, J., 2017. Development of a thermosensitive HAMA-containing bio-ink for the fabrication of composite cartilage repair constructs. Biofabrication 9, 015026.

Nixon, A.J., Fortier, L.A., Williams, J., Mohammed, H., 1999. Enhanced repair of extensive articular defects by insulinlike growth factor-I-laden fibrin composites. J Orthop Res 17, 475-487.

Nixon, A.J., Rickey, E., Butler, T.J., Scimeca, M.S., Moran, N., Matthews, G.L., 2015. A chondrocyte infiltrated collagen type I/III membrane (MACI® implant) improves cartilage healing in the equine patellofemoral joint model. Osteoarthritis and Cartilage 23, 1-13.

Salonius, E., Rieppo, L., Nissi, M.J., Pulkkinen, H.J., Brommer, H., Brünott, A., Silvast, T.S., P. René Van Weeren, P.R., Muhonen, V., Brama, P.J., Kiviranta, I., 2018. Critical-sized cartilage defects in the equine carpus. Connective Tissue Research, 1-12.

Schuurman, W., Khristov, V., Pot, M.W., van Weeren, P.R., Dhert, W.J., Malda, J., 2011. Bioprinting of hybrid tissue constructs with tailorable mechanical properties. Biofabrication 3, 1-7.

Schwab, A., Kock, L., Mouser, V.H.M., Stichler, S., Abbadessa, A., Schro¨n, F., Hansmann, F., Ehlicke, F., Walles, F., 2016. Screening novel hydrogels in an ex vivo cartilage defect model. Eur Cells Mater 31, 7.

Seegers, W.H., 2013. Blood Clotting Enzymology, New York. London, Academic Press.

Slaughter, B.V., Khurshid, S.S., Fisher, O.Z., Khademhosseini, A., Peppas, N.A., 2009. Hydrogels in regenerative medicine. Adv Mater 21, 3307-3329.

Smith, G., Knutsen, G., Richardson, J.A., 2005. Clinical review of cartilage repair techniques. Bone Joint J 87, 445-449.

Steinert, A.F., Ghivizzani, S.C., Rethwilm, A., Tuan, R.S., Evans, C.H., No¨th, U., 2007. Major biological obstacles for persistent cell-based regeneration of articular cartilage. Arthritis Res Ther 9, 804-814.

Stichler, S., Bertlein, S., Ju¨ngst, T., Bo¨ck, T., Hesse, E., Renz, Y., Seebach, E., Mancini, I., Van Weeren, R., Richter, W., 2016. Thiol-ene cross-linked polyglycidol-hyaluronic acid hybrid hydrogels: preparation, cell loading, 3D printing, and in vivo evaluation. Front Bioeng Biotechnol, In: Conference abstract: 10th World Biomaterials Congress.

Temenoff, J.S., Mikos, A.G., 2000. Review: tissue engineering for regeneration of articular cartilage. Biomaterials 21, 431-440.

Thorn, J., Sørensen, H., Weis-Fogh, U., Andersen, M., 2004. Autologous fibrin glue with growth factors in reconstructive maxillofacial surgery. Int J Oral Maxillofac Surg 33, 95-100.

Vasara, A.I., Hyttinen, M.M., Lammi, M.J., Lammi, P.E., La°ngsjo¨, T.K., Lindahl, A., Peterson, L., Kelloma¨ki, M., Konttinen, Y.T., Helminen, H.J., 2004. Subchondral bone reaction associated with chondral defect and attempted cartilage repair in goats. Calcif Tissue Int 74, 107-114.

Vindas Bolaños, R.A., Cokelaere, S.M., Estrada McDermott, J.M., Benders, K., E.M., Gbureck, U., Plomp, S.G.M., Weinans, H., Groll, J., van Weeren, P.R., Malda, J., 2017. The use of cartilage decellularized matrix scaffold for the repair of osteochondral defects: the importance of long-term studies in large animal model. Ostearthritis and Cartilage 25, 413-420.

Visser, J., Melchels, F.P., Jeon, J.E., Van Bussel, E.M., Kimpton, L.S., Byrne, H.M., Dhert, W.J., Dalton, P.D., Hutmacher, D.W., Malda, J., 2015. Reinforcement of hydrogels using three-dimensionally printed microfibres. Nat Commun 6.

White, A.A., Panjabi, M., Southwick, W., 1977. The four biomechanical stages of fracture repair. J Bone Joint Surg Am 59, 188-192.

Yang, Z., Shi, Y., Wei, X., He, J., Yang, S., Dickson, G., Tang, J., Xiang, J., Song, C., Li, G., 2009. Fabrication and repair of cartilage defects with a novel acellular cartilage matrix scaffold. Tissue Eng Part C Methods 16, 865-876.

Supplementary material
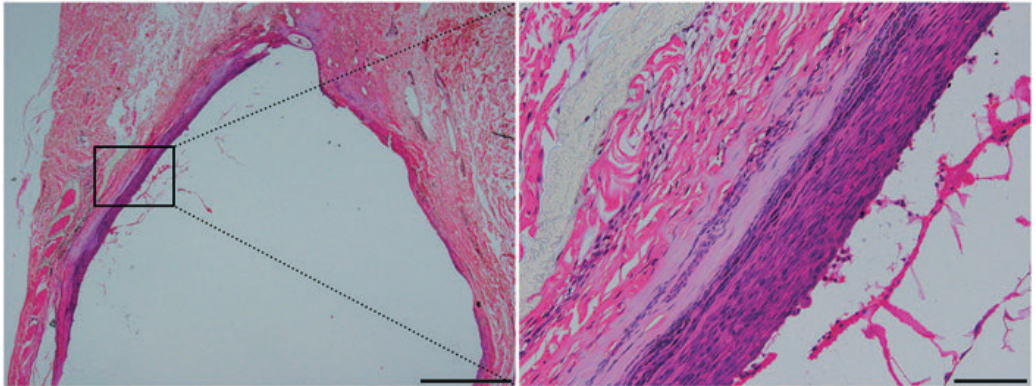
Supplementary fig S1. Histological section of tissue surrounding PCL after implantation in an equine ectopic model for 14 days. PCL is dissolved during processing of sections, and the remaining front of contact appears infiltrated mostly by fibroblasts, some macrophages, and neutrophils (right black bar = 200, left black bar = 100). PCL, polycaprolactone.
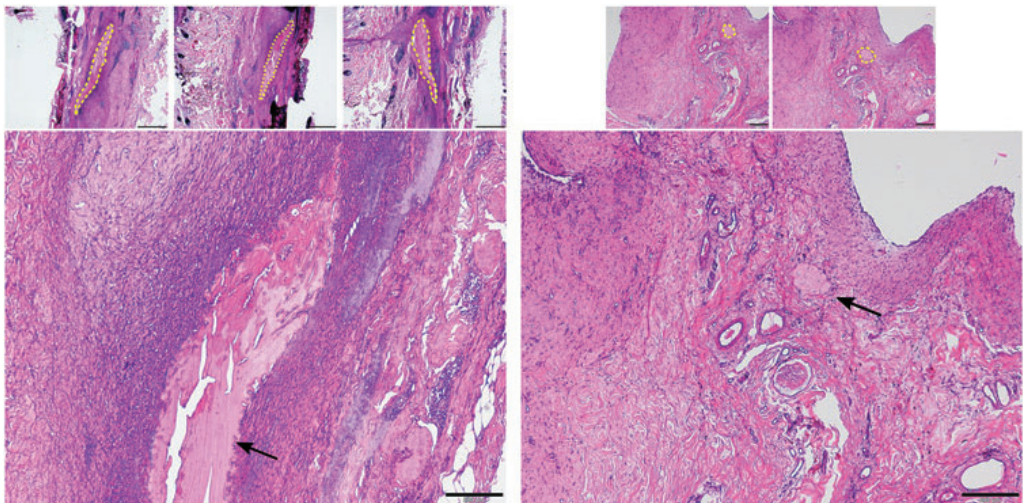
Supplementary fig S2. Figure 4 alternative with outlines and illustration of three-dimensional aspect of constructs throughout the tissue.

Supplementary Table S3

Study	N. animals	Location	Duration	Findings and conclusions
Fixation potential of CFG for hydrogel based constructs	9	Orthotopic	1-2-4 weeks	Some bone loss was detected in all defects, independently of time, material or animal. Only common factor was CFG, used in all defects.
Comparison of CFG and AFG	2	Ectopic	2 weeks	Cell recruitment in CFG showed prevalence of neutrophils and macrophages. AFG degraded more rapidly and was difficult to detect, less immune cells recruitment.
Comparison of fixation potential of AFG and PCL osteal anchor	3	Orthotopic	2 weeks	Fixation of constructs with AFG proved to be less efficient than with osteal anchor.

Chapter VI

The use of a cartilage decellularized matrix scaffold for the repair of osteochondral defects: the importance of long-term studies in a large animal model

Summary

Objective: To investigate the effect of decellularized cartilage-derived matrix (CDM) scaffolds, by itself and as a composite scaffold with a calcium phosphate (CaP) base, for the repair of osteochondral defects. It was hypothesized that the chondral defects would heal with fibrocartilaginous tissue and that the composite scaffold would result in better bone formation.

Methods: After an 8-week pilot experiment in a single horse, scaffolds were implanted in eight healthy horses in osteochondral defects on the medial trochlear ridge of the femur. In one joint a composite CDM-CaP scaffold was implanted (+P), in the contralateral joint a CDM only (-P) scaffold. After euthanasia at 6 months, tissues were analysed by histology, immunohistochemistry, micro-CT, biochemistry and biomechanical evaluation.

Results: The 8-week pilot showed encouraging formation of bone and cartilage, but incomplete defect filling. At 6 months, micro-CT and histology showed much more limited filling of the defect, but the CaP component of the +P scaffolds was well integrated with the surrounding bone. The repair tissue was fibrotic with high collagen type I and low type II content and with no differences between the groups. There were also no biochemical differences between the groups and repair tissue was much less stiff than normal tissue (P < 0.0001).

Conclusions: The implants failed to produce reasonable repair tissue in this osteochondral defect model, although the CaP base in the -P group integrated well with the recipient bone. The study stresses the importance of long-term *in vivo* studies to assess the efficacy of cartilage repair techniques.

Introduction

In the quest for techniques to produce a cartilage repair tissue that will remain functional life-long, a wide range of approaches have been explored (Richter et al., 2016). Although some techniques, such as various variants of autologous chondrocyte implantation (ACI) (Bekkers et al., 2013) and joint distraction (Wiegant et al., 2013), yield promising clinical results, none of these approaches has yet been proven to fully restore proper hyaline cartilage. An alternative technique that has yielded very promising results in other areas of regenerative medicine, such as restoration of bladder, trachea and gut, is the use of scaffolds based on decellularized extracellular matrix (ECM) (Badylak, 2007). The advantage of this technique is that an environment of natural ECM elements is created that may still contain a variety of appropriate bioactive cues without the presence of cellular components, hence avoiding immunological issues (Crapo et al., 2011; Gawlitta et al., 2015) . Moreover, it does allow for a xenogenic approach as ECM proteins are highly conserved across species (Badylak, 2007).

In vitro studies have already demonstrated the potential of cartilage-derived matrix (CDM) scaffolds, as abundant new glycosaminoglycan (GAG)- and collagen type II-containing cartilaginous matrix was formed by cultured mesenchymal stromal cells (Benders et al., 2014). The potency was further underscored by *in vivo* studies in small animal models both at ectopic (Gawlitta et al., 2015; Visser et al., 2015a) and orthotopic locations (Kang et al., 2014; Yang et al., 2010). The CDM scaffolds are potentially interesting for the repair of osteochondral defects, as they can be custom-shaped into osteochondral plugs that can be inserted in a press-fit fashion, avoiding insecure or complicating fixation techniques that may induce damage to the surrounding and opposing tissue (Panseri et al., 2012) . They also have the potential to become an off-the-shelf product, as there is no need for pre-implantation culturing. This approach, however, requires the simultaneous regeneration of both bony and cartilaginous tissues. This can in theory be realized by using either a composite scaffold, or a single scaffold that will allow formation of both tissues, depending on the surrounding original tissue.

In this study, a CDM-based scaffold is developed and used. The CDM consists of predominantly collagen type II, in the absence of GAGs and cells (Benders et al., 2013) and is used either on its own, or combined with a three-dimensionally (3D) printed calcium phosphate (CaP) cement-based proven osteogenic scaffold (Gbureck et al., 2007; Habibovic et al., 2008) to fill osteochondral defects in the femoropatellar joints of horses. The equine model is seen as one of the best and most challenging models for orthopaedic ailments (McIlwraith et al., 2011; Moran et al., 2016). It was hypothesized that the chondral portion of the osteochondral defects would heal with neo-tissue coming close to hyaline cartilage and that the composite scaffold would show better bone formation and lead to better overall anatomical reconstitution.

Methods

Animals
The protocols and studies described were approved by the ethical and animal welfare committees of Utrecht University (pilot study) and National University of Costa Rica (long-term study). For the pilot study one Dutch Warmblood horse (age: 6 years, 490 kg) was used, while for the long-term study eight healthy Criollo breed horses (age 4-9 years; weight 275-350 kg) were used. The horses were free of lameness and without any clinical or radiographic evidence of acute or chronic injuries. They were housed in individual boxes, and fed a standard maintenance ration of concentrate with hay ad libitum and free access to water.

Scaffold preparation
Full-thickness cartilage was harvested from cadaveric femoropatellar joints of horses (n= 5; age 3-10 years), euthanized for reasons other than joint disease, with owner permission. The cartilage particles were pooled and decellularized according to a protocol previously described (Panseri et al., 2012) Finally, particles were milled in liquid nitrogen (A11 basic analytical mill, IKA, Staufen, Germany) and sieved through pores of 300 μm.

The CaP scaffold [Fig.1(A), (B)]was manufactured by 3D printing of tricalcium phosphate (TCP) powder with diluted phosphoric acid, as described previously (Gbureck et al., 2007). Briefly, TCP was synthesized by heating a mixture of $CaHPO_4$ and $CaCO_3$ (both Merck, Germany) in a 2:1 molar ratio to 1400°C for 5 h, followed by quenching to room temperature. The sintered cake was manually crushed and sieved <125 μm and finally ground in a ball mill (PM400, Retsch, Germany) for 10 min. Printing was performed on a Z-Corp 310 powder printer (Z-Corporation, Burlington, USA) by using the TCP powder and 20 wt% phosphoric acid as printing liquid.

The suspended decellularized particles were placed in a 11 mm diameter cylindrical mould, either directly (-P) or placed on top of the CaP scaffolds (+P) while ensuring that they penetrated all macropores of the CaP scaffold. The scaffolds were then lyophilized for 24 h and subjected to ultraviolet light overnight to allow for crosslinking, before sterilization using ethylene oxide gas.
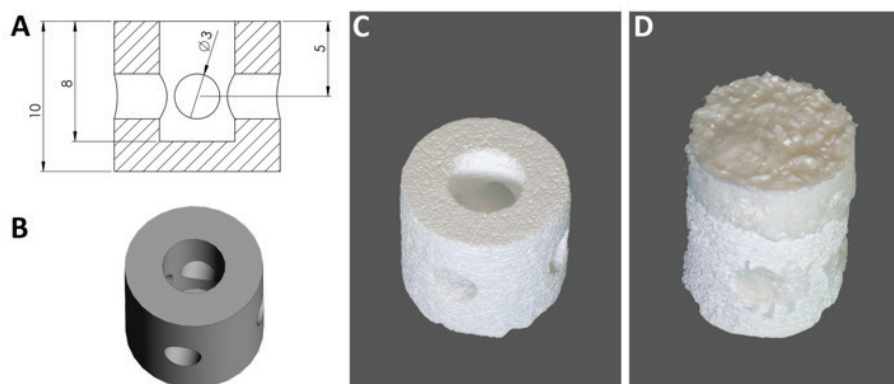
Fig. 1. Macroscopic views of scaffolds. The 3D design (A; all distances in mm), rendering (B) and printed CaP scaffold (C), which was subsequently combined in a mould with the CDM scaffold (D).

Experimental design
Scaffolds were implanted in 11 mm diameter and 10 mm deep cylindrical defects that were surgically created at the axial side of the medial femoral trochlear ridge. The 8-week pilot study was performed to evaluate the short-term response to the CDM scaffold. To reduce the use of experimental animals, a horse was used that was destined to be sacrificed for educational purposes. No CaP scaffold was used in this case. In the main 6-month study, each horse received both the treatment with CDM scaffold alone (-P) and with a composite scaffold consisting of CDM and a 3D printed CaP scaffold (+P). Horses 1-4 received treatment -P and +P for the left and right femoropatellar joints, respectively. For horses 5-8 this was inverted.

Surgical procedure
After premedication with xylazine (1.1 mg/kg, Pisa) intravenously (IV), horses were induced with ketamine (2.2 mg/kg, Holliday) and midazolam (0.05 mg/kg, Holliday) IV and positioned in dorsal recumbence. General anaesthesia was maintained with isoflurane in oxygen.
A cranial femoropatellar mini-arthrotomy was performed through a 5 cm incision made between the middle and medial patellar ligaments (McIlwraith and Robertson, 1998). Osteochondral defects at the middle aspect of each medial femoral trochlear ridge were created using a power-driven drill. Defect site and joints were flushed with saline solution (Careflex) before implantation. Scaffolds were press-fit implanted into each defect. Wounds were sutured in four layers (joint capsule, deep fascia, superficial fascia, and skin) and a stent bandage was applied over the incision.

Post-operative care and rehabilitation
Post-operatively, horses received antibiotics for 8 days (procaine penicillin 15,000 IU/kg intramuscularly SID, Alfasan, and IV gentamicin 6.6 mg/kg BID, Alfasan), and non-steroidal anti-inflammatory drugs (phenylbutazone (2.2 mg/kg, Lisan, orally BID)) during the first 14 days.
The pilot horse was subjected to the following rehabilitation protocol during the next 8 weeks: from week 2, the horse was hand-walked daily starting with 5 min/day with increments of 5 min per week until 20 min/day was reached. In the main study, from week 3, horses were hand-walked starting with 5 min/day with increments of 5 min/week, until 30 min/day was reached, which was then kept stable until week 16. In months 5 and 6, horses were walked, trotted and cantered for 2 min at each gait.

Monitoring during experimental period
The animals were subjected to daily monitoring of clinical parameters (temperature, heart rate and respiratory rate). Blood parameters were checked and lateromedial radiographs of the femoropatellar joints were taken before surgery and at months 1, 2, 4 and 6 after the intervention to check for general health.

Euthanasia and sample harvesting
The pilot horse was euthanized at 8 weeks by a combination of detomidine (0.01 mg/kg, Vetoquinol), ketamine (2 mg/kg, Vetoquinol), midazolam (0.1 mg/kg, Actavis) and pentobarbital (50 mg/ kg, AST Farma). The horses of the main study were euthanized at 6 months using a combination of xylazine (1 mg/kg IV, Pisa) and ketamine-midazolam (3 mg/kge0.05 mg/kg IV, Holliday) to induce profound anaesthesia. After this, a bolus of oversaturated magnesium sulphate (200 g/l) and chloral hydrate (200 g/l) solution was administered to effect.
After opening the femoropatellar joint, macroscopic pictures were taken and blocks of tissue containing the defect were excised. A piece containing one half of the treated defect was fixed in 10% formalin for micro-CT analysis and histological evaluation after embedding in polymethylmethacrylate (MMA). The remainder of the tissue was snap-frozen in liquid nitrogen and stored at -80°C until further processing for paraffin-based histological, biomechanical and biochemical analyses.

Micro-CT imaging and CaP scaffold analysis
To visualize the calcified tissue at the defect site, the formalin fixed tissue underwent micro-CT analysis (Quantum FX-Perkin Elmer) with scan parameters 90 kV tube voltage, 180 mA tube current, 60 μm resolution and 3 min scan time. Reconstruction of 2D projections was automatically performed using the inbuilt software; image calibration and noise reduction was undertaken with Analyze-11.0 software.

Remnants of CaP scaffolds were analysed by XRD analysis (D5005, Siemens, Karlsruhe,

Germany) using monochromatic Cu Kα1 radiation in a 2Theta range of 20-40° with a step size of 0.02°. Diffraction patterns were qualitatively analysed using the following reference patterns from the powder diffraction database: brushite (PDF-No. 09-0077), monetite (PDF-No. 09-0080), β-tricalcium phosphate (β-TCP) (PDF-No. 09-0169), α-tricalcium phosphate (α- TCP) (PDF-No. 09-0348) and hydroxyapatite (HA) (PDF-No. 09- 0432).

Biomechanical testing
Micro-indentation experiments were performed on both healthy cartilage and defect tissue from the same animal. A displacement-controlled nano-indenter machine (Piuma, the Netherlands) with a spherical indenter (radius: 73 µm, cantilever stiffness: 15.6 N/m) was used to obtain indentation-based load displacement curves (Pathak and Kalidindi, 2015). A 3 X 3 matrix of indentation (n = 9) covering 600 x 600 µm^2 area, corresponding with 300 µm distance between each point, was performed. The actual indentation depth was in the range of 8 microns. The Young's modulus was calculated based on the Oliver-Pharr theory using the initial slope of the unloading curve and estimated Poisson's ratio of 0.5 (Jin and Lewis, 2004).

After biomechanical testing, half of the sample was fixed in formalin and further processed for paraffin embedding. From the remaining tissue sample, the soft tissue of the defect was excised and processed for biochemical analysis.

Histological processing
Formalin-fixed samples were embedded in MMA and cut with a Leica 4 SP1600 Saw Microtome system (Leica, Germany) to yield 20-30 µm sections. Sections were stained with methylene blue (Merck, 1.06045)/basic fuchsine (Klinipath, 800561).

Formerly frozen tissue samples were, after fixation in 10% formalin, decalcified in ethylene diamine tetra acetic acid (EDTA) and dehydrated through a graded ethanol series, cleared in xylene, embedded in paraffin, and sectioned (5 µm). To visualize cells, sections were stained with haematoxylin (Klinipath) and eosin (Merck, 115935). To visualize collagen fibre orientation, a picrosirius red staining (Klinipath, 80115) was performed. A triple stain of haematoxylin, fast green, and Safranin-O (both from Sigma) was also applied to identify the presence of GAGs. Stained sections were examined using a light microscope (Olympus BX51). Immunohistochemistry was used to identify collagen type I (Rabbit monoclonal from Abcam (AB138492); 1:500 dilution) and II (Mouse monoclonal Antibody DSHB, II-II6B3; 1:1500 dilution) after deparaffinization and rehydration of the sections following a protocol described previously (Gawlitta et al., 2015).

Biochemical analyses
Tissue derived from the defect area after biomechanical testing was used for DNA, GAG and hydroxyproline (HYP) quantification. Samples were digested overnight in papain solution, 200 ml per sample (0.01 M cysteine, 250 mg/ml papain, 0.2 M NaH2PO4 and 0.01 M EDTA) at 60°C. Total DNA was quantified on the papain digest using the Qubit 2.0 fluorimeter with the Qubit dsDNA BR Assay Kit (Q32853) according to the manufacturer's instructions.

Total GAG content was determined after reaction with dimethyl methylene blue as described previously (Visser et al., 2015a). Collagen was quantified by using a HYP assay. Samples were freeze-dried overnight and hydrolysed at 108°C overnight in 4 M NaOH. HYP was measured after reaction with Dimethylaminobenzaldehyde, the absorbance was read at 570 nm using a microplate reader (Tecan).

Statistics
Data are presented as mean and confidence interval. Statistical significance was determined, using SPSS software, for biochemical and biomechanical quantification a paired t-test was used, and for biomechanical testing a Wilcoxon signed ranks test was used.

Results

Scaffold preparation
The composite scaffold consisted of the CaP custom-designed 3D printed base [Fig. 1(A)e(C)], to promote bone regeneration, and the CDM scaffold [Fig. 1(D)] for the restoration of the cartilage compartment. After lyophilisation a good integration of the CDM scaffold was obtained and the CDM compartment was trimmed to 2 mm allowing for good accessibility of internal pores.

Pilot experiment
The horse in the pilot experiment recovered well from anaesthesia and had an uneventful post-operative period. At 8 weeks, an indentation of the cartilage surface was observed macroscopically, but regeneration of both the bone and cartilage phase was evident at a microscopic level [Fig. 2(A)]. There was excellent integration of newly formed trabecular bone with the original subchondral bone.
There was intense staining for proteoglycans [Fig. 2(A)] and collagen type II [Fig. 2(B)] and there were indications for integration with the pre-existent tissue at the margins of the defect at this level. Nevertheless, the cartilage phase showed some cleft formation and disorganisation of collagen structures, as evidenced by picrosirius red staining [Fig. 2(C)] andwas positive for collagen type I (data not shown).
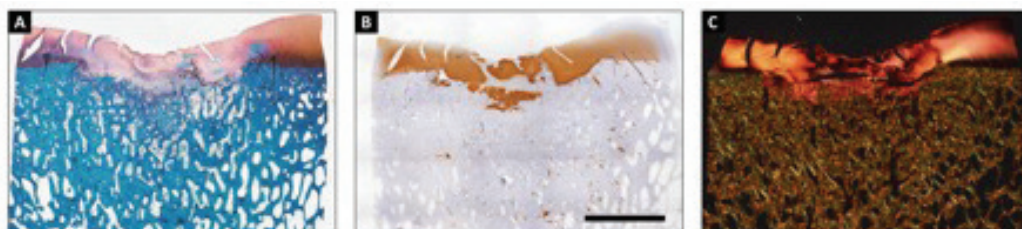
Fig. 2. Histological view of the artificial defect treated with a decellularized CDM scaffold after 8 weeks. Newly formed tissue was rich in GAGs (GAGs stain red with safranin-O (A)); and rich in collagen type II (brown in B) with clear distinction between cartilage and bone phases. Picrosirius red staining demonstrates under polarized light the disorganisation in the collagen fibril organisation (C). Scale bars represent 500 µm.

Surgery and clinical and radiographic observations during experimental period
For the 6-month study, horses recovered uneventfully and could cope well with the post-surgical rehabilitation period. After the initial recovery period, no significant lameness was observed in six of eight horses. The remaining two showed intermittent mild lameness that responded well to treatment with non-steroidal analgesics. In all horses, clinical and blood parameters remained within normal physiologic limits. The radiographs taken at 2 months after surgery showed evidence of the artificial defects, with a clear difference between the sides treated with -P and +P implants (Suppl. Fig. 1). Whilst the +P scaffolds had a radio dense appearance [Suppl. Fig. 1(B)], around the -P scaffolds a sclerotic rim was visible [Suppl. Fig. 1(D)].

Macroscopic appearance at necropsy
At the time of euthanasia, the surgical sites were readily recognizable by an indentation in the cartilage (Fig. 3); whilst at the time point of implantation implants had been carefully placed level with the surrounding cartilage. All sites had a similar appearance without macroscopically visible differences between treatments.
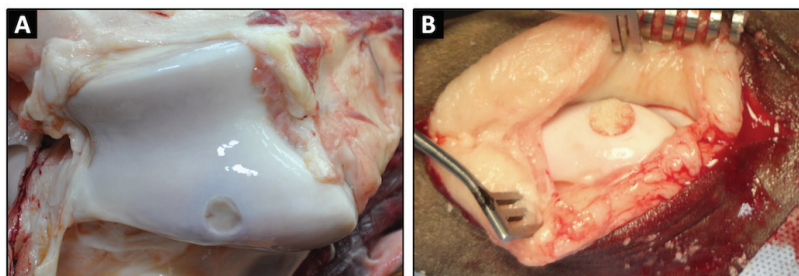

Fig. 3. Macroscopic view of the surgical site at necropsy (6 months after implantation).

Micro-CT and analysis of the CaP scaffold

Micro-CT analyses showed that filling of the bony part of the defect was very limited and considerably less than observed in the *in vivo* pilot experiment in all cases, although the CaP component of the +P scaffolds appeared well integrated with the surrounding bone (Fig. 4). Prior to implantation, the 3D printed scaffolds were composed of a mixture of brushite ($CaHPO_4.2H_2O$), monetite ($CaHPO_4$), β-TCP and α-TCP. Analysis of the remnants of the retrieved CaP scaffold by XRD showed that most of the scaffolds had dissolved during the implantation period since no brushite, monetite and α-TCP could be detected in all samples. Only in few cases, small residues of crystalline β-TCP could be found. All analysed samples contained nanocrystalline HA, which either originates from direct conversion of brushite (or α-TCP), or it stems from newly formed bone matrix [Fig. 4(E)].
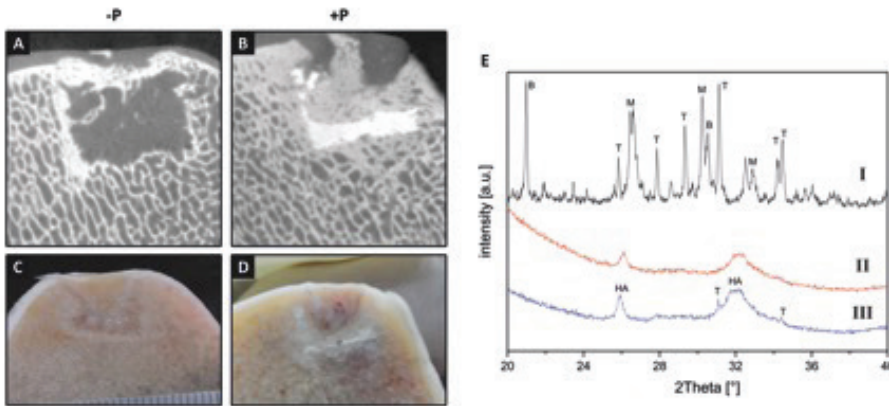

Fig. 4. Micro-CT and macroscopic pictures, respectively, of implantation sites at 6 months for _P (A, C) and þP (B, D) scaffolds. XRD analysis of 3D printed CaP scaffolds (E); I indicates a sample before implantation, whilst II and III indicate samples at necropsy. The most prominent peaks are labelled as: B: brushite (PDF-No. 09-0077), M: monetite (PDFNo. 09 0080), T: b-tricalcium phosphate (PDF-No. 09-0169) and HA: hydroxyapatite (PDF-No. 09 0432).

Biomechanical analysis

Biomechanical testing showed that the repair tissue in both -P and +P treated defects was very soft(mean Young's modulus 302KPa (CI 177-427) for -P and 261 KPa (CI 148-374) respectively) and the stiffness was significantly less than that of normal adjacent cartilage (mean Young's modulus for -P 2385 KPa (CI 2009-2761), for +P 2372 KPa (CI 2036-2708) ($P < 0.0001$)). There was no difference between repair tissue of the -P and +P groups ($P > 0.05$) (Fig. 5).
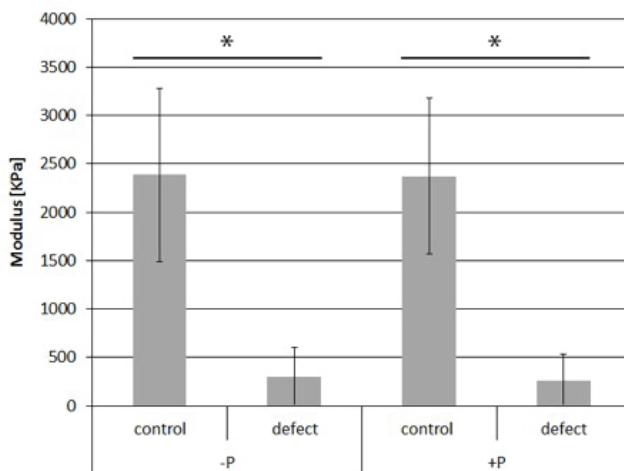
Fig. 5. Young's modulus of repair tissue vs normal cartilage from lesions treated with CDM only (-P) or CDM plus CaP scaffolds (+P). *P < 0.0001, n ¼ 8 for all groups.

Biochemistry

In line with the histological observations, there was limited GAG production in the defects. Values for GAG, DNA and GAG/DNA for the -P condition were 25.67 (CI 17.27-34.07) mg/mg tissue, 1.57 (CI 1.35-1.79) mg/mg tissue and 16.54 (CI 12.09-20.99) respectively. For -P these were 12.32 (CI 9.88-14.82); 1.74 (CI 1.63-1.85) and 7.13 (CI 6.63-8.63) respectively. For the collagen parameter HYP values were 11.63 (CI 10.47-12.79) and 8.78 (CI 7.03-10.53) Hyp/ mg tissue. There were no significant differences in the GAG and collagen content between the -P and +P groups (Fig. 6).
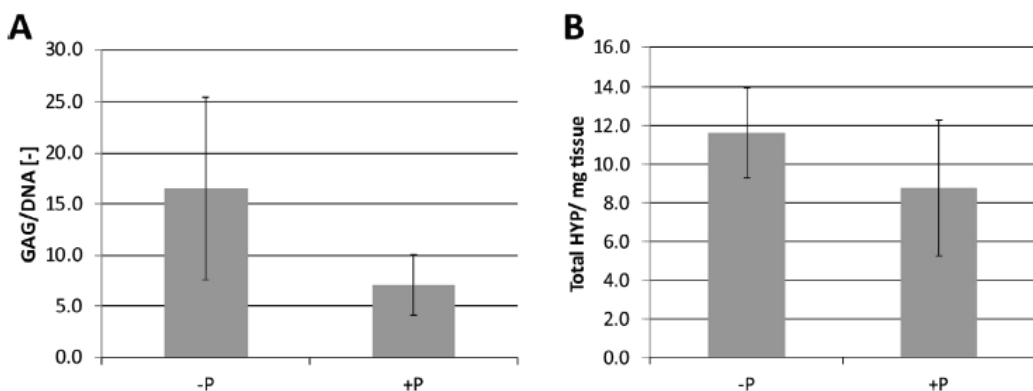

Fig. 6. Average GAG (A) and hydroxyproline (HYP, mg/mg dry weight; (B) content, as a measure of collagen content, of the repair tissue after 6 months.
Histology

Histological staining of paraffin-embedded samples from the edges of both +P and -P treated defects demonstrates that a predominantly fibrotic repair tissue had been formed (Fig. 7) without obvious differences between the groups. The neo tissue contained very limited amounts of GAGs and collagen type II, while abundant staining for collagen type I was observed (Suppl. Fig. 2).

The MMA sections showed substantial retention of the CaP scaffold at 6 months [Fig. 8(A)] with good to very good adherence of the surrounding trabecular bone to the scaffold [Fig. 8(B)].
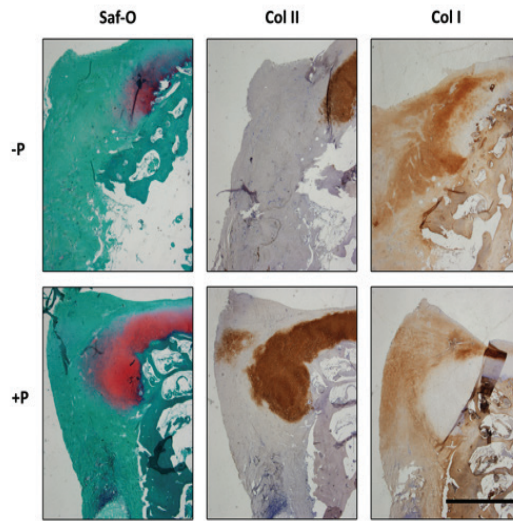

Fig. 7. Histological evaluation of the composition of the repair tissue after 6 months. Positive safranin-O staining (red) was predominantly observed at the edges of the defect, and co-localized with the immunolocalisation of collagen type II (brown). Immunolocalisation of collagen type I (brown) was homogeneous in the fibrous repair tissue. Scale bar represents 2 mm.
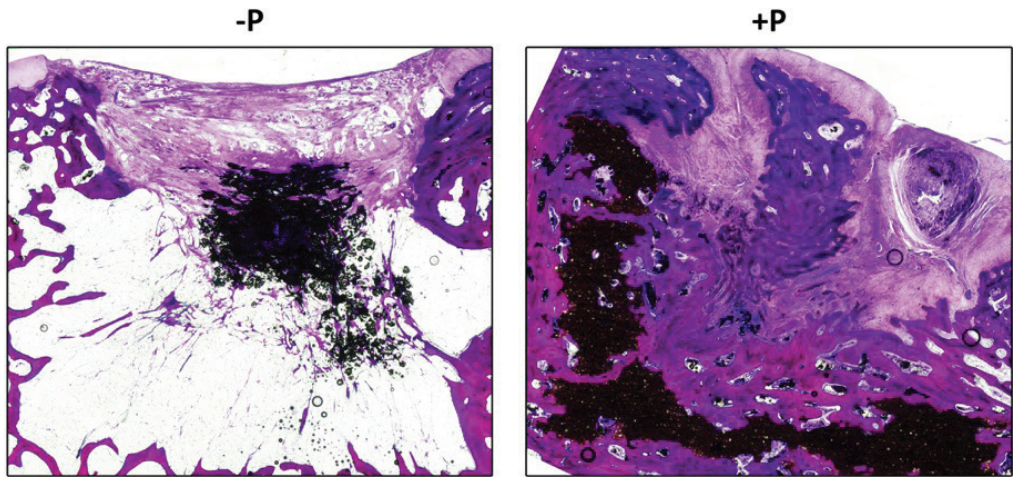
Fig. 8. MMA embedded section of a defect with a scaffold with a CaP base (+P) stained with methylene blue/basic fuchsine. The overview (A) shows substantial retention of the scaffold (in black) that is well connected to the bone, as shown by higher magnification (B). Scale bars represent 3 mm (A) and 1 mm (B).

Discussion

Since the early days of tissue engineering, articular cartilage has been one of the target tissues (Vacanti, 2006). However, it soon became clear that extensive *in vitro* testing in the classic smaller laboratory species, while still being of absolute necessity in the initial developmental phase, were not sufficient for evaluation of any therapy aiming at cartilage repair or regeneration in clinical circumstances (Hurtig et al., 2011).

Of the larger models, the equine model is regarded as one of the best, but also as one of the most challenging (Moran et al., 2016). Advantages include the size and accessibility of the joints, the thickness and biochemical composition of the cartilage, which are close to those in humans (Malda et al., 2012), and the fact that the subchondral plate is closed, which is not the case in many of the smaller species. Among the disadvantages of the model perhaps the immediate load-bearing after surgery may be most important (Ahern et al., 2009). An important ethical consideration with respect to the equine model is that horses are animals that are primarily bred and kept for their athletic potential. This makes the horse, unlike any other species with the possible exception of the dog, into an experimental species, as well as a target species, with a clear clinical need for better treatment of (osteo)chondral articular disorders (Williams et al., 2001).

In this study, the equine model was used to evaluate the effect of filling an artificial

osteochondral defect with a cell-free CDM scaffold, with (+P) or without (-P) a ceramic base for press-fit anchoring in the subchondral bone. Results of the implantation of a CDM only implant in the 8-week pilot study were in line with previous promising results from *in vivo* ectopic studies with these scaffolds (Gawlitta et al., 2015; Visser et al., 2015a), as well as the orthotopic implantations in rabbits (Kang et al., 2014; Yang et al., 2010). At the site of the scaffold, regeneration of both the bone and cartilage phase were seen, although a marked indentation of the articular surface could be noted. Nevertheless, the outcome of the pilot study was deemed encouraging enough to justify a larger longer-term study.

While in the main study clinical signs, such as lameness or joint effusion, were limited and not seen in all horses, defect filling at necropsy at 6 months was disappointing and clearly less than in the pilot horse in all treated animals. Macroscopic and histological analysis confirmed large indentations and the presence of inferior repair tissue. Biomechanically, this tissue was on average 90% less stiff than samples from healthy cartilage from the same horse. In contrast, the 3D printed CaP cement from the bony part of the scaffold was well integrated in the surrounding bone tissue, similar to previous orthotopic studies (Habibovic et al., 2008; Tamimi et al., 2014). Although a major part of the cement had been resorbed and replaced by newly formed bone, remaining fragments were still visible within the implantation site. X-ray diffraction (XRD) analysis clearly confirmed that brushite and monetite as main components of the scaffolds were fully resorbed and only a minor amount of residual β-TCP could be found, likely due to the lower solubility of β-TCP (~0.4 mg/l) compared to brushite (85 mg/l) and monetite (41 mg/l) (Holzapfel et al., 2013). All diffraction patterns revealed nanocrystalline HA as the major component given the broad peaks around 2Theta =25.8˚ and 31-35˚. This HA might be formed either directly after scaffold implantation from hydrolysis of α-TCP to calcium deficient HA (Carrodeguas and De Aza, 2017), or after longer times by the conversion of brushite into HA in the presence of Ca^{2+}. The latter often appears for brushite based biocements following orthotopic implantation (Kanter et al., 2014), as the compound is thermodynamically instable at physiological pH values. Since the lateral resolution of the used XRD is in the order of several mm^2, the HA may also stem from newly formed bone mineral next to the scaffold residues.

Several factors may have contributed to the limited performance of the implants in the long-term study. In decellularized scaffolds the efficacy of the decellularization process is known to affect the host response and *in vitro* more aggressive decellularization was associated with a shift in macrophage phenotype predominance from M1 to M2 (Keane et al., 2012) . Although not well researched, the clinical impression among veterinarians exists that the horse is a relatively sensitive animal to immunogenic stimuli compared to other species, which may also have affected the fate of the implanted scaffolds in this study. Another potentially very important factor is the initial biomechanical loading, both shear and compression, the implanted scaffolds have been subjected to from the very moment the horses recovered from anaesthesia. This is a well-known drawback

of the equine model (Ahern et al., 2009), which is due to the inability of the horse to unload one of its limbs for any prolonged period of time without severe complications. Additionally, the limited overall mechanical properties of the CDM scaffold may have contributed to failure by hampering the transfer of the forces to the underlying bone, ultimately resulting in bone loss in these regions. This stresses the need for more mechanically stable, e.g., fibre-reinforced constructs (Boere et al., 2014; Visser et al., 2015b), for the treatment of defects in these mechanically challenging locations. Outcomes might also further have been improved by the inclusion of regenerative cells to further enhance the tissue formation. However, this will be a complicating factor when an off-the-shelf solution, i.e., a cell-free construct, is envisioned.

Taken together, the poor outcomes of the long-term equine study were not in line with the observed promising results of the *in vitro*, ectopic *in vivo* and the short-term *in vivo* pilot studies. While the horses did surprisingly well clinically only with exhibition of relatively mild lameness, in the long-term study very limited defect filling was observed compared to the outcomes of the 8- week pilot study. This study thus underscores the need for long-term studies in a challenging model when evaluating regenerative approaches to treat joint defects, even if the outcome of *in vitro* work and even short-term *in vivo* studies may be promising, as the performance of treatments may otherwise be overestimated. The outcome also suggests there may be substantial added value of more and more in-depth monitoring during long-term studies, for example, through imaging technologies or advanced profiling of the synovial fluid composition.

Author contributions
R.V.B., S.M.C., K.E.M.B., U.G., R.W. and J.M. contributed to the conception and design of the study. R.V.B., S.M.C., J.E.E.M., K.E.M.B., S.G.P., and J.M. performed the experiments. R.V.B., S.M.C., K.E.M.B., U.G., S.G.P., H.W., J.G., R.W. and J.M. contributed to the analysis and interpretation of data. All approved the submitted manuscript.

Conflict of interest
The authors have nothing to disclose.

Acknowledgements

References

Ahern, B.J., Parvizi, J., Boston, R., Schaer, T.P., 2009. Preclinical animal models in single site cartilage defect testing: a sistematic review. Ostearthritis and Cartilage 17, 705-713.

Badylak, S.F., 2007. The extracellular matrix as a biologic scaffold material. Biomaterials 28, 3587–3593.

Bekkers, J.E., Creemers, L.B., Tsuchida, A.I., van Rijen, M.H., Custers, R.J., Dhert, W.J., 2013. One-stage focal cartilage defect treatment with bone marrow mononuclear cells and chondrocytes leads to better macroscopic cartilage regeneration compared to microfracture in goats. Osteoarthritis Cartilage 21, 950-956.

Benders, K.E., Boot, W., Cokelaere, S.M., Van Weeren, P.R., Gawlitta, D., Bergman, H.J., 2014. Multipotent stromal cells outperform chondrocytes on cartilage-derived matrix scaffolds. Cartilage 5, 221-230.

Benders, K.E.M., van Weeren, P.R., Badylak, F., 2013. Extracellular matrix scaffold for cartilage and bone regeneration. Trends in Biotechnology 31, 169-176.

Boere, K.W., Visser, J., Seyednejad, H., Rahimian, S., Gawlitta, D., van Steenbergen, M.J., 2014. Covalent attachment of a threedimensionally printed thermoplast to a gelatin hydrogel for mechanically enhanced cartilage constructs. Acta Biomater 10, 2602-2611.

Carrodeguas, R.G., De Aza, S., 2017. alpha-Tricalcium phosphate: synthesis, properties and biomedical applications. Acta Biomater 7, 3536-3546.

Crapo, P.M., Gilbert, T.W., Badylak, S.F., 2011. An overview of tissue and whole organ decellularization processes. Biomaterials 32, 3233-3243.

Gawlitta, D., Benders, K.E., Visser, J., van der Sar, A.S., Kempen, D.H., Theyse, L.F., 2015. Decellularized cartilage-derived matrix as substrate for endochondral bone regeneration. Tissue Eng Part A 21, 694-703.

Gbureck, U., Vorndran, E., Muller, F.A., Barralet, J.E., 2007. Low temperature direct 3D printed bioceramics and biocomposites as drug release matrices. J Control Release 122, 173-180.

Habibovic, P., Gbureck, U., Doillon, C.J., Bassett, D.C., van Blitterswijk, C.A., Barralet, J.E., 2008. Osteoconduction and osteoinduction of low-temperature 3D printed bioceramic implants. Biomaterials 29, 944-953.

Holzapfel, B.M., Reichert, J.C., Schantz, J.T., Gbureck, U., Rackwitz, L., Noth, U., 2013. How smart do biomaterials need to be? A translational science and clinical point of view. Adv Drug Deliv Rev 65, 581-603.

Hurtig, M.B., Buschmann, M.D., Fortier, L.A., Hoemann, C.D., Hunziker, E.B., Jurvelin, J.S., Mainil-Varlet, P., McIlwraith, C.W., Sah, R.L., Whiteside, R.A., 2011. Preclinical Studies for Cartilage Repair: Recommendations from the International Cartilage Repair Society. Cartilage2(2):137-52. doi: 2, 137-152.

Jin, H., Lewis, J.L., 2004. Determination of Poisson's ratio of articular cartilage by indentation using different-sized indenters. J Biomech Eng 126, 138-145.

Kang, H., Peng, J., Lu, S., Liu, S., Zhang, L., Huang, J., 2014. In vivo cartilage repair using adipose-derived stem cell-loaded decellularized cartilage ECM scaffolds. J Tissue Eng Regen Med 8, 442-453.

Kanter, B., Geffers, M., Ignatius, A., Gbureck, U., 2014. Control of in vivo mineral bone cement degradation. Acta Biomater 10, 3279-3287.

Keane, T.J., Londono, R., Turner, N.J., Badylak, S.F., 2012. Consequences of ineffective decellularization of biologic scaffolds on the host response. Biomaterials 33, 1771-1781.

Malda, J., Benders, K.E.M., Klein, T.J., de Grauw, J.C., Kik, M.J.L., Hutmacher, D.W., Saris, D.B.F., van Weeren, P.R., Dhert, W.J.A., 2012. Comparative study of depth-dependent characteristics of equine and human osteochondral tissue from the medial and lateral femoral condyles. Ostearthritis and Cartilage 20, 1147-1151.

McIlwraith, C.W., Robertson, J.T., 1998. Equine Surgery. Advanced Techniques.

McIlwraith, W.C., Fortier, L.A., Frisbie, D.D., Nixon, A.J., 2011. Equine Models of Articular Cartilage Repair. Cartilage 2, 317-326.

Moran, C.J., Ramesh, A., Brama, P.A., O'Byrne, J.M., O'Brien, F.J., Levingstone, T.J., 2016. The benefits and limitations of animal models for translational research in cartilage repair. J Exp Orthop 3.

Panseri, S., Russo, A., Cunha, C., Bondi, A., Di Martino, A., Patella, S., Kon, E., 2012. Osteochondral tissue engineering approaches for articular cartilage and subchondral bone regeneration. Sports Traumatol Arthrosc 20, 1182-1191.

Pathak, S., Kalidindi, S.R., 2015. Spherical nanoindentation stressestrain curves. Mater Sci Eng Rep 91, 1-36.

Richter, D.L., Schenck, J.R.C., Wascher, D., Treme, G., 2016. Knee articular cartilage repair and restoration techniques: a review of the literature. Sports Health 8, 153-160.

Tamimi, F., Torres, J., Al-Abedalla, K., Lopez-Cabarcos, E., Alkhraisat, M.H., Bassett, D.C., 2014. Osseointegration of dental implants in 3D-printed synthetic onlay grafts customized according to bone metabolic activity in recipient site. Biomaterials 35, 5436-5445.

Vacanti, C.A., 2006. The history of tissue engineering. J Cell Mol Med 10, 569-576.

Visser, J., Gawlitta, D., Benders, K.E., Toma, S.M., Pouran, B., van Weeren, P.R., Dhert, W.J., Malda, J., 2015a. Endochondral bone formation in gelatin methacrylamide hydrogel with embedded cartilage-derived matrix particles. Biomaterials 37, 174-182.

Visser, J., Melchels, F.P., Jeon, J.E., Van Bussel, E.M., Kimpton, L.S., Byrne, H.M., Dhert, W.J., Dalton, P.D., Hutmacher, D.W., Malda, J., 2015b. Reinforcement of hydrogels using three-dimensionally printed microfibres. Nat Commun 6.

Wiegant, K., van Roermund, P.M., Intema, F., Cotofana, S., Eckstein, F., Mastbergen, S.C., 2013. Sustained clinical and structural benefit after joint distraction in the treatment of severe knee osteoarthritis. Osteoarthritis Cartilage 21, 1660-1667.

Williams, R.B., Harkins, L.S., Hammond, C.J., Wood, J.L., 2001. Racehorse injuries, clinical problems and fatalities recorded on British racecourses from flat racing and National Hunt racing during 1996, 1997 and 1998. Equine Vet J. 33, 478-486.

Yang, Z., Shi, Y., Wei, X., He, J., Yang, S., Dickson, G., Tang, J., Xiang, J., Song, C., Li, G., 2010. Fabrication and repair of cartilage defects with a novel acellular cartilage matrix scaffold. Tissue Eng Part C Methods 16, 865-876.

Supplementary data
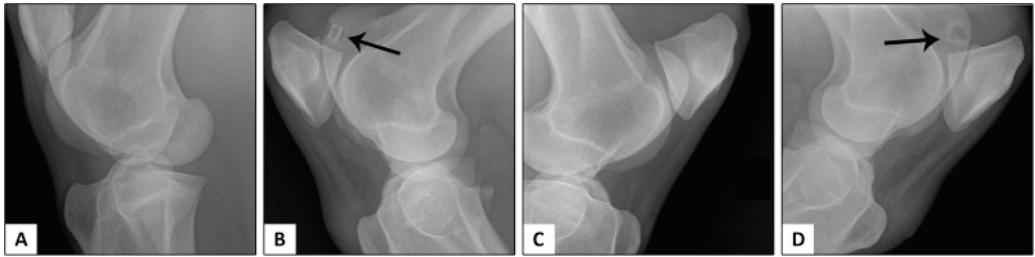
Supplementary Fig. S1. Representative radiographs of a left femoropatellar joint before surgery (A) and at 2 months after implantation of a +P scaffold (arrow, B). Representative radiographs of a right femoropatellar joint before surgery (C), and at 2 months after implantation of a −P scaffold (arrow, D).
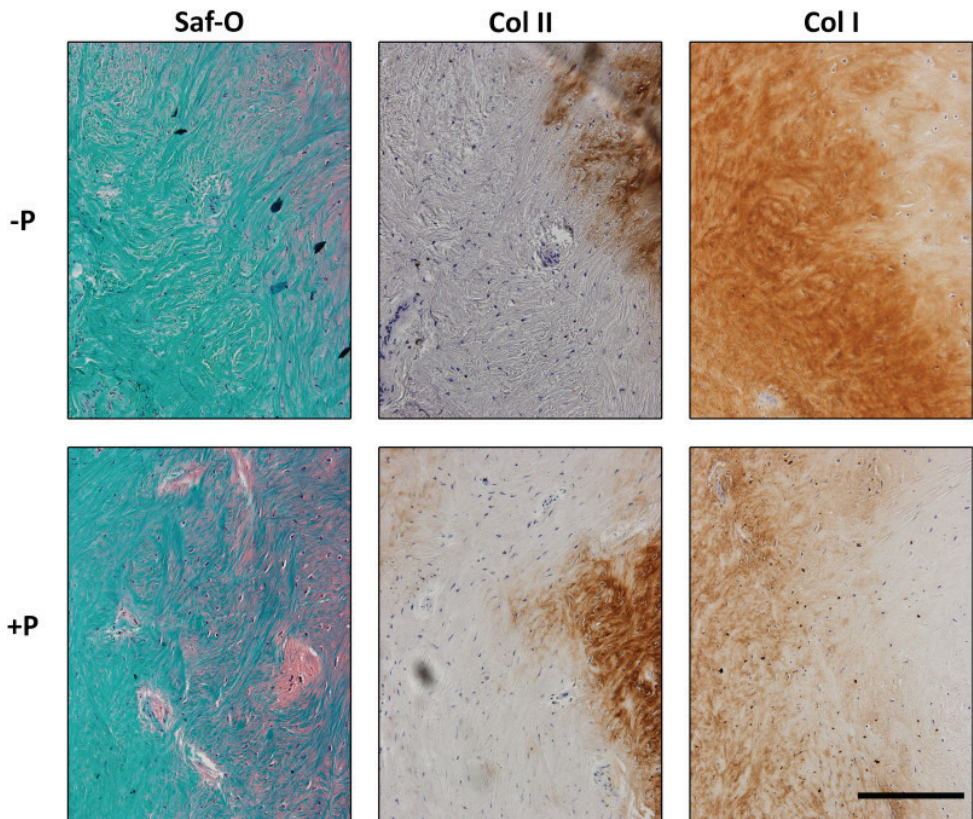
Supplementary Fig. S2. Histological evaluation of the composition of the repair tissue after 6 months. Positive safranin-O staining (red) was predominantly observed at the edges of the defect, and co-localized with the immunolocalisation of collagen type II (brown). Immunolocalisation of collagen type I (brown) was homogeneous in the repair tissue. Scale bar represents 200 μm.

Chapter VII

Use of a self-sealing hydrogel for chondral defects of articular cartilage: a long-term follow-up study in an equine chondral defect model

(Manuscript in preparaton)

Use of a self-sealing hydrogel for chondral defects of articular cartilage: a long-term follow-up study in an equine chondral defect model

Rafael A. Vindas Bolaños*[a], Sanne K. Both*[b], Stefan M. Cokelaere[c], Mariëlle Vullers[c], Nicoline M. Korthagen[c,d], Bram Zoetebier[b], Pieter J. Dijkstra[b], Anders Lindahl[e], Janny C. de Grauw[c], P. René van Weeren[c], Marcel Karperien[b]

[a] Catedra de Cirugía de Especies Mayores, Escuela de Medicina Veterinaria, Universidad Nacional, Costa Rica

[b] Developmental BioEngineering, Faculty Technical Nature Science, University of Twente, Drienerlolaan 5, 7522 NB, Enschede, The Netherlands

[c] Department of Equine Sciences, Faculty of Veterinary Medicine, Utrecht University, Yalelaan 112, 3584 CM, Utrecht, The Netherlands

[d] Department of Orthopaedics, University Medical Center Utrecht, Heidelberglaan 100, 3584 CX, Utrecht, The Netherlands

[e] Clinical Chemistry and Transfusion Medicine, Sahlgrenska University Hospital, SE 413 45, Gothenburg Sweden.

* shared first authorship

Corresponding author
Rafael A. Vindas Bolaños, Catedra de Cirugía de Especies Mayores, Escuela de Medicina Veterinaria, Universidad Nacional, Campus Benjamín Núñez, Lagunilla, Heredia, Costa Rica. E: rafael.vindas.bolanos@una.cr T: +506 8351 1313

Keywords
Cartilage repair, hydrogel, horse, nanofracture

Summary

Objectives: The aim of the current study was to evaluate the regenerative potential of a self-sealing hydrogel compared to nanofracture for the treatment of chondral defects in a long-term *in vivo* study in the equine stifle joint.

Methods: Left and right stifle joints of n = 8 horses were randomly allocated to be treated with either the hydrogel or nanofracture as a control treatment. One partial-thickness chondral defect (1 mm depth) was created via mini-arthrotomy in the mid-medial trochlear ridge of each stifle joint by the same surgeon (SC) using a 7-mm diameter biopsy punch. Defects were either treated with three perforations into the subchondral bone (nanofracture) or with a self-sealing hydrogel, and repair tissue was studied after 7 months using histology (ICRS-II scores) and micro-CT analysis.

Results: Horses recovered well from surgery and did not show lameness over the 7 month follow-up. Cartilage mean total ICRS-II score at 7 months was significantly worse in the nanofracture group (48% ± 10%; mean± SD) compared to the hydrogel group (72% ± 7%; mean ± SD, where 100% denotes normal cartilage; p = 0.0007). Hydrogel treated joints showed significantly better scores for every ICRS-II criterion assessed except matrix staining. Defects treated with nanofracture contained mainly fibrous and fibrocartilaginous repair tissue, as evidenced by relatively poor cell morphology, surface architecture and collagen II immunohistochemical staining; subchondral bone and calcification abnormalities were appreciable in the nanofracture but not the hydrogel treated defects. Micro-CT showed altered subchondral bone microarchitecture in all nanofracture treated defects 7 months post-operatively, compared to no such disturbance in hydrogel treated joints.

Main limitations: Outcome was evaluated at a single time point. No advanced longitudinal monitoring (SF analysis, repeat arthroscopy) nor biomechanical testing of repair tissue was performed.

Conclusion: The clinical and histological outcome of this first long-term large animal study using the described injectable hydrogel seems promising, and further research into this avenue of articular regenerative medicine is warranted.

Introduction

The natural capacity for functional healing of articular cartilage defects is very limited. As a consequence, individuals with chondral defects are predisposed to the development of osteoarthritis (OA), a debilitating disease with a staggering incidence in the human adult population (Lawrence et al., 2008).

The standard care of chondral defects, *i.e.* lesions that do not penetrate into the subchondral bone, is the use of bone marrow stimulation techniques, in which defect repair is stimulated by making perforations through the subchondral bone plate, creating a pathway for stem cell migration from underlying bone marrow into the defect (Bedi et al., 2010). Although these methods initially have a good clinical effect, they predominantly result in generation of less resilient fibrocartilage and induce changes in the subchondral bone plate, ultimately also leading to OA (Bae et al., 2006; Goyal et al., 2013; Kreuz et al. 2006a; 2006b; Mithoefer et al., 2016). Because of the poorer long term clinical outcome and substantial subchondral bone damage associated with bone marrow stimulation techniques, novel methods to facilitate cartilage defect healing and thus prevent secondary OA are continuously being sought.

Recently, it has become clear that, contrary to William Hunter's dogma that cartilage *"… when destroyed, [it] is never recovered"* (Hunter 1743), the joint may possess intrinsic repair capacity. This is evidenced by the presence of stem or progenitor cell populations in the synovial membrane (Kubosch et al., 2018), synovial fluid (Garcia et al., 2016)) and cartilage itself (Williams et al. 2010). Cell tracing studies in mouse knee joints have identified migration of cells into cartilage defects contributing to repair (Decker et al., 2017). These observations have spurred the development of a cell free treatment of cartilage defects, by filling the defect with an appropriate biomaterial that essentially should serve two functions: 1) provide mechanical support and protection against further erosion due to wear and tear, and 2) serve as a scaffold facilitating the ingrowth of resident stem- or progenitor cell populations that subsequently replace the biomaterial with *de novo* cartilage. The choice of biomaterial for such approaches is critical for the extent and quality of defect filling obtained, as well as for eventual clinical outcome (Levato et al., 2017).

Injectable and *in situ* gelating hydrogels are ideally suited for the development of such a biomaterial. Critical design parameters for such a gel include ease of application (preferably via arthroscopy), retention of the gel in the defect (Mancini et al., 2017), as well as appropriate biomaterial properties (e.g. porosity, biochemical and mechanical cues) facilitating cell ingrowth and tissue formation (Levato et al., 2017). Previously, we have developed an injectable and in situ gelating hydrogel based on dextran – tyramine and hyaluronic acid – tyramine conjugates that crosslink in an enzymatic reaction using horse radish peroxidase and minute non-toxic amounts of hydrogen peroxide (Jin et al.,

2010a, 2010b; Moreira Teixeira 2011, 2012). The gelation can be tuned to take between 20 and 30 seconds (Jin et al., 2010a) and results in covalent bonding of the hydrogel to the surrounding tissue (Wang et al., 2014). When combined with chondrocytes or mesenchymal stem cells, the hydrogel supports cartilage formation (Jin et al., 2011) and facilitates cell ingrowth (Moreira Teixeira 2012) *in vitro* and *ex vivo*, and appears a good candidate for facilitating intrinsic cartilage repair.

Clinical outcome in humans may only be evaluated once pre-clinical large animal studies have shown favorable results. In order for such studies to function as a predictive model for human clinical response, follow-up needs to be sufficiently long (Vindas Bolanos et al., 2017). The equine stifle joint has proved to be one of the closest approximations to the human knee joint in terms of cartilage thickness and composition (Malda et al., 2012), which is why the horse is one of the preferred models to test interventions intended for the human knee joint (Cook et al. 2014). The aim of the current study was to evaluate the regenerative potential of a self-sealing hydrogel for the treatment of chondral defects in a long-term *in vivo* study using the equine stifle joint model.

Methods

Hydrogel synthesis and preparation

Dextran-tyramine (Dex-TA, 40 kDa) and hyaluronic acid-tyramine (HA-TA, 25 kDa) were synthesized as previously described (Wennink et al., 2011) and dissolved in sterile PBS to obtain a 10 w/v% dilution. Hydrogen peroxide 30% (Sigma-Aldrich Cat No. 7722-84-1) was dissolved in PBS to obtain a 3% dilution. Dex-TA and HA-TA were mixed in a 1:1 ratio by resuspension and then split up in two equal parts. HRP was added to one part of the mixture at 20% v/v (1 part dissolved HRP in 4 parts polymer solution) and H_2O_2 was added to the second part to obtain a final concentration of 0.03%. The sterile gel was applied via a double chamber syringe into the defect were in situ gelation occurred.

In vivo study

Animals

The protocols and studies described were approved by the ethical and animal welfare committees from the Veterinary School at the National University of Costa Rica. Eight healthy adult Criollo breed horses (mean age 7.1 years, range 5 - 9 years; mean weight 319 kg, range 275 – 375 kg) with no history of stifle joint pathology were used. Horses were clinically sound on lameness examination, had normal hematology and serum biochemistry results, and showed no radiographic abnormalities of either stifle joint. They were housed in individual box stalls and fed a standard maintenance ration of

concentrate with hay ad libitum and had free access to water during the first three months of the study. After this period, they were maintained at free pasture at the University farm with unlimited excess to hay and water.

Surgical procedure

After IV premedication with xylazine (1.1 mg/kg; Pisa, Mexico), a 12G jugular venous catheter was placed and phenylbutazone (2.2 mg/kg; Holliday, Argentina) administered IV for peri-operative analgesia. Anaesthesia was induced with midazolam (0.05 mg/kg; Holliday, Argentina) IV and ketamine (2.2 mg/kg; Holliday, Argentina) IV and the horse was positioned in dorsal recumbence. General anesthesia was maintained with isoflurane in oxygen.

Prior to surgery, left and right stifle joints were randomly allocated to be treated with either the hydrogel or nanofracturing (a novel technique with potential advantages over routine microfracturing; Cokelaere et al. manuscript in preparation) as a control treatment (Figure 1). One partial-thickness chondral defect (1 mm depth) was created via mini-arthrotomy in the mid-medial trochlear ridge of each stifle joint by the same surgeon (SC) using a 7-mm diameter biopsy punch. Remnants of cartilage in the defect bed were removed using a sharp curette. For nanofracture, each cartilage lesion was treated with three perforations distributed across the 7-mm defect. Defects were flushed with sterile saline (Baxter, USA) before and after application of the hydrogel or nanofracturing, to remove any left-over debris. Hydrogel was applied using a sterile applicator, taking care to make the hydrogel level with the surface of the cartilage. Incisions were routinely closed in four layers (joint capsule, deep fascia, superficial fascia, and skin) and a stent bandage was applied over the incision. Horses were allowed to recover from anesthesia and returned to their stalls immediately after surgery.

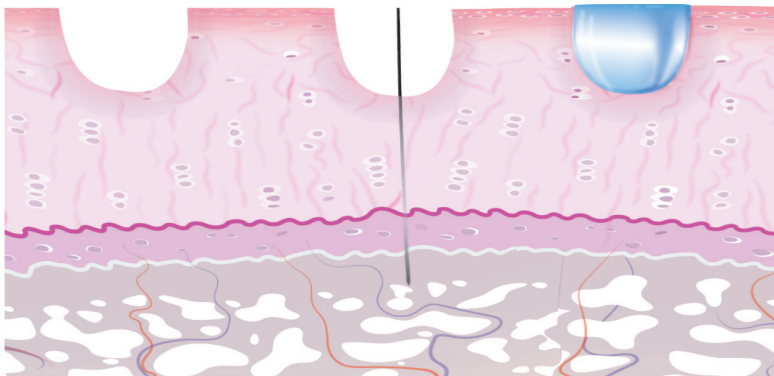**Figure 1** Schematic diagram of surgically created partial cartilage thickness defects before treatment (left), treated with nanofracture, penetrating the subchondral bone plate to engage bone marrow stem cells and trophic factors (middle), or treated with an experimental self-sealing hydrogel that covalently binds to the defect walls and leaves the underlying bone intact (right).

Post-operative care and monitoring

Post-operatively, horses received antibiotics for 5 days (procaine penicillin (Phenix, Belgium) 15000 IU/kg IM SID and gentamicin (Kepro BV, the Netherlands) 6.6 mg/kg IV SID) and non-steroidal anti-inflammatory drugs (phenylbutazone (Lisan, Costa Rica; 2.2 mg/kg PO BID) during the first 10 days. Horses were clinically monitored on a daily basis for rectal temperature, heart rate and respiratory rate, as well as stance, demeanor and general appearance; routine hematology and serum biochemistry were investigated one, three and six months post-operatively. Gait was evaluated at walk daily, with a more comprehensive lameness examination performed if irregularities were noticed. From three months post-operatively, horses were turned out at free pasture allowing natural exercise until the end of the experiment.

Euthanasia and sample harvesting

Horses were euthanized 7 months post-operatively. Deep anaesthesia was induced with a combination of xylazine (1.1 mg/kg IV, Pisa, Mexico) followed by ketamine and midazolam (3 mg/kg IV and 0.05 mg/kg IV respectively; Holliday, Argentina), after which a bolus of oversaturated magnesium sulphate (200 g/L; Agreagro S.A., Costa Rica) and chloral hydrate (200 g/L) solution was administered IV to effect and death was confirmed by absence of breathing, ictus and corneal reflex.

After opening the femoropatellar joint, macroscopic pictures were taken using multiple focal distances and angles. Subsequently, blocks of tissue containing the defect were excised. Each piece containing the defect was fixed and stored in 10% formalin in individual plastic container and sent to Utrecht University, the Netherlands, for further analysis.

Macroscopic assessment

The ICRS-I Visual Assessment Scale (Table 1) was used for macroscopic scoring of defect repair on photographs taken after opening of the femoropatellar joint. Three images of each cartilage defect (perpendicular overview, zoomed in on the defect with immediately adjacent tissue, and at an angle to the trochlear ridge) were selected. These images were randomly labelled and scored by three blinded observers, who scored all images twice within one week.

Table 1 – International Cartilage Repair Society Visual Assessment Score (ICRS-I; Van den Borne et al., 2007)

Cartilage repair assessment ICRS	Points
Degree of defect repair	
In level with surrounding cartilage	4
75% repair of defect depth	3
50% repair of defect depth	2
25% repair of defect depth	1
0% repair of defect depth	0
Integration to border zone	
Complete integration with surrounding cartilage	4
Demarcating border < 1mm	3
¾ of graft integrated, ¼ with notable border > 1mm width	2
½ of graft integrated with surrounding cartilage, ½ with a notable border >1mm	1
From no contact to ¼ of graft integrated with surrounding cartilage	0
Macroscopic appearance	
Intact smooth surface	4
Fibrillated surface	3
Small, scattered fissures of cracks	2
Several, small or few but large fissures	1
Total degeneration of grafted area	0
Overall repair assessment	
Grade I: normal	12
Grade II: nearly normal	8-11
Grade III: abnormal	4-7
Grade IV: severely abnormal	1-3

Microscopic assessment

Formalin-fixed osteochondral plugs were procured from the formalin-stored tissue blocks and used for histopathologic analysis. They were embedded in paraffin and sections were processed and stained for routine histopathologic analysis. Stains included Safranin-O (SAF-O), Alcian Blue (AB), Hematoxylin-Eosin (HE) and collagen-II immunohistochemistry (IHC) using a rabbit polyclonal anti-COLII primary antibody (Abcam, Cambridge, UK). An osteochondral plug of a healthy horse was used as a

normal control for all histological scoring, and non-immune controls (without the primary antibody) were included for IHC. Microscopic assessment was performed using the ICRS-II scoring system (Mainil-Varlet et al., 2010; see results Table 2 for scoring criteria) on number-coded images (Nanozoomer 2.0-RS slide scanner, Hamamatsu) of HE, SAF-O and AB stained slides obtained from each border of the defect as well as mid-defect. Scores were assigned by three observers blinded to horse, joint and treatment. One observer (JG) also assessed collagen II immunohistochemistry images of each defect.

Micro-CT

The samples were removed from formalin, dried and manually positioned in the μCT system (μ-CT 80, ScancoMedicalAG, Switzerland). Specific settings of the μCT system included voltage of 90 kV, current of 200 μA, field of view (FOV) of 20 mm and scan time of 4.5 minutes. Settings were the same for all samples and created 512 μCT images per sample. Fiji software (version ImageJ1.52g) was used to edit μCT images for further analyses using manual selection of regions of interest (ROI) for subchondral bone plate thickness as well as for cartilage thickness estimation both mid-defect and at a set distance from the defect ('adjacent').

Statistical analysis

Statistical analysis of macroscopic scoring and μCT results was performed using R version 3.5.1 (R Foundation for Statistical Computing; 2018) and the ggplot2 package. Histological scores were statistically analyzed using SPSS software (SPSS, IBM statistics, version 25.0).

The macroscopic scores were loaded into R and partially converted to factorial numbers to allow analysis. A One Way ANOVA completely randomized full-factorial design was used to assess the effect of treatment on the overall repair assessment score. A Tukey test was used to compare between treatments, and p values <0.05 were considered significant.

As exact cartilage defect location on the medial trochlear ridge showed some variation between horses (Figure 1), statistical analysis of μCT data for cartilage thickness was performed on the ratio of cartilage thickness mid-defect divided by that at a set distance from the proximal defect edge ('adjacent'):

y_{ij}= (Cartilage Thickness Mid-Defect$_i$/ Cartilage Thickness Adjacent$_j$) *100

where y is the cartilage thickness ratio. A paired t-test was used to compare the effect of treatment on cartilage thickness ratio as well as on subchondral bone plate thickness immediately underlying the defect.

Results

Post-operative course and clinical monitoring

One of the horses showed dehiscence of the skin wound, which was immediately treated by re-suturing which resulted in further uneventful healing of the wound. Over the 7 months follow-up, 7 out of 8 horses recovered uneventfully and coped well during the post-surgical rehabilitation period. Two months postoperatively, one horse unfortunately died due to an unrelated traumatic head injury; osteochondral tissue blocks were harvested but no photographs were obtained from this horse. In the remaining horses, no significant (≥ 1/5 on AAEP scale) lameness was observed at any time, and clinical parameters as well as routine hematology and serum biochemistry parameters remained within normal physiologic limits throughout the experiment. Radiographs were taken at baseline but not subsequently, as the clinical course was deemed very satisfactory.

Macroscopic assessment

At the time of euthanasia, defect sites were still readily recognizable by an indentation in the cartilage. Nanofracture treated joints typically showed more extensive visible filling of the defect with repair tissue than hydrogel-treated joints (Figure 2). Inter-observer agreement for visual assessment using the ICRS-I scoring system performed by three blinded observers was good (Cronbach's alpha = 0.86; p <0.001). Median overall repair assessment score was significantly higher, indicating better visual appearance of repair, for nanofracture treated (median 9, interquartile range (IQR) 7 – 10) compared to hydrogel treated defects (median 5, IQR 3 – 7; $p < 0.001$). Similar significant differences were found for each individual item of the visual assessment scoring system (i.e., degree of defect repair, integration to border zone, and macroscopic appearance; p <0.001, p = <0.001, and p <0.001, respectively).
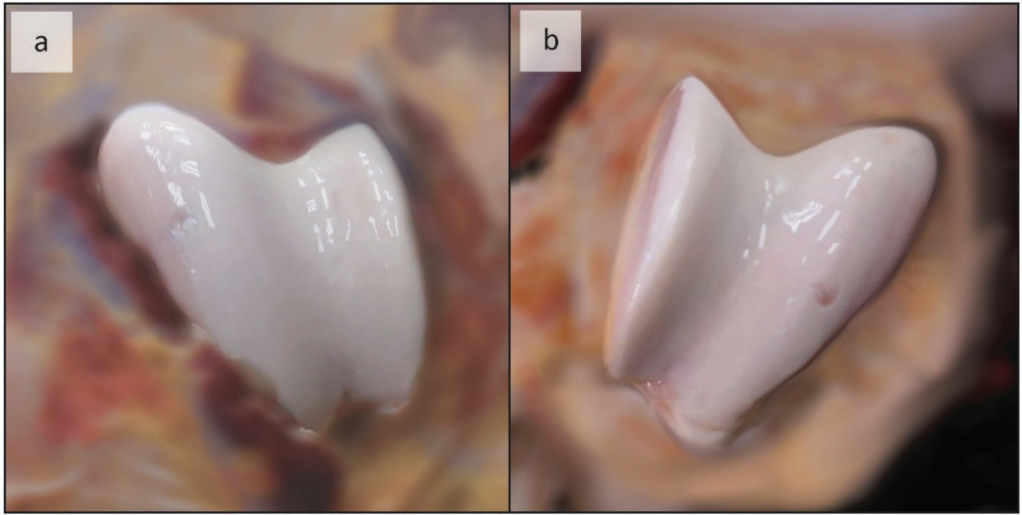
Figure 2 Typical macroscopic appearance of a nanofracture (a) and hydrogel (b) treated partial thickness cartilage defect 7 months after surgical application of either technique in contralateral stifle joints of the same horse. Despite the slightly different camera angle, it can be appreciated that defect location varied by approximately one centimeter between sides.

Histopathologic analysis

Results of microscopic cartilage repair assessment using the ICRS-II scoring system averaged over three blinded observers are shown in Table 2. Reliability analysis of scoring performed by three blinded observers yielded a Cronbach's alpha of 0.78, which is acceptable (where > 0.8 is rated as good). One of the 14 ICRS-II criteria, tissue morphology, was not assessed, as polarized light microscopy was not performed. Mean total ICRS-II score was significantly worse in the nanofracture group (48% ± 10%; mean± SD) compared to the hydrogel group (72% ± 7%; mean ± SD, where 100% denotes normal cartilage; p = 0.0007; Table 2). Hydrogel treated joints showed significantly better scores for every ICRS-II criterion assessed except matrix staining (Table 2). Defects treated with nanofracture contained mainly fibrous and fibrocartilaginous repair tissue, as evidenced by relatively poor cell morphology, surface architecture and collagen II immunohistochemical staining; subchondral bone and calcification / tidemark abnormalities were appreciable in the nanofracture but not the hydrogel treated defects (Figure 3).

Table 2 - Histologic scoring results, using the ICRS-II scoring system (Mainil-Varlet et al., 2010) for cartilage repair tissue assessed by three blinded observers 7 months after nanofracture (n = 7) or hydrogel (n = 7) treatment of experimentally created chondral defects in the equine stifle joint.

Scoring item	Mean score (%)	SD	Mean score (%)	SD	P-value
	Nanofracture		**Hydrogel**		
1. Tissue morphology	---------------------Not scored-------------------				
2. Matrix staining	41	7	48	4	**0.071**
3. Cell morphology	33	9	58	7	**< 0.01**
4. Chondrocyte clustering	57	24	88	8	**0.021**
5. Architecture of surface	37	11	54	7	**0.011**
6. Basal integration	67	9	86	10	**< 0.01**
7. Calcification front / tidemark	51	21	81	13	**0.016**
8. Subchondral bone abnormalities	45	17	85	10	**< 0.01**
9. Inflammation	76	9	91	7	**0.011**
10. Abnormal calcification	52	16	86	10	**< 0.01**
11. Vascularization in repair tissue	59	13	83	9	**0.020**
12. Surface / superficial assessment	32	12	50	10	**< 0.01**
13. Mid / deep zone assessment	38	16	68	9	**< 0.01**
14. Overall assessment	33	12	60	8	**< 0.01**
Mean total score	***48***	***10***	***72***	***7***	***< 0.01***
Collagen II immunohistochemistry	***55***	***17***	***86***	***11***	***< 0.01***

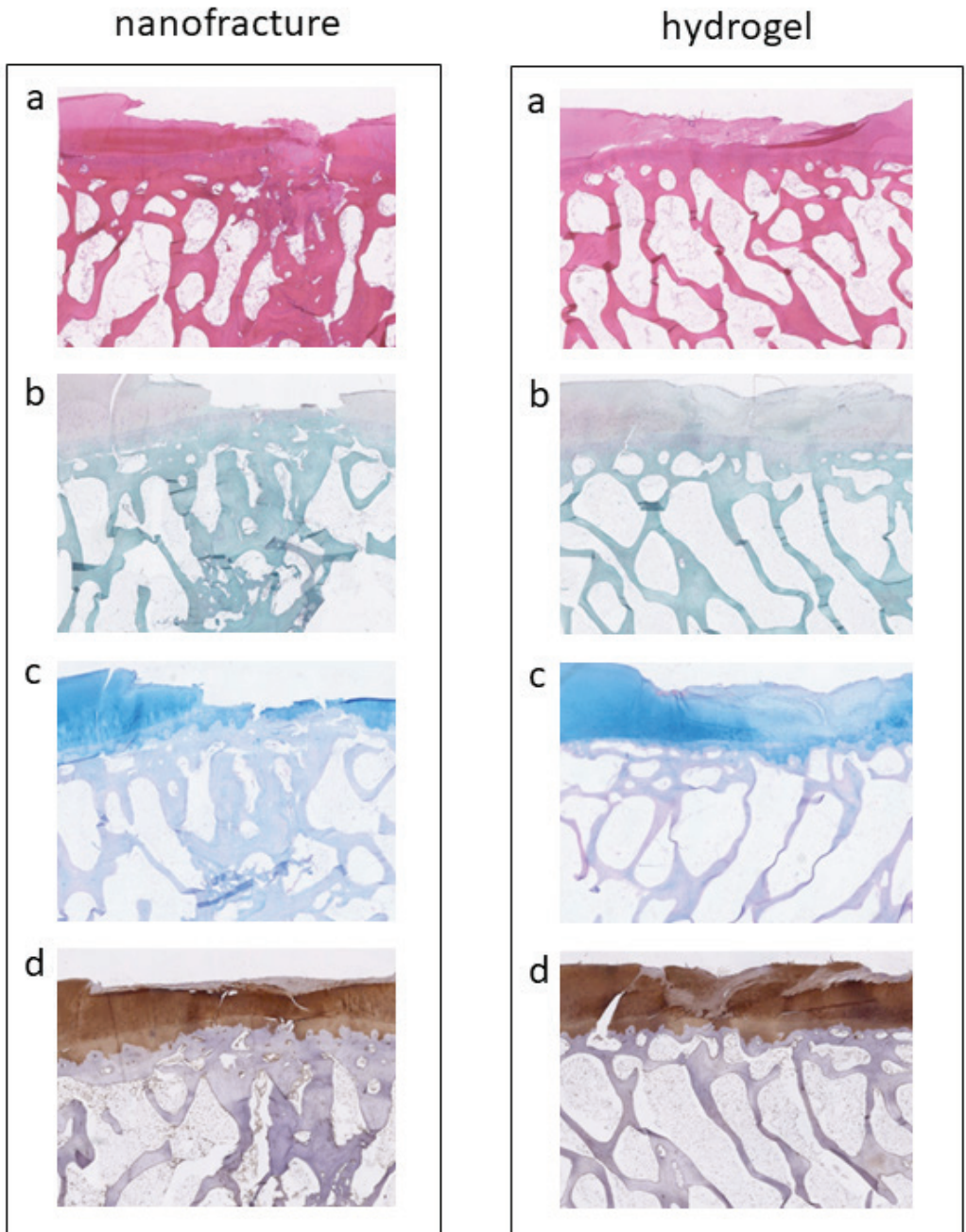## nanofracture

hydrogel

Figure 3 Histological outcome 7 months after nanofracture (left) or hydrogel (right) treatment of partial thickness cartilage defects in contralateral stifle joints of the same horse. (a) Hematoxyllin-Eosin stained section mid-defect (b) Safranin-O stained section mid-defect (c) Alcian Blue stained section mid-defect.

MicroCT analysis

Mean cartilage thickness mid-defect was 97.6 ± 7.7% (mean ± SD) of adjacent cartilage thickness in nanofractured defects, compared to 87.1 ± 16.3% (mean ± SD) in hydrogel treated defects (p = 0.12). Subchondral bone plate thickness underlying the defect likewise did not differ significantly between treatment groups (p = 0.95). MicroCT image analysis showed substantially altered subchondral bone microarchitecture in all nanofracture treated defects 7 months post-operatively (Figure 2b), compared to no such disturbance in hydrogel treated joints.

Discussion

This is the first long-term *in vivo* large animal study on the effects of an injectable and *in situ* gelating hydrogel for the repair of experimentally created partial thickness cartilage lesions. The horse was used as the animal species, as it is generally considered the closest to the human situation in a technical sense, but also as a very challenging model because of the relatively high biomechanical loads and the immediate weight-bearing after surgery (Cook et al. 2014, McIlwraith et al. 2011, Moran et al. 2016). In this particular case, horses of the local Criollo breed were used, which are not only a little more sturdy, but also on average much lighter than the breeds that are more commonly used (Warmbloods, Standardbred trotters or Thoroughbreds), which may have been an advantage for this study.

Injectable and *in situ* gelating hydrogels offer many potential advantages in comparison to other articular regenerative medicine approaches that have been developed and tested to a greater or lesser extent *in vivo.* An important advantage is that the gel, thanks to its capacity to almost instantaneously form cross-links with the native cartilage, obviates the need for fixation of the material in the defect. Fixation of articular cartilage grafts, especially in shallow partial thickness defects, is not a trivial issue (Mancini et al., 2017). Suturing the graft itself or covering it by a sutured membrane, be it a periosteal flap or a custom-made collagen membrane, has been reported, but may lead to OA development (Hunziker and Stähli, 2008). The feasibility of the use of trans-osseous sutures or biodegradable pins depends on the nature of the scaffold and will anyhow affect the structure of the latter (Bekkers et al., 2010). The use of commercially available fibrin glue to retain grafts is well accepted in human orthopaedic surgery (Bekkers et al., 2013), but there are serious concerns with respect to the suitability of the product for use in several animal species, among which are the goat and the horse (Brehm et al., 2006; Mancini et al., 2017). The alternative as suggested by Mancini et al. (2017), *i.e.* the use of a composite osteochondral implant, solves the fixation problem as these can be implanted in a press-fit manner, but creates a much larger osteochondral lesion which, at least intuitively, does not seem the best approach for

treating shallow partial thickness chondral defects. Another advantage of the currently tested hydrogel is that it relies on ingrowth of locally available stem cells and thus obviates the need for both the use of allogenic cells and for a two-stage procedure, as is common in ACI or MACI procedures (Brittberg et al., 1994). This avoids (almost insurmountable) regulatory hurdles and also greatly reduces treatment costs, thereby greatly enhancing the chance of acceptance by the health care industry. A further technical advantage is that the absence of (vulnerable) cells during the manufacturing process of the scaffold puts far fewer constraints on this process.

The clinical outcome of the current study was considered excellent. Apart from superficial wound dehiscence without further consequences in a single horse, all animals recovered well and rapidly after surgery and showed no lameness at all during the entire course of the experiment. The one horse that was lost to follow-up for the study sustained a traumatic head injury and suffered a highly complicated mandibular fracture, for which it was euthanized, but showed no negative effect whatsoever of the experimental intervention.

Macroscopically, the control joints that underwent nanofracturing showed significantly better assessment scores than the hydrogel treated joints particularly for degree of defect filling and integration to border zone. Median overall macroscopic assessment score was 'near-normal' for nanofracture, compared to 'abnormal' for hydrogel treated defects. Importantly however, histologically, the hydrogel treated defects scored significantly better on every single item of the ICRS-II scoring system, with only the criterion 'matrix staining' just failing to reach statistical significance. The better macroscopic appearance could be attributed to a more advanced covering of the defect site by fibrocartilaginous scar tissue that tends to form over lesions treated with micro- or nanofracturing (Frisbie et al., 1999). Histologically however, this repair tissue was characterized by relatively poor cell morphology and surface architecture, disordered collagen II immunohistochemical staining, and calcification abnormalities. The superior macroscopic appearance of the nanofracture treated defects is therefore of questionable clinical value, as it is well-known that such fibrocartilaginous tissue, though providing visually good defect filling, is biomechanically inferior to native hyaline cartilage, and therefore less resistant to wear and tear, in the end giving way to OA (Bae et al., 2006; Goyal et al., 2013; Kreuz et al. 2006a; 2006b; Mithoefer et al., 2016).

The blinded histologic assessment of the repair tissue in hydrogel treated defects was considerably and significantly better than that of nanofractured control defects. The individual scoring items (criteria) showing the biggest differences between treatments, with hydrogel treatment scoring at least 30% higher than nanofractured defects, were: chondrocyte clustering, calcification front / tidemark, abnormal calcification,

subchondral bone abnormalities and superficial assessment. The better maintenance of the calcification front, reduced abnormal calcification within the repair tissue, and reduced subchondral bone abnormalities (mean score of 45% for nanofracture vs. 85% for hydrogel treatment, where 100% denotes normal hyaline cartilage) together corroborate what is one the main purported advantages of the hydrogel compared to bone marrow stimulation or osteochondral implant techniques that require bone anchors: the lack of subchondral bone disturbance.

This was also supported by microCT analysis, which revealed changes to subchondral bone microarchitecture in all nanofractured defects 7 months after surgery, compared to no such changes in hydrogel treated joints. While this is likely due to the absence of subchondral bone penetration with the hydrogel treatment, it also shows that at least within this follow-up time, no secondary changes to the subchondral bone due to inadequate biomechanics of the overlying repair tissue had occurred (DeFalco et al., 2003). Despite the clearly superior histologic assessment of hydrogel treated defects compared to control defects, it should be noted that also in hydrogel treated defects, repair tissue was still far removed from native hyaline cartilage with a score of 72% compared to 100% for normal cartilage. This discrepancy is also underlined by the relatively poor mean score for matrix staining (48%). In this respect, it is a shame that no polarized light microscopy was undertaken, as this would have helped provide an additional insight in repair tissue matrix organization (Hoemann et al., 2011). It is therefore not unlikely that a considerable discrepancy remains between the functional characteristics of the repair tissue and those of native cartilage. However, the histologic appearance of the tissue after 7 months in the demanding equine *in vivo* situation was substantially better than what was seen in an earlier experiment with a similar set-up, in which a scaffold based on decellularized extracellular matrix was tested under comparable circumstances (Vindas Bolaños et al., 2016). Hence, the conclusion that the current results should be considered an encouraging achievement seems warranted.

The study as reported here has several limitations that should be noted. Importantly, biomechanical analysis of repair tissue was not performed. As the ultimate test of cartilage repair tissue is not how it looks macroscopically or microscopically but how it performs under normal joint loading conditions (Brommer 2005), it would have been very helpful if static and dynamic modulus testing or even simple clinical cartilage indentation had been performed. Other limitations include the relatively low number of animals (which is a well-known limitation of large animal studies for ethical, economic and logistic reasons) and the lack of advanced longitudinal monitoring (other than clinical data) during the course of the experiment. The equine model, in contrast to many other animal models, offers good opportunities for close monitoring of the animals over time (*e.g.* serial collection of synovial fluid, repeat arthroscopies, kinetic and kinematic measurements), thus reducing the total reliance on endpoint

measurements (Vindas Bolaños et al., 2016). Unfortunately, these attributes could not be taken advantage of during this experiment because of practical constraints associated with the geographic location of the study.

As always in articular cartilage research where the goal is lifetime survival, the duration of the experiment may be considered a limitation as well. Six months is often seen as the lower limit of a long-term (large) animal study, so this experiment was only just of sufficient duration. Economic constraints are of course an issue in this respect, but any novel intervention that provides promising results should ideally be subjected to further experimental *in vivo* testing with a minimum duration of follow-up of one year (McIlwraith and Frisbie, 2010).

It can be concluded that the clinical and histological outcome of this first long-term large animal study using the described injectable and in situ gelating hydrogel seems promising, and further research into this avenue of articular regenerative medicine is warranted.

Acknowledgements

References

Bae, D.K., Yoon, K.H., Song, S.J., 2006. Cartilage healing after microfracture in osteoarthritic knees. Arthroscopy Apr;22, 367-374.

Bedi, A., Feeley, B.T., Williams, R.J.r., 2010. Management of articular cartilage defects of the knee. .J Bone Joint Surg Am 92, 994-1009.

Bekkers, J., Tsuchida, A., Malda, J., Creemers, L., Castelein, R., Saris, D., Dhert, W., 2010. Quality of scaffold fixation in a human cadaver knee model. Osteoarthritis Cartilage 18, 266-272.

Bekkers, J.E., Tsuchida, A.I., van Rijen, M.H., Vonk, L.A., Dhert, W.J., Creemers, L.B., Saris, D.B., 2013. Single-stage cell-based cartilage regeneration using a combination of chondrons and mesenchymal stromal cells comparison with microfracture. . Am J Sports Med 41, 2158-2166.

Brittberg, M., Lindahl, A., Nilsson, A., Ohlsson, C., Isaksson, O., Peterson, L., 1994. Treatment of deep cartilage defects in the knee with autologous chondrocyte transplantation. N Engl J Med 331, 889-895.

Brommer, H. 2005. Towards Detection of Functional Failure of Equine Articular Cartilage. The Metacarpophalangeal Joint Under Scrutiny.PhD, Utrecht, The Netherlands.

Cook, J.L., Hung, C.T., Kuroki, K., Stoker, A.M., Cook, C.R., Pfeiffer, F.M., Sherman, S.L., Stannard, J.P., 2014. Animal models of cartilage repair. Bone Joint Res 3, 89-94.

Decker, R.S., Um, H.B., Dyment, N.A., Cottingham, N., Usami, Y., Enomoto-Iwamoto, M., Kronenberg, M.S., Maye, P., Rowe, D.W., Koyama, E., Pacifici, M., 2017. Cell origin, volume and arrangement are drivers of articular cartilage formation, morphogenesis and response to injury in mouse limbs. Dev Biol 426, 56-68.

DeFalco, R.A., Ricci, A.R., Balduini, F.C., 2003. Osteonecrosis of the knee after arthroscopic meniscectomy and chondroplasty: a case report and literature review. Am J Sports Med. Nov-Dec;31, 1013-1016.

Frisbie, D.D., Trotter, G.W., Powers, B.E., Rodkey, W.G., Steadman, J.R., Howard, R.D., Park, R.D., McIlwraith, C.W., 1999. Arthroscopic subchondral bone plate microfracture technique augments healing of large chondral defects in the radial carpal bone and medial femoral condyle of horses. . Vet Surg. Jul-Aug;28, 242-255.

Garcia, J., Wright, K., Roberts, S., Kuiper, J.H., Mangham, C., Richardson, J., Mennan, C., 2016. Characterisation of synovial fluid and infrapatellar fat pad derived mesenchymal stromal cells: The influence of tissue source and inflammatory stimulus. Sci. Rep 6, 1-11.

Goyal, D., Keyhani, S., Lee, E.H., Hui, J.H., 2013. Evidence-based status of microfracture technique: A systematic review of level I and II studies. Arthroscopy: The Journal of Arthroscopic and Related Surgery 29, 1579-1588.

Hoemann, C., Kandel, R., Roberts, S., Saris, D.B., Creemers, L., Mainil-Varlet, P., Méthot, S., Hollander, A.P., Buschmann, M.D., 2011. International Cartilage Repair Society (ICRS) Recommended Guidelines for Histological Endpoints for Cartilage Repair Studies in Animal Models and Clinical Trials. Cartilage Apr;2, 153-172.

Hunter, W., 1995. Of the structure and diseases of articulating cartilages. 1743. Clin Orthop Relat Res. Aug;(317), 3-6.

Hunziker, E.B., Stähli, A., 2008. Surgical suturing of articular cartilage induces osteoarthritis-like changes. Osteoarthritis Cartilage 16, 1067-1073.

Jin, R., Moreira, T.L.S., Dijkstra, P.J., van Blitterswijk, C.A., Karperien, M., Feijen, J., 2010a. Enzymatically-crosslinked injectable hydrogels based on biomimetic dextran-hyaluronic acid conjugates for cartilage tissue engineering. Biomaterials Apr;31, 3103-3113.

Jin, R., Moreira, T.L.S., Dijkstra, P.J., van Blitterswijk, C.A., Karperien, M., Feijen, J., 2011. Chondrogenesis in injectable enzymatically crosslinked heparin/dextran hydrogels. Journal of Controlled Release 152, 186-195.

Jin, R., Moreira, T.L.S., Dijkstra, P.J., Zhong, Z., van Blitterswijk, C.A., Karperien, M., Feijen, J., 2010b. Enzymatically crosslinked dextran-tyramine hydrogels as injectable scaffolds for cartilage tissue engineering. Tissue Engineering - Part A 16, 2429-2440.

Kreuz, P.C., Erggelet, C., Steinwachs, M.R., Krause, S.J., Lahm, A., Niemeyer, P., Ghanem, N., Uhl, M., S¨udkamp, N., 2006a. Is microfracture of chondral defects in the knee associated with different results in patients aged 40 years or younger? . Arthroscopy November,22, 1180-1186.

Kreuz, P.C., Steinwachs, M.R., Erggelet, C., Krause, S.J., Konrad, G., Uhl, M., S¨udkamp, N., 2006b. Results after microfracture of full-thickness chondral defects in different compartments in the knee. Ostearthritis and Cartilage Nov;14, 1119-1125.

Kubosch, E.J., Lang, G., Furst, D., Kubosch, D., Izadpanah, K., Rolauffs, B., 2018. The Potential for Synovium-derived Stem Cells in Cartilage Repair. Curr. Stem Cell Res. Ther 13, 174-184.

Lawrence, R.C., Felson, D.T., Helmick, C.G., Lesley, M., Arnold, M.D., Hyon Choi, H., Deyo, R.A., Gabriel, S., Hirsch, R., Hochberg, M.C., G. Hunder, G.G., Jordan, J.M., Katz, J.N., Kremers, H.M., Wolfe, F., 2008. National Arthritis Data Workgroup. Estimates of the prevalence of arthritis and other rheumatic conditions in the United States. Part II. Arthritis Rheum Jan;58, 26-35.

Levato, R., Webb, W.R., Otto, I.A., Mensinga, A., ., Zhang, Y., van Rijen, M., van Weeren, R., Khan, I.M., Malda, J., 2017. The bio in the ink: cartilage regeneration with bioprintable hydrogels and articular cartilage-derived progenitor cells. Acta Biomater Oct 1, 41-53.

Mainil-Varlet, P., van Damme, B., Nesic, D., Knutsen, G., Kandel, R., Roberts, S., 2010. A new histology scoring system for the assessment of the quality of human cartilage repair ICRS II. Am J Sports Med May;38, 880-890.

Malda, J., Benders, K.E.M., Klein, T.J., de Grauw, J.C., Kik, M.J.L., Hutmacher, D.W., Saris, D.B.F., van Weeren, P.R., Dhert, W.J.A., 2012. Comparative study of depth-dependent characteristics of equine and human osteochondral tissue from the medial and lateral femoral condyles. Ostearthritis and Cartilage 20, 1147-1151.

Mancini, I.A.D., Vindas Bolaños, R.A., Brommer, H., Castilho, M., Ribeiro, A., van Loon, J.P.A.M., Mensinga, A., van Rijen, M.H.P., Malda, J., van Weeren, P.R., 2017. Fixation of Hydrogel Constructs for Cartilage Repair in the Equine Model: A Challenging Issue. TISSUE ENGINEERING 23, 804-814.

McIlwraith, W.C., Fortier, L.A., Frisbie, D.D., Nixon, A.J., 2011. Equine Models of Articular Cartilage Repair. Cartilage 2, 317-326.

McIlwraith, W.C., Frisbie, D.D., 2010. Microfracture: Basic Science Studies in the Horse. Cartilage 1, 87-95.

Mithoefer, K., Venugopal, V., Manaqibwala, M., 2016. Incidence, degree, and clinical effect of subchondral bone overgrowth after microfracture in the knee. Am J Sports Med. 44, 2057-2063.

Moran, C.J., Ramesh, A., Brama, P.A., O'Byrne, J.M., O'Brien, F.J., Levingstone, T.J., 2016. The benefits and limitations of animal models for translational research in cartilage repair. J Exp Orthop 3.

Moreira, L.S.T., Bijl, S., Pully, V.V., Otto, C., Jin, R., Feijen, J., van Blitterswijk, C.A., Dijkstra, P.J., Karperien, M., 2012. Self-attaching and cell-attracting in-situ forming dextran-tyramine conjugates hydrogels for arthroscopic cartilage repair. Biomaterials 2012, 3164-3174.

Moreira, L.S.T., Feijen, J., van Blitterswijk, C.A., Dijkstra, P.J., Karperien, M., 2011. Enzyme-catalyzed crosslinkable hydrogels: Emerging strategies for tissue engineering. Biomaterials 33, 1281-1290.

R Foundation for Statistical Computing; version 3.5.1.3.5.1., R.F.f.S.C.v., Vienna, Austria, 2018., https://www.R-project.org.

Vindas Bolaños, R.A., Cokelaere, S.M., Estrada McDermott, J.M., Benders, K., E.M., Gbureck, U., Plomp, S.G.M., Weinans, H., Groll, J., van Weeren, P.R., Malda, J., 2017. The use of cartilage decellularized matrix scaffold for the repair of osteochondral defects: the importance of long-term studies in large animal model. Ostearthritis and Cartilage 25, 413-420.

Wang, R., Leber, N., Buhl, C., Verdonschot, N., Dijkstra, P.J., Karperien, M., Technologies, P.f.A., 2014. Cartilage adhesive and mechanical properties of enzymatically crosslinked polysaccharide tyramine conjugate hydrogels. 25, 568-574.

Wennink, J.W.H., Niederer, K., Bochyńska, A.I., 2011. Injectable Hydrogels by Enzymatic Co- Crosslinking of Dextran and Hyaluronic Acid Tyramine Conjugates. Macromol Symp 309-310.

Williams, R., Khan, I., M, Richardson, K., Nelson, L., McCarthy, H.E., Analbelsi, T., Singhrao, S.K., Dowthwaite, G.P.-., Jones, R., E. , Baird, D.M., Lewis, H., Roberts, S., Shaw, H.M., Dudhia, J., Fairclough, J., Briggs, T., Archer, C.W., 2010. Identification and clonal characterisation of a progenitor cell sub-population in normal human articular cartilage. PLoS ONE 5, p. e13246.

Chapter VIII

Summarizing Discussion

Naturam si sequemur ducem, nunquam aberrabimus[1] *(If we follow Nature as a guide, we will never go astray). These wise words by Marcus Tullius Cicero (106-43BC) could easily be the motto of modern regenerative medicine. However, as with many things, this is easier said than done. Where Nature has taken millions and in some cases billions of years to develop today's highly sophisticated and extremely complex living beings, humanity has only recently started its Odyssey of trying to artificially mimic biological function in an attempt to counteract accidental damage, disease, or simply wear and tear, in order to improve longevity and quality of life. Like Ulysses' epic journey, this endeavour is far from easy and characterized by rare moments of quick progress and joy, severe backlashes and long periods of stagnation. These last aspects become particularly and painfully evident when trying to evaluate regenerative medicine solutions for the repair of diarthrodial joints in the harsh and utterly unforgiving environment of long-term large animal models. However, like the Greek hero, modern scientists will not give up and stubbornly continue their own epic journey, driven by the hope that one day they'll come up with an approach for lasting functional repair of articular cartilage damage and hence find themselves washed upon Ithaca's promising shores. This thesis is the account of a part of this epic journey.*

The osteochondral unit: a masterpiece of natural engineering

The main function of the musculoskeletal system is to provide structure to the body and to enable locomotion. This is accomplished through a complicated system of hinged rigid bones, powered by muscles as active units and indirectly by energy-storing tendons, and interconnected by passive tendinous and ligamentous structures. The forces this system has to accommodate are those generated by the mechanical interaction of the body and the environment, which is the ground surface in the case of terrestrial locomotion. These ground reaction forces can be considerable, especially in large animals that are moving fast. In the horse, ground reaction forces have been measured during a variety of activities. Even minor athletic performance (a 60cm jump) led to an increase in ground reaction force (and thus limb loading) of a single forelimb of a 600 Kg horse from 1800 N when standing to 12,000 N, *i.e.* two times body weight and an almost 7-fold increase (Brama et al., 2001). More strenuous exercise, such as higher jumps or flat racing, will increase this figure manifold.

As in any complex structure that is made up of interconnected rigid bodies, the contact points of those rigid bodies (*i.e.* in the case of a living being the body segments) are most prone to damage and wear and tear. These points are the articulations between the rigid skeletal parts and especially the so-called diarthrodial joints that permit maximal range of motion. Diarthrodial joints are always synovial joints and their motion is limited only by periarticular or intraarticular capsular or ligamentous structures, not by the nature of the joint itself. Virtually all joints of the appendicular skeleton of both horses and humans are diarthrodial joints (van Weeren, 2016). The high challenge to these diarthrodial joints is dealt with by nature through the combination of articular cartilage (AC) and subchondral bone (SCB), which together form the osteochondral unit

---

1   Cicero: *De officiis* I, 100.

that facilitates the absorption and attenuation of the forces generated by locomotion, and allows almost frictionless gliding of articular surfaces. In this interplay of tissues, it is the cartilage that in first instance dissipates and to a certain extent redistributes the forces acting on the joint and that provides the low-friction surface that enables the supple gliding of the cartilage-capped ends of the (long) bones within the joint. These functional biomechanics of articular cartilage are enabled by the highly specialized composition and specific architecture of the cartilage, in the form of a fibrillar type II collagen network with interspersed proteoglycan aggregates. Because of the high degree of sulphation of the latter, these molecules are highly hydrophilic and attract water, leading to swelling of the extracellular matrix (ECM). This expansion of the ECM is restricted by the collagen network of which the collagen fibrils are stiff, non-elastic structures, generating an intrinsic pressure within the ECM that is maintained by the balance of osmotic pressure and the resistance of the collagen network. Loading will lead to exclusion of water, while during release of pressure water is drawn in again because of the osmotic forces.

This system will only work properly when the tissue's macro-architecture is as homogeneous as possible, which may account for the lack of structures such as blood vessels or nerves in articular cartilage. Lack of vascularization may in its turn explain the extremely long turnover times of type II collagen in the mammalian joint. The turnover time of human femoral head cartilage has been estimated at up to 350 years (Maroudas et al., 1992) and in a more recent study, human articular collagen was shown to be laid down in early puberty not to be replaced after that age at all, irrespective of whether the individual concerned suffered from osteoarthritis (OA) or not (Heinemeijer et al., 2016). Proteoglycans have a much faster turnover time, but substantial loss will inevitably alter the mechanical properties of the cartilage (Malemud, 1991). Any substantial compromise of either the hydrophilic properties of the proteoglycans or the integrity of the collagen network will lead to (partial) failure and increase the vulnerability to further damage. However, given the difference in turnover time, it will be clear that especially damage to the collagen network may have grave consequences.

The subchondral bone absorbs most of the loading, particularly in the trabecular part of it. This part is much less deformable than articular cartilage, but is still approximately 10 times more deformable than cortical bone (Mankin and Radin, 1993), making it very well suitable for the attenuation of forces, but also prone to fatigue and ensuing failure. A great advantage of subchondral bone is that it retains its capacity to remodel and adapt according to Wolff's law throughout life (Gartner, 2017; Stewart and Kawcak, 2018). Subchondral bone should not be viewed as a mere passive supporting structure for the overlying cartilage; not only are subchondral bone changes (sclerosis, marrow oedema, remodelling) an intricate element of clinical OA (Saltzman and Riboh, 2018), the subchondral bone marrow is an important endogenous source of regenerative

potential in the form of progenitor cells and trophic factors. Because there are limitations even to the large regenerative capacity of bone with major bone defects not healing spontaneously, there is a clinical need for the improvement of healing of both extensive subchondral pathology and of these large bone defects. In both instances, biomaterial-based interventions may prove the best approach to restore bone regenerative capacity.

When resilience succumbs to incessant overcharging

The mechanical challenges posed to the musculoskeletal system may be quite severe, as pointed out above. However, more than the sheer magnitude of forces, it is the repetitive nature of these stresses and strains that seems to be most injurious. Even the strongest or most resilient system will fail when falling victim to either single events of massive overcharging, or, more likely and more frequently, to relentless minor overcharging with insufficient time for repair, resulting in cumulative micro-damage (Goldring, 2012; McIlwraith et al., 2012; Stewart and Kawcak, 2018). This so-called micro-trauma occurs frequently in both humans and horses and may manifest as very bothersome and performance-hampering, but not life-threatening, repetitive strain injuries, but may also lead to dramatic fatalities (*e.g.* subchondral bone disease in racing Thoroughbreds, culminating in catastrophic fracture (Whitton et al., 2018)). In Thoroughbred racing it is known that not so much the top speed during racing or training is a risk factor for catastrophic injuries, but the accumulation of high-load training events (Janes et al., 2017), which lead to accumulated micro-damage that cannot be fully repaired in time. For cartilage the same mechanism (insidious wear and tear leading to gradual degradation) applies. The lack of repair capacity as outlined above is a strongly complicating factor that makes cartilage degradation and the ensuing development of OA into a progressively invalidating chronic condition.

Size matters: mice ain't men

Mice (and to a lesser extent rats and rabbits) are often the experimental animals of choice in the biomedical sciences. They have many advantages: they come in inbred strains reducing inter-individual variation, knock-out and knock-in mutants can be easily generated, they are cheap and they have little appeal to the general public, facilitating the acceptance of their use as experimental animals. In musculoskeletal research they have the huge drawback that, due to their size and weight, their biomechanics are crucially different from larger animals. As the biomechanical performance is essentially the main, if not the only, functional output of the musculoskeletal system, this means these animals are inherently unsuitable to test functional outcome in any form of regenerative medicine approach to musculoskeletal repair. Importantly, these small mammals have higher cartilage cellularity (Malda et al., 2013) and higher intrinsic regenerative ability than humans and larger animals (Muschler et al., 2010). Also, they are short-lived, where in musculoskeletal research it is long-term outcome that matters most (Ahern et al., 2008; Cook et al., 2014; Di Pietro et al., 2018; Kreuz et al., 2006a; Moran et al., 2016).

These drawbacks have been recognized and it is now generally accepted that for orthopaedic applications, testing in large animal models is preferred. All of these models (dogs, sheep, goats and horses) have their pros and cons (Cook et al., 2014), but of these, the equine model is seen as the most relevant, be it also the most challenging (Chu et al., 2009; Kreuz et al., 2006a; Malda et al., 2012a; McIlwraith et al., 2011). Further, the horse is also the animal in which there is a clear and urgent need for better orthopaedic care, as orthopaedic ailments account for the vast majority of equine veterinarian consultations (Loomans et al., 2007). In these, joints play an important role. In a survey of US horse owners in 1998, 60% of all lameness cases were related to OA, and approximately $145 million was spent on veterinary bills relating to the problem (Anonymous, 2000).

Given the importance of the horse both as a translational animal model and as a target species for orthopaedic regenerative medicine, the entire work described in this PhD thesis focused on *in vivo* work in the equine model.

The benchmark

It has been known for long that the intrinsic repair capacity of (mature) articular cartilage is virtually nil (Hunter, 1743), impeding the healing of partial thickness lesions. However, this does not apply to other articular tissues, most importantly the subchondral bone. A logical step to tap into the body's own regenerative capacity was thus surgical involvement of the underlying subchondral bone, permitting the recruitment of stem cells and other endogenous anabolic factors from the subchondral bone through the created connection between the subchondral bone and the articular cartilage. In fact, the current standard of care for the surgical treatment of articular cartilage defects in both humans and horses is indeed debridement of the affected area, which is then followed by micro-fracturing of the subchondral bone plate (Steadman et al., 2001). This will result in the defect becoming covered by a collagen I-based fibrocartilaginous repair tissue. While biomechanically inferior to and less resistant than the original hyaline cartilage, this tissue will initially provide clinical relief and may hold for a while before finally yielding to development of severe osteoarthritis (Curl et al., 1997; McIlwraith et al., 2012; Pot et al., 2016). Studies in horses initially focused on the validation of the technique for human use (Frisbie et al., 1999), but later the technique also became common practice in equine surgery. In many cases it is therefore the preferred control treatment for novel regenerative medicine (RM)-based approaches to address articular cartilage damage (McIlwraith and Frisbie, 2010; Steadman et al., 2001).

In this thesis the micro-fracturing technique was refined by use of a new commercial device, developed to create much smaller subchondral bone perforations, limiting subchondral bone disturbance (Chapter II). This device had not previously been used in the horse, but proved to work well, despite the known hardness of the equine subchondral bone (Chu et al. 2010). The technique was performed as part of a larger

study, where it was used as a control for another biomaterial-based intervention (reported in Chapter VII) applied in the contralateral stifle joint, and there was no direct control in the form of a similar defect treated with classical micro-fracture. However, the macroscopic assessment was very favourable, with near-normal grading of repair tissue overall, while histology revealed mainly fibrocartilaginous tissue as expected; subchondral microarchitecture was deemed acceptable based on microCT evaluation.

The bony base

From a biomechanical viewpoint, the osteochondral unit serves a single purpose, but it is composed of two very different tissues with highly different biomechanical characteristics. This means that any RM attempt to repair or regenerate the unit, as is necessary in case of full thickness lesions, should take these differences into account and aim at creating a composite structure in which both the osteal and cartilaginous layer are mimicked in a functional sense (Brittberg et al., 2016; Lajeunesse and Reboul, 2003; Nukavarapu and Dorcemus, 2013). The same applies if an osteochondral solution is preferred for the treatment of partial thickness lesions because of issues related to the fixation of the implant (see later).

After the initial stages of *in vitro* development, it would seem prudent to perform the first *in vivo* studies on the suitability of biomaterials intended to serve as a scaffold for bone repair or as a bone anchor in a given species in an osteal, and not the more complicated osteochondral, environment. For this reason, we tested such novel scaffolds in a novel site: the tuber coxae of the horse. The tuber coxae is an anatomical site that is easily accessible in the standing horse, thus obviating the need for general anaesthesia, which is a great practical advantage and also greatly reduces the risk of anaesthetic complications. Further, the site gives access to a compact bone structure of substantial size that permits implantation of scaffolds of likewise considerable size (easily up to 15 mm diameter). Additionally, the area does not suffer easily from external contamination, is not biomechanically loaded, is nowhere near any joints that are relevant for locomotion and is in an area with hardly any movement beneath the skin of the underlying bony parts, unlike other areas nearby where bones are situated at little depth from the skin, such as the minor and major trochanters of the femur (van Weeren et al., 1990). In goats, pigs and sheep, tibial and femoral defect models have been developed and characterized (McGovern et al., 2018) that provide valuable translational insights for human applications. Given the advantages and considerations listed above it is perhaps a bit surprising that the equine tuber coxae has not previously been used for the testing of (bone) grafting materials. However, it is a well-known location for harvesting material for autologous bone grafts (Richardson et al., 1986).

In Chapters III and IV we show that a 3D-printed CaP-based scaffold made of tricalcium phosphate (TCP, synthesised by heating a mixture of $CaHPO_4$ and $CaCO_3$), allowed for good integration in the native bone and hence would be an excellent candidate

for the osteal part of composite implants. The study in Chapter III describes the first time this specific material, which had undergone ample characterisation and fine-tuning in an *in vitro* setting, was used in a long-term large animal study. The Chapter shows, in a mostly qualitative fashion, that the material served its intended use well, including ingrowth of bone from the neighbouring native tissue and concomitant cell-driven break-down and remodelling of the scaffold. Chapter IV gives further proof of the scaffold's suitability, now also in more quantitative terms. It is clear that the material used in Chapters III and IV holds great promise for clinical use in regenerative medicine of bone, as has also been shown with comparable material types (Nguyen et al., 2015; Yuan et al., 2010). The material is, therefore, also a good candidate for the creation of more complex osteochondral scaffolds, though it should be realised that the requirements for these more complex structures are different to those for the more simple application in (unloaded) bone.

Smaller is not necessarily simpler

For smaller and shallower partial thickness lesions, theoretically a chondral-only approach would be preferable, as the osteal part of the osteochondral unit is not affected and using an osteochondral scaffold would require provoking additional damage. This poses the problem of fixing a small chondral scaffold of not more than 1-2 mm thickness into the surrounding native cartilage, which is a non-negligible technical issue.

In human clinical practice this issue is dealt with when using the autologous chondrocyte implantation (ACI) and Matrix-associated ACI (MACI) techniques. The classic ACI uses periosteal flaps to cover the defect and prevent escape of the suspension containing the seeded cells (Brittberg et al., 1994). In the MACI approach the cells are seeded in scaffolds (*e.g.* hyaluronan or collagen-based), which are then tailored to fit within the defect and secured with fibrin glue (Kraeutler et al., 2018). However, these and similar techniques cannot be copied directly to the horse, as here one of the disadvantages of the equine model surfaces. In humans the period prescribed until full weight-bearing is variable, but was never less than 6 weeks in a recent systematic review (Kraeutler et al., 2018); in the horse immediate postoperative loading is the rule and cannot be avoided. This combines very badly with the greatly reduced stiffness (compared to native cartilage) of almost all hydrogel-based scaffolds and leads easily to early loss of the scaffold, as demonstrated in the series of pilot studies on scaffold fixation in Chapter V.

Chapter V also unveiled another disadvantage of the equine model: there was a significant immune response to a commercially available fibrin glue (made of human components), which is commonly used to fixate partial thickness scaffolds and is also commonly used as a negative control. Even a fibrin glue that was custom-made and was largely (but not entirely) based on autologous equine components did prove to be

far from inert and provoked a sizeable inflammatory response. Here the fact that the equine model is much closer to the clinical reality comes into play. Unlike many mouse strains, the horse is a fully immunocompetent outbred animal.

Chapter V had to conclude that with the current state of the technique, it is not very well feasible to fixate any form of implant or scaffold in a partial thickness cartilage defect in the equine stifle osteochondral defect model to which immediate weight-bearing and the related considerable biomechanical compression and shear forces are inherent. For this reason, it was recommended to use in the equine model at all times, when prefabricated scaffolds are used, osteochondral implants that can surgically be press-fit secured . The forcibly more complex implant and the larger surgical defect that has to be created should be taken for granted.

Decellularized extracellular matrix as a two-in-one solution: a bridge too far?
Accepting the limitations set by the equine model for the way of fixating the implant as outlined in the paragraph above and Incited by the great advances made in RM of other tissues than those pertaining to the musculoskeletal system by using decellularized extracellular matrix (Badylak, 2007) and by the favourable outcome of a 10-week pilot in a horse using a decellularized collagen type II matrix, it was decided to launch a long-term (6 months) study in a larger group of horses (Chapter VI). In the one-horse pilot study good bone formation was seen alongside the formation of an acceptable tissue layer at the level of the articular cartilage (Benders et al., 2013a). A scaffold consisting of decellularized extracellular matrix (DCM) alone was compared to a composite scaffold consisting of DCM with a base of the above-mentioned CaP- based scaffold (Chapters III and IV). Unfortunately, the outcome was disappointing. Where the CaP-scaffold showed substantial retention of the CaP at 6 months with good to very good adherence of the surrounding trabecular bone to the scaffold, thus confirming the promising results from Chapters III and IV, the CDM matrix had largely disappeared and given way to predominantly fibrotic repair tissue that featured a Young's modulus that was 8- to 10-fold less than that of healthy cartilage from the same joint, hence worth nothing in a biomechanical sense (Vindas Bolaños et al., 2017). An encouraging feature, on the other hand, was that there were no indications of strong immunologic or otherwise adverse reactions.

Disappointing results almost invariably teach lessons. The lesson learnt here was that the study emphasized the need for long-term studies in a challenging model when evaluating regenerative approaches for joint defects. This should be done for any construct or other potential therapy that is seriously considered for clinical use, even if the outcome of *in vitro* work or even short-term *in vivo* studies seems promising. The fact that clinical performance of the animals was good, despite the disappointing tissue-level outcome, led to the conclusion that there may be added value of more advanced monitoring during long-term studies, for which the equine model offers

ample possibilities, but which could unfortunately not be incorporated in the present work due to practical (financial, logistic and geographical) constraints.

If we can't fix it, can we stick it?

The fixation issue mentioned above could possibly be addressed by using another primary material for the scaffold that needs to fill the defect, especially matrices that have intrinsic adherent properties. Such a so-called sealing gel that adheres to the native extracellular matrix would then fill the irregularities of the cartilage layer not unlike the techniques used in plastering. Such a cell-free injectable hydrogel, based on the use of dextran-tyramine conjugates developed by the University of Twente, had shown excellent capacities of adherence to native cartilage in *in vitro* and *ex vivo* experiments (Moreira Teixeira et al., 2012; Moreira Teixeira et al., 2011). Short-term pilot work in horses using such a hydrogel (unpublished data) showed good retention and even migration of cells through the gel. This encouraging outcome led to the long-term experiment described in Chapter VII.

In this long-term experiment, no clinical adverse effects were noted and the outcome at histological level was far superior to the nano-fractured control side. Not surprisingly this applied to the subchondral bone, as no perforating injury had been made, but also to the repair tissue at the level of the cartilage layer. Nano-fracture, although perhaps comparing favourably with historical controls for micro-fracture as detailed in Chapter II, resulted in the expected fibrocartilaginous repair tissue. The hydrogel-treated defects showed significantly better outcome in 12 of the 13 ICRS scale histological outcome parameters that were scored and with that performed considerably better than the decellularized matrix scaffold that had been tested in Chapter VI. It should be acknowledged that also the histological aspect of the repair tissue that had replaced this gel was still distinct from that of native hyaline cartilage, but the material stood the harsh test of the long-term equine model relatively well and further research and development in this category of gels therefore seems warranted.

Conclusions and directions for future research

This thesis is entirely dedicated to the use of the horse as a model for orthopaedic regenerative medicine, focusing on the repair of chondral or osteochondral damage. The huge quantity of literature aiming at repair of joint damage (of which only a very tiny fraction deals with *in vivo* experiments and even less with applications in the clinical situation, which may be telling) shows that this is an endeavour that should not be taken lightly. Thus far, there is no publication on any approach that has demonstrated the regrowth of hyaline cartilage showing both a biochemical composition and an architecture that is similar (or, in the case of architecture, even close) to the native tissue. This might well be related to the relative neglect of the importance of the biomechanical function of articular cartilage compared to the more biological aspects, and to holding on to the paradigm in regenerative medicine that native tissue in the

end should replace any temporary scaffold or other material.

That paradigm may certainly hold true for bone, whose tissue is known to adapt to loading for life according to Wolff's law and the mechanostat theory (Frost, 2000), which has even been further developed in the horse because of the species' great translational value (Wang et al., 2016). Good regrowth of bone was indeed seen in scaffold-treated defects made in the tuber coxae model as reported in this thesis (Chapters III, IV and VI). However, there are many arguments to state that in the case of articular cartilage, which is infamous for the extremely long turnover times of the collagen network (Maroudas et al., 1992) that disable any substantial repair during an individual's lifetime (Heinemeijer et al., 2016), this paradigm entirely disregards Cicero's wise words that were cited at the start of this chapter, as we are **not** following nature when applying this same paradigm to articular cartilage. Therefore, for this specific tissue, an approach in which our constructs will contain a permanent, non-resorbable core structure might prove a more rewarding way to go, even if, or perhaps a little more provocatively, because this approach defies the prevailing paradigm.

Throughout this entire thesis the *equine* model was used for *long-term* testing. Both words in italics in the preceding sentence represent enormous challenges. A well-known quote from one of the pioneers in equine orthopaedic regenerative medicine, professor C. Wayne McIlwraith from Colorado State University, is: *"Nothing better to ruin your results than long-term follow-up"* (McIlwraith, 2016). Apart from hilarious, this statement is, unfortunately, utterly true, certainly in the case of attempts at joint repair. However, it is the longevity and durability of the solutions that are key in orthopaedics when trying to address chronic disorders such as osteoarthritis. This is certainly true in horses, for which only short-term palliative relief is available at present, but also for humans in which species there are more options for longer lasting clinical effect in the form of implants. However, these prostheses are prone to wear, not self-healing, and have an average life span of 10-15 years before needing extensive surgery upon revision. Such a revision is costly (>€50k€), is frequently associated with complications and is even less durable. Due to an ageing population and more active lifestyles, the yearly number of joint replacement surgeries is expected to increase by ca. 30% within the next 10 years to 1.5 million per year in the UK, Germany, France and Italy alone (Millennium Research Group, 2013). How challenging and discouraging it may be, long-term follow-up should be regarded as a must for any attempt at joint repair.

Equine is the other word written in italics. There is no doubt that the equine model is a very challenging one, and it might even be too challenging given the necessity of immediate and formidable weight-bearing and thus loading of any construct. It further may pose some immunologic hurdles (Mancini et al., 2017), but this obstacle is probably easier to overcome. Ethically, the model might come under more and

more pressure, given the increasing societal resistance to animal experimentation and resulting pressure from legislators to further reduce, replace and refine animal experiments (Marr, 2014). All factors together urge the development of new *in vitro* or *ex vivo* models that can accurately reflect the intra-articular conditions in terms of joint homeostasis and biomechanical environment and that can contribute to what might be considered a long-term goal: comprehensive *in silico* modelling of the human (and animal) diarthrodial joint with good predictability of the effect of interventions on joint homeostasis and tissue integrity. Such development, which may seem far away still but may be nearer than thought given recent developments in the human field (Lin et al., 2018), will allow for the gradual phasing out of the horse as an experimental model for musculoskeletal research. The animal will then still retain its role in end-stage testing of newly developed experimental treatments in randomised clinical trials, to the benefit of both the equine and the human species that share a great and urgent need for such treatments.

In the epic journey of articular regenerative medicine, the shores of Ithaca are still hidden beyond the horizon and one can even wonder whether there is any firm ground in sight at all. However, such a situation did not deter Ulysses from continuing his voyage and it will neither dissuade the scientific community from continuing to chase the Holy Grail of fully functioning and lifelong lasting cartilage repair. The members of that community may feel comforted by a citation of another famous Roman writer, the poet Ovid (Publius Ovidius Naso, 43BC-18AD): **Perfer et obdura; multo graviora tulisti**[2] *(Don't complain and carry on, you've gone through more difficult things).*

---

2   Ovidius : *Tristia, 5.11.7*

References

Ahern, B.J., Parvizi, J., Boston, R., Schaer, T.P., 2008. Preclinical animal models in single site cartilage defect testing: a systematic review. Osteoarthritis and Cartilage 2009, 705-713.

Anonymous, 2000. Lameness and laminitis in US horses. National Animal Health Monitoring Systems 2000, Veterinary Services – Centers for Epidemiology in Animal Health. Fort Collins, CO.

Badylak, F., 2008. The extracellular matrix as a biological scaffold material. Biomaterials 28, 3587-3593.

Benders, K.E.M., van Weeren, P.R., Badylak, F., 2013. Extracellular matrix scaffold for cartilage and bone regeneration. Trends in Biotechnology 31, 169-176.

Brama, P.A.J., Karssenberg, D., Barneveld, A., van Weeren, P.R., 2001. Contact areas and pressure distribution on the proximal articular surface of the proximal phalanx under sagittal plane loading. Equine vet. J. 33, 26-32.

Brittberg, M., Gomoll, A.H., Canseco, J.A., Far, J., Lind, M., Hui, J., 2016. Cartilage repair in degenerative ageing knee. Acta Orthopaedica 87, 26-38.

Brittberg, M., Lindahl, A., Nilsson, A., 1994. Treatment of Deep Cartilage Defects in the Knee with Autologous Chondrocyte Transplantation. New England Journal of Medicine. 331 14, 889–895.

Cook, J.L., Hung, C.T., Kuroki, K., Stoker, A.M., Cook, C.R., Pfeiffer, F.M., Sherman, S.L., Stannard, J.P., 2014. Animal models of cartilage repair. Bone Joint Res 3, 89-94.

Curl, W.W., Krome, J., G.ordon, E.S., Rushing, J., Smith, B.P., Poehling, G.G., 1997. Cartilage injuries: A review of 31,516 knee arthroscopies. Arthroscopy: The Journal of Arthroscopic & Related Surgery 13, 456-460.

Chu, C.R., Szczodry, M., Bruno, S., 2010. Animal Models for Cartilage Regeneration and Repair. Tissue Engineering 16. Part B, 105-115.

Di Pietro, C., La Sala, G., Matteoni, R., Marazziti, D., Tocchini-Valentini, G.P., 2018. Genetic ablation of Gpr37l1 delays tumor occurrence in Ptch1+/- mouse models of medulloblastoma. Exp Neurol Nov 16;312:33-42..

Frisbie D.D. (2012). Synovial joint biology and pathobiology. In: Auer J.A., Stick J.A. (eds). Equine Surgery (4th ed) (pp. 1096-1114). St. Louis, MO: Elsevier-Saunders.

Frisbie, D.D., Trotter, G.W., Powers, B.E., 1999. Arthroscopic subchondral bone plate microfracture technique augments healing of large chondral defects in the radial carpal bone and medial femoral condyle of horses. Vet Surg 28, 242-255.

Frost, H.M., 2000. The Utah paradigm of skeletal physiology: an overview of its insights for bone, cartilage and collagenous tissue organs. J Bone Mineral Metab 18, 305-316.

Gartner, L.P, 2017. Textbook of Histology, 4th ed. Elsevier, Philadelphia,USA.

Goldring, S.R., 2012. Alterations in periarticular bone and cross talk between subchondral bone and articular cartilage in osteoarthritis. Ther Adv Musculoskelet Dis 4, 249–258. 154

Heinemeier, K.M., Schjerling, P., Heinemeijer, J., M.B., M., Krogsgaard, M.R., Grum-Schwensen, T., Petersen, M.M., Kjaer, M., 2016. Radiocarbon dating reveals minimal collagen turnover in both healthy and osteoarthritic human cartilage. Sci Transl Med 8, 346-390.

Hunter, W., 1743. Of the structure and diseases of articulating cartilages. Phil Trans R Soc London 9, 514-521.

Janes, J.G., Kennedy, L.A., Garrett, K.S., Engiles, J.B., 2017. Common lesions of the distal end of the third metacarpal/metatarsal bone in racehorse catastrophic breakdown injuries. J Vet Diagn Invest Jul;29, 431-436.

Kraeutler, M.J., Belk, J.W., Carver, T.J., McCarty, E.C., 2018. Is delayed weightbearing after Matrix-Associated Autologous Chondrocyte Implantation in the knee associated with better outcomes? A Systematic Review of Randomized Controlled Trials. Orthop J Sports Med 6, 1-10.

Kreuz, P.C., Erggelet, C., Steinwachs, M.R., Krause, S.J., Lahm, A., Niemeyer, P., Ghanem, N., Uhl, M., S¨udkamp, N., 2006. Is microfracture of chondral defects in the knee associated with different results in patients aged 40 years or younger? Arthroscopy November,22, 1180-1186.

Lajeunesse, D., Reboul, P., 2003. Subchondral bone in osteoarthritis: a biologic link with articular cartilage leading to abnormal remodeling. Current opinion in rheumatology 15, 628-633.

Lin, Y.C., Walter, J.P., Pandy, M.G., 2018. Predictive Simulations of Neuromuscular Coordination and Joint-Contact Loading in Human Gait. Ann Biomed Eng. Aug;46, 1216-1227.

Loomans, J.B.A., Stolk, P.W.T., van Weeren, P.R., 2007. A survey of the workload and clinical skills in current equine veterinary practice in The Netherlands. Equine Vet Educ 19, 162-168.

Malda, J., Benders, K.E.M., Klein, T.J., de Grauw, J.C., Kik, M.J.L., Hutmacher, D.W., Saris, D.B.F., van Weeren, P.R., Dhert, W.J.A., 2012. Comparative study of depth-dependent characteristics of equine and human osteochondral tissue from the medial and lateral femoral condyles. Osteoarthritis and Cartilage 20, 1147-1151.

Malda, J., de Grauw, J.C., Benders, K.E.M., Kik, M.J.L., van de Lest, C.H.A., Creemers, L.B., Dhert, W.J.A., van Weeren, P.R., de Grauw, J.C., Benders, K.E.M., Kik, M.J.L., van de Lest, C.H.A., Creemers, L.B., 2013. Of Mice, Men and Elephants: The Relation between Articular Cartilage Thickness and Body Mass. PLOS ONE 8, 1-8.

Malemud, C.J., 1991. Changes in proteoglycans in osteoarthritis: biochemistry, ultrastructure and biosynthetic processing. J Rheumatol Suppl Feb;27, 60-62.

Mancini, I.A.D., Vindas Bolaños, R.A., Brommer, H., Castilho, M., Ribeiro, A., van Loon, J.P.A.M., Mensinga, A., van Rijen, M.H.P., Malda, J., van Weeren, P.R., 2017. Fixation of Hydrogel Constructs for Cartilage Repair in the Equine Model: A Challenging Issue. TIissue Engineering 23, 804-814.

Mankin, H., Radin, E., 1993. Structure and function of joints. In: McCarthy D.J. (ed.). *Arthritis and allied conditions: a textbook of rheumatology* (12th ed) (p. 189). Philadelphia, PA: Lea & Febiger [cited by Frisbie, 2012].

Maroudas, A., Palla, G., Gilav, E., 1992. Racemization of aspartic acid in human articular cartilage. Connect Tissue Res 28, 161-169. 155

Marr, C.M., 2015. Ethical animal research – a pathway to zero tolerance. Equine Vet J 47, 3-5.

McGovern, J.A., Griffin, M., Hutmacher, D.W., 2018. Animal models for bone tissue engineering and modelling disease. Dis Model Mech. Apr 23;11, 1-14.

McIlwraith, W.C., 2016. Second Havemeyer Conference on Regenerative Medicine, Bonita Springs (FL), USA, November 5-9.

McIlwraith, C.W., Frisbie, D.D., Kawcak, C.E., 2012. The horse as a model of naturally occurring osteoarthritis. Bone Joint Res 1, 297-309.

McIlwraith, W.C., Fortier, L.A., Frisbie, D.D., Nixon, A.J., 2011. Equine Models of Articular Cartilage Repair. Cartilage 2, 317-326.

Mcllwraith, W.C., Frisbie, D.D., 2010. Microfracture: Basic Science Studies in the Horse. Cartilage 1, 87-95.

Millennium Research Group, European markets for large joint reconstructive implants., 2013.

Moran, C.J., Ramesh, A., Brama, P.A., O'Byrne, J.M., O'Brien, F.J., Levingstone, T.J., 2016. The benefits and limitations of animal models for translational research in cartilage repair. J Exp Orthop 3(1):1.

Moreira Teixeira, L.S., Bijl, S., Pully, V.V., Otto, C., Jin, R., Feijen, J., van Blitterswijk, C.A., Dijkstra, P.J., Karperien, M., 2012. Self-attaching and cell-attracting in-situ forming dextran-tyramine conjugates hydrogels for arthroscopic cartilage repair. Biomaterials 33, 3164-3174.

Moreira Teixeira, L.S., Feijen, J., van Blitterswijk, C.A., Dijkstra, P.J., Karperien, M., 2011. Enzyme-catalyzed crosslinkable hydrogels: Emerging strategies for tissue engineering. Biomaterials 33, 1281-1290.

Muschler GF, Raut VP, Patterson TE, Wenke JC, Hollinger JO., 2010. The design and use of animal models for translational research in bone tissue engineering and regenerative medicine. Tissue Eng Part B Rev. 16(1):123-45.

Nguyen, T.B.L., Min, Y., Lee, B.T., 2015. Nanoparticle Biphasic Calcium Phosphate Loading on Gelatin-Pectin Scaffold for Improved Bone Regeneration. Tissue Engineering 21, 1376-1387.

Nukavarapu, S.P., Dorcemus, D.L., 2013. Osteochondral tissue engineering: Current strategies and challenges. Biotechnology Advances 31, 706-721.

Pot, M., W., Gonzales, V., K., Buma, P., IntHou, J., van Kuppevelt, T., H., de Vries, R., B.M., Daamen, W.F., 2016. Improved cartilage regeneration by implantation of acellular biomaterials after bone marrow stimulation: a systematic review and meta-analysis of animal studies. PeerJ. Sep 8;4:e2243.

Richardson, G.L., Pool, R.R., Pascoe, J.R., Wheat, J.D., 1986. Autogenous cancellous bone grafts from the sternum in horses comparison With other donor sites and results of use in orthopedic surgery. Vet. Surg 15, 9-15.

Saltzman, B.M., Riboh, J.C., 2018. Subchondral Bone and the Osteochondral Unit: Basic Science and Clinical Implications in Sports Medicine. Sports Health 10, 412-418. 156

Steadman, J.R., Rodkey, W.G., Rodrigo, J.J., 2001. Microfracture: surgical technique and rehabilitation to treat chondral defects. Clin Orthop Relat Res Oct;(391 Suppl), S362-369.

Stewart, H.L., Kawcak, C.E., 2018. The importance of Subchondral Bone in the Pathophysiology of Osteoarthritis. Frontiers in Veterinary Science 5, 1-9.

van Weeren, P.R., 2016. General anatomy and physiology of joints. In: *Joint Disease in the Horse*, 2nd ed. Eds: McIlwraith, C.W., Frisbie, D., Kawcak, C.E. and van Weeren, P.R. Elsevier: St. Louis MO.

van Weeren, P.R., van den Bogert, A.J., Barneveld, A., 1990. Quantification of skin displacement in the proximal parts of the limbs of the walking horse. Equine Vet. J. Equine Vet. J., Suppl. 9: 110-118.

Vindas Bolaños, R.A., Cokelaere, S.M., Estrada McDermott, J.M., Benders, K., E.M., Gbureck, U., Plomp, S.G.M., Weinans, H., Groll, J., van Weeren, P.R., Malda, J., 2017. The use of cartilage decellularized matrix scaffold for the repair of osteochondral defects: the importance of long-term studies in large animal model. Osteoarthritis and Cartilage 25, 413-420.

Wang, X., Thomas, C.D., Clement, J.G., Das, R., Davies, H., Fernandez, J.W., 2016. A mechanostatistical approach to cortical bone remodelling: an equine model. Biomech Model Mechanobiol 15, 29-42.

Whitton, R.C., Ayodele, B.A., Hitchens, P.L., Mackie, E.J., 2018. Subchondral bone microdamage accumulation in distal metacarpus of Thoroughbred racehorses. Equine Vet J. Nov;50, 766-773.

Yuan, H., Fernandes, H., Habibovic, P., de Boer, J., Barradas, A.M., de Ruiter, A., Walsh, W.R., van Blitterswijk, C.A., de Bruijn, J.D., 2010. Osteoinductive ceramics as a synthetic alternative to autologous bone grafting. PNAS 107, 13614-13139.

Summary

This thesis focuses on *in vivo* studies in horses for the long-term evaluation of various regenerative approaches for articular cartilage and bone repair using cell-free techniques. It is concluded that the equine stifle joint and the tuber coxae represent reliable models to study the regeneration of cartilage and bone, respectively, in a truly translational sense, as they yield highly valuable information on potential for clinical use both in horses and humans. The high costs (both financially and in terms of animal welfare and ethics) of this work are justified by the vast economic and welfare needs of both humans and horses suffering from osteoarthritis (OA), for whom more effective treatments to aid the regeneration of cartilage and bone are urgently sought in order to improve their quality of life (Chapter I).

Chapter II is a technical note on the first use in the horse of a new nano-fracture technique that has been developed to replace the current standard-of-care micro-fracturing for the surgical treatment of focal cartilage defects and that was adopted from earlier studies in other animals and humans. Like micro-fracturing, this technique also aims at stimulating the ingrowth of cells from the subchondral bone marrow. Nano-fracturing however uses a very thin (1 mm) needle made of nitinol (a nickel and titanium alloy) to allow penetration to a standardized stop-controlled depth, rather than a larger-diameter standard microfracture awl. This procedure has been reported to cause less damage to the subchondral bone than conventional micro-fracture. The technique proved easy to use in a time-efficient way during surgery, and macroscopically bleeding from the needle perforations was confirmed. Micro-computed tomography showed moderate subchondral bone disruption surrounding the nano-fracture channels. Histologically, the defects demonstrated ample but mainly fibrocartilaginous repair tissue with a total ICRS-II score of 48% ± 10% (mean ± SD), where 100% denotes normal cartilage. Importantly, no direct comparison with routine microfracture was performed in this study. However, the preliminary results at 7 months were deemed promising and the technique seems to be a viable alternative for micro-fracturing in the horse, both with an outlook for clinical treatment of focal cartilage defects and as a control treatment for the study of novel regenerative interventions.

In Chapters III and IV, the equine tuber coxae was introduced as a novel site to study bone defect repair and bone regeneration, an important issue in a species in which orthopaedic injuries caused by athletic activities are common. In these studies, scaffolds based on tricalcium phosphate and produced by additive manufacturing techniques were used. The tuber coxae bone defect model proved convenient, mainly because of its anatomical features: The elevated location keeps the site remote from the soil, reducing the risk of contamination. Far away from articulations, tendons or ligaments, there is also hardly any effect on the locomotion of the animals. Furthermore, surgical access is relatively easy and surgery can be done in the standing animal, obviating the

need for general anesthesia. Last but not least, the horse is an animal that is easy to handle and the size of the anatomical structure allows upscaling of defect size more readily than in many of the more frequently used model species (such as goats and sheep), favoring translation to large bone defects in humans.

In Chapter III it was demonstrated that scaffolds based on tricalcium phosphate had been incorporated into the surrounding tissue six months after implantation. The scaffolds showed clear osteoconductivity and the capacity for new bone formation was evident, compared to the empty defects that served as controls, and which were mostly covered with fibrous tissue. This study confirmed the suitability of the tuber coxae model for long-term *in vivo* evaluation of biomaterial-based bone regeneration. In chapter IV we followed up on this work with a comparative study of different pore-architectures of printable calcium phosphate based scaffolds. One of the constructs comprised a gradually changing vertical porosity in which the diameter of the pores varied from 750 μm at the base to 450 μm at the top, while the other featured a constant macro-porosity of 750 μm. It was concluded that the scaffold with constant porosity achieved enhanced bone formation with more advanced degradation of the scaffold compared to the construct with the gradually changing pore size. It was speculated that the presence of the polycaprolactone (PCL) cap that was placed on one end of the scaffold provided a microenvironment that could be representative of non-healing large bone defects, in which pore structure may be a limiting factor, and that delays in bone regeneration in one region of the construct affect regeneration in neighboring regions.

Concurrent studies were carried out on articular cartilage regeneration in the same horses, reducing the number of experimental animals needed. Firstly, for these it was necessary to determine the optimal fixation strategy for chondral implants. In Chapter V, commercial and autologous-derived fibrin glue were evaluated, but it was concluded that both approaches had significant drawbacks. Commercial fibrin glue, which is made of components harvested from humans, appeared to cause severe adverse immunological reactions in the horse. The autologous form of the fibrin glue did not appear to be a good alternative, as the preparation process was rather complex and it still caused an immunological response. Therefore, a suitable alternative appeared to be the use of a PCL-based bone anchor, to which the chondral part of the implant could be fixed to allow press-fit implantation.

In Chapter VI, we investigated the possibility of regeneration of cartilage and subchondral bone comparing two types of scaffolds. One scaffold existed completely of decellularized cartilage-derived matrix (CDM) (-P), the other was a composite scaffold made of the same CDM for the cartilage phase combined with a three-dimensionally (3D) printed calcium phosphate (CaP) cement-based proven osteogenic scaffold (+P). In a first pilot experiment, very satisfactory results had been obtained at 8 weeks, using scaffolds

of decellularized cartilage only (-P), but in the main experiment little hyaline tissue was found at 6 months, leading to the conclusion that given the demanding *in vivo* situation in fully loaded large animal joints, long-term studies of putative regenerative approaches are always needed, irrespective of the outcome of short-term pilot experiments. With respect to the bone phase, the potential for adaptation, osteoconductivity, osteogenesis and scaffolding reabsorption of the +P scaffolds was evidenced by Micro CT and histopathology, providing useful data for later follow-up studies.

Chapter VII reports preliminary results of a recent investigation. Here, an alternative solution for the issue of fixation of an implant in a chondral, not osteochondral, defect is investigated. The approach used in Chapter VII relies on a so-called self-sealing hydrogel that adheres to the adjacent cartilage surrounding the defects by the formation of covalent bonds. This hydrogel was evaluated over a 7-month timeframe and compared to nano-fracture treated defects in the contralateral stifle joints. The hydrogel treated joints showed poorer scores for macroscopic cartilage repair, which may in part have been due to translucency of the hydrogel creating the appearance of less extensive or dense defect filling. Microscopically however, repair tissue histology (both superficially and at the tidemark and subchondral bone level) was markedly and statistically superior to that seen in the nano-fracture treated defects. MicroCT confirmed the absence of subchondral bone abnormalities in the hydrogel-treated joints, compared to obviously disturbed microarchitecture mid-defect in the underlying subchondral bone in contralateral joints 7 months after nano-fracture treatment. Though preliminary, the outcome for the hydrogel seems promising, and further exploration of the avenue is certainly warranted.

The body of work covered by this thesis, including the difficulties and challenges that were encountered along the way and the possible ways to handle these obstacles in further work, is discussed in Chapter VIII, the "Summarizing Discussion". This chapter underlines the need to continue this type of research in order to improve the quality of life of humans and horses alike and urges researchers to do so by taking cues from mother Nature. This in line with the great ancient Greek philosophers, when they spoke about "the search for the truth", *i.e.* getting to know what we currently do not know, guided by Nature itself. There is still a long way to go. We have reached the 21st century, but thus far we have not been successful in finding an effective treatment that has the capacity to regenerate the articular cartilage of an adult mammal. To ensure true progress in the biomedical sciences, we need to re-assert and re-think some of our assumptions. For this, we might need to re-assess our *in vitro* and *in vivo* models and our methodologies, using the advances of current technology. For this, scientific soundness and ethical acceptability are paramount and ideally, this would be done within the framework of the One Health – One Medicine concept, in order to take the badly needed steps forward in Regenerative Medicine that will allow a better quality of life for future generations.

Resumen

Esta tesis se enfoca en estudios *in vivo*, en equinos, evaluando varias matrices regenerativas a largo plazo para la reparación de cartílago articular y hueso, mediante técnicas acelulares. Se concluyó que la rodilla y la tuberosidad coxal del equino son modelos representativos para estudiar la regeneración del cartílago y hueso, respectivamente, con un verdadero sentido traslacional, debido al alto valor de información y al potencial para la aplicación clínica en equinos y humanos. Los altos costos (financieros, éticos y de bienestar animal) de este trabajo, se justifican por la necesidad económica y de bienestar en los equinos y humanos que sufren de osteoartritis (OA), quienes requieren urgentemente de nuevos tratamientos más eficientes en la regeneración de cartílago y hueso, que les permita tener una mejor calidad de vida. (Capítulo I).

El capítulo II es una nota técnica del primer uso en equinos de una técnica de nano-fractura que ha sido desarrollada para reemplazar la técnica actual de micro-fractura para tratamientos quirúrgicos de defectos focales del cartílago y que se adoptó de recientes estudios en otros animales y humanos. Al igual que la microfractura, ésta técnica pretende estimular el crecimiento de células que provienen de la médula del hueso subcondral. Sin embargo, la nanofractura usa una aguja muy delgada (1mm) hecha de nitinol (aleación de níquel y titanio), para permitir la penetración a una profundidad con una detención controlada estandarizada, en vez de un punzón de microfractura estándar que es de mayor diámetro. Se ha reportado que este procedimiento causa menos daño al hueso subcondral que el producido por la técnica convencional de microfractura. La técnica se realizó con facilidad y en un tiempo eficiente durante las cirugías, confirmándose macroscópicamente la salida de sangre a través de las perforaciones realizada por la aguja en el hueso subcondral. La micro tomografía computarizada mostró moderada disrupción del hueso subcondral alrededor de los canales de la nanofractura. Histológicamente, los defectos mostraron amplia reparación de tejido, pero principalmente de fibrocartílago, con una puntuación total de 48% ± 10% (mean ± SD), donde el 100% se refiere al cartílago normal. Es importante señalar que en este estudio no hay una comparación directa con la técnica de microfractura. Sin embargo, los resultados preliminares encontrados a los 7 meses del estudio son prometedores y la técnica parece ser una alternativa viable a la microfractura en equinos, ambas para tratamientos focales de cartílago y como un tratamiento de control para estudios de nuevas intervenciones regenerativas.

En el capítulo III y IV se utilizó por primera vez la tuberosidad coxal del equino para estudios de reparación de defectos óseos y medicina regenerativa de hueso, siendo un problema importante en esta especie por las comunes lesiones ortopédicas producidas en las actividades deportivas. En estos estudios se utilizaron andamios a base de fosfato

tricálcico, producidos mediante técnicas de fabricación aditiva. El modelo de defecto óseo en la tuberosidad coxal resulto conveniente, principalmente por sus características anatómicas: La localización elevada mantiene las heridas a una gran distancia del suelo, reduciendo el riesgo de contaminación. Al estar lejos de articulaciones, tendones y ligamentos, no hay efectos negativos relacionados con la locomoción de los animales. Además, es de fácil acceso quirúrgico y la cirugía puede realizarse con el animal en pie, obviando la necesidad de la anestesia general. Por último, pero no menos importante, el caballo es un animal de fácil manejo y el tamaño de la estructura anatómica permite aumentar el tamaño del defecto con mayor facilidad que en muchas de las especies modelo utilizadas con mayor frecuencia (como cabras y ovejas), favoreciendo la traslación a los grandes defectos óseos en humanos.

En el capítulo III se logró demostrar que los andamios a base de fosfato tricálcico, se habían incorporado al tejido aledaño a los seis meses de ser implantados. Los andamios mostraron una clara osteoconductividad y la capacidad de formación de nuevo tejido óseo fue evidente, en comparación con los controles o defectos vacíos, que fueron cubiertos en su mayoría por tejido fibroso. Este estudio confirmó el potencial del modelo de la tuberosidad coxal a largo plazo, para la evaluación *in vivo* de regeneración ósea basada en biomateriales. En el capítulo IV se continuó con el estudio comparativo de diferentes poro- arquitecturas de andamios impresos a base de fosfato de calcio. Uno con porosidad vertical gradual que variaba el diámetro de los poros desde 750 μm en la base hasta 450 μm en la cima, mientras que el otro con macro porosidad constante de 750 μm. Al final del estudio se concluyó que el andamio con porosidad constante logró una mayor formación de tejido óseo y una degradación más avanzada del andamio en comparación con el de porosidad gradual. Se especuló que la presencia de la tapa de policaprolactona (PCL) que se colocó en un extremo del andamio, proporcionó un microambiente que podría ser representativo de defectos óseos grandes que no cicatrizan, en los cuales la estructura de los poros puede ser un factor limitante que retrasa la regeneración ósea en una región del constructo, afectando la regeneración de las regiones vecinas.

Paralelamente se realizaron estudios en regeneración de cartílago en los mismos equinos, reduciendo el número de animales experimentales que se necesitaban. Como primer paso, para ello, fue necesario buscar alternativas óptimas de fijación de los implantes condrales. En el capítulo V se evaluó la goma de fibrina comercial y la de fibrina autóloga, concluyéndose que ambas tenían inconvenientes importantes. El pegamento de fibrina comercial que está hecho de componentes de humanos, parece causar reacciones inmunológicas adversas severas en el equino. La goma de fibrina autóloga no pareciera ser una buena opción, debido a su complejo proceso de preparación y que también causó una respuesta inmunológica. Por lo tanto, una adecuada alternativa parece ser, el uso de PCL como base de anclaje ósea, mediante el cual el implante podría ser fijado a presión.

En el capítulo VI se investigó la posibilidad de regeneración de cartílago y hueso subcondral, comparando dos tipos de andamios. Un andamio a base de una matriz de cartílago completamente descelularizada (CDM) (-P) y el otro hecho con la misma base CDM para la fase de cartílago combinado con la impresión en tercera dimensión (3D) de fosfato de calcio (CaP) como base, para probar la capacidad osteogénica del andamio (+P). En un primer experimento piloto se obtuvieron resultados muy satisfactorios a las 8 semanas, utilizando solamente andamios de cartílago descelularizado (-P), pero en el experimento principal se encontró poco tejido hialino a los 6 meses, concluyendo que siguen siendo una demanda las investigaciones *in vivo* de articulación en las grandes especies de animales, y que los estudios de matrices regenerativas a largo plazo son siempre necesarios, independientemente de los resultados en experimentos piloto de corto plazo. Con respecto a la fase ósea, el potencial de adaptación, osteoconductividad, osteogénesis y reabsorción del andamio fue evidenciada mediante la microtomografía computarizada y la histopatología, proporcionando datos útiles para estudios de seguimiento.

El capítulo VII reporta de manera preliminar resultados de una reciente investigación. Consiste en una solución alternativa de fijación de un implante a investigar en un defecto condral, no osteocondral.
El anclaje utilizado en el capítulo VII se conoce como hidrogel auto adherible, ya que se adhiere al cartílago de los alrededores de los defectos por la formación de enlaces covalentes. Este hidrogel fue evaluado a los 7 meses y comparado con los defectos tratados con la técnica de nanofractura de las articulaciones de las rodillas contralaterales. El hidrogel tratado en las articulaciones mostró menor grado de reparación de cartílago, lo que puede haber sido en parte debido a la translucidez del hidrogel, creando la aparición de un relleno de defectos densos menos extenso. Sin embargo, a nivel microscópico, la reparación histológica de tejido (tanto a nivel superficial, de tidemark (línea limitante basófila) y del hueso subcondral), fue evidentemente superior que los vistos en los defectos tratados con nanofractura. A pesar de ser algo preliminar, los resultados de la utilización del hidrogel parecen ser prometedores y la exploración futura esta ciertamente garantizada.

Todo este proceso de investigación con las dificultades y los retos que fueron encontrados a lo largo del trayecto y los posibles caminos para manejar los obstáculos en futuros trabajos son discutidos en el capítulo VIII "Summarizing Discussion". En este capítulo se resalta la necesidad de continuar este tipo de investigaciones para mejorar la calidad de vida de los humanos y los equinos, e insta a los investigadores a hacerlo siguiendo los pasos de la Madre Naturaleza. Es decir, siguiendo la línea de lo que los antiguos filósofos griegos mencionaban sobre "la búsqueda de la verdad", ante aquello que no logramos conocer, guiados por la misma naturaleza. Hay un camino que continuar. Llegamos al siglo XXI y no hemos tenido éxito en encontrar un tratamiento efectivo,

que tenga la capacidad de regenerar el cartílago articular de un mamífero adulto. Para asegurar un verdadero progreso en las ciencias biomédicas, necesitamos reafirmar y repensar algunas de nuestras suposiciones. Es por ello que los modelos *in vitro* e *in vivo* y nuestras metodologías deben orientarse usando los avances de la tecnología actual. Para ello, la solidez científica y la aceptabilidad ética son primordiales, e idealmente, esto debe hacerse en el marco del concepto Una Salud-Una Medicina, con el fin de dar los pasos necesarios en la Medicina Regenerativa, que permitirán una mejor calidad de vida para las futuras generaciones.

Samenvatting

Dit proefschrift heeft als thema het onderzoeken van een aantal celvrije regeneratieve technieken voor het herstel van gewrichtskraakbeen en bot door middel van *in vivo* studies die gebruik maken van het paard als modeldier. Een hoofdconclusie van het werk is dat het kniegewricht en de heupbeensknobbel, of *tuber coxae*, van het paard zeer geschikte modellen vormen om de translationele aspecten van kraakbeen- en botherstel te bestuderen omdat deze modellen bijzonder waardevolle informatie leveren over de toepasbaarheid van die verschillende technieken bij zowel de mens als bij het paard zelf. De rechtvaardiging van de hoge kosten die gepaard gaan met het onderzoek (zowel in economische zin als in termen van dierenwelzijn) ligt in de sterke noodzaak die er is vanuit gezondheidszorg, economie en welzijn voor zowel mensen als paarden om betere behandelingen te ontwikkelen voor het herstel van kraakbeen- en botschade om zo de kwaliteit van leven van velen te kunnen verbeteren (Hoofdstuk I).

Hoofdstuk II is een korte technische beschrijving van het gebruik van een nieuwe chirurgische nano-fractuur techniek. Het betreft hier een techniek die in het in het proefschrift beschreven onderzoek voor het eerst bij het paard gebruikt wordt en die, bij de mens en andere diersoorten, ontwikkeld is om de huidige klinische standaardbehandeling, de zogenaamde micro-fractuurtechniek te vervangen. Net zoals bij de micro-fractuurtechniek heeft deze techniek tot doel een influx van cellen in een kraakbeendefect te genereren door een verbinding te maken met het onderliggende subchondrale bot. Het verschil is dat de nano-fractuur techniek hiertoe gebruik maakt van veel dunnere instrumenten (van een legering van nikkel en titanium gemaakte dunne naalden van ca. 1 mm doorsnede) en zodoende veel minder weefselschade maakt dan de conventionele techniek. De techniek bleek eenvoudig en op efficiënte wijze toepasbaar en resulteerde in de gewenste bloedtoevoer vanuit het subchondrale bot. Na 7 maanden bleek uit computer tomografische beelden dat er maar geringe schade was ontstaan aan het bot rond de met de nano-fractuur techniek gemaakte kanalen. Histologisch onderzoek liet zien dat het defect grotendeels opgevuld was met fibreus kraakbeen dat 48±10% (gemiddelde ± standaarddeviatie) scoorde op de ICRS-II schaal (waarin een 100% score normaal (hyalien) kraakbeen betekent). In deze studie is geen directe vergelijking gemaakt met de conventionele micro-fractuur techniek, maar de voorlopige resultaten werden als zeer positief gezien en de conclusie was dat de techniek een prima alternatief biedt voor de conventionele techniek en goed toepasbaar is in de klinische behandeling van gelokaliseerde kraakbeendefecten bij het paard dan wel als controle behandeling voor de toepassing van experimentele regeneratieve technieken.

In de Hoofdstukken III en IV wordt het *tuber coxae* van het paard voor de eerste keer gebruikt als model voor de studie van botregeneratie. Dat is een belangrijk onderwerp bij de mens, maar ook bij een diersoort als het paard waar sportblessures

194

vaak voorkomen. Er werd bij deze studies gebruik gemaakt van scaffolds die via een driedimensionale (3D) printtechniek gemaakt waren op basis van tri-calciumfosfaat. Het *tuber coxae* bleek goed te voldoen voor deze soort studies. Het is een deel van het skelet dat zich ver van de grond bevindt en dus weinig gevoelig is voor contaminatie. Verder bevindt het zich ook niet dicht in de buurt van gewrichten en (bewegende) pezen of banden en heeft een ingreep ter plekke dus weinig invloed op de locomotie. De goede toegankelijkheid van de locatie laat het toe de ingreep bij het staande dier uit te voeren waardoor algehele anesthesie niet nodig is. Verder is het paard een dier dat doorgaans makkelijk in de omgang is en komen de afmetingen van de botten veel beter met die van de mens overeen dan van vele laboratoriumdiersoorten, wat de translatie naar de mens makkelijker maakt. De grootte van de anatomische structuur laat het opschalen van implantaten beter toe dan bij andere gebruikelijke grote diermodellen, zoals het schaap en de geit.

Hoofdstuk III liet zien dat de op tri-calciumfosfaat gebaseerde scaffolds 6 maanden na implantatie goed geïncorporeerd waren in het omliggende natieve bot. De osteoconductiviteit en het vermogen tot de vorming van nieuw bot waren duidelijker zichtbaar in de met de scaffolds behandelde defecten in vergelijking met de niet behandelde controledefecten die slechts gevuld waren met enig fibreus weefsel. Nadat op deze manier de potentiële waarde van deze scaffolds duidelijk was geworden, werd er een vervolgstudie ingezet (Hoofdstuk IV), waarin ook printbare calciumfosfaat scaffolds gebruikt werden, maar nu met twee verschillende vormen van porositeit. In de ene vorm nam de grootte van de poriën geleidelijk aan af langs de centrale as van het cilindervormige implantaat (van 750 μm basaal tot 450 μm apicaal), net zoals ook *in vivo* de porositeit van het subchondrale bot afneemt naarmate de osteochondrale overgang verder genaderd wordt. De andere vorm had een constante poriëngrootte (750 μm) door het hele implantaat. De eindconclusie was dat het implantaat met de constante poriëngrootte betere botvorming en gelijktijdige afbraak van het *scaffold* materiaal liet zien dan het implantaat met verlopende poriëngrootte. Op basis van de resultaten werd er gespeculeerd dat de aanwezigheid van een polycaprolactone (PCL) omhulsel dat aan het implantaat grotendeels omgaf een micro-omgeving creëerde die representatief zou kunnen zijn voor de situatie van een niet genezend bot defect waar de poriëngrootte een beperkende factor zou kunnen vormen. Verder zou het zo kunnen zijn dat verstoringen in de botvorming op een bepaalde plaats binnen het implantaat een effect zouden kunnen hebben op de botregeneratie op andere plaatsen.

Parallel met de bovenstaande studies werd er ook gewerkt aan kraakbeenregeneratie. Een belangrijke vraag op dat terrein was de fixatie van implantaten in chondrale defecten (die dus niet dieper gaan dan de kraakbeenlaag zelf). In Hoofdstuk V wordt een vergelijking gemaakt tussen een commercieel verkrijgbare fibrinelijm (die gemaakt is op basis van humane componenten) en een autologe vorm daarvan, gebaseerd op componenten gewonnen bij het dier zelf. Beide benaderingen bleken niet te voldoen.

De commerciële fibrinelijm bleek belangrijke immunologische reacties bij het paard te veroorzaken. De autologe vorm deed dat in veel mindere mate, maar bleek slechts te produceren via een zeer gecompliceerd proces. De beste oplossing bleek om het chondrale concept vaarwel te zeggen en het subchondrale bot erbij te betrekken. In een osteochondraal defect kon succesvol een *custom-made* botanker gemaakt van PCL geplaatst worden dat als drager voor de scaffold van de kraakbeenlaag kon fungeren.

In Hoofdstuk VI wordt uitgegaan van scaffolds die gebaseerd zijn op een collageen basis die verkregen is door natief kraakbeen te decellulariseren. Er worden twee types vergeleken die alleen in het botdeel van elkaar verschilden. In de ene vorm was de hele scaffold gemaakt van alleen het gedecellulariseerde collageen type II (-P), in de tweede vorm was er sprake van een samengesteld implantaat waarbij het kraakbeendeel identiek was aan die van het eerste implantaat, maar waarbij voor het botdeel een driedimensionaal geprinte scaffold gebruikt werd die gebaseerd was op calcium fosfaat en die in eerdere studies al bewezen had osteogene capaciteiten te bezitten (+P). Het experiment was gebaseerd op een bijzonder veelbelovend *pilot experiment* van 8 weken waarin het alleen de (-P) vorm gebruikt was die een goede defectvulling had laten zien. In de lange termijn studie vielen deze resultaten (zowel voor -P als voor +P) voor de kraakbeenvorming echter sterk tegen en de conclusie was dat er, hoe goed de *pilot* ook mag zijn, altijd behoefte zal blijven aan lange termijn studies. Het botdeel liet een goede potentie voor osteoconductiviteit, botvorming en resorptie van de samengestelde (+P) scaffold zien op basis van micro-CT en histologie. Deze resultaten vormen een goede basis voor verder onderzoek.

Hoofdstuk VII bevat een deelrapportage van een groot recent experiment waarvan de verwerking van de resultaten nog gaande is. In dit onderzoek wordt de fixatie van implantaten in een ondiep chondraal defect anders benaderd dan in Hoofdstuk V. Hoofdstuk VII maakt gebruik van een bijzonder soort *"sealing gel"* die in het defect aangebracht wordt en zich met speciale chemische verbindingen hecht aan het omringende natieve kraakbeen. Deze gel werd gedurende 7 maanden getest en vergeleken met de effecten van nano-fractuur aan de contralaterale zijde. Macroscopisch leek de met de nieuwe geel behandelde kant minder goed te scoren, maar dat was mogelijk te wijten aan het transparante karakter van de gel waardoor de indruk gewekt werd dat de defecten minder goed gevuld waren. Microscopisch was de uitkomst aan de met de gele behandelde zijde echter beduidend beter. Micro-CT liet zien dat er geen afwijkingen waren in het subchondrale bot aan de met de gel behandelde kant terwijl er nog duidelijke schade aanwezig was aan de gemicrofractureerde zijde. De uitkomst is nog steeds preliminair, maar lijkt heel veelbelovend en zal waarschijnlijk aanleiding zijn voor verder onderzoek naar deze benaderingswijze.

Het afsluitende Hoofdstuk VIII, de *"Summarizing Discussion",* presenteert een overzicht van het gehele in het proefschrift opgenomen werk en gaat in op de mogelijke manieren waarop de vele uitdagingen en moeilijkheden die gerezen zijn aangepakt kunnen worden. Het hoofdstuk benadrukt de grote vraag die er is om tot betere behandelwijzen te komen en stelt dat dit alleen mogelijk zal zijn door de natuurlijke mogelijkheden en onmogelijkheden te erkennen en daar mee om te gaan op een manier die geïnspireerd wordt door de Natuur. Dit in navolging van de grote Griekse filosofen wanneer zij spraken over "de queeste voor de waarheid", dat wil zeggen het te weten komen van wat nog niet bekend is, op geleide van de Natuur zelf. Er is nog wel een zekere weg te gaan. We zijn inmiddels in de 21^e eeuw aangeland, maar we kunnen nog steeds geen gewrichtskraakbeen bij volwassen individuen herstellen. Om echte voortgang te maken in de biomedische wetenschappen zullen we onze *in vitro* en *in vivo* modellen en onze methodologieën kritisch onder de loep moeten nemen. Hiervoor zijn de wetenschappelijke validiteit en ethische acceptatie van zeer groot belang en idealiter wordt dit gedaan in het kader van het *"One Health – One Medicine"* principe. Op die manier kunnen we de noodzakelijke stappen zetten op het gebied van de regeneratieve geneeskunde en een betere kwaliteit van leven voor toekomstige generaties mogelijk maken.

all the support in this PhD project.

Thanks to the staff of the Equine Clinic at Utrecht University, especially to Dr. Harold Brommer, and Dr. Stefan Cokelaere and Dr. Thijs van Loon, of which the first two were part of this project. Thanks a lot my friends!

Thanks to the staff of the University Medical Center of Utrecht (UMCU) and the Regenerative Medicine Center Utrecht (RMCU), especially to Saskia Plomp, Miguel Castilho, Riccardo Levato, Paweena Diloksumpan, Mattie van Rijen, Mariëlle Vullers, Nicoline, Behdad Pouran, Anneloes Mensinga, Kim Benders, Alexandro Ribeiro and Harrie Weinans. Also many thanks to our collaborators from Würzburg: Jürgen Groll and Uwe Gbureck.

Thanks to the collaborators from the University of Twente, especially Sanne Both, Bram Zoetebier, Piet Dijkstra and Marcel Karperien.

Thanks to the Department of Clinical Chemistry and Transfusion Medicine, Sahlgrenska University Hospital, Gothenburg Sweden, especially to Anders Lindahl.

Thanks to the secretaries of the Utrecht Equine Hospital, Marloes and Suzanne.

Thanks to my friends, Francina de Pater and her Family, Maarten Pieterse and his wife Karin, Irina Mancini and her husband Fred, Federico Vilaplana and Janneke Boere.

Thanks to the team that collaborated in the design, formatting and revision of the thesis:
Christian J. Alfaro Rojas, Raquel Hernández Rojas and Erica Wilson (USA).
Thanks to all the organizing staff of the Regenerative Medicine PhD Program, especially to Sarah Opitz, Dr. Koen Braat, and Professor Paul Coffer.

Many thanks to the Institutions that gave financial or technical support to the work that lies at the basis of the thesis:
- Universidad Nacional, Costa Rica.
- Ministerio de Ciencia, Tecnología y Telecomunicaciones (MICITT), Costa Rica.
- Stichting ReumaNederland programmalijn LLP-22, The Netherlands.
- Utrecht University, the Netherlands.
- University Medical Center Utrecht (UMC), the Netherlands.
- Twente University, the Netherlands.
-
Thanks to my family, my parents Rafael Vindas Zamora and Victoria Bolaños Blanco, my wife Ariella Solís Amaya and my children Rafael, Gabriel and Michelle, for their unconditional support, love, and for helping me make this dream come true.

Thanks my God for giving me strength and confidence to achieve this dream.

Curriculum vitae

Rafael Ángel Vindas-Bolaños was born on February 15, 1968 in Zarcero, Alajuela, a beautiful rural mountain town in the northern part of Costa Rica, where he received his primary and secondary education. As a student of the School of Veterinary Medicine (Escuela de Medicina Veterinaria) of the Universidad Nacional de Costa Rica (National University of Costa Rica), he worked as an assistant in the Library and in the Pathology Department. He completed his final 7-month traineeship practicing surgery, ambulatory care and anesthesia of large animals at Utrecht University in the Netherlands in 1994. Rafael, obtained his DVM title from the Universidad Nacional de Costa Rica in 1995. Once graduated, he worked part-time as a professor of physiology, clinical training and large animal surgery at the Universidad Nacional de Costa Rica. For the remainder of his time, he worked as supervisor of the Program for the Eradication of the Screwworm and Surveillance of Exotic Diseases, a collaborative program between the Ministry of Agriculture and Livestock of Costa Rica and the Department of Agriculture of the United States of America (1995-2010). During this time, he also published his book, "Dislocaciones del Abomaso" (Abomasal Displacements), and was recognized as a professor and distinguished civil servant for both institutions. In 2004, he obtained the title of Professional Specialist in Medicine, Surgery and Reproduction of Equids. He also taught farm animal surgery at the Escuela de Medicina Veterinaria San Francisco de Asis of the Universidad Veritas de Costa Rica (School of Veterinary Medicine San Francisco de Assisi, Veritas University of Costa Rica) in the years 2003-2008. He has received training in surgery, internal medicine, ambulatory care, exotic diseases, regenerative medicine and epidemiology from the universities of Utrecht (the Netherlands); Hannover (Germany); Guelph (Canada); Colorado State University (USA) and the Plum Island Animal Disease Center (USA). He has further been professionally active in Argentina, Mexico and Panama. Rafael has been recognized for his work in national emergencies, for his professional collaboration in low-income communities in marginal areas of Costa Rica, for his participation in national and international traceability projects and for implementing quality systems with international ISO standards. From 2010-2012, he was the coordinator for the Comité de Educación Continua del Colegio de Médicos Veterinarios de Costa Rica (Committee for Continuing Education of the College of Veterinary of Costa Rica) where he was involved in the creation of a Departamento de Educación Continua del Colegio de Médicos Veterinario (Department for Continuing Education of the College of Veterinary). He has published and spoken at conferences and congresses on the topics of quality, disease surveillance, regenerative medicine and surgery of large Animals. In December 2012, he began his PhD program in regenerative medicine in equines at the University of Utrecht in the Netherlands. From 2010 to 2015, he continued as a professor of surgery in large species in the Escuela de Medicina Veterinaria of the Universidad Nacional de Costa Rica (School of Veterinary Medicine of the National University of Costa Rica) and was elected vice-dean of the Facultad de Ciencias de la Salud (Faculty of Health Sciences). In 2015, Rafael was appointed as dean of this faculty, which position he will hold until November 1, 2020. At present, he lives in Lagunilla, Heredia, in Costa Rica where he enjoys spending time with his family, watching movies, playing sports and visiting the beach in his free time.